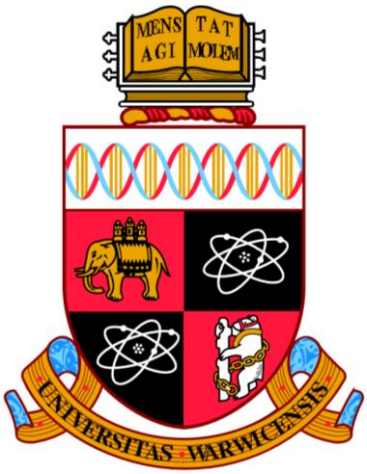

Design of a Resorption Transformer to Upgrade Industrial Waste Heat

By

Samuel John Hinmers

A thesis submitted in partial fulfilment of the requirements for the degree of Doctor of Philosophy

University of Warwick, School of Engineering

March 2022

Summary

A design for a 3 kW resorption thermal transformer reactor has been presented. The design uses the pair calcium chloride and manganese chloride salts with ammonia as the refrigerant, using the same internal geometry in both reactors. The reactor design was informed by extensive experimental testing of the two salts mentioned and barium chloride, which were identified as principal salts to test. Testing was comprised of Large Temperature Jump (LTJ) testing using a specially designed reactor. The experimental apparatus was further developed to observe key reaction data. This has enabled a methodology to be presented for analysing new salts reacting with ammonia for the development of resorption reactor design. The LTJ testing observed the evolution of the reaction, and enabled the equilibrium data to be recorded, and observed phenomena in the salts that appeared as a metastate (or metastable state). One further development was the 'shell-side' LTJ reactor, this enabled empirical data for adsorbent material analogous in scale and geometry to a working resorption machine to be documented. The shell-side reactor was further modified to record Isosteric Temperature Change (ITC) data, which enabled accurate heats of reaction to be recorded. The experimental data enabled a design to be produced considering the Coefficient of Performance (COP) and the power density. This identified the importance of considerations into the heat transfer resistance and hysteresis. The 3 kW design presented could have a COP in the range of 0.4 with heat recovery processes applied. The system is designed at an expected power density of 1.4 kW/litre. The calcium chloride reactor overall length is 605 mm with a diameter of 114 mm, and hosts seven tubes with 16 mm A/F hexagonal forms of the composite adsorbent. The hexagonal forms were tested in the LTJ and performed well.

Contents

List of Figures

List of Tables

Nomenclature

Abbreviations

COP	Coefficient of Performance
DAQ	Data Acquisition
ENG	Expanded Natural Graphite
HVAC	Heating Ventilation and Air Conditioning
HT	High Temperature
HTS	High Temperature Salt
ID	Inner Diameter (mm)
ITC	Isosteric Temperature Change
OD	Outer Diameter (mm)
LTJ	Large Temperature Jump
LT	Low Temperature
LTS	Low Temperature Salt
SCP	Specific cooling power (Wkg^{-1})
SMP	Specific Mean Power (Wm^{-3})
TC	Thermocouple
TIT	Temperature Indicator Transmitter
PEEK	Polyether ether ketone
PIT	Pressure Indicator Transmitter
PTFE	Polytetrafluoroethylene

Latin

A_r	Arrhenius constant in rate equation

C Kinetic coefficients (s^{-1})

C_A Concentration of material A (mol·litre^{-1})

C_n Molar heat capacity (J mol^{-1}K^{-1})

C_p Specific heat (J kg^{-1} K^{-1})

c_V Specific heat at constant volume (J kg^{-1} K^{-1})

dm Increment of mass (kg)

dt increment of time becoming a time step in the simulation (s)

E Psuedo-energies of activation (K^{-1})

h Specific enthalpy (J kg^{-1})

K_a Kinetic coefficient (m^{-2}s^{-1})

K_r Kinetic coefficient (m^{-2}s^{-1})

k_0 Kinetic constant (s^{-1})

MC_p Heat capacity- comprised of ENG and salt fixed masses (J K^{-1})

M_r Kinetic coefficient

m mass (kg)

m_1, m_2, m'_1, m'_2 Psuedo-orders of reaction

N_g Number of reacting moles of gas per grain

n Constant in reaction rate equation

p Pressure (Pa)

P Pressure (bar)

Q Total heat (W)

P_i Interfacial pressure (Pa)

R Gas constant (J kg^{-1} K^{-1})

RMM Relative molecular mass (gmol^{-1})

r_A Rate of reaction (mol·Litre^{-1}s^{-1})

r_c interface radius in the grain (m)

SHF Sensible heat factor

t Time (s)

T Temperature (K)

T_c Constraint temperature (K)

u Specific Internal Energy (J kg^{-1})

V Volume (m^3)

X Degree of 1st reaction 0 to 1 (mol/mol)

Y Degree of 2nd reaction 0 to 1 (mol/mol)

Greek

$\Delta h, \Delta H_r$ Heat of reaction/Enthalpy of Reaction (kJ/kmol)

ρ Density (kg m^{-3})

ρ' Density factor (kg m^{-3})

ΔQ Heat entering system (J)

Δs Change in entropy (J kg^{-1} K^{-1})

ΔU Change in internal energy (J)

Subscripts

A Pertaining to type A adsorbate with .A mols of ammonia

AB Reaction from type A to type B

ADS Adsorbate

ads Adsorption process

B	Pertaining to type B adsorbate with .B mols of ammonia
BC	Reaction from type B to type C
C	Pertaining to type C adsorbate with .C mols of ammonia
d	Desorption
des	Desorption process
E	Expansion vessel
e	Equilibrium
ENG	Expanded Natural Graphite
eq	Equilibrium
GAS	Gas
HYS	Hysteresis
high	at the higher condition
in	Inlet
low	at the lower condition
mid	at the mid condition
NR	Non-reacting portion
out	Outlet
PROD	Product
R	Reacting portion
REACT	Reactant
SALT	Salt
S	sorption
V	Void

Acknowledgements

Throughout my research project I have had a great deal of support from my supervisor Professor Critoph, whose impressive expertise and many years of experience in this field has been invaluable in completing this work. I am immensely grateful and also appreciate all the related opportunities that working with him has given me. Thank you for taking me on four years ago.

I would also like to express my gratitude to all my colleagues in the STET research group. Every single one past and present has given me useful advice and knowledge, and I have thoroughly enjoyed my time working with them; particularly at the start of my studies, awaiting the chorus of phone pings across the office for coffee. Thanks to Charlie Joyce for his technical help and to George Atkinson my comrade in research, for their practical assistance. I must also mention special thanks Dr van der Pal for his guidance.

I am also deeply grateful to my parents for always pushing me and encouraging me down this path, and my late grandfather John Norman who inspired me so much. Without the support of my entire family, I would not have got here. Thank you also to my girlfriend Molly Hopwood for her unwavering support and encouragement, ensuring I never stray towards pessimism. Finally, my thanks to the Hopwoods, who have always been excited to hear about my studies and given me much encouragement.

Thank you to EPSRC (Doctoral Training Partnership) and TNO (under the project, Efficient Ad-Sorption for Industrial Energy Recovery — EASIER) (formally ECN) for funding my research project.

Declaration

This thesis is submitted to the University of Warwick in support of my application for the degree of Doctor of Philosophy. It has been composed by myself and has not been submitted in any previous application for any degree.

The work presented (including data generated and data analysis) was carried out by the author except in the cases outlined below:

The mathematical model presented in appendix 8.1 was produced by the project supervisor Professor Critoph. The initial MATLAB model that used the mathematical model was also written by Professor Critoph.

Parts of this thesis have been published by the author, and the list of publications is as follows:

Journal Papers

S. Hinmers, G.H. Atkinson, R.E. Critoph, M. van der Pal, “Resorption Thermal Transformer Generator Design,” *Energies,* 2022, *15*(6), 2058.

S. Hinmers, G.H. Atkinson, R.E. Critoph, M. van der Pal, “Modelling and Analysis of Ammonia Sorption Reactions in Halide Salts,” *International Journal of Refrigeration*, 2022, Volume 137, May 2022, Pages 188-211.

S. Hinmers, R.E. Critoph, “Modelling the Ammoniation of Barium Chloride for Chemical Heat Transformations,” *Energies,* 2019, *12*, 4404.

Conference Papers

S. Hinmers, G.H. Atkinson, R.E. Critoph, M. van der Pal, “Ammonia-Salt Reactions for Heat Pumping and Thermal Transforming Applications,” Heat Powered Cycles (HPC), Bilbao, Spain, 16–19 September 2021 (postponed to 10–13 April 2022). *HPC 2022 proceedings*, 2021.

S. Hinmers, G.H. Atkinson, R.E. Critoph, J. Locke, "Ammonia-salt Large Temperature Jump Experimental Technique Advances," International Sorption Heat Pump Conference (ISHPC), Berlin, DE, 23–26 August 2020 (postponed to 22–25 August 2021 virtual). *ISHPC 2021 Proceedings,* 2020.

S. Hinmers, R.E. Critoph, “Experimentation and analysis of ammonia-salt reactions for resorption cycles” International Symposium on Innovative Materials and Processes in Energy Systems (IMPRES), Kanazawa, Japan, 20–23 October 2019, *Impress 2019 Proceedings,* 2019.

S. Hinmers, R.E. Critoph, “Methanol and its Sorption Heat Pump and Refrigeration

Potential” Heat Powered Cycles (HPC), Bayreuth, Germany, 16–19 September 2018. *HPC 2018 proceedings*, 2018.

1 Introduction

1.1 Background

In recent years, the application of heat recovery and heat integration has become increasingly important and financially attractive. In 2014, a report by *elementenergy* for the UK government highlighted that 48 TWh/year of heat is emitted as waste heat from UK industry. They highlight the importance of reducing this to achieve emission goals relating to climate change, and the economic incentives of doing so; they indicate that an estimate 10-40 TWh/year could be recovered for use (elementenergy, 2014). Since the beginning of this project the importance of reducing waste heat has become yet more exigent. COP26 took place in Glasgow, drawing more attention to the issues of climate change and the challenge of meeting emission targets; and as the world recovers from the pandemic, there is an ongoing energy crisis. The crisis has caused the wholesale gas price in the UK to rise by 212 per cent in a year (between the third quarter of 2020 and the third quarter of 2021) (BEIS, 2021). Reducing waste heat is now more important than ever. Future industry is expected to move towards using: hydrogen; carbon capture utilisation and storage; biogas; or electricity, for future energy requirements. As it stands, all these options are expensive, so the challenge of high energy prices will become more acute.

Valorising waste heat and using it, is key to building resilience in industry and making green fuels viable in the near future. One of the best ways to utilise waste heat is with sorption technologies. These are gaining more interest with various heat driven absorption refrigeration or heat pumping technologies on the market; these are getting more commonly employed in industry and alongside large heating infrastructure. A major component of the waste heat which is currently emitted to the atmosphere is low grade or ultra-low grade heat—under 100 °C. Heat at this temperature has a low exergy and limited direct application for recovery within industrial

processes; it has been and is used in district heating networks and for space heating on-site. But in many cases, there is no application for this heat (or there is too much) and it is just emitted.

A vital technology to combat the deluge of wasted low exergy heat is thermal transformer technology. Thermal transformers are a concept that have been around for a long time, with absorption transformers having been in operation in Europe as far back as the 1980s (Cudok et al., 2021). Quite simply, a thermal transformer is able to upgrade the temperature of waste heat using its internal exergy, to a useful temperature. There have been surges of interest in the 1980s and now in recent years but no systems have made it to the UK. This is likely due to the size of the technology, seemingly bulky and heavy, and the high capital investment cost. The size and cost may dissuade process engineering firms due to the scale of commitment for both space and financial planning—to receive the return on investment for a thermal process they may not be familiar with.

The employment of transformer technology in Asia from companies such as Hitachi, highlights the potential for resorption transformers. A major challenge to uptake of even the simplest heat recovery processes in UK industry is capital cost. Resorption transformers present a simple system comprised of two beds, and without expensive components like condensers and evaporators. The beds themselves are simple heat exchangers and the salts (and graphite matrix in this example) are relatively cheap; which means that manufacture and component cost, could be a fraction of that for absorption systems. This could provide reduced capital cost and payback times even lower than those presented by Cudok et al. for absorption systems (Cudok et al., 2021) — making resorption transformers an attractive investment in the UK.

Heat transformers, effectively split the waste heat flow; producing a high temperature heat that is recoverable and low temperature heat near to environmental temperature which is emitted. The waste heat is provided below 100 °C, upgraded to a useful temperature in excess of 120 °C with low

temperature heat emitted around 40 °C. This is the same for absorption transformers and resorption transformers and so resorption systems should target the same industrial processes.

There are a number of key industries where transformer technology is viable. Currently absorption transformers are employed in the chemical, food and paper industries (Cudok et al., 2021). The most evident processes where transformers can be installed will for example: already apply heat recovery and even pinch technology; occupy remote locations or be in industrial areas (no way to market the waste heat); or use steam to provide process heat. Ling-Chin et al. collate the date from various industrial processes and detail the forms of waste heat (flue gas, etc.) and the related temperatures (Ling-Chin et al., 2019). Their work illustrates the application of steam condensate; but also shows other potential sources such as dyed waste water from the textiles industry (90-94 °C); or waste steam from flushing furnaces in the paper industry (95-100 °C). Hammond and Norman's work collates the temperature and quantity of waste heat from a number of industries that could also benefit from resorption transformers: food and drink, lime production, and pulp and paper all produce low grade heat at the scale of TJ per site per year (Hammond and Norman, 2014). The most practical and common waste heat source to work with is steam condensate, which is the proposed basis for the design presented in this work. Future systems could exploit a broader range of heat sources to abate considerably more emissions and raise industrial process efficiency.

One possible application yet to be explored is the use of thermal transformers to power carbon capture utilisation and storage. Absorption transformers are regularly installed directly to power distillation processes in the chemical industry—waste heat is provided from a different part of the process (Cudok et al., 2021). The most common method used for the capture component of Carbon Capture Utilisation and Storage (CCUS), is absorption stripping technology, which makes use of an amine solvent/sorbent. These absorption stripping systems require temperatures of 105-110 °C in the

stripper to liberate the CO_2 (Warudkar et al., 2013). Because of this CCUS processes can suffer from an 'efficiency penalty' of 8-16 % (Supekar and Skerlos, 2015). This means CCUS is expensive, and there is no direct return on investment unless the CO_2 is utilised. Therefore, the potential incorporation of transformer technology is an interesting concept, and the system could provide heat to the stripping process. Regardless, the applications of transformers are broad, and with high gas prices and expensive fuels like hydrogen on the horizon, transformers will only garner more interest.

1.2 Objectives of this work

The objectives of this project were as follows:

- Understand the reaction processes well enough to inform a model to simulate the reaction processes.
- Obtain relevant reaction data for three salts identified: barium chloride, calcium chloride, and manganese chloride.
- Use the model to inform a design for a 3 kW resorption demonstration experiment.
- Build and test the 3 kW machine in the ThermExS rig at the University of Warwick.

A 3 kW machine presents a reasonable size to test in the lab to gain empirical data with some potential to scale up.

1.3 Evaluating this Work and Thesis Outline

The objectives of the project were met except for building and testing of the demonstration experiment. However, the research project has been very successful. The literature review identified an absence of empirical evidence used in designing resorption machines, and important data that has been omitted. The work in this project was able to report new and accurate reaction data, identifying key components to the kinetics and observing phenomena not previously reported. The experimental data validated the

model developed by Professor Critoph; which is the first presented to consistently predict the reaction behaviour over dynamic conditions. The experiment was developed for further analysis and enabled a methodology to be developed (which is presented) for how to rapidly test and design a reactor for different and new salts. Finally, a design has been produced for a resorption reactor using the empirical data to optimise performance. Furthermore, experimental data has been obtained to provide empirical evidence for its potential performance with like for like samples tested and the specific mean power estimated. The design that is presented in this thesis can be used as a demonstration for resorption thermal transformers, and dynamic data obtained from testing this design will be crucial in raising the technology readiness level of resorption transformers.

The project began with the literature review observing the omissions of dynamic data in past work, and identifying the salt contenders to be evaluated. This was followed by developing the large temperature jump test cell and categorising barium chloride reacting with ammonia using an initial model presented in the literature. The LTJ test cell was developed to enhance its output for more reliable data, and then was used to gather experimental data on manganese chloride, and calcium chloride. Results were then used to evaluate a new model derived by Professor Critoph; which proved effective at simulating reaction data, and enabled the observation of reaction kinetic parameters to model the reaction for designing. The shell side LTJ was then developed to evaluate sizing of composite adsorbent expected in reactors, and the model was validated further. The shell side LTJ was adapted to perform ITC tests, this resulted in a much-improved estimate for the heat of reaction—a single value for adsorption and desorption believed to be the true value. The model was then tested against the previous results deriving final values for the kinetics; then it was applied to observe specific mean power, and to inform optimising the design of a reactor. Efforts were then made to reduce the heat transfer resistance to samples. A reactor design was developed by optimising the power density

and thermal efficiency, the former was performed by measuring the specific mean power (SMP) in kW/litre; and thermal efficiency by the Coefficient of Performance (COP), or useful heat out over total heat input.

2 Literature Review

Resorption transformers can be used to recover and upgrade low grade waste heat from industrial processes — that would otherwise be lost — to be reused within the processes on site to reduce overall energy consumption. This will be essential for many industries where valorising this waste heat in district heating networks will not be possible due to remoteness of industrial sites. Moreover, the simplicity of resorption machines which lack expensive components like evaporators and condensers, provide a compelling argument for their development.

The simplicity of a resorption transformer can also reduce the footprint of the technology. Crucial to achieving this will be ensuring a high-power density whilst maintaining a viable coefficient of performance (COP). Ammonia-salt reactions used in resorption transformers are documented to have fast reaction times in the scale of minutes (Atkinson et al., 2021, van der Pal and Critoph, 2017), this leads to high power densities, with the potential in multibed systems to produce a continuous high grade heat output.

Resorption systems comprise of pairing two halide salts in separate reaction vessels with (in this case) ammonia as a refrigerant. The two reactors are permanently connected and are thus at the same pressure. The system, driven by heat inputs and outputs, is cycled between upper and lower pressure limits. For a thermal transformer, at the upper limit, ammonia is desorbed from the low temperature bed and absorbed by the high temperature bed. At the lower limit the ammonia flow is in the opposite direction. The process is illustrated by **Figure 1** and **Figure 2** Such systems are well documented for applications of heat pumping, cooling, and

transforming (Vasiliev et al., 2004, Bao et al., 2012, Goetz et al., 1993). This work details an initial design for the generators, or reaction vessels, for a resorption transformer, evidenced by experimental tests, and followed with a discussion of the various hurdles to be addressed for an effective machine to reach prototype and production.

2.1 Working Concept

The resorption machine cycle has two main phases of operation and transitions between them, the resorption cycle illustrated in **Figure 1**, is explained as follows:

The first phase is the high-pressure phase. Waste heat is delivered to the low temperature salt, the salt desorbs the ammonia and the pressure rises in the system. Ammonia begins to adsorb in the high temperature bed and the temperatures in both beds climb the Clapeyron lines until at the P_{high} condition in **Figure 2**. At this point, high temperature (useful) heat is recovered and returned to the industrial process. The transition between pressures takes place over a short period, and the heat is delivered over an extensive period.

The second phase resets the system. Cooling water is delivered to the low temperature bed initiating ammonia adsorption and the system pressure begins to fall. The beds drop down the Clapeyron lines to the low-pressure condition. Whilst this occurs, the waste heat is fed to the high temperature bed to provide the endothermic heat. The process continues at low pressure until the exothermic adsorption reaction is complete in the low temperature bed, resetting the cycle.

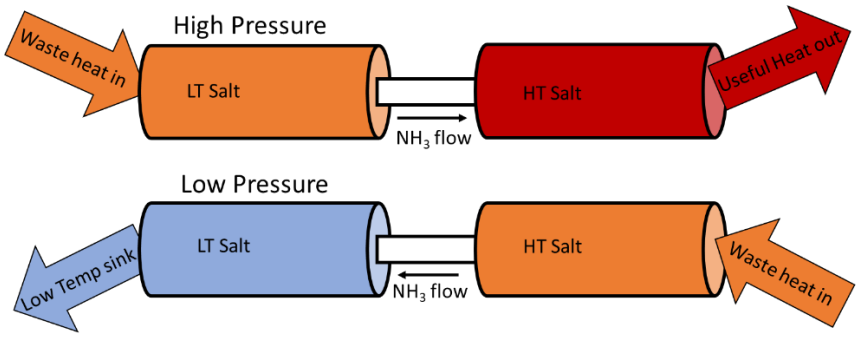

Figure 1 Simplified resorption machine, at low and high-pressure phases of operation.

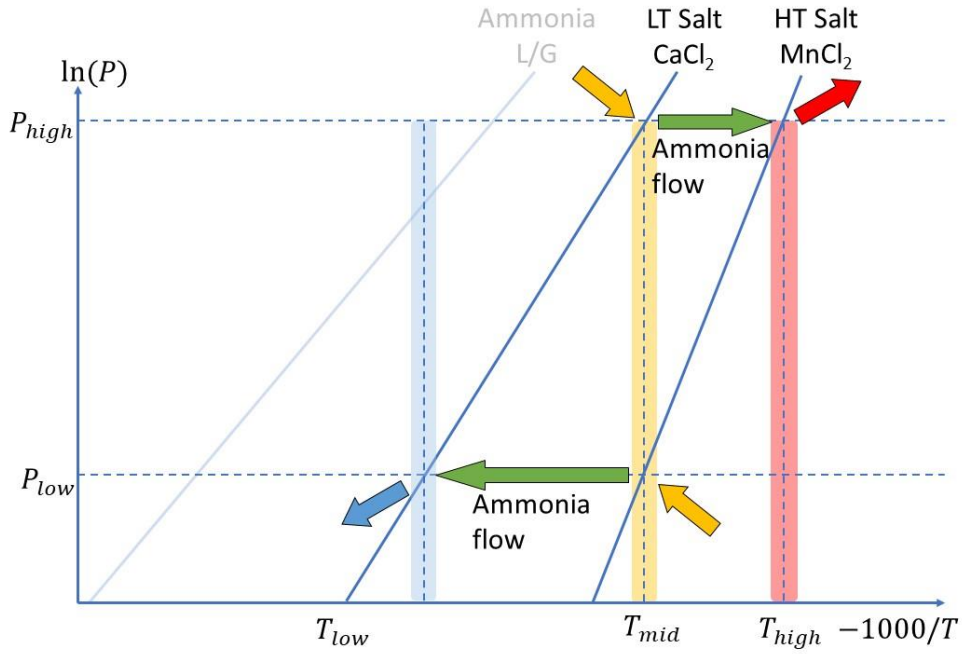

Figure 2 Resorption Machine Clapeyron Diagram

Relatively little electric power is required in the process, apart from fluid movement, fans, instrumentation and control. The absence of evaporator and condenser within a resorption system creates the opportunity for cheap manufacture, whilst operation requires limited electrical power input. Fluid movement may require some energy, but processes likely to find transformers appealing will either have steam condensate or may already have heat recovery and pinch analysis incorporated (and therefore already pumping fluids). These factors and simple operation mean resorption machines can play a key role in decarbonisation.

2.2 Thermal Transformers

The concept of thermal transformers has already reached the market. There are 17 absorption thermal transformers that are operational as detailed by Cudok et al., these are mostly in Asia, saving several thousand tonnes of CO_2 per year (Cudok et al., 2021). This highlights the efficacy of heat transformers. Yet, absorption transformation isn't a new idea. Tyagi discusses the thermodynamics of an absorption transformer system and compares them with a resorption heat transformer 35 years ago. Tyagi shows that an absorption transformer can outperform a resorption transformer for lift and COP with the use of ultra-low-grade heat, but this has limited scope and is not useful for industrial heat recovery (upgraded heat is lower than 100 °C); the work describes double effect systems in detail, but their key observation is 'The pump work and heat regenerator duty are less for the resorption heat transformer than for the absorption heat transformer' (Tyagi, 1987). More contemporary work by Ma et al. discusses this further but the applications are restricted due to maximum temperatures less than 100 °C (Ma et al., 2016). Similarly Hernández-Magallanes et al. shows how utilising a double effect transformer increases the temperature lift as much as up to 60 °C but achieves lower COPs than would be expected for an optimal resorption heat transformer (Hernández-Magallanes et al., 2017). On Hitachi industrial's website, they detail two examples of absorption systems that have been commissioned and installed. A system in a machinery company using cooling water from an engine; the transformer delivers 133-137 °C at a scale of 150 kW. Another system they have delivered is used in the alcohol industry utilising hot alcohol vapour (presumably a distillate, as the recovered heat is used to feed a distillation tower), and upgraded heat is produced at 107-112°C in a 2475 kW system (HITACHI, 2019).

Furthermore, one of the most useful things that can be found is within Hitachi's 'features' section for the industrial system on their website, this is a plot showing operating temperatures seen in **Figure 3** (heat source

temperature, regeneration temperature and heat sink temperature) (HITACHI, 2019). This gives us the quoted operating conditions for the technology on the market, providing a benchmark for a resorption system and will be discussed again later. The challenges to achieve wide adoption of transformers are especially important when considering a UK market. These are: size of technology; high capital cost; and length of cycle times, as detailed by Cudok et al (Cudok et al., 2021). When considering the hypothesis of Tyagi, this might be overcome by resorption systems as long as they provide a reasonable temperature lift.

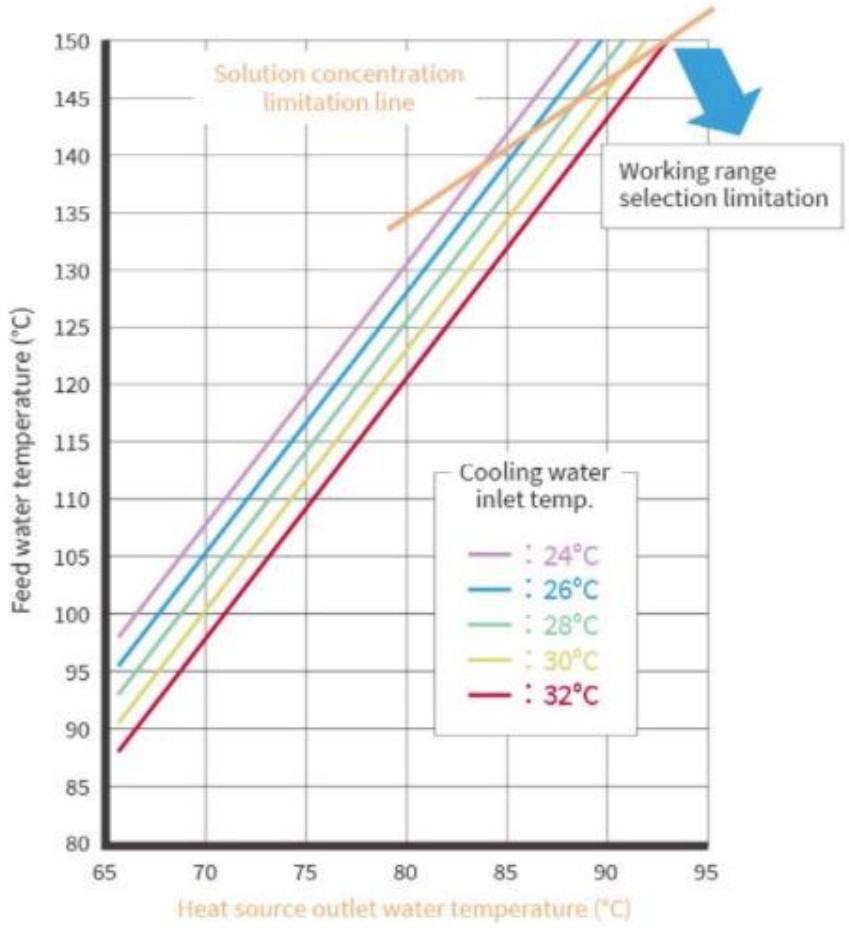

Figure 3 Operating temperatures of Hitachi's thermal transformer, this graph is taken from a Hitachi webpage for their absorption type2 heat pump (HITACHI, 2019).

2.3 Ammonia and Salts

The first observation of the potential of chemisorption of ammonia into halide salts was by Faraday in 1823 (Faraday, 1823). He observed a significant uptake of the ammonia adsorbed into the salt silver chloride. Upon heating the ammoniated salt in a sealed bent tube (the other end simultaneously cooled), he noticed the ammonia condensing in the other end of the tube. He then removed the tube from the heat and allowed the chloride to adsorb the ammonia, this produced significant heat; and as the ammonia evaporated from the other end of the tube, he observed significant cold. This observation of artificial cooling is one of the first and is an important moment in the development of HVAC. In the '80s and '90s more interest arose in the adsorption of ammonia into salts for the potential of sorption machines. This was perhaps eclipsed by the development of vapour compression systems that now dominate the market. But in recent years since, interest has rebounded as heat driven cycles present new ways to better utilise energy.

One of the first suggestions for the application of ammonia reacting with salts for the upgrading of waste heat—with a transformer—was presented by Goetz, et al. (Goetz et al., 1993), this is presented as an alternative to the previously mentioned absorption transformers with water-ammonia systems (Tyagi, 1987). Ammonia reacting with salts in a resorption machine are compelling as this presents an option for cheap manufacture, and potentially smaller footprint of device which is key to making transformers a more attractive investment. To comprehend the interactions between salts and ammonia it is sensible to explore other refrigerants and sorbents discussed in the literature. A good place to begin with solid state sorption is the research by Offenhartz et al., they produced a solar driven heat pump and refrigeration machine, using methanol as a refrigerant and calcium chloride as the sorbent. They reported a COP of 1.6 and 0.6 for heating and cooling respectively (Offenhartz et al., 1980, Offenhartz et al., 1981). This is equal to or greater than COPs recorded even to this day utilising

physisorption, which require heat recovery to achieve similar performance (Chekirou et al., 2016). The main limitation of methanol is its lack of stability above 120°C limiting its application to heat pumps as documented (Iedema, 1984, Aittomäki and Härkönen, 1988), rather than for waste heat transforming. A more appropriate sorbate to the applications of heat pump or thermal transformer is ammonia. Work by Critoph considered a number of refrigerants and although methanol is a strong contender for heat pumping and refrigeration, he concluded ammonia has the best potential (Critoph, 1989). The problem with water and methanol systems is these tend to operate at sub-atmospheric pressure due to their boiling temperatures. Consequently, mass transfer phenomena can considerably affect the rates of reaction. Such refrigerants are better suited to refrigeration and energy storage applications. Ammonia is a more suitable refrigerant for thermal transformer applications, and this appears to be why it garners the recommendation by Goetz et al. (Goetz et al., 1993).

The broad applications of ammonia and salt reactions for chemical heat pumps were well discussed in the nineties; work by Neveu and Castaing collated the reaction equilibrium data from a large number of chloride salts, whilst discussing in detail choices of salts. The data is tabulated with the corresponding enthalpies and entropies that equate to the Clapeyron relationship equilibrium lines (Neveu and Castaing, 1993). Their paper begins to discuss the potential of a resorption system citing the paper by Goetz et al. (Goetz et al., 1993), highlighting the advantages due to the direct heating and cooling effects from the solid-gas reactor. The paper by Goetz et al. considers a number of different operating cycles and is discussed later in this report. More recent work by Donkers et al., considers many different ammoniation reactions and the complexes formed with a large number of salts. It analyses data from as early as 1860, with enthalpy and entropy values for Clapeyron equilibriums (Donkers et al., 2016). This paper overlaps with work done by Touzain et al., which considers 350 different solid salt-ammonia reactions, this also proposes some of the best candidates for

applications (Touzain, 1999). There is data missing for some salts such as the number of moles of ammonia in the crystalline structure after deammoniation. Utilising the Clapeyron equation data from this paper enables the evaluation of any salt pair for their potential in resorption systems.

Salt-sorption systems are very promising but the main issues to overcome are agglomeration of the salt crystals and low conductivity of the reactive medium. Gordeeva and Aristov reviewed the progress of composite sorbent materials and impregnation of salts into conductive or other mediums (Gordeeva and Aristov, 2012). This paper is most valuable when considering the process of the impregnation and the physical chemistry of the reaction with the composite. Methods are presented for production of the composite sorbent as well as reporting the different outcomes; this includes a discussion into the effect pore diameter has, and discussion into vapour transport as a function of the size of the pores. An optimal pore size is required to ensure that a crystalline phase of salt forms that reacts to form a salt ammoniate, rather than an amorphous phase developing in the presence of ammonia. Furthermore, they consider work into the effects of binary salt systems (salt mixtures), which appears to move the sorption isobars between those of the two single salt composites (Gordeeva and Aristov, 2012). This means salt mixtures could be very promising, and the possibility of new isosteres in the middle of existing salts, has the potential for fine tuning pairs to suit any operation conditions.

Trudel et al. discussed the hysteresis of the reaction between cobalt chloride and ammonia in the development of a chemical heat pump. They present a number of explanations of the hysteresis such as swelling of the crystalline structures, which requires a driving force to cause the expansion in the crystals, perhaps even an activation barrier which may need to be crossed in adsorption but not during desorption. Another explanation they proposed is a lag between the temperature in the gas phase and solid phase, which will be very different depending on whether the adsorption or desorption

process is occurring (Trudel et al., 1999). This paper is valuable for considering the challenges when designing an ammonia-salt system with explanations and solutions. Pan and Zhou, considered the application of salts (with water) for high temperature energy storage for industrial applications. This was also incorporated into a hybrid design (Pan and Zhao, 2017).

A favourable host matrix for salt is Expanded Natural Graphite (ENG), due to its pore size and high conductivity. Kiplagat et al. used sodium bromide within ENG to create the composite sorbent material for use in an air conditioner; their design utilised a condenser and evaporator. The reactor was formed by producing a slurry of ENG and NaBr, which was manually filled between fins on the outside of a tube which are then consolidated into a bundle within a steel cylindrical case. Their conclusion was that NaBr is applicable to solar air conditioning due to its capacity to operate with a low source temperature. A range of COPs are discussed with relation to cycle conditions, but present a value of 0.41-0.45 under typical conditions (Kiplagat et al., 2013). Van der Pal and Critoph also utilise ENG as a matrix producing a composite of roughly a kilogram of calcium chloride, within a kilogram of ENG. This is utilised in a reactor for the development of a transformer concluding that the reaction of $CaCl_2$(4-8)NH_3 shows little hysteresis but also suggest that the kinetic rate constants for the reaction are different to that from $CaCl_2$(2-4)NH_3, highlighting the importance to evaluate both reactions and model them separately. They predict that calcium chloride in a transformer could produce values for the COP of 0.35-0.4 (van der Pal and Critoph, 2017). An interesting application into the use of salts is detailed by Aristov. He proposes the application of thermal transformation to upgrade heat in cold climates; this system works by transforming heat from a large lake or underground to heat a home, sinking heat to Siberian winter temperatures well below zero. It is noted that special attention is required in considering the materials and system dynamics due to low operating temperatures and pressures to enable such a system to

work (Aristov, 2017). This novel concept utilised a lithium chloride salt within vermiculite and methanol as a refrigerant.

Reversible reactions between ammonia and halide salts are monovariant equilibrium reactions; this means operation of a resorption machine can be represented by a Clapeyron diagram like in **Figure 2**. The reason halide salts reacting with ammonia are promising for resorption (particularly for thermal transformers) is due to their high uptake and relatively quick reaction rates (van der Pal and Critoph, 2017). Furthermore, resorption systems are able to make use of the extensive variety of salts that can be paired, creating enormous flexibility and the opportunity to tailor operating conditions to temperatures required (Neveu and Castaing, 1993). For future applications it is worth noting that in the case of pairs of salts with different anions (e.g., sulphates and bromides) the equilibrium lines may cross on the Clapeyron diagram; this creates further applications, with multiple temperature outputs analogous to a quadripole. The exergetic quadripole can be optimised for a double transformer effect or combined heat and refrigeration, enhancing its performance (Goetz et al., 1993).

2.4 Introduction to Thermodynamic Characteristics and Reaction Kinetics

Key to developing a design for a resorption machine is understanding the reaction kinetics during a reaction cycle between ammonia and the halide salt (usually within a matrix). A number of approaches were taken in the nineties to develop a model for the reaction behaviour which were then evaluated against various experiments. Contemporary adsorption testing tends to use either a gravimetric suspension balance test cell, or large temperature jump testing. This is then applied to a model, often based upon the methods presented in the nineties. First it is sensible to consider the various testing methods taken previously, before reviewing the different approaches to modelling that have been taken, and what insight they give into reaction behaviour.

2.4.1 Testing Methods from Literature

Much work in the nineties considered the broad applications of ammonia and salt reactions for chemical heat pumps. Neveu and Castaing collated the Clapeyron relationships of a large number of chloride salts reacting with ammonia. The data is tabulated with the corresponding enthalpies and entropies that equate to the Clapeyron equilibrium lines (Neveu and Castaing, 1993). The data cited presents only single equilibrium lines. The paper starts to review the potential applications for ammonia-salt reactions, and highlights the surge of interest in testing and experimental data that began around that time. A paper published just prior is by Moundanga-Iniamy and Touzain; they studied sorption reactions between magnesium chloride and ammonia for the purpose of energy storage, highlighting the high energy storage density (Moundanga-Iniamy and Touzain, 1992). They tested pure magnesium chloride and a magnesium chloride-natural graphite powder mix at a molar ratio of 1:5, and observed three Clapeyron relationship lines for different changes in moles of adsorbed ammonia (6-2, 2-1 and 1-0 moles). Unfavourably, the production of the composite appears challenging, requiring six hours of heating a mixture of graphite powder and manganese chloride at 580°C (Moundanga-Iniamy and Touzain, 1992). Touzain and Moundanga-Iniamy build on this work, and also with their colleague Atifi; they observed the addition of graphite increases the heat and mass transfer and avoids agglomeration, and report improved reaction cycles of 30 minutes. Interestingly they also recorded X-ray diffraction and neutron diffraction data of the composite and ammoniate and were able to deduce the shape of the lattice structure when bonded to the ammonia (Touzain and Moundanga-iniamy, 1994, Touzain et al., 1994). The structure of the material when ammoniated is under-explored and the chemistry involved is still not fully understood.

Mazet et al. undertook tests by packing a reaction chamber with nearly 700 grams of calcium chloride. The simple experiment involved external heating and monitoring the temperature at a number of points across the radius. A

notable observation was "…the quasi-simultaneous evolution of the two reactions". Their conclusion is based on observing smooth temperature profiles. This is interesting, although different stationary temperatures can be seen in some of the more external radial readings during the evolution of the reaction. Also, the radial conversion plot has anomalous results which need to be considered or the tests repeated. In this paper the results typically show distinct reactions but this is dictated by the reaction isosteres which are not mentioned. Their main observation, was that the size of their reactor bed enabled large temperature gradients to be observed during the process, and they conclude it is vital to optimise the thickness of the salt bed (Mazet et al., 1991).

Goetz and Marty used a Setaram DSC 111 to observe the reactions between manganese chloride and ammonia, their experiment was pressure controlled with a cell held at a fixed temperature. They observed extensive hysteresis, which they detail as the pseudo-equilibrium area, in which no reaction occurs. More recently there have been two main approaches to testing: using gravimetric magnetic suspension balance equipment; and using the large temperature jump technique (LTJ). Gravimetric suspension balance testing has been popular (Zhong et al., 2009, An et al., 2020b, Trudel et al., 1999), this is again a pressure-controlled test method; typically operated by holding the test cell at a fixed temperature whilst changing the pressure using a liquid ammonia reservoir. The cell is suspended and measures a change in mass as the sorption reaction occurs. The test process is therefore gradual, and the temperature of the material is not monitored. This should raise questions about its effectiveness for providing empirical data for sorption machine design and the results often show extensive hysteresis. The LTJ method appears more effective as it is designed to mimic the behaviour in sorption machines. Dawoud and Aristov pioneered the LTJ method to observe the evolution of sorption reactions (Dawoud and Aristov, 2003), and it has been used many times to observe reaction dynamics (Veselovskaya and Tokarev, 2011, Aristov, 2013). Gordeeva and Aristov used

the LTJ method with success analysing the sorption of methanol into lithium chloride (Gordeeva and Aristov, 2011), and Metcalf et al. used the method to produce and test generator designs for ammonia-carbon systems (Metcalf et al., 2021). Adapting this method to test ammonia-salt reactions has proven effective to observe phenomena that would be missed by gravimetric methods. For example, Atkinson et al. observed a peculiar behaviour at low pressures when ammonium chloride reacts with ammonia; a spike in the temperature and change of reaction behaviour (Atkinson et al., 2021). The LTJ method utilise a large expansion volume which ensures the pressure change is low, similar to the conditions in sorption machines. The simple design also enables measurement of the material temperature improving understanding of the reaction behaviour.

Sharma et al. deployed a testing method which essentially employs pressure jumps, and tested ammonium chloride and potassium iodide (Sharma et al., 2021). Their testing does not appear to be robust; they concluded that different isosteres occur at different concentrations of ammonia within the salt, this conclusion is uncertain due to the test method. They chose to perform calculations neglecting this finding which further brings this conclusion into question. They stated that isobaric conditions were used to plot their differing isosteres, but the lines used clearly show a graduation in the pressure where the values are taken so the isobaric assumption is incorrect (N.B. the plot is a log scale exacerbating the error). This is important particularly as this is obtained from a construction line, and then construction is not shown for one of the salts which shows a local maximum in the pressure scale at low concentrations (early in the reaction), before dropping and then rising again, which is not isobaric behaviour; this leads one to wonder where the reading could be taken. Their methodology is also confusing as the material is left to reach equilibrium, but '*equilibrium state-points'* are recorded when the behaviour is transient and changing (Sharma et al., 2021). The values they observed present extensive hysteresis. However, the effects of hysteresis should not be observed if the conditions

were left to reach equilibrium, as hysteresis is irreversible behaviour and a function of transients of transport phenomena which will not occur when this system is at equilibrium by definition. A better approach would be monitoring the final conditions after the pressure jump (when equilibrium conditions are reached along the isostere), and not attempting to draw a straight line across dynamic temperature behaviour; this could produce a unified line for the isosteres. Much of their work focused on the idea that hysteresis always occurs, but an improved practical example which contradicts their work is shown by van der Pal and Critoph. In their work, van der Pal and Critoph stepped a large reactor up and down the isostere by changing the temperature, they observed no hysteresis (van der Pal and Critoph, 2017). The *stepping-up* effect is to change the conditions and then leave to settle and then change again, thus observing the material under equilibrium conditions. It is also worth noting that some salts appear to never exhibit hysteresis and so it cannot be assumed. Atkinson et al, observed no hysteresis when testing ammonium chloride in an LTJ (Atkinson et al., 2021). It is clear that LTJ testing is the most effective way to observe the reactions, presenting a simple case that can be modelled and removing uncertainties found with other methods.

2.4.2 Modelling the Reaction Kinetics

Key to analysing experimental results is constructing an effective model; in the literature there are a number of approaches that have been taken. Some work has taken the approach to approximate a reaction rate equation, simply by fitting the reaction-rate or rate of advancement to an exponential function. Other approaches have been highly theoretical with consideration of the transport phenomena. An et al. have provided possibly the most comprehensive review of the mechanisms and kinetic models used to predict the behaviour of ammonia-halide salt reactions [25]. This work details the methods taken by researchers over the last 30 years and unpacks the approaches so we can infer the motives of the cited work. In this section, some relevant models will be covered briefly to inform the practices in this

work. The terms and nomenclature (particularly those not described in the body of text) are defined in the **Nomenclature** section.

As An et al. conclude in their review paper, little attention has been paid to reaction kinetics in the years prior to its publication; rather researchers have focussed on performance results (An et al., 2018). A prime example of this is the work using an exponential function with a time constant. This was capable of approximating reaction performance (Veselovskaya et al., 2010, Veselovskaya and Tokarev, 2011, Veselovskaya et al., 2012), but this black-box type approach lacks flexibility and is prone to error when scaling up. A theoretical approach was taken by Lebrun and Spinner; this was perhaps one of the first methods used to dimension a working system from dynamic reaction results (Lebrun and Spinner, 1990a, Lebrun and Spinner, 1990b, Lebrun, 1990). Lebrun and Spinner presented reaction kinetics in an analogical form, assuming that the limiting factor is the chemical reaction rate. They based this conclusion on two reactions between methylamine and calcium chloride and derive the following equations (Lebrun, 1990):

General form of equation:

$$\frac{dX}{dt} = f(x)k_0 \exp\left(\frac{-E}{T}\right)\ln\left(\frac{P}{P_e}\right) \quad (1)$$

Adsorption

- Reaction (I)

$$\frac{dX}{dt} = (1-X)^{n_1} C_1 exp\left(\frac{-E_1}{T}\right)\ln\left(\frac{P}{P_{e1}}\right) \quad (2)$$

- Reaction (II)

$$\frac{dY}{dt} = (1-Y)^{m_2} X^{n_2} C_2 exp\left(\frac{-E_2}{T}\right)\ln\left(\frac{P}{P_{e1}}\right) \quad (3)$$

Desorption

- Reaction (I)

$$\frac{dX}{dt} = X^{n'_1}(1-Y)^{m'_1}C'_1 exp\left(\frac{-E'_1}{T}\right)\ln\left(\frac{P}{P_{e1}}\right) \quad (4)$$

- Reaction (II)

$$\frac{dY}{dt} = Y^{m'_2}C'_2 exp\left(\frac{-E'_2}{T}\right)\ln\left(\frac{P}{P_{e1}}\right) \quad (5)$$

Where:

Pseudo-orders of reaction in adsorption or desorption respectively: n_1, n_2, and m_2; n'_1, m'_1 and m'_2

Kinetic coefficients: C_1, C_2, C'_1 and C'_2

Psuedo-activation energies: E_1, E_2, E'_1 and E'_2

The structure of the kinetics is derived from Arrhenius' law, based around the rate equation for surface kinetics on a catalyst:

$$-r_A = kC_A^n = k_0 C_A^n e^{-E/RT} \quad (6)$$

Where the rate of reaction is nth order in respect to the concentration of species A, indicated by C_A (Levenspiel, 1999). The concentration is replaced by a term for the conversion and there is no longer an order of reaction described in the rate expression. Instead, a pseudo-order of reaction is presented as a constant, but has no effect relating to the concentration of reacting species (or order of the reaction). The functions can also be seen to have pseudo-reaction energies that incorporate the gas constant and contain a pseudo pre-exponential factor. They evaluate two consecutive and potentially simultaneous reactions, hence (I) and (II). The method is very interesting and has inspired much subsequent work including this project, but the number of constants makes the process unnecessarily complex; too much weight is put on the pseudo-orders of reaction, when they infer that all but one are equal to 1. The kinetic coefficients can be seen to change depending on the packing density and the proportion of binder. The fact that these values have an optimum—and this is presented as a way to optimise the composite performance—suggests perhaps this value is responding to improved conductivity and thus reaction rate, and not actually predicting the

kinetics. The flaw in this method appears to be that they: "…consider only the global exchanges between the reacting medium and the heat transfer fluid." (Lebrun and Spinner, 1990a). For such a complex approach to the reaction rate equations, it would have been more instructive and a more accurate test if the model used local variables. None the less this work is a key step in design based on dynamic reaction results (Lebrun and Spinner, 1990a).

Another approach was taken by Mazet et al., again observing the reaction between methylamine and calcium chloride (Mazet et al., 1991, Mazet and Amouroux, 1991). Their approach was to decouple the kinetic and thermal equations and resolve the kinetic equation $dx/dt = f(x, T, P)$ for x, independently of heat transfer. This can then be used in part to derive the local heat transfer effects. They again present two kinetic equations for two reactions, with the potential for simultaneous reactions occurring.

$$\frac{dX}{dt} = (1 - X)^{m_x} \cdot A_{r,X} \cdot \frac{p - p_{eq}}{p} \tag{7}$$

$$\frac{dY}{dt} = ([1 - Y]X)^{m_y} \cdot A_{r,Y} \cdot \frac{p - p_{eq}}{p} \tag{8}$$

$$k(p, T) = f'(p, T) \cdot s \exp(-E/RT) \tag{9}$$

$$f'(p, T) = (p - p_{eq})/p \tag{10}$$

Mazet et al. describe $f'(p, T)$ from equation (9) as a term to weight the expression for reversible heterogeneous reactions by the difference between operating conditions and equilibrium conditions. Therefore the final kinetic equation is in a similar form to that for surface kinetics for catalytic reactions, as shown in equation (11) (Levenspiel, 1999); dX/dt for the rate of conversion, is a function of the conversion X, to the power of a pseudo-order m_x, multiplied by a rate of reaction term that encompasses kinetic term and the displacement from equilibrium (derived from equation 11).

$$Rate\ of\ reaction = \frac{(kinetic\ term)(driving\ force/displacement\ \ from\ \ equilibrium)}{resistance\ term} \quad (11)$$

The choice of a displacement from equilibrium term is important when we consider that the preponderant effect on the adsorption reaction, is the driving force created by the extent of the negative deviation—or the lower the temperature relative to the equilibrium conditions. For example. during adsorption in equation (9) the Arrhenius term would decrease but an increased reaction rate is observed even as the negative temperature displacement increases (highlighting the dominance of the displacement from equilibrium). Additionally, the preponderance of the deviation from equilibrium can also be seen in the desorption reaction. The choice of $p - p_{eq}\ /p$ to express the deviation from equilibrium conditions rather than temperature, ensures the separation of the kinetic and thermal expressions in their model, but still reflects the driving force.

Their function describes global advancement and is shown to predict with success. They explain the Arrhenius term A_r has a limited effect, as the reaction rate is dominated by the deviation from equilibrium; furthermore, it is *'practically equivalent to a constant'*, and it is therefore not possible to extract the parameters s and E. Inadvertently, the global model appears to be replaced with a local (one dimensional) model where X, Y and T are a function of the radius (Mazet et al., 1991). Tests in a later section such as in **Figure 18**, show the individual phase changes in equilibrium when calcium chloride reacts with ammonia; these appear to occur consecutively. This may be a local effect and global simultaneous reactions occur or perhaps it is more complex. Mazet et al. suggest that both reactions can occur simultaneously with methylamine, but no results are shown or equilibrium data. The simplified approach presented by Mazet el al. is a big improvement on the previous work, and is cited in the papers that present these subsequent kinetic equations.

Goetz and Marty used an unreacted core model for manganese chloride ammonia salt reactions (this is analogous to shrinking nucleus/core model) which models the evolution of the reaction through a grain of salt (Goetz and Marty, 1992). The composite sorbent is manganese chloride in graphite binder, and in developing the model they considered the medium as spherical grains within a pellet. The kinetic equation (12), is designed for spherical grains with spherical coordinates, and dN_g equates to change in number of moles of reactive gas per grain. The spherical coordinates are for the surface area of the reaction interface as the *unreacted-core* shrinks. An advancement is presented as X in equation (13) being related to the ratio of the reaction interface and the original grain radii; this relates to the reaction rate and is intrinsic to the energy balance.

The reactive medium was within a cylindrical reactor and the kinetic equation was then integrated into an energy balance with conductive heat in the radial direction (Goetz and Marty, 1992). The specific rate term is dictated by the K_a value and the components within parentheses, therefore the reaction rate is dictated by the thermodynamic conditions and the reacting interface which shrinks as the reaction proceeds. The model used by Lepinasse et al. is very similar utilising a reaction interface within a grain with the kinetics as shown in equation (14) (Lépinasse et al., 1994). They emphasised the importance of understanding the thermal behaviour, and utilise the same radial ratio of reactive surface as part of the reaction advancement. They modelled the transformation between 0.1 and 0.9 values of X typical of the extremes of transformation that would be realised in practical cycles.

$$\frac{dN_g}{dt} = 4\pi r_c^2 K_a \left[\frac{P - P_e(T)}{P_e(T)}\right] \tag{12}$$

$$X = 1 - \left(\frac{r_c}{r_g}\right)^3 \tag{13}$$

$$\frac{dN_g}{dt} = 4\pi r_c^2 K_a \left[\frac{P}{P_e(T)} - 1\right]^M \tag{14}$$

$$\frac{dN_g}{dt} = 4\pi r_c^2 K_r exp\left(-\frac{M_r}{RT_c}\right)\left(\frac{P_i - P_e(T_c)}{P_e(T_c)}\right) \quad (15)$$

Similar work by Lu et al. published just earlier, develops a phenomenological model that helps to further our understanding of some of the transport phenomena involved (Lu et al., 1996, Lu et al., 1997). The model evaluates a case where the rate limitation is both heat and mass transfer, and uses the kinetic rate equation (15); we can observe the similarity of form to discussed earlier in this section kinetic rate equations. The model is presented for a halide salt reacting with ammonia and considers the reactions at grain and pellet level in the form of a shrinking core reaction model. They compare a "simplified" and "general" model for their effectiveness (Lu et al., 1997). Their tests on pure salt shows cycles that occur over hours. The method is novel and shows some insight into the performance when mass transfer limitations need to be considered (Lu et al., 1996). Cycles of this duration are restricted to energy storage processes but much work has been done on ammonia-salt reactions in some form of graphite composite that overcome any issues with mass transfer and cycle quickly.

More recent work has looked at analogical models to predict the kinetics, An et al. evaluated the effectiveness of an exponential function, power function, and a linear model. They concluded that only the *linear* model is (relatively) reliable in predicting the kinetics (An et al., 2020b, An et al., 2020a). The form of this model is similar to that presented by Mazet discussed earlier in this section. Adsorption is shown in equation (16) and desorption in equation (17).

$$\frac{dX}{dt} = k_s\left(1 - \frac{P_{eq}}{P_c}\right)(1 - X)^m \quad (16)$$

$$\frac{dX}{dt} = -k_d\left(\frac{P_{eq}}{P_c} - 1\right)X^m \quad (17)$$

They used the equations to predict the behaviour of a manganese chloride and expanded natural graphite composite, reacting with ammonia. A plot is

presented showing results between ± 20% deviation (An et al., 2020a). Furthermore, even within these large bounds, they show that the constants vary between the different tests, i.e. they are not true constants. The challenge when interpreting is that they did not publish simulation results from the model; if the enthalpy of reaction is calculated from results from the Rubotherm magnetic balance, this could be the source of some of the error.

2.5 Resorption Experiments from Literature

In the literature, there are a number of resorption test machines that have been built. The effectiveness of the machines has been mixed; the earlier experiments appear to be more successful. Research in the 21st century has tended to be driven by novelty rather than results, these tests tend to have little consideration into key design parameters such as thickness of composite and optimisation of design; typically, a cylinder with a central gas channel packed into an arbitrary vessel. Often this is just placed in a thermostatic bath rather than a heat exchanger (style reactor). The choice of external heating (in this way or otherwise) is not practical when we consider the ratio of thermal masses to active mass and the effects this would have on the COP or power density of the generators; this is perhaps why many papers appear to neglect the thermal masses of the heat transfer fluid. This means results have acceptable appearing values for COP, but this startling omission perhaps explains why systems have not developed to prototype yet.

One of the first papers published where they test a resorption refrigeration machine is by Lépinasse et al. (Lépinasse et al., 1994). They used graphite (35% w/w) mixed with barium chloride and manganese chloride, the material had a relatively low conductivity of 8 W/mK. The composite was tested in a Seteram DSC, the results were used to model the reaction as consumption over a grain (of salt). A ‘catalytic type’ reactor was used to test the resorption beds; this is essentially a shell and tube heat exchanger, with

baffles in the shell and the reactive material hosted in the tubes. The COP was calculated accounting for the thermal masses and with a degree of transformation between 0.1 and 0.9 (of stoichiometric adsorbed mass of ammonia). The COP result was 0.33, but it appears this value was not calculated from dynamic data, it was an estimate calculated using the heat of reactions without much detail given. It is a shame the COP was not calculated using dynamic data as this would be a valuable observation, furthermore, the theoretical value presented could have been calculated without constructing the machine. Limited results are published and no data on thermal masses, so the real COP cannot be determined (Lépinasse et al., 1994).

Goetz et al. followed on from this work (the two papers have each other as co-authors and a different third co-author); they modelled and tested another resorption machine for chilling (Goetz et al., 1997). This time reactors are used with thermal fluid in a shell, hosting a cylinder of composite material with a central gas channel. They note that their tests are '…focussed on cooling at low pressure and not defined for automatic cycling', the system is modelled using work in a previous paper (Goetz and Marty, 1992), and experimental data is compared to the model. The data was again obtained using a microcalorimeter, and interestingly barium chloride shows hysteresis but nickel chloride does not. Their model is complex but seems to have some limits. For example, the fluid temperature is calculated as a mean of the in versus out, and the wall temperature is assumed the same as the fluid temperature due to turbulence in the fluid. If heat transfer to the composite is at a level suitable for a machine, (i.e., for a case with a reasonable COP or SCP,) then there would be a difference in wall and fluid temperature during dynamic conditions. The main finding was that when the reactions occur at stable pressures (at point of heat delivery) the mass flow of ammonia produced in the low temperature bed during decomposition is consumed by the high temperature bed in synthesis. They then challenge the hypothesis that, if conversion in one bed is equal to in

the other, then the ratio of heat transfer over heat of reaction should be equal. They then show that the ratio is actually 1.2 times higher in the high temperature reactor, concluding that the heat transfer and grain kinetics are coupled and greatly decrease the cooling power at low temperatures. This point appears to be an important conclusion and it is a shame it is not described in more detail, as it alludes to limits on the operation, but it could just point to the importance of heat transfer on the rate of reaction (Goetz et al., 1997). No value is given for COP but that was seemingly not the purpose of the test, rather to evaluate the operation at limiting conditions to extend application.

Following this Lépinasse et al. develop a cooling storage device which used resorption (Lépinasse et al., 2001). This arrangement used lead chloride and manganese chloride to chill an insulated box. The device would have to be removed to regenerate at a higher temperature, so it is not designed for cycling. The system has a relatively low SCP, and no COP is reported. The intent is to perhaps define and prove a new application. The resorption chiller can keep the box cool for 3 hours (Lépinasse et al., 2001). They describe the application of a relief valve to the system can reduce the rate of the cycle. The valve operation is not detailed and the reduced reaction rate just ensures a longer cycle time with reduced cooling power. Generally speaking, the system just seems to counter heat flow into the box rather than actively having a cooling effect, and the device would need to be removed to recharge so the application is perhaps less effective than a simple phase change material (cold block). Lead chloride is also incredibly toxic, so the application for chilling food may not be suitable.

Vasiliev et al. built a resorption heat pump (Vasiliev et al., 2004). This system made use of active carbon fibre ‘busofit’ to host the salt and form the composite. Disks of ‘busofit’ are cut in cog shapes, but the actual production method is not explained. The concept was to reduce the thermal mass as the ‘busofit’ is a sorbent and this can enhance the system COP ‘close to 90% of [the] theoretical limit’. Barium chloride and nickel chloride were used for the

resorption heat pump. The ‘busofit’ disks were placed between fins, and heat was provided internally with the disks placed over a central tube. The heat transfer fluid entered a head space, before flowing down a central tube and then returning counter flow through an annulus (internal radius being the central tube) with the outer surface in contact with the active material. The des

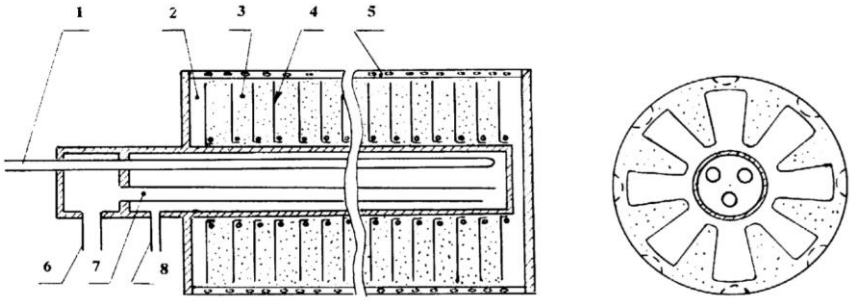

Figure 4 Resorption reactor sorbent bed, from Vasiliev et al., numbered labels: 1—water heat exchanger; 2—ammonia vapor distribution volume; 3—sorbent bed; 4—fin; 5—reactor envelope; 6––water vapor entrance (to the thermosyphon condenser); 7—heat pipe vapor channel; 8—heat pipe liquid exit. (Vasiliev et al., 2004)

A COP calculation was performed without using dynamic data presenting a value of 1.2, in their conclusion it is described as near 1.2 which raises some questions. The system is designed to operate as a high temperature heat pump, raising 120-130 °C from a 200 °C heat source, with extensive cycle times at around 2 hours. A four-bed system is proposed, but it does not appear to actually have been built. It is suggested this arrangement would raise the COP, and a speculative value is presented between 1.4-1.5 due to heat and mass recovery, the basis of this calculation is not presented (Vasiliev et al., 2004). It is a shame that this is the case, an effective high temperature heat pump at a COP of 1.2 could find a place in the market, certainly a COP of 1.3 would be attractive. The thermal masses of their system would appear to be very large, particularly with their heat transfer arrangement, perhaps the trade off in their reasonable predicted COP is quelled by a very low power density due to the massive cycle times. This pairing of salts should be evaluated in more detail for this application, with the intention of producing more reliable data.

A resorption transformer was built by van der Pal et al (Van der Pal et al., 2009). The transformer utilised lithium chloride and magnesium chloride impregnated in metal foam. The impregnated metal foam was supported by fins and placed in the shell of a two-pass tube-side heat exchanger. The results are very interesting from an operational perspective, the high temperature bed seems to operate at a fairly consistent upper temperature throughout every stage of the cycle, straying from the HTS equilibrium line. This may be due to the fact this is driven by the low temperature bed and there is extensive hysteresis for synthesis and decomposition. The lift appears good but a middle temperature is not met for both reactors, so perhaps not a full cycle or a different form of operation is shown. The system needs more explanation and they highlight some shortcomings: such as with a high temperature lift the COP tends to zero; and in the tests they performed the salt cycles only around 40% of the ammonia which is very low. The cycle times can be seen to have been slow and the material has a conductivity of 0.5 W/mK which is very low and could hinder the performance, they also recorded the process as limited by the rate of heat transfer. They did note however, that the system had stable performance over 100 cycles (Van der Pal et al., 2009).

The baton of resorption appears to pass to Shanghai after this. Wang et al. built a resorption heat transformer utilising calcium chloride and manganese chloride (Wang et al., 2010). They considered a very simple system and the effect of ‘valve control’ or ‘closed protocol’ using a valve which meant the system was left to pressurise before the valve was opened, kick-starting the reaction in the other bed. They recorded COP values of around 0.2, and did not account for thermal masses as their simple experiment had the beds submerged in thermostatic baths.

Li et al. built a more advanced refrigeration resorption test cell (Li et al., 2010). The salts used were barium chloride and manganese chloride in expanded graphite, but with little detail of the production process. This was packed inside a flanged reactor to form a hollow cylinder with a central gas

channel, with fluid flowing through the shell. Actual test data is published, but the COP is not calculated from dynamic results. The authors make some relevant statements about how the theoretical COP of an adsorption heat pump is lower than a resorption heat pump; therefore, design of a resorption heat pump is extremely important as the sensible heating effects can limit the performance. It is very disappointing that this is not explored in their work as that is the problem to be addressed, and previous work has already shown theoretical effectiveness. The conclusions are therefore rather disappointing as the practical work does not align with addressing the propositions. They also noted that the SCP may be affected by slower reaction rates that may occur in resorption machines at low pressure during the useful cooling phase which is key to evaluate and potentially resolve (Li et al., 2010).

More work from Shanghai considers different pairs for a resorption refrigerator, by Bao et al (Bao et al., 2011). Manganese chloride was used as a high temperature salt and barium chloride; sodium bromide; and ammonium chloride were evaluated for their performance as the low temperature salt. The test cell was a reactor filled with compressed blocks of ENG that were soaked in salt in solution and then dried. The blocks were quite tall, no diameter is presented but from the diagram they appear thick, with heights of 124; 96; 88; and 147 mm for ammonium chloride, sodium bromide, barium chloride and manganese chloride respectively. The reactors were placed in thermostatic baths. The cycles appeared to take more than an hour, with high pressure and low pressure periods taking 30 and 50 minutes respectively. The authors calculate COPs for the machine but neglected the thermal mass of fluid; this gives a more positive picture than the reality, with values of 0.3/0.31 depending on low temperature salt (Bao et al., 2011). The problem to address is the ratios of the thermal masses and to have a system that cycles enough material quickly to have a high COP and SCP. The relatively poor COPs in this system (even with neglected thermal masses of fluids) show the process was actually very hindered. The

arrangement presented by Bao et al. has a high material to metal ratio and so should have a much higher COP, adjustments to the design to enhance SCP would only drop the COP further unless thermal resistance and material conductivity is improved (Bao et al., 2011). Bao et al. furthered their work by applying the resorption concept to cold storage and long distance refrigeration (Bao et al., 2012). Their experimental set up was quite similar, with some modification for their test purpose. The COP calculation again neglected thermal mass of the fluid and presents values of 0.3. What is interesting to observe is how their -1000/T versus ln(pressure) plots for dynamic data show incredible divergence from the equilibrium lines for the high temperature salt which is not explained and is particularly curious. A questionable conclusion was made, “The experimental results also indicated that if one intends to maximize the SCP instead of the COP, the cooling period should be no longer than 20–30 min” this is true as they evidence this conclusion by citing the work by Goetz et al. which has a much higher SCP. However, this does not get to the crux of the matter, there is a superficial trade off with COP, but improved heat transfer means a large mass of reactant can cycle quickly; meaning a design with a high COP can have a high SCP.

Xu et al. followed with a similar system design of cylinders of manganese chloride and ammonium chloride with gas channels. The connected reactors were again placed in thermostatic baths. They attempted to use the heat and cold produced simultaneously. The system has cycle times of six hours. The COP values calculated neglect the thermal mass of the heat transfer fluid presenting values from 0.27-0.35. One conclusion presented is the chiller COP performance could be upgraded by using the heat to simultaneously drive a silica gel-water chiller to give a COP of 0.82 (Xu et al., 2011). The calculation to get to this value is not presented and the initial COP is an overestimate so it needs to be considered with caution. Jiang et al. used another packed cylinder of material, but this system has a proper heat exchanger design with fluid in the shell. They considered manganese

chloride, calcium chloride and ammonium chloride in a composite 14 mm thick. COP calculations are performed again without thermal masses with yet lower values for the COP at 0.25-0.27, some isobar plots are given but the data is slightly confusing (Jiang et al., 2016).

There are a number of examples of resorption systems being built, but the more contemporary work has failed to learn from the work in the '90s or build from their successes. There are clear and simple steps to be made in enhancing performance to bring the technology towards a prototype. However, what is noted is that there are no publications which document the thermal masses of the fluids (as well as shell and composite) that utilise dynamic data to calculate the COP of a system. A clear omission is data values for masses (and volumes) for readers of the papers, the failure to report thermal masses is thoroughly discussed by (Gluesenkamp et al., 2020). Another observation is that power density measurements of systems have seemed to be relatively poor; cycle times of beds have been relatively long which has in some cases improved the COP results, but this is at the detriment of the SCP or SMP. Earlier research has highlighted the need to focus on bed design as heat transfer is key to optimal performance, so work really needs to be done to enhance conductivity of the composite and improve heat transfer from the composite to the shell wall and to the fluid. There is a lot of scope to develop resorption and the work in the '90s still shows promise for the technology while current research highlights the appeal of resorption transformers; there is definitive scope to design resorption generators with optimised design enhancing heat transfer to provide a useful power density with a reasonable COP. An effective design at 3 kW scale could show the efficacy of the technology and incremental future gains would provide a marketable product. If a resorption transformer can be built with good performance (similar to the temperature lifts shown in **Figure 3** with a COP of around 0.4), this would be attractive for the same reasons as the existing absorption systems and the simplicity,

smaller footprint, and cheap manufacture cost would open new markets, making this a lucrative and disruptive technology.

3 Testing Methodology

As concluded in section, **2.4.1 Testing Methods from Literature**, the best method for testing is that of the Large Temperature Jump (LTJ) method. This method was realised by Dawoud and Aristov for the testing of the dynamics of water sorption (Dawoud and Aristov, 2003), which was developed further into a methodology by Aristov et al., in later work (Aristov et al., 2008). In their test-rig, the reactor consisted of a heated reactor, with a plate on which sorbent grains sit and exchange heat with the jacket of the reactor. The results enable the users to initiate the temperature jump and observe the sorption kinetics over a desorption or adsorption test. The system contains a vapour vessel which is temperature controlled and loaded to the correct pressure. The pressure transducers observe the pressure within the system, and enable the amount of adsorbed or desorbed water to be determined (Dawoud and Aristov, 2003). The simplicity of this experimental test is what makes it so effective compared to gravimetric or calorimetric tests.

Ammonia-salt systems operate at higher pressures than hydrate systems. The aim when designing an LTJ system is to mimic a heat exchanger design that is similar to a full-sized sorption system. This would ensure the system produced reliable data, with performance that could be expected at scale. Veselovskaya and Tokarev designed a large temperature test cell for a barium chloride–vermiculite composite (Veselovskaya and Tokarev, 2011), they designed it to evaluate the kinetic behaviour and it follows the design by Dawoud and Aristov. The reactor has a measuring cell which hosts grains of the sorbent, and this cell is heated by the jacket. The tests are effective and they observe the kinetics but the test cell is more of a container with loose grains within, and practical system would likely have the grains fixed in a heat exchanger, potentially between fins. Warwick has some experience

with large temperature jump testing particularly for carbon-ammonia systems. A test cell was developed and used to extract heat transfer parameters (Jegede and Critoph, 2016), this has been updated in design and used to validate sorbent performance for finned-tube adsorption generator design (Metcalf et al., 2021). The systems now test the carbon in the form expected for a machine; with the recent work testing like-for-like modular sections including fins. The carbon-ammonia LTJ, is simulated with a two-dimensional heat transfer model. Measured fluid temperature and flow rate were used to simulate temperatures and the process which is presented by Rivero-Pacho et al. (Rivero-Pacho et al., 2017). When considering the salt-ammonia reactions, the salt-ENG composite is anticipated to be conductive enough in the ENG to not need fins, as the results from van der Pal and Critoph showed (van der Pal and Critoph, 2017).

When considering testing the ammonia-salt reactions in an LTJ, it is clear particularly from work in the literature, that heat transfer is a key component. Therefore, a sensible approach in the testing is to rapidly heat and cool the composite in a small sample, so that (large) temperature gradients do not occur. In doing this, the objective is to extract equilibrium and reaction kinetics data, and to provide the opportunity to simply model the heat transfer and evaluate with empirical data. This therefore suggests a tube in tube heat exchanger design, with the external tube acting as a jacket. The aim was to measure the wall temperature or approximate it with a thermocouple against the surface. To explore a range of salts at different conditions it is essential to have a broad temperature range from 15-200 °C. This means the heat transfer fluid must be silicon oil, rather than water. The use of the oil which flows in a laminar fashion had a high heat transfer resistance from the wall, and also a large surface area in contact with the thermocouple (relative to thermocouple wall contact). Therefore, it quickly became important to consider the practicalities of accurately measuring the wall temperature.

3.1 Choosing Salts to Test

Of primary importance to the effectiveness of a resorption system is choosing the correct pairs of salts. The position of the isosteres will be important to the temperature lift, performance, and operating pressure. Optimal performance in a resorption system will come from paired salts with near parallel reaction isosteres. Much work has looked at (di)chloride salts in the past which have isosteres quasi-parallel in nature. If we consider the collation of chloride salt equilibrium lines by Neveu and Castaings, we can see that of these salts, barium chloride, calcium chloride and manganese chloride appear to react in a suitable temperature range (Neveu and Castaing, 1993). Goetz et al. also suggest these salts for a variant of the transformer process (Goetz et al., 1993). The most likely pairing is $CaCl_2$(8-4)-$MnCl_2$(6-2): the operating pressures and temperatures are in a suitable region, additionally van der Pal and Critoph have shown the applicability of calcium chloride and consider both calcium chloride reactions for use in a system (8-4) and (4-2) (van der Pal and Critoph, 2017), both isosteres are close together and react in the correct range, and this would increase the sorption capacity of the calcium chloride. In **Figure 5** the Clapeyron lines for calcium and manganese chloride can be seen with a single or double calcium chloride reaction. Another option presented by Goetz et al. is the pairing of $BaCl_2$(8-0)-$CaCl_2$(4-2). This operates at higher pressure which could prove beneficial, but the stoichiometry could lead to excessive thermal mass of calcium chloride due to the lower molar uptake of ammonia. The Clapeyron lines for this pair can be seen in **Figure 6.** Barium chloride also has a single reaction which desorbs all the ammonia, presenting a simple case to start testing and modelling.

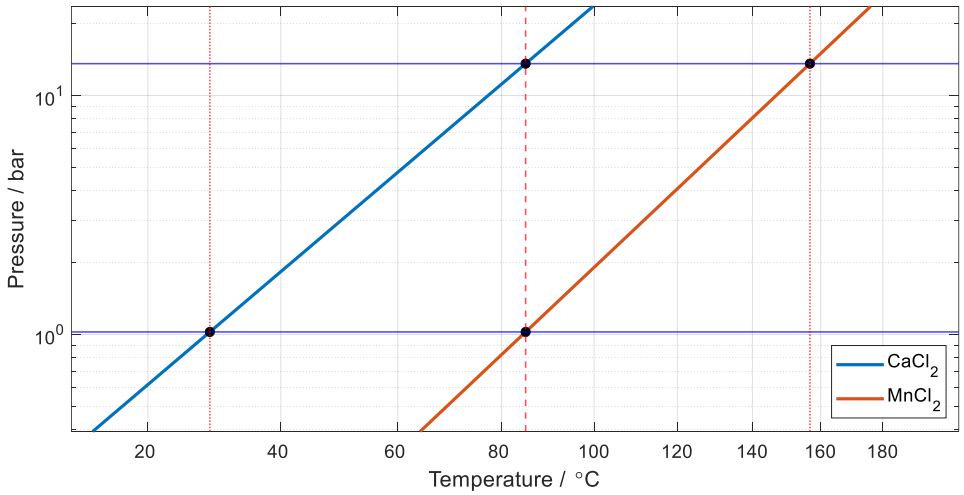

(a)

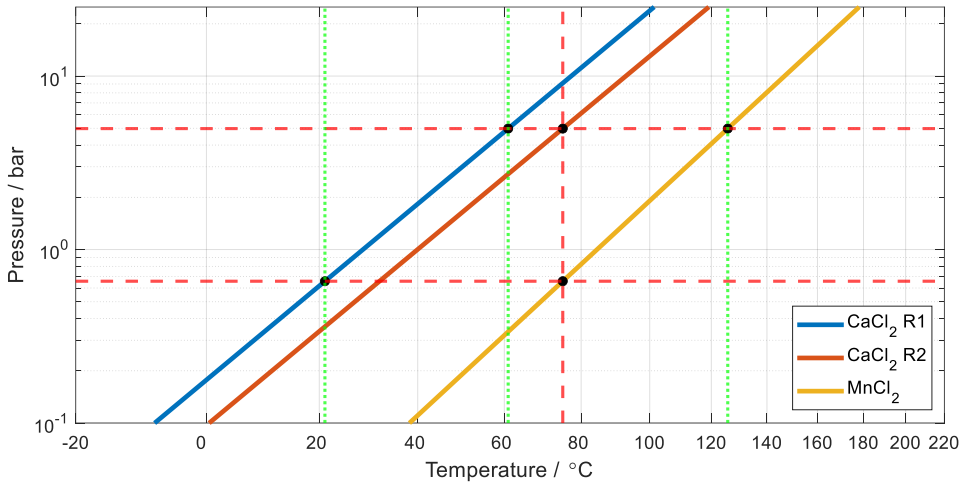

(b)

Figure 5 Resorption pairing Clausius-Clapeyron Diagram for pairs: (a) $CaCl_2$(8-4)-$MnCl_2$(6-2); (b) $CaCl_2$(8-4-2)-$MnCl_2$(6-2). Waste heat is provided at 85 °C and the lift and sink temperature can be seen by the vertical dotted lines. The isosteres are plotted for desorption obtained from the ITC, revisited later in this paper.

Understanding the working temperatures is essential to predict the COP of a resorption system using any of these pairs. To do this, single isosteres were plotted in **Figure 5** and **Figure 6** (isostere data identified later in this work has been used to plot **Figure 5** and **Figure 6**, as this is more exact than the quoted data in literature). The temperatures can be seen on the plots; the waste heat temperature is provided as the middle temperature, and the heat sink and recoverable heat as the lower and higher temperatures

respectively. To ensure a temperature difference, heat will be supplied to the reactor 10 °C above (the middle temperature), and recovered 10 °C below (the high and low temperatures). When this is considered, the temperatures are close to those presented by HITACHI shown in **Figure 3.**

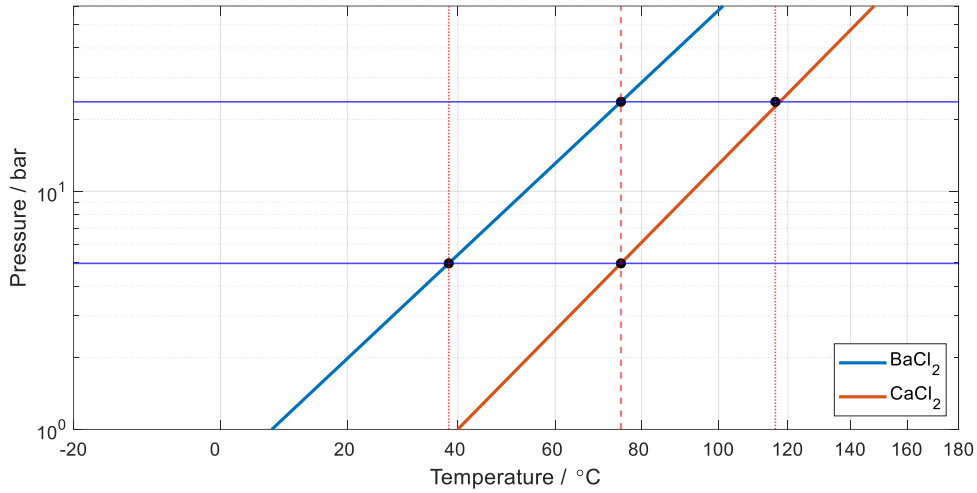

Figure 6 Clausius-Clapeyron Diagram for $BaCl_2$(8-0)-$CaCl_2$(4-2) Resorption Transformer. Waste heat is provided at 75 °C and the lift and sink temperature can be seen by the vertical blue dotted lines. The isosteres are plotted for desorption obtained from the ITC, revisited later in this paper.

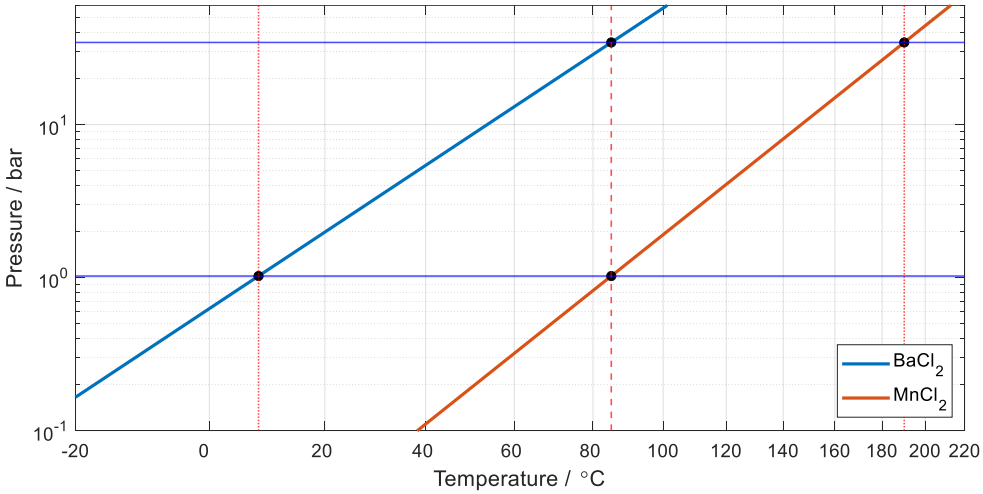

Figure 7 Clausius-Clapeyron Diagram for $BaCl_2$(8-0)-$MnCl_2$(6-2) Resorption Transformer. Waste heat is provided at 85 °C and the lift and sink temperature can be seen by the vertical blue dotted lines. The isosteres are plotted for desorption obtained from the ITC, revisited later in this paper. The high temperature is 190 °C. This pairing is unlikely but when comparing three salts this is the final combination so can easily be reviewed as perhaps a control pairing.

As three salts are being tested; the final paired combination—although not likely to be used—is $BaCl_2$(8-0)-$MnCl_2$(6-2), the temperatures are just out of range (particularly the lowest) but this combination can be easily considered, and may provide further incite or understanding about larger

temperature lifts; the Clapeyron plot for $BaCl_2$(8-0)-$MnCl_2$(6-2) can be seen in **Figure 7**.

The reversible ammonia-salt reaction equations for the three salts to test are as follows:

Barium chloride (0-8)

$$BaCl_2 + 8NH_3 \rightleftharpoons BaCl_2 \cdot (NH_3)_8 + \Delta H_{r,BaCl_2(0-8)}$$

Calcium Chloride (4-8)

$$CaCl_2 \cdot (NH_3)_4 + 4NH_3 \rightleftharpoons CaCl_2 \cdot (NH_3)_8 + \Delta H_{r,CaCl_2(4-8)}$$

Calcium Chloride (2-4)

$$CaCl_2 \cdot (NH_3)_2 + 2NH_3 \rightleftharpoons CaCl_2 \cdot (NH_3)_4 + \Delta H_{r,CaCl_2(2-4)}$$

Manganese Chloride (2-6)

$$MnCl_2 \cdot (NH_3)_2 + 4NH_3 \rightleftharpoons MnCl_2 \cdot (NH_3)_6 + \Delta H_{r,MnCl_2(2-6)}$$

The adsorption of ammonia in the salts (in whatever state) is an exothermic reaction and so there is a ΔH_r value for the heat of reaction for heat that is released, an equivalent heat is consumed by desorption (there is a negligible difference, this is explained further in the **section 4.1.3**). This reversible process is fundamental to the working of sorption systems. Throughout this thesis the reactions will be described as the species followed by the number of moles that change within brackets as above, to differentiate the reactions.

3.2 Composite Material Production

The reactive material was comprised of halide salts impregnated in a conductive matrix of expanded natural graphite (ENG). The challenges with using salts are the propensity for the material to agglomerate and the low conductivity of the material. As detailed in the **Literature Review section 2**., many approaches have been taken to address these, with composites using graphite flake, or ENG mixed with the salt. The best approach was taken by van der Pal and Critoph, using ENG sheet (van der Pal and Critoph, 2017).

The use of ENG sheet ensures the composite is able to exploit the high conductivity of layer of graphite in the plane, as this ensures the continuous structure of the material. This advantage can be lost when mixing flakes and salt. The ENG sheet is also very workable, easy to cut and can be prepared uniformly to requirements. The ENG has a conductivity of 26 W/mK in plane and a conductivity of 8 W/mK through plane (SGL Carbon, 2020). An important part of testing the salts is also to evaluate the uptake of salt, and then the potential mass of adsorbate.

The discs for each sample were cut from SGL Sigratherm board L10/1500, with a density of 1500 g/m^2. The board is 10 mm thick and was cut using a water jet cutter into disks of 10.8 mm to fit into half-inch stainless steel tubes (of 10.8 mm bore). Cutting with a hole saw was explored, but this gave a smooth finish, whereas the waterjet cutter has a rough finish that was preferable as visually it appeared to not obstruct pores. A 1 mm hole was drilled in the centre to receive a stainless-steel sheathed thermocouple. Larger samples (shell side, see section 3.3.3) were cut with an outer diameter of 34.5 mm on the waterjet cutter. The centre hole was then drilled with a custom hole saw that was made with a diameter of 11.9 mm to ensure a tight fit around a half inch tube.

Aqueous salt solutions (manganese chloride; calcium chloride; barium chloride) were prepared near to saturation at room temperature, on a hot plate stirrer with warming and agitation. It is worth noting that the solvation of anhydrous manganese chloride in water is very exothermic and can result in an oxide forming, observations of this are detailed in **Appendix 8.2.** Cut discs were dried and then weighed, they were then placed in containers and submerged in the salt solution, weighted down to prevent them floating. The containers with the submerged samples were then placed in a bell jar connected to a vacuum pump and evacuated. They were left under vacuum for twenty-four hours before removal and then dried in an oven at 200 °C for an hour to remove all moisture. They were dried at this temperature following guidance in lab material preparation books for the anhydrous form

(Armarego and Chai, 2009, Daintith, 2008). Once dried, the samples were then weighed again, before being placed in the reactor. The rig was then connected to a vacuum pump and evacuated for 2 hours while the reactor was heated to 60 °C. Time in the air is minimised to reduce any hygroscopic effect with moisture in the air.

The primary factor affecting salt uptake was the concentration of the solution, more so than other factors such as length of time evacuated. Potentially a higher concentration could be obtained by heating the solution—but to ensure the solution entered the pores of the ENG, it could not be left to cool down below saturation so that the salt could crystalise before entering the ENG. When the material was exposed to the vacuum, one could observe tiny bubbles leaving the ENG. There must be a minimum time required for the sample to be under a vacuum, but 24 hours provided confidence for the solution filling the pores. Future work could further examine production of the composite, considering an optimal method. The final salt uptakes can be seen in **Table 1 and**

Table 2.

Table 1 Salt preparation data, for tube side LTJ samples. This were constituted of 5 disks of 10.88 mm diameter, with a 1 mm central drilled hole, and a depth of 9.5 mm.

Salt	$MnCl_2$	$BaCl_2$	$BaCl_2$	$CaCl_2$
(Prepared with)	$MnCl_2 \bullet 4H_2O$	$BaCl_2 \bullet 2H_2O$	$BaCl_2 \bullet 2H_2O$	$CaCl_2 \bullet 2H_2O$
Weight Dry Salt (g)	0.791	0.586	0.655	0.656
Weight ENG (g)	0.651	0.639	0.649	0.900

Solution (g/100 ml)	150	43	36	36.75
Test index	TA	TB	TC	TD

Table 2 Salt preparation data, for shell side LTJ samples. These had an inner diameter of 12.7 mm. SC barium sample was a hexagon, the given diameter is a circle with equivalent surface area to (35 mm hexagon with 17.5 mm apothem)

Salt	$MnCl_2$	$BaCl_2$	$BaCl_2$	$CaCl_2$
(Prepared with)	$MnCl_2 \bullet 4H_2O$	$BaCl_2 \bullet 2H_2O$	$BaCl_2 \bullet 2H_2O$	$CaCl_2 \bullet 2H_2O$
Weight Dry Salt (g)	4.038	2.936	3.095	2.819
Weight ENG (g)	2.594	2.556	2.008	2.759
Solution (g/100 ml)	150	43	44.3	36.75
Number of Disks	2	2	2	2
Test index	SA	SB	SC	SD
Heat Transfer Fluid	Silicone Oil	Silicone Oil	Water	Silicone oil
Diameter of Disks	34.5	34.5	33.6 (32 hex)	34.5
Test Index	SA	SB	SC	SD

3.3 Experimental Test Rig Design

The initial large temperature jump (LTJ) design conceived was in the form of a 'jacketed reactor' or a simple double pipe heat exchanger as shown in **Figure 8**. The vessel was comprised of a one-inch stainless steel tube welded around a half-inch tube with cuffs to form a jacket. The first iteration had only one thermocouple fitting welded and can be seen in **Figure 9** (a) (compared to the final iteration (b)). The length of reactor, was nominally chosen to be oversized to ensure a uniform flow of oil through the jacket

(with negligible velocity variation around the circumference) delivering heat to the reactor contents. The intention was always to test a small amount of material (5 or 6 sample discs).

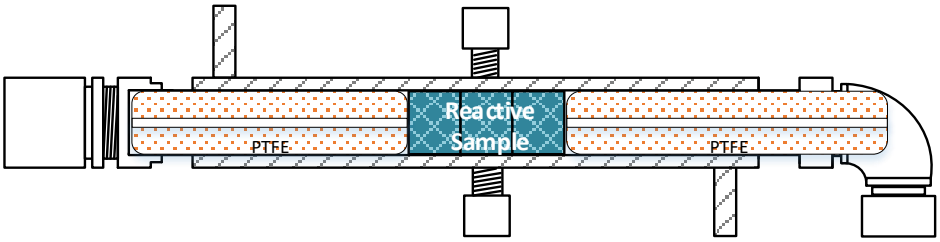

Figure 8 Early iteration of large temperature jump reactor design.

3.3.1 Improvements to the LTJ Rig

The downside of the long reactor (shown in **Figure 9** (a)) was that the large void volume caused heating up of the gas and this meant the pressure would not settle after a reaction, but continue to increase (or decrease) due to sensible heating of the gas. The initial design instrumentation was connected to an Omega data acquisition device (OMB-DAQ-2408-2AO) and a LabVIEW program was written and used to log the data. Another issue was caused by the Swagelok® connections on each end, these were standard ferrule sealed connectors (one end had a cap that was drilled and tapped), and they had to be tightened every time it was loaded. Tightening up each time to ensure a good seal further pinched the ferrule, this caused the pipe to deform and the inner diameter to reduced, affecting the ability to insert the samples (and subsequent PTFE slugs).

The thermocouples (TCs) measuring the wall temperature were initially inuslated K type (as were the others). It soon became clear that the wall thermocouple reading was nearer to the oil temperature than that of the wall. The biased temperature reading was produced due to the thermal resistance between the TC and the wall, as well as thermal conduction to the large surface area of the TC sheath in the oil (there is also significant heat transfer resistance between the oil and the tube). It also became clear that noise was an issue in the data sampling. The pressure transducer was connected to the mains, this put a voltage across the whole rig and thermocouples were not isolated from the rig, thus the signal interferred

with the readings on the DAQ device. Efforts to ground the signals and remove this were thwarted because the pressure transducer appeared to put a voltage across the whole board of the DAQ device, through its input. The pressure transducer was also sensitive to noise; it was able to pick up a signal induced on the electrical mains loop in the lab. This signal was transferring from the lab's earth loop through the earth pin on the Huber baths' power supply and inducing a voltage on the rig. The voltage induced (and the noise read) were caused by a flickering light in the lab which induced this voltage on the earth.

To overcome these issues:

- The Swagelok® was changed to O-ring face sealed Swagelok®. This made sure the experiment could be dismantled and put together at will, sealing on an O-ring rather than a ferrule.
- The void volume in the reactor was filled with PTFE which was drilled with a 1.2 mm central hole. This held the material in the centre of the reactor and filled the void volume but left a gas channel for ammonia to flow and hosted the sample measuring TC.
- Grounded TCs were installed in place of the K type for the wall measurement. By taking the opposite polarity connections from a pair of grounded TCs on opposite sides of the reactor, the TC junction becomes the reactor wall, rather than the welded tip. Thus, the voltage reading from the thermocouple pair provides an average wall temperature at diametrically opposed points of the pipe.
- The Omega DAQ device was switched to a NI CompactDAQ device (cDAQ-9178), this had isolated modules for temperature and pressure measurement. Grounded connections were then effective and prevented grounding loops or similar and noise was reduced to an acceptable level. The TC module was a NI 9214 TC module, with isothermal housing block to prevent cold junctions on the TCs. The pressure transducer was connected to NI 9220 Voltage module.
- The flickering light was also exchanged for an LED bulb.

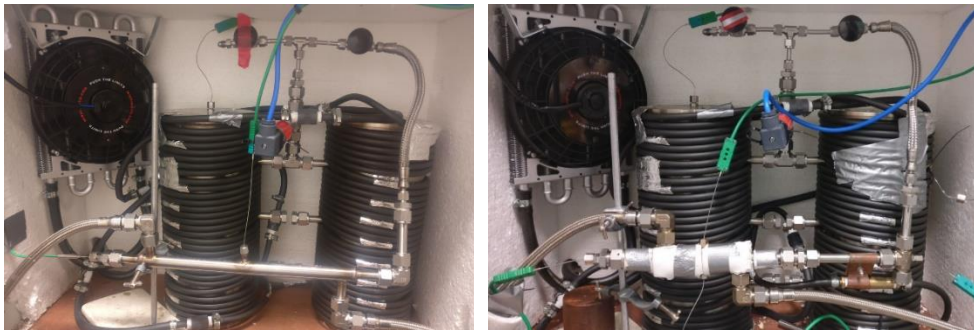

(a) (b)

Figure 9 LTJ reactor designs: (a) First iteration of LTJ rig, this had only one thermocouple measuring the wall; (b) The second iteration of LTJ rig, the reactor now wrapped in insulation. The pipework TC was also added to observe in case any odd behaviour could be explained with this.

The intial and final LTJ tube-side reactors can be seen in **Figure 9**. The final design was reached as described, with the result that a few samples could fit and the heat transfer could be modelled simply in one (radial) dimension.

3.3.2 Final LTJ Design

The final LTJ reactor design can be seen in **Figure 11**, compared to the initial design. The reactor comprised of 15 cm of half-inch tube surrounded by 12cm of three-quarter inch tube. Cuffs were welded to each end form a shell, and machines bosses welded which were tapped and host Spectite fittings that seal the grounded TCs. The full test rig PFD (not based on final reactor) can be seen in **Figure 10**. The reactor was fed thermal fluid, *silicone oil*, from two Huber™ baths. The baths are connected to a valve array which was controlled by an electric switch; one bath would be isolated (and circulating round a dead loop) while the other fed the reactor. Switching would cause the bath feeding the reactor to instantaneously switch and cause the temperature to rapidly jump.

During the temperature jump the reaction conditions are monitored with the following instrumentation: The LTJ wall (heat transfer area between the salt and the fluid) TIT L1 & TIT L4 used K type grounded thermocouples; the centre of the sample TIT L2, gas temperature in connected pipework TIT L3, temperature of gas within expansion vessels TIT E1, temperature of expansion vessel wall TIT E2 were K type insulated thermocouples; and the pressure of the system PIT 01 was a Danfoss AKS 32 pressure transmitter.

The pressure transmitter was successfully checked for accuracy with a deadweight pressure tester, and results of this can be seen in **appendix 8.5**. The sampling frequency rate was set to 1 Hz.

The valves were pneumatic valves with solenoid actuators, connected to the laboratory 8 bar gas supply and the electric signal was from a power bank, delivered by a household light-switch. An integral bonnet needle valve was used to isolate the rig and the expansion vessels, enabling gradual opening to not cause damage to materials. Another was used to seal the rig and enable gradual filling or emptying (particularly after pressure testing with argon). This would routinely become obstructed and became a repeat offender when leaking was observed so a quarter turn ball valve was used to isolate and seal the entire rig. In preparation for testing the rig was evacuated for 2 hours with a vacuum pump, and then loaded to a set ammonia pressure in the expansion vessels. The LTJ reactor was isolated so that the mass of ammonia in the system could be calculated before any adsorption occurred. Each sample was run through a number of tests at different nominal pressures, typically from 8 bar dropping incrementally to 0.5 bar. During each pressure change the cell was isolated, so the pressure was dropped in just the expansion vessels. This meant the new total mass of ammonia in the system could be derived. In operation, the baths were set to temperatures away from the phase change, based on the data presented by Neveu and Castaing (Neveu and Castaing, 1993), and stepped across to pinpoint the conditions at which the reaction occurs.

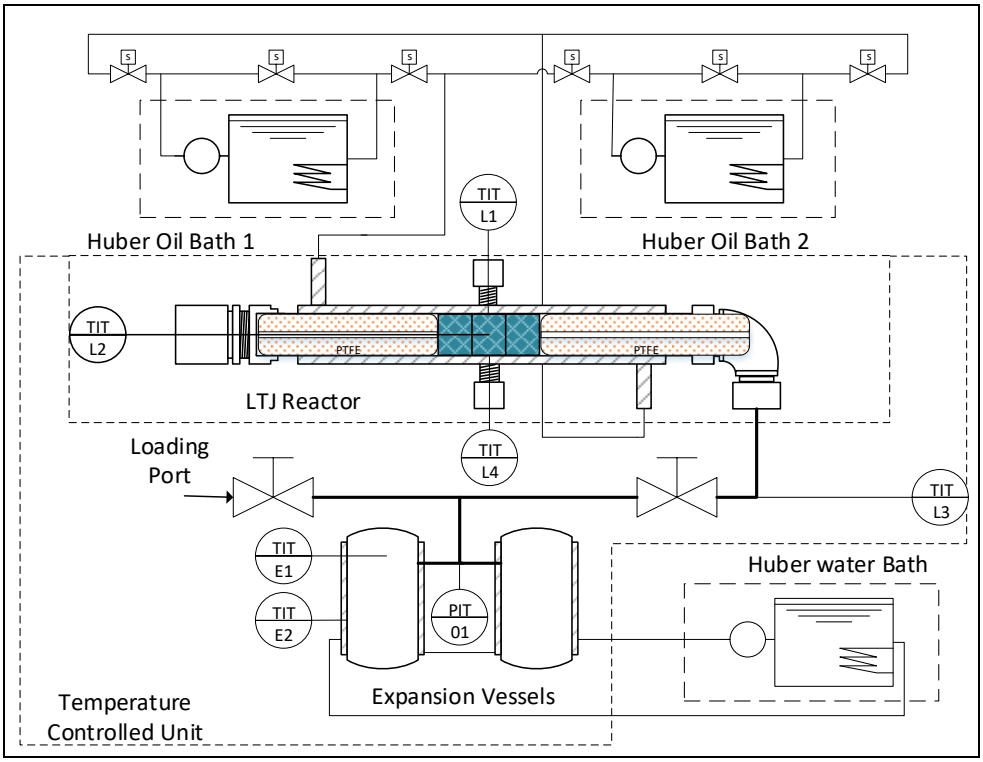

Figure 10 Process flow diagram of entire LTJ rig.

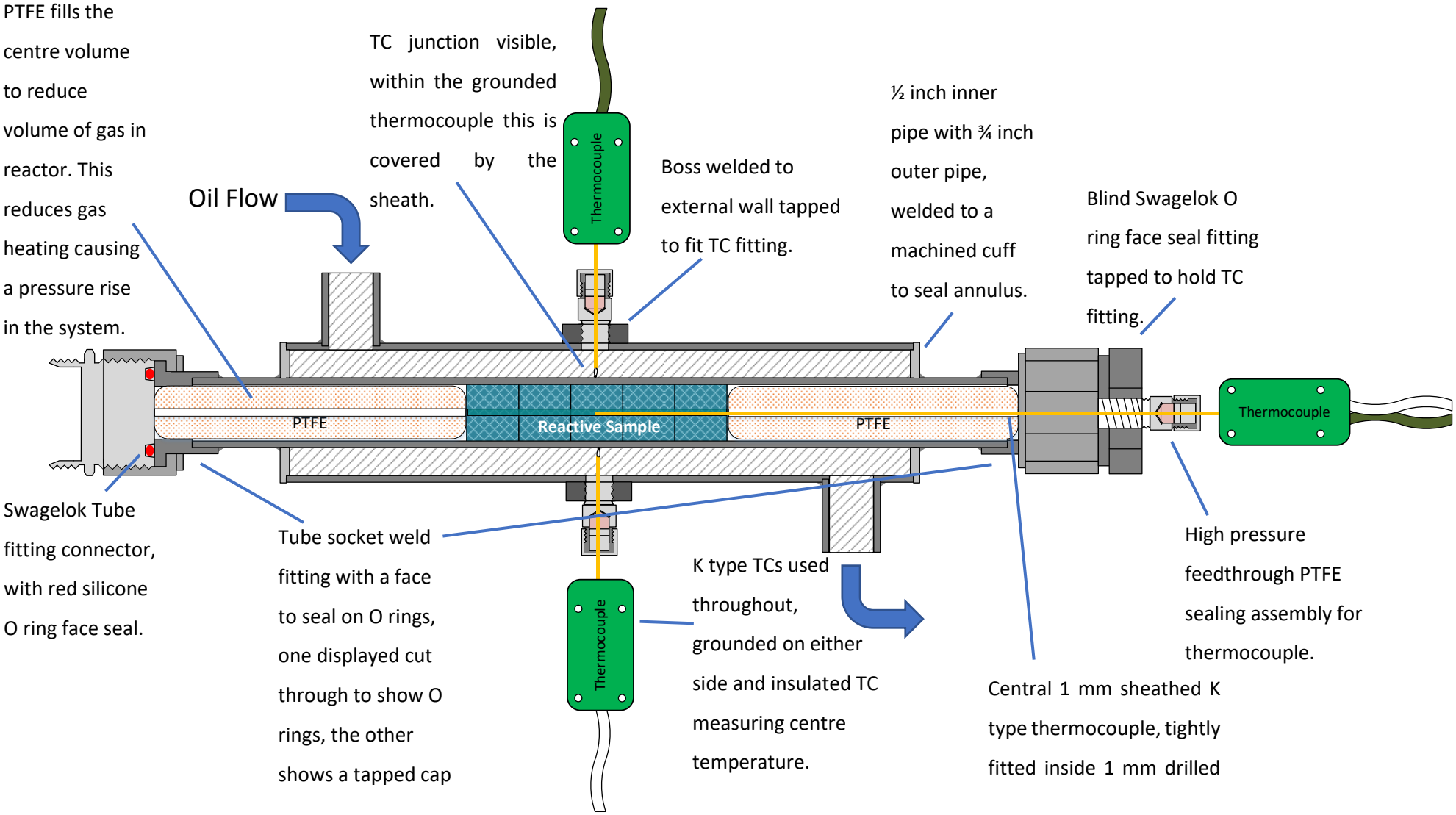

Figure 11 Diagram of final LTJ with samples in the tube, note alternative terminals from thermocouples measuring wall temperature.

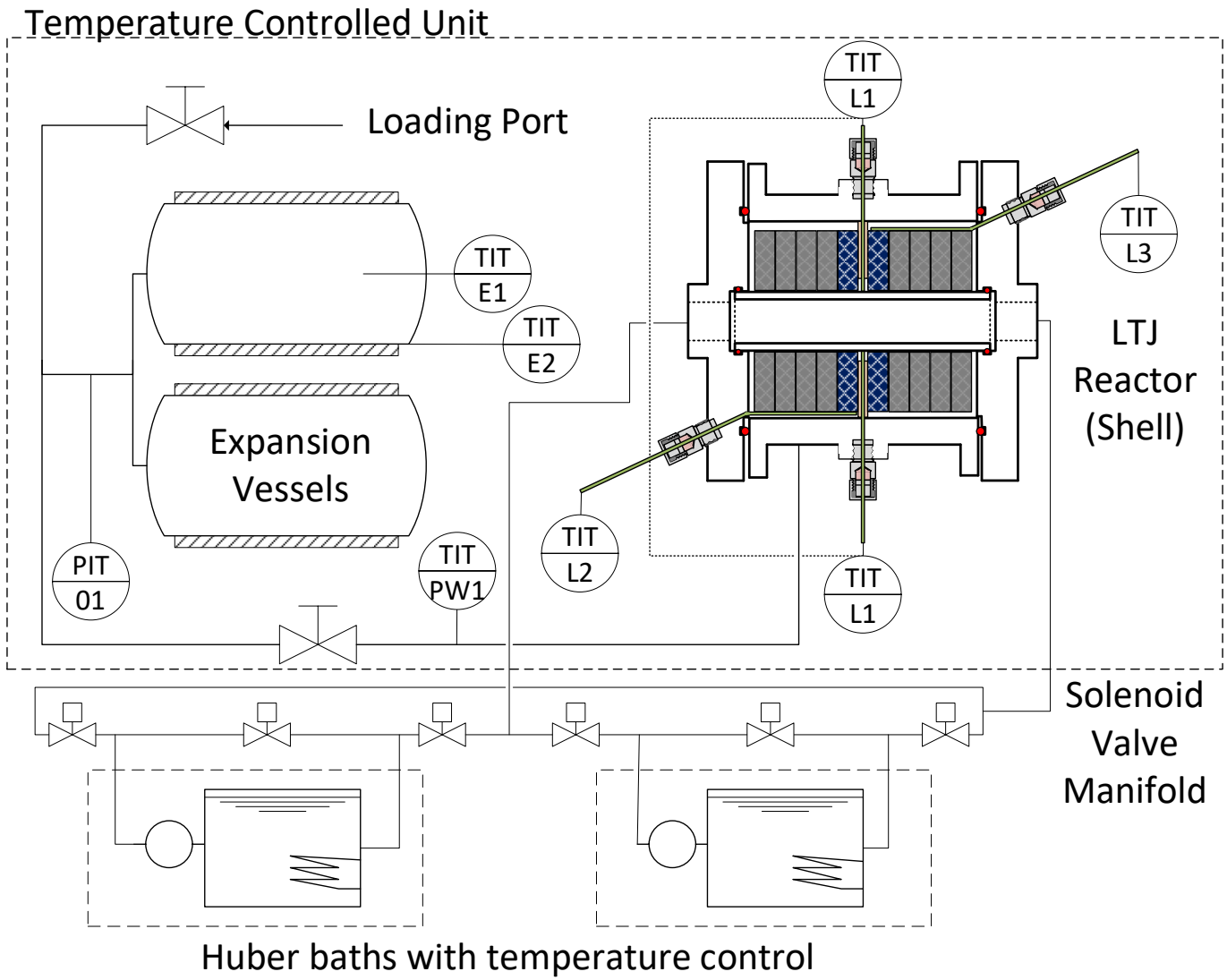

Figure 12 Process Flow Diagram of LTJ Test Rig with shell-side LTJ reactor. The active samples are shown in blue; these are held in place by expanded natural graphite disks that have no salt in, which appear grey in the diagram.

3.3.3 Shell-side LTJ for Further Testing

To further evaluate the model, a reactor that hosts the sorbent material in the shell (of a shell and tube heat exchanger) was designed, as shown in **Figure 12, Figure 14 & Figure 15**. This is installed in place of the previous tube side LTJ reactor, as **Figure 12** shows. The reactor was designed to enable tests on samples of a size expected in a full-scale machine, with some flexibility so that once a size was chosen, it could be evaluated before committing to final design.

Figure 13 Grounded thermocouple contact with central pipe; a sample can be seen underneath.

The shell-side reactor is formed of a central stainless-steel tube, through which the silicone oil flows (rather than the external annulus of the tube side reactor) and has an aluminium shell. The reactive samples fit tightly around the stainless-steel tube and the samples are isolated from the shell with a gas gap to reduce heat transfer. A two-millimetre ring of thermoplastic PEEK, (which was not in contact with the central tube as seen in **Figure 13**,) was used to direct the central thermocouples radial to the oil flow, allowing a

measurement of the wall temperature. The guiding holes in the PEEK ring were drilled at a slight angle to encourage the thermocouples to bend to create a spring force, ensuring contact on the pipe as shown in **Figure 13**. This was necessary as again, grounded thermocouples using opposite polarities were used to produce the '*wall*' or tube temperature. It was much more difficult in this case to ensure good contact, as the thermocouple was within the reactor rather than external. This meant that once it was loaded, little could be done to adjust contact due to risk of causing a leak. In **Figure 14** it can be seen that ENG discs without salt were used to hold the sample in place and align the thermocouples. A previous iteration used PEEK cylinders with a gap to isolate from the central pipe, but the thermoplastic provided too much thermal mass and the thermocouple readings were less reliable. A diagram and results of a test can be seen in **Appendix 8.3**, which presents the barium results in the shell. The results in **Appendix 8.3** shows the thermocouples inserted axially—measuring the outside of the sample—can be observed to drift from expected readings whilst the pressure rise in the system still provided a reasonable basis for measuring the rate of reaction and was predicted accurately by the model.

Similar to the previous design, grounded thermocouples were used in contact with the centre pipe to provide a temperature reading of the pipe wall. Sheathed thermocouples were fed through the tapped flange and aligned using the blank ENG to provide a temperature reading on the outer surface of the samples. The machined flanges and shell were sealed with silicone rubber O-rings (indicated in red in **Figure 14**). A tapered Swagelok fitting in the shell (seen in **Figure 15** on the right side) connects the reactor to the expansion vessels.

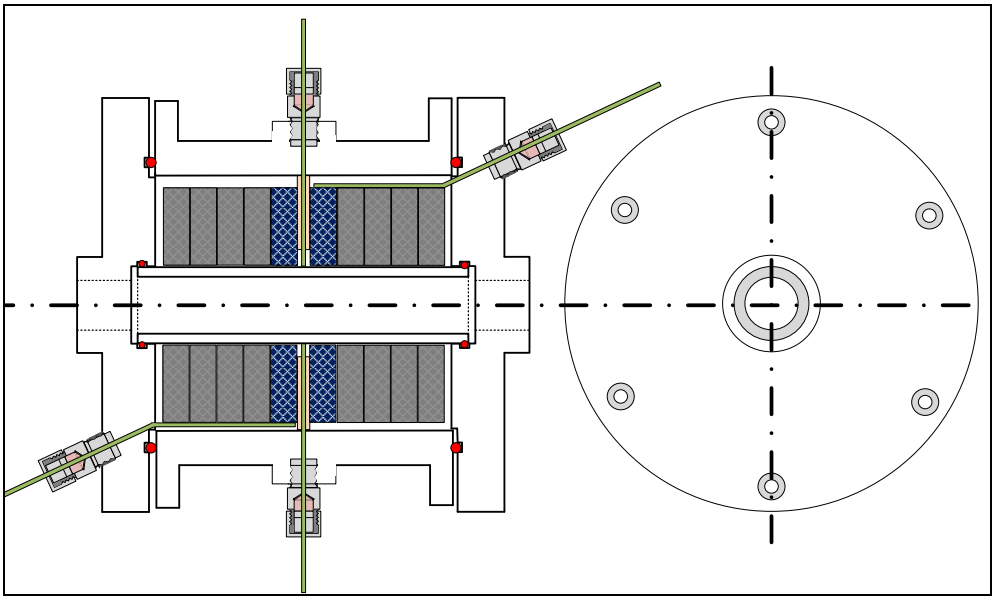

Figure 14 Shell-side reactor design section. Positions of thermocouples can be seen in green. Red circles show O-rings in section. A port connecting the reactor to the pipework as in ***Figure 15*** *is perpendicular to the radial TC tapped fittings and cannot be seen in this diagram.*

Figure 15 Shell side reactor. The main shell is manufactured from a single piece of aluminium machined down to include bosses to mount TC fittings and a BSP fitting to connect to expansion vessels. The two flanges also made from the same piece of aluminium, the top and bottom are tapped with BSP Swagelok elbow connection and gasket seal. The end of the shell is sealed with large silicone O rings and the ½" central tube is sealed with two silicone O rings.

3.3.4 Instrumentation Error

Some attention was taken to consider error in results. Generally, error in signal outputs was not a concern, as most reported results utilised rates of change rather than exact values (such as ITC results). To provide confidence in the assertion that error was no issue, some tests were done. The

thermocouple error is most likely to come from the cold junction where the TCs are connected to the DAQ device; to reduce any effect from fluctuations in room temperature an isothermal terminal block was used with the DAQ NI module. To further evaluate the error, the thermocouples were placed in a vacuum insulated vessel with hot water, their temperature readings were monitored as the water cooled over a period of around an hour. This was used to calculate a standard deviation in the readings. The quoted typical value of error (not the maximum value) from the NI 9214-module specification sheet, at high resolution sampling at 100 °C and 0 °C is +/- 0.37 °C and 0.36 °C respectively. The measured deviation was well within this value. See **Appendix 8.4** for further details. The pressure transducer (Danfoss AKS 32) was checked for accuracy using a deadweight pressure tester. The device error is quoted at 0.8 %. The deadweight test results showed the mean of the absolute deviation from the absolute pressure value was 0.17 % and ignoring the first value in the test was at 0.13 %. Details can be seen in **Appendix 8.5**.

The potential for error of ± 0.0104 bar at the high-pressure end of testing (8 bar) is insignificant. Particularly because the reported values were using rates of change of dynamic results, ensuring the error is trivial. The isosteres observed for the onset of reaction were obtained from fixed data points and used an average value to improve accuracy.

3.4 Measuring the Heat of Reaction

The equilibrium is commonly described by the Clapeyron relationship. Ideally there is a single equilibrium line that relates the pressure and temperature of the reaction, whether adsorption or desorption. The well-known relationship is given by:

$$ln(p) = \frac{\Delta s}{R} - \frac{\Delta h}{RT} \tag{18}$$

Where Δs is the change in entropy J/kg K, Δh is the enthalpy of reaction in J/kg, T is temperature in Kelvin and R is the gas constant in J/kg K.

Measurement of the line experimentally is normally used to determine the heat of reaction via the slope. However, salt-ammonia reactions in real applications and with realistic reaction speeds exhibit hysteresis with adsorption and desorption at the same pressure being up to 10 or more degrees apart. The position of the separate adsorption and desorption lines can be measured experimentally in LTJ tests as described in **Section 4 Experimental Results**. A complication is that in general the two lines do not have the same slope. In this case the slope cannot in any case be used to calculate reaction heats since equation 18 assumes the process to be reversible and hysteresis is of course irreversible.

If a cycle consists of a) isobaric heating from the adsorption line (fully adsorbed) to the desorption line (fully desorbed), followed by b) isobaric cooling back to the original state is considered, Critoph proposed that (Hinmers et al., 2022):

$$\Delta h_{ads} - \Delta h_{des} = \Delta T_{HYS}(c_{v\,ads} - c_{v\,GAS}) \tag{19}$$

where the term on the left is the difference between the adsorption and desorption enthalpy changes and the term on the right is the difference in the sensible heat of the gaseous and adsorbed ammonia phases when changing in temperature by ΔT_{HYS} the temperature difference between the desorption and adsorption lines at that pressure. If typical values for the salts under consideration are inserted Δh_{ads} and Δh_{des} differ by only as much as one part in a thousand and so for practical purposes the terms can be considered equal.

Any enthalpy values recorded from the onset of reaction were very different, therefore, it was necessary to find a unified value for Δh. The concept was to employ very slow heating rates, ensuring a large pressure and temperature swing up and down the isostere without completing the reaction. To perform this isosteric process, the shell-side reactor was utilised with many samples and the expansion volumes were disconnected from the rig. The shell reactor was heated by setting one of the Huber baths to ramp

up and down in cycles in excess of 8 hours. This methodology is described as a Isosteric Temperature Change (ITC). The approach was taken as it resembles the testing performed by van der Pal and Critoph (van der Pal and Critoph, 2017); they found they could step up and down the equilibrium of calcium chloride in a large reactor (where there was a large pressure swing), the approach taken here did not leave the process to reach equilibrium, but the results showed reduced hysteresis with negligible difference in gradient between adsorption and desorption. A process flow diagram that illustrates the simplicity of the ITC can be seen in **Figure 16**.

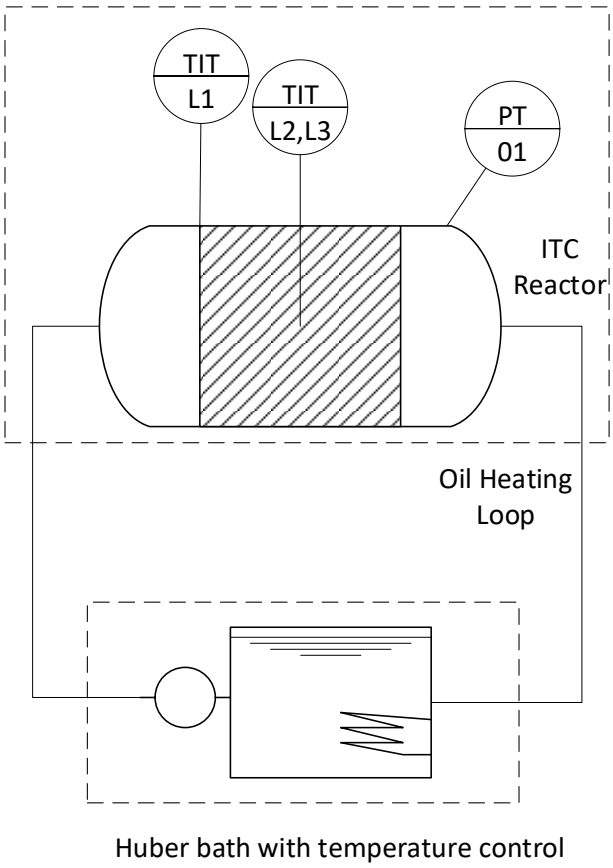

Figure 16 Diagram showing a representation of the ITC experiment.

4 Experimental Results

During an LTJ cycle the adsorption or desorption reaction was initiated by switching the temperature controlled- baths circulating silicone oil through the reactor. Once the pressure had stabilised, the baths were switched again so the reverse reaction could proceed. The LTJ is designed with a relatively

large expansion volume, so the reaction occurs near isothermally while the pressure steadily rises by a fraction of a bar. The nature of an LTJ experiment mimics the reaction behaviour in a resorption machine. A complete barium chloride cycle can be seen in **Figure 17.** The temperatures and pressure are plotted against time, with the pressure scale on the right-hand y axis. The baths are switched at around 5 seconds causing the temperature to jump; this initiates desorption and the pressure rises linearly as the reaction progresses. The reverse effect for adsorption can be seen at 250 seconds. A calcium chloride cycle with two phase changes can be seen in **Figure 18**.

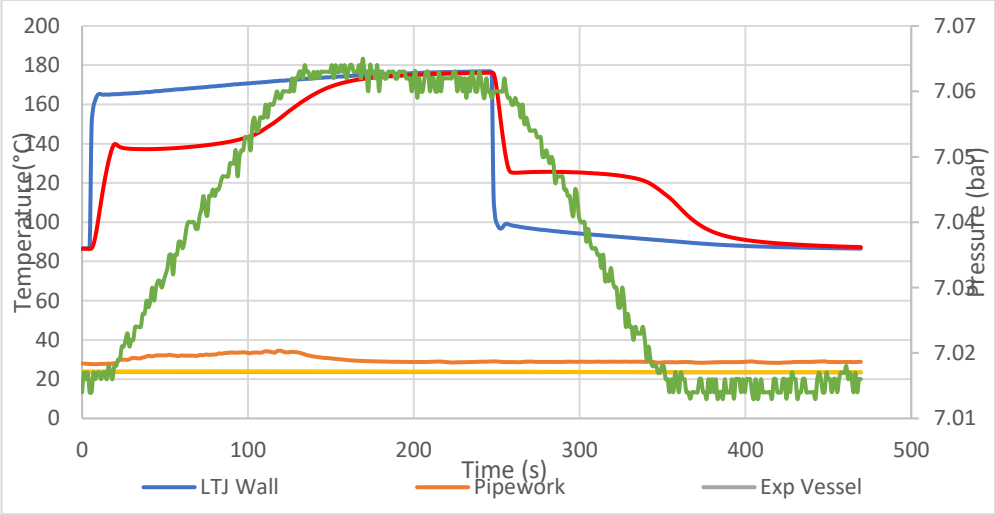

Figure 17 LTJ tube-side cycle of manganese chloride (test d), desorption followed by adsorption. Pressure on the right-hand scale. The legend values are as follows: LTJ wall is TIT L1; Pipework is TIT PW1; Exp Vessel is Expansion volume TIT E2; Expansion Vessel wall is the expansion vessel wall reading TIT E1; ENG is the temperature of the centre of the sample or surface TIT L2 (and in the shell, also TIT L3).

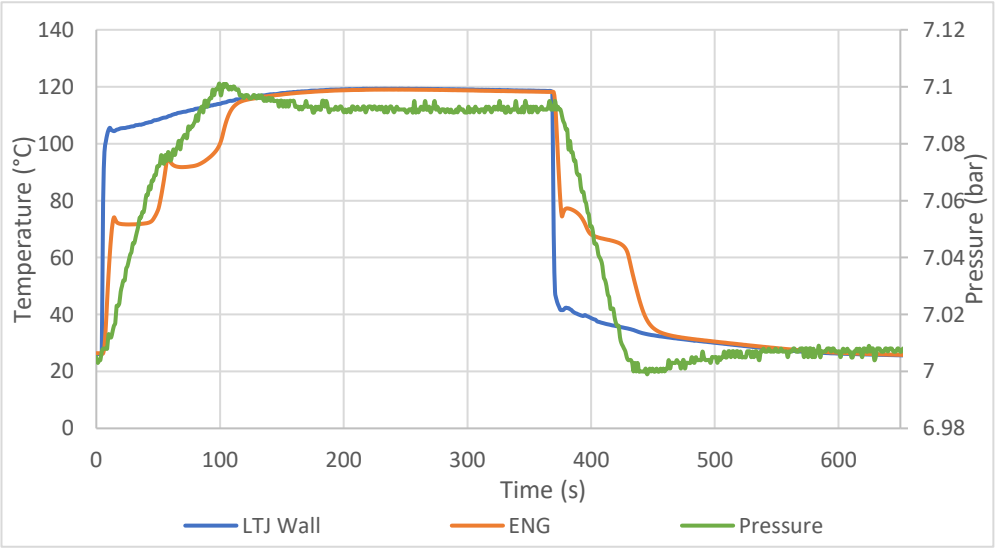

Figure 18 Calcium chloride LTJ result at around 7 bar, the ammoniate phase changes can be seen: first 8-4 and then 4-2; 2-4 and 4-8 reactions follow after around 370 seconds. ENG denotes the salt-ENG composite.

4.1 Equilibrium Data Results

To be able to develop an accurate model it was important to predict the point at which the reaction occurs. If incorrect isosteres were used for this, it would affect the results. The prime reason is because the driving temperature and rate of heat transfer is key to the process. An incorrect equilibrium line would cause the reaction to initiate at the wrong conditions, this could reduce the delta T driving force of the reaction and produce a poor prediction of the reaction rate.

One of the first observations in the new LTJ was of a superheating effect discussed in the **section 4.1.1.** The effect shows the salt exceeding the temperature at which the reaction occurs, before returning to it and reacting isothermally. This effect is not described in the literature and illustrates the value of the LTJ versus gravimetric methods which do not measure the sample temperature; a gravimetric test would produce results that suggest the reaction initiates at the peak, which would present even further hysteresis. The effectiveness of the LTJ is discussed further in **section 6.** The relationship between pressure and temperature at the equilibrium change are described by the Clapeyron relationship, the values for the enthalpy and entropy are derived from the isothermal reaction conditions after the metastate.

4.1.1 Observation of a Metastate in LTJ results

During the cycle, the temperature reading of the sample tracks the reactor wall temperature until the phase change conditions are met. Rather than the process temperature reaching a stationary point at onset of reaction, a metastable superheated state occurs. The temperature briefly exceeds the equilibrium conditions, before reducing when the reaction initiates. This is similar to behaviour observed in phase change materials and it is hypothesised a similar effect, where initiation requires more energy to cause

the crystalline lattice structure to reform. Once these conditions are overcome the phase change proceeds as expected. The superheat behaviour can be observed in the cycle plot in **Figure 17** (it can also be seen in **Figure 18**). The metastable state is visible on the red plot (ENG) as the local maximum at around 20 seconds for the desorption reaction and similarly a local minimum can be observed around 260 seconds for the adsorption reaction. After this peak, the temperature reading returns rapidly to an isothermal reaction temperature, which appears to be the true reaction conditions. The reactions should always proceed provided the initial peak is overcome.

4.1.2 The Clapeyron Relationships for the Onset of Reactions

The reversible reactions between ammonia and salts are monovariant equilibrium reactions; this means that the changes in equilibrium conditions can be described by the Clapeyron relationship. The Clapeyron relationship—equation (18)—describes the equilibrium pressure as a function of the temperature T, enthalpy Δh (not the real heat of reaction), the entropy Δs, and the universal gas constant R. Extensive testing was carried out in the LTJ reactor, to observe the conditions at which the reactions occurred. Tests were performed at different pressures between 8 and 0.5 bar. Cycles were performed a number of times so that at each pressure condition there were different scales of temperature jump and a variety of cases. To obtain each data point at the conditions the reaction occurs, the mean of 5 consecutive data points was used, from a single temperature jump. These were taken just after the metastate during the isothermal reaction. For the different conditions and each different test, the obtained average data points were plotted on the scale $-1/T$ and $\ln(p)$ to form a correlation. This can be seen in **Figure 19**. A line of best fit using the excel tool was then applied, and from this line the Clapeyron relationship terms were derived. As described in **section 3.4** the reactions observe hysteresis between adsorption and desorption, therefore different values were recorded for each.

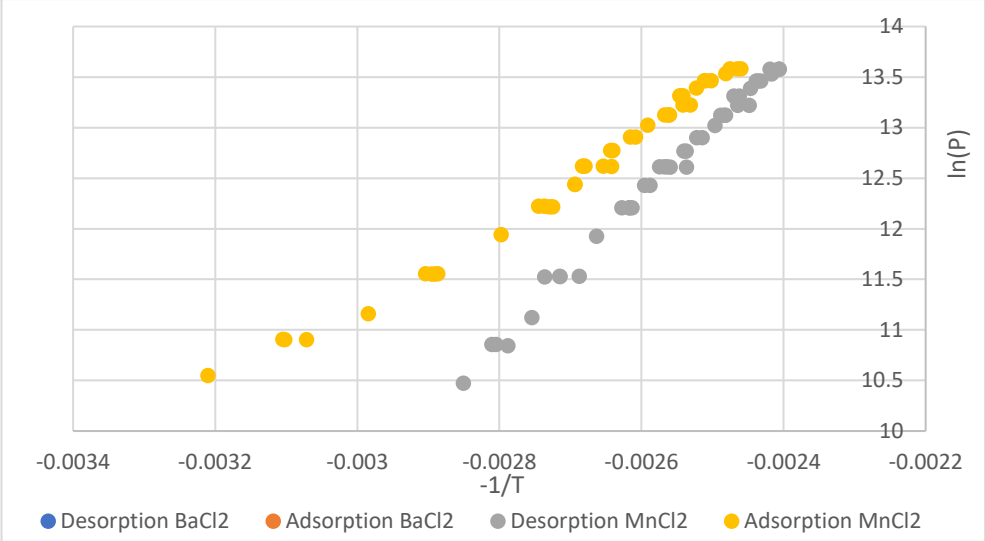

Figure 19 Data points for the reaction isosteres.

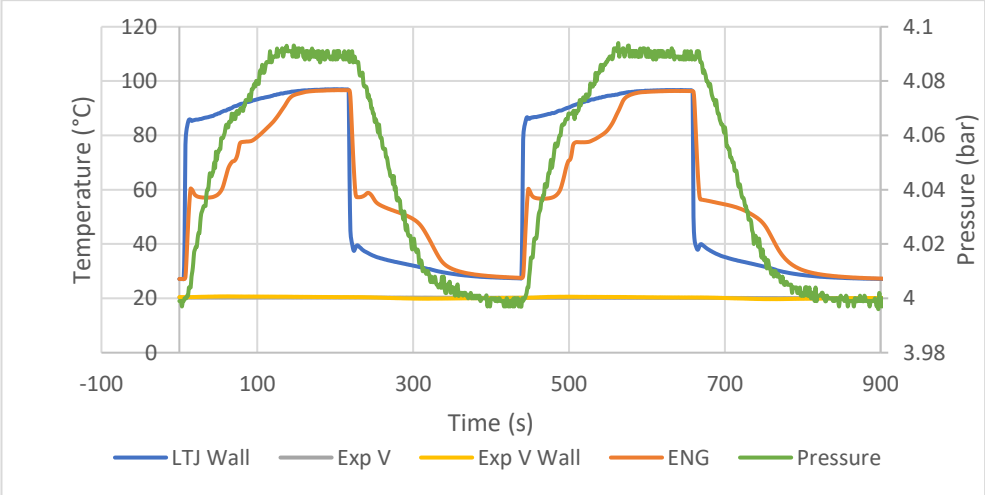

Figure 20 Calcium chloride LTJ result at around 4 bar. In adsorption, the first cycle shows the subcooling effect and the returning to the phase change temperature of the 8-4 reaction, the second cycle under the same conditions appears not to show sub-cooling and a single phase change is observed.

Calcium chloride has two reaction isosteres within a reasonable temperature range. These can be seen over a single temperature jump with a large ΔT as shown in Figure 18. In some cases, a single adsorption reaction (that spans both phase changes) can be seen as shown in **Figure 20**. The temperature difference appears to be enough that the conditions are in place for both reactions to occur, this is particularly amplified as the hysteresis can be seen to bring the equilibrium lines very close at the lower conditions. At all pressures it was possible to study each phase change independently by controlling the temperatures to include only one reaction.

The single reaction data points are plotted in **Figure 21**.Error! Reference source not found. as 'Adsorption 2-8*'.

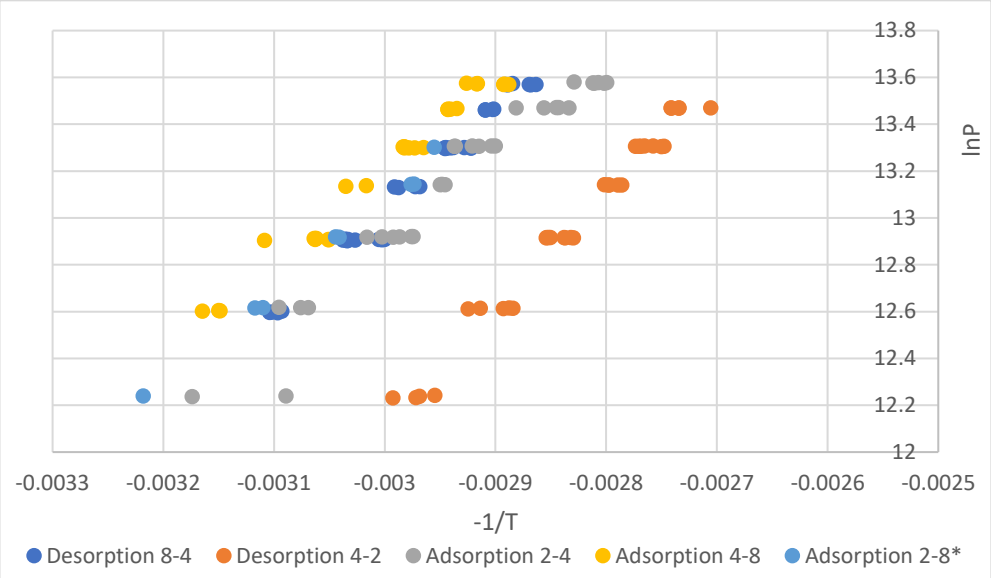

Figure 21 Data points for reaction isosteres for calcium chloride phase changes.

The resultant ΔH and ΔS values from the data in **Figure 19** and **Figure 21** can be seen in **Table 3.** The 8-2 data points are ignored, if it does occur it is an interesting phenomena; perhaps larger salt grains are completing the first reaction whilst smaller grains have completed and are in the process of the second. This cannot be monitored by the TC reading, and the uniform nature of the discretised nodes in the program would miss it too. The nature of the process is not so important in this case though, in practice the driving temperature would just ensure the second reaction occurred, and actual temperature is not so important.

Table 3 Measured values for the Clapeyron relation for the onset of adsorption and desorption reactions. ΔH terms are not the heat of reaction.

Salt	$BaCl_2$	$CaCl_2$		$MnCl_2$
NH_3 mole change	8-0	8-4	4-2	6-2
$\Delta H_{desorption}$ (kJ/kmol)	48924.790	36365.790	41202.320	58196.253
$\Delta H_{adsorption}$ (kJ/kmol)	37360.200	32844.620	31699.720	36611.107
$\Delta S_{desorption}$ (kJ/kmol K)	263.993	217.432	224.432	253.641
$\Delta S_{adsorption}$ (kJ/kmol K)	229.454	208.302	202.390	202.865

The Clapeyron relationships from the data in **Table 3** is plotted in **Figure 22**. These provide an accurate estimate for the conditions at which the onset of reactions occur. The plots are taken against those found in the appendix from Neveu and Castaings who collated a number of results (Neveu and Castaing, 1993), these formed the basis of much work since and have been referenced by many of the publications mentioned in the literature review. Work that does not use their data usually takes gravimetric data which as has been stated, is inaccurate.

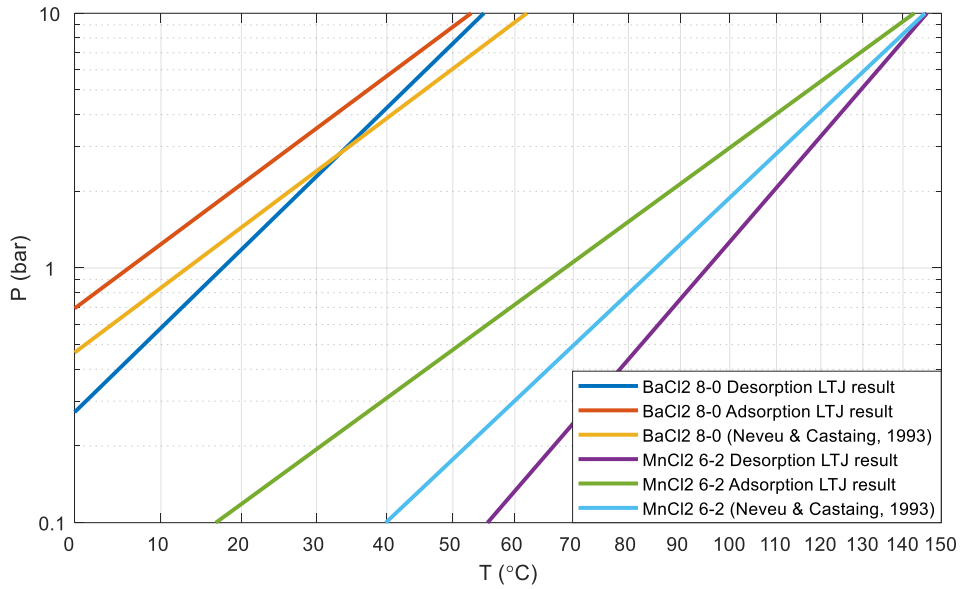

(a)

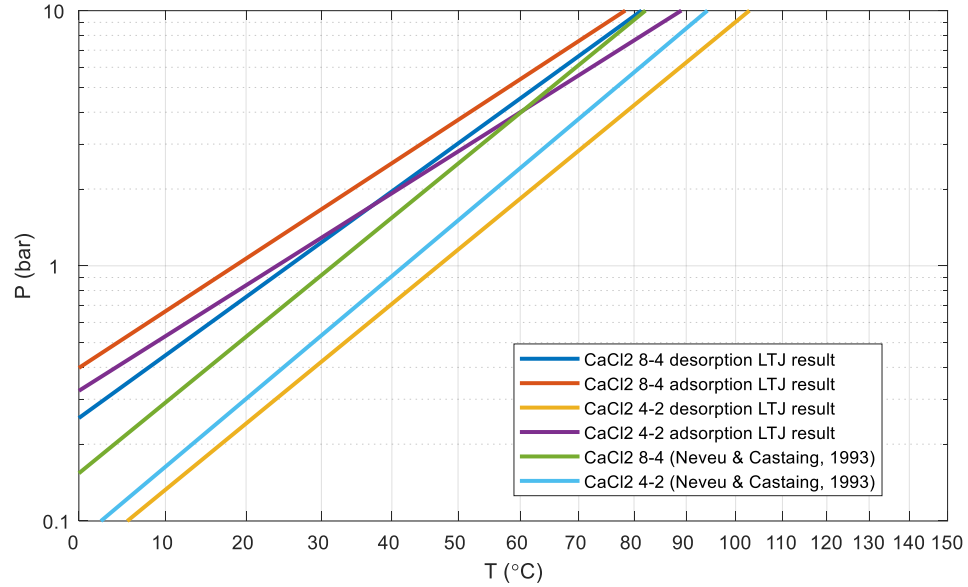

(b)

Figure 22 Clapeyron plots of experimentally observed equilibrium lines (for the onset of reactions) versus results from literature (Neveu and Castaing, 1993): (a) barium chloride (8-0), and manganese chloride (6-2); (b) calcium chloride (8-4), and (4-2).

4.1.3 Obtaining an Accurate Heat of Reaction (ITC Results)

As detailed in **section 3.4**, the data in **Table 3** does not provide a heat of reaction as there must be a unified value for adsorption and desorption. To find this the ITC testing method was realised, using slow temperature cycles and large pressure swings to climb up and down the isostere. The idea is the slower rate of reaction and the reduced volume produce large pressure swings across the temperature, tracking much closer to the isostere and not finishing the reaction. The concept of the ITC does not leave things to reach

equilibrium, but by reacting slowly, the results track the isostere well enough that adsorption and desorption produce (quasi) parallel lines. If this was not the case, behaviour may have been observed to indicate the true line or influence steps forward. Fortunately, the results gave a good approximation, the envelope of the cycle was reduced to between the previous reaction lines—and typically the lines were quasi parallel. This gave a good approximation for the true isostere and thus a unified heat of reaction was derived. An example of the results testing manganese chloride can be seen in **Figure 23**, together with the steps towards deriving the enthalpy. The process was not fool-proof, and there were challenges with obtaining the calcium chloride 4-2 reaction. Reaction times in this case had to be made so slow that diurnal effects were noticed or minute leaks in the rig; over many tests, periods of stability were observed. These lines appeared to be close to parallel in both adsorption and desorption, so to obtain a value the average of all values was used — which should reduce any error. What provided further confidence in this result is that for the other three salts, when the construction ITC lines were plotted — the gradients from these lines enabled the derivation of the reaction heats — against the lines reported by Neveu and Castaing, they all appeared parallel.

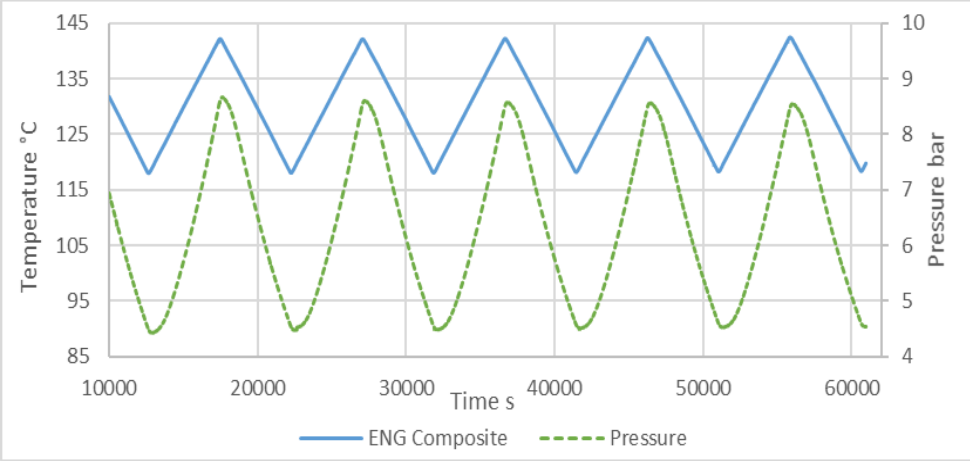

(a)

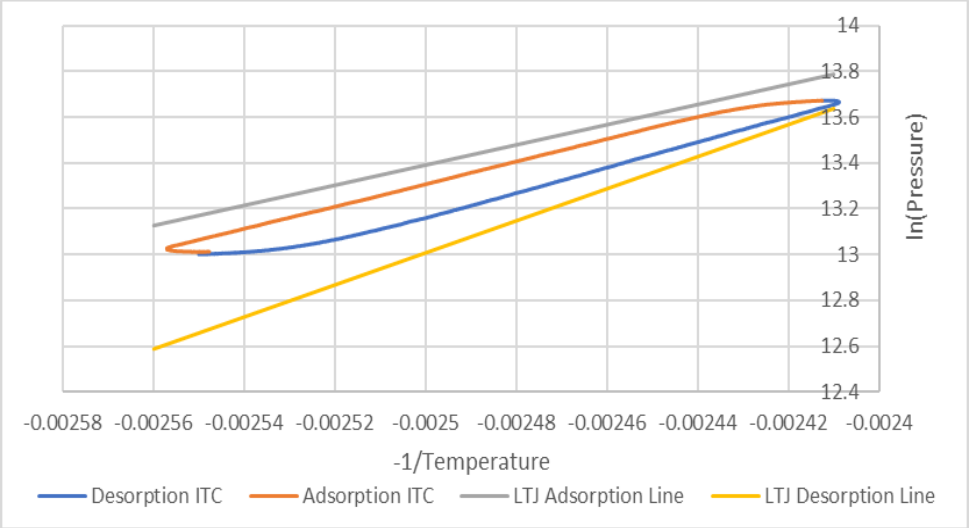

(b)

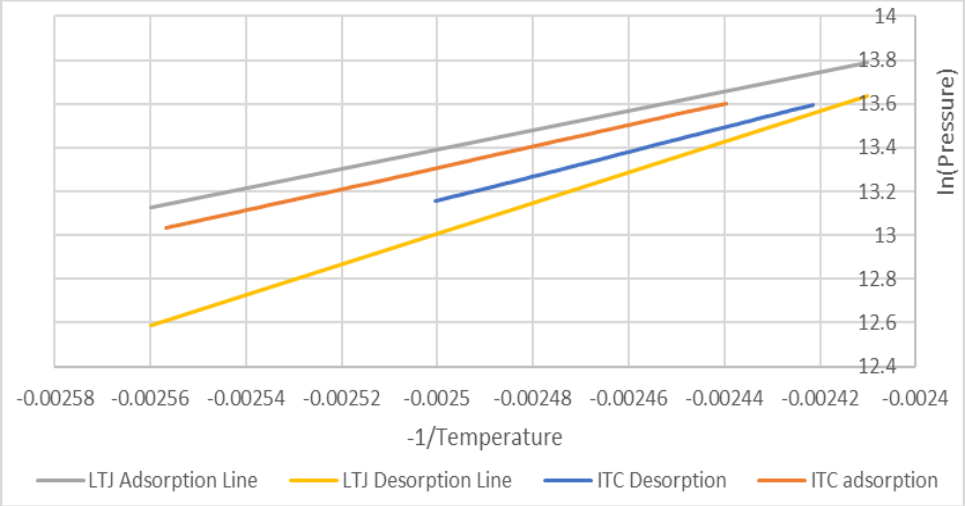

(c)

Figure 23 ITC test results: (a), raw data showing the repeating cycles plotted over time; (b), plotting the natural log of pressure versus temperature of part of the cycle, it can be seen between the reaction onset isosteres, illustrating the reduced hysteresis; (c), straight sections of the line, the average gradient of the two is then used to derive a value for the enthalpy.

As it can be seen **Figure 23** the ITC data falls within the previously obtained lines for the onset of reaction, and the lines are near to parallel providing a more accurate estimate for the heat of reaction ΔH_{REACT}. ITC plots from both of calcium chloride's isosteres and the single manganese chloride isostere can be seen in **Appendix 8.6.**

Table 4 Heat of reaction values for salts, obtained from ITC.

Salt	$BaCl_2$	$CaCl_2$		$MnCl_2$
NH_3 mole change	8-0	8-4	4-2	6-2
Heat of Reaction ΔH_{REACT} (kJ/kmol)	40745	42080	39948	42523

4.2 Modelling Dynamic Data and Results

With an accurate value for the heat of reaction, and isosteres to predict the onset of reaction, it was now possible to simulate the reaction data from the LTJ. This was done using the derived model presented in **Appendix 8.1**. The model was derived by Professor Critoph, who then wrote a MATLAB® programme to use for simulation. I took the programme and adapted it, and then used it to identify the key parameters.

4.3 Simulation Methodology

In order to characterise the salt-ENG reaction behaviour, a finite difference model has been developed. To match the geometry in the tube and shell side reactor, the model is based on a cylindrical structure in which the composite ENG with its impregnated salt is either externally heated or cooled within a tube (tube-side), or internally heated from a central tube (shell-side). Any number of radial nodes can be used but only one axial node. Conduction heat transfer is assumed between elements, and the heat transfer between the tube wall and the adjoining node is simulated by the resistance of a static 'gap' layer of gaseous ammonia between the two. For each time step the heat fluxes into and out of each element are calculated; this is ultimately what drives the adsorption or desorption. An estimated pressure rise is assumed for the time step which must be iterated to arrive at the final value. Chemical reaction rate equations are used to determine

the masses of ammoniated complexes changing from one state to another using the assumed pressure rise and current progression of the reactions taking place. This enables the temperature changes in the nodes to be calculated using an energy balance. It is then possible to calculate the total mass of ammonia (gaseous or adsorbed) in the system. This must of course be constant, and the estimated pressure rise is varied (using the MATLAB® fzero function) until this is between prescribed limits.

The modelling assumptions are as follows:

(i) Ammonia acted as a perfect gas

(ii) Gas is desorbed at the temperature of the salt

(iii) Heat transfer occurs only in the radial direction within the reactor (1 dimensional model)

(iv) The process is adiabatic, apart from the heat flow to and from the tube/wall in the reactor

To ensure the assumption that ammonia behaved as an ideal gas, the ideal gas constant was compared to a value for ammonia calculated from a polynomial at a number of conditions to prove the error relating to this was low.

Table 5 Ideal gas constant versus value calculated for ammonia as a function of temperature and pressure.

P(bar)	T(°C)	R J/mol K	R J/mol K	R difference
7.5	140	8.128484	8.3145	0.022372
1	50	8.239578	8.3145	0.009011
8	200	8.184794	8.3145	0.0156
3	100	8.205721	8.3145	0.013083

The model is presented in **Appendix 8.1** and the MATLAB® programme is available in linked in the research document section of the paper it was presented in (Hinmers et al., 2022).

The kinetic equation is based on the form of the equation presented by Mazet et al. shown in the following equation:

$$\frac{dX}{dt} = (1 - X)^n A_r \frac{p_{eq} - p}{p}$$

But in this case derived based on a function of the masses.

The derived equation is presented as follows, for the case of desorbing from state $A\ to\ B$:

$$\frac{dm_{SALT\ A\ to\ B}}{dt} = (m_{SALT\ A} + m_{SALT\ B}) \left(\frac{m_{SALT\ A}}{m_{SALT\ A} + m_{SALT\ B}}\right)^{n_{AB}} A_{r_{AB}} \frac{p_{eq\ AB} - p}{p}$$

4.3.1 Methodology for Fitting Dynamic Data

In simulating the results from the LTJ the key values to identify were as follows:

i) An active fraction of the stoichiometric mass of adsorbed ammonia which readily reacts.
ii) A value for the thermal resistance between the composite and tube wall (heat transfer surface). In this case simulated by a static 'gap' of gaseous ammonia.
iii) Values for the kinetic constants n and A_r from **equations (33-36) Appendix 8.1.**

The simulations were then compared against all experimental test results at different pressures and with differing temperature jumps. The constants identified and used within the model are effective at simulating the kinetics, and particularly effective at predicting the rate of the reaction.

The first step (i) in fitting the results was done by adjusting an active fraction of the salt so that the pressure rise was equal to a stoichiometric mass of desorbed ammonia. This was calculated from the mass of gas in the expansion volume assuming for an ideal gas. Values for active fraction were consistent throughout the results; they also match up with Lépinasse et al., they modelled between values for the conversion of 0.1 and 0.9 (Lépinasse

et al., 1994), and for all intents and purposes the active fraction for these salts is 0.8. Further adsorption/desorption may occur but is limited by the rate of diffusion into or out of the crystal, or through a product layer. In practice, a starting and finishing point is clearly observed (presenting the mass that is active during the *fast* reactions) and the rate beyond this is very low if not unobservable during the cycles, therefore deemed inactive. The remaining mass (inactive) is accounted for in the model as an adsorbed thermal mass. In a working machine the ammonia would either stay in the adsorbed state, or not adsorb during a cycle (creating these boundary operating conditions for the active fraction). The consistency in the value between the tests in the tube and the larger shell-side supports this to be true in the ENG-salt composite which largely overcomes mass transfer issues.

The second step (ii) of fitting was to adjust size of the gap simulating the heat transfer resistance. The gap is adjusted such that the simulated reaction time matches that of the experimental reaction time. An accurate measurement of the reactor wall temperature (obtained by the grounded thermocouples) enables an accurate value for the rate of heat transfer between the sorption material and the stainless-steel wall to be identified, reducing the need for also identifying a heat transfer coefficient for silicone oil to the stainless-steel wall. The conductivity of the stainless-steel and the ENG are both relatively large compared to the 'gap' conductivity between the two surfaces. This means the heat transfer resistance is dominated by the resistance between the two surfaces, this was observed in the results as discussed later by the linear reaction rate. Only simple conduction occurs across the gas 'gap', which quantified the heat transfer coefficient between the two materials. It was taken that the '*gap*' or contact can vary between different salts since they swell by differing amounts within the material as shown in **Figure 24**.

Figure 24 Picture to illustrate the difference in swelling of samples once used. Left to right: a sample dosed with barium chloride with limited swelling; ENG without salt; and a manganese chloride sample that has increased slightly in outer diameter and height.

Finally, (iii) the equation parameters n and A_r were adjusted and identified. This was done by trial and error, to match simulated and experimental data. Because the rate of reaction is dominated by the rate of heat transfer, the constants n and A_r have limited effect on the reaction rate. However, adjusting the constants produces a better fit of the temperature curve and the pressure curve. The model was deemed effective as the constants were observed to be consistent under different conditions and for different samples, in contrast with some of the work in literature.

These steps were performed for each salt, the values that were identified are shown in Table 6.

4.3.2 Simulation Results with best-fit heat transfer and kinetic constants (Tube-Side)

Table 6 shows the best-fit values of kinetic constants, established by trial and error as described above.

Table 6 Kinetic constants from the reaction model.

Salt	$MnCl_2$	$BaCl_2$	$CaCl_2$	$CaCl_2$
NH_3 mole change	6-2	8-0	8-4	4-2
A_r adsorption	2	2	2	2
n adsorption	3	0.1	1.5	3
n desorption	3	2	2	1.5
A_r desorption	3	3	3	2.5
Active fraction	0.8	0.78	0.8	0.8

Tube-side experimentally measured pressure and temperatures plus the matching simulation results for manganese chloride can be seen in **Figure 25, and Figure 26**; barium chloride simulation results can be seen in **Figure**

27, and Figure 28; and calcium chloride results in **Figure 29, Figure 30, Figure 31, and Figure 32**. The model simulates the results across a number of conditions well. In the case of calcium chloride, the model simulates across both reactions, consecutively or individually. These results illustrate that the constants identified in **Table 6** predict well and remain constant. The case where a single adsorption reaction appears to occur as in **Figure 20**, has also been simulated, the results can be seen in **Appendix 8.7.** Two phase changes appear in the simulation, but the reaction rate is consistent with the LTJ results.

The results in the tube-side, are consistently well predicted by the model and the format of the test is very simple. This makes it easy formulate a model of the process which can be applied to larger samples in the shell-side configuration. There is some divergence in the manganese chloride results (relative to others) which may need more consideration; the difference is in the overall pressure change during the process. Overall, the temperatures, the pressures and the conversion rates are predicted within about ±2 °C, $\pm 0.01 \times 10^5$ Pa and ±0.5 mol/mol respectively.

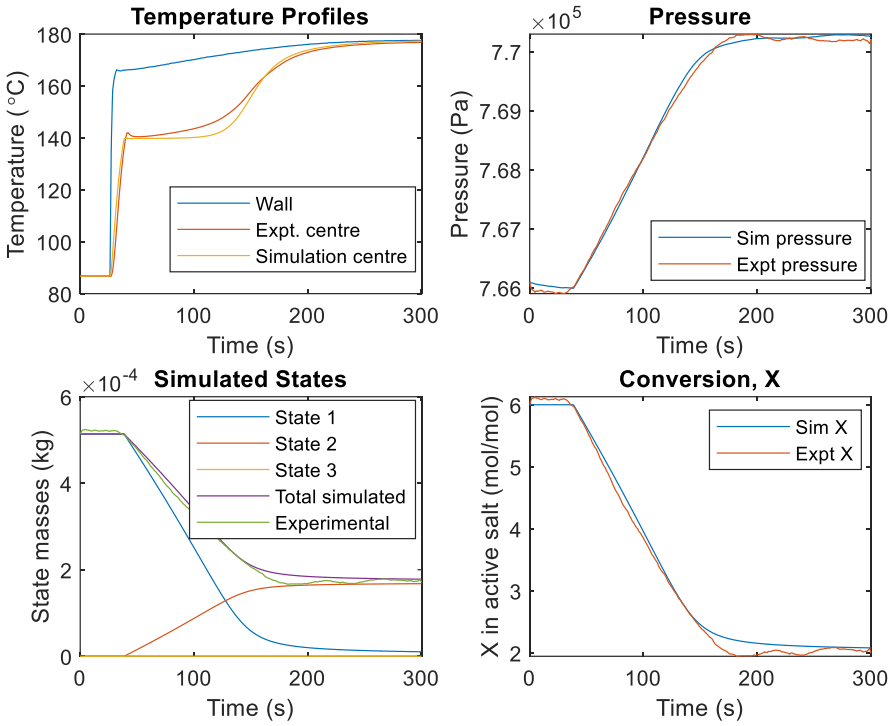

(a)

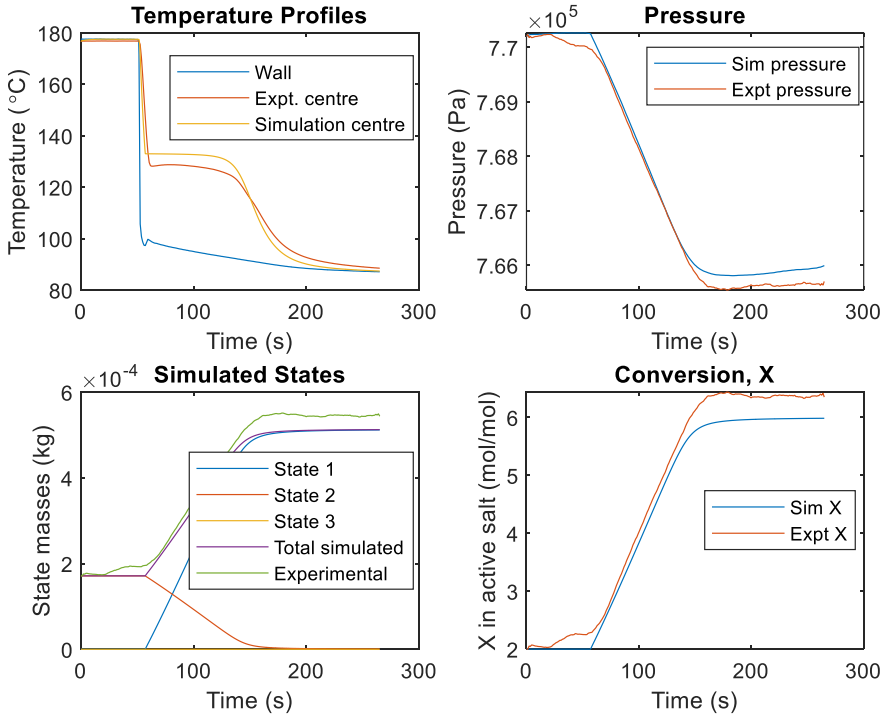

(b)

Figure 25 Simulation results for manganese chloride plotted against experimental results from the tube-side LTJ testing manganese chloride (test TA): (a) Desorption at 7.6 bar; (b) adsorption at 7.6 bar.

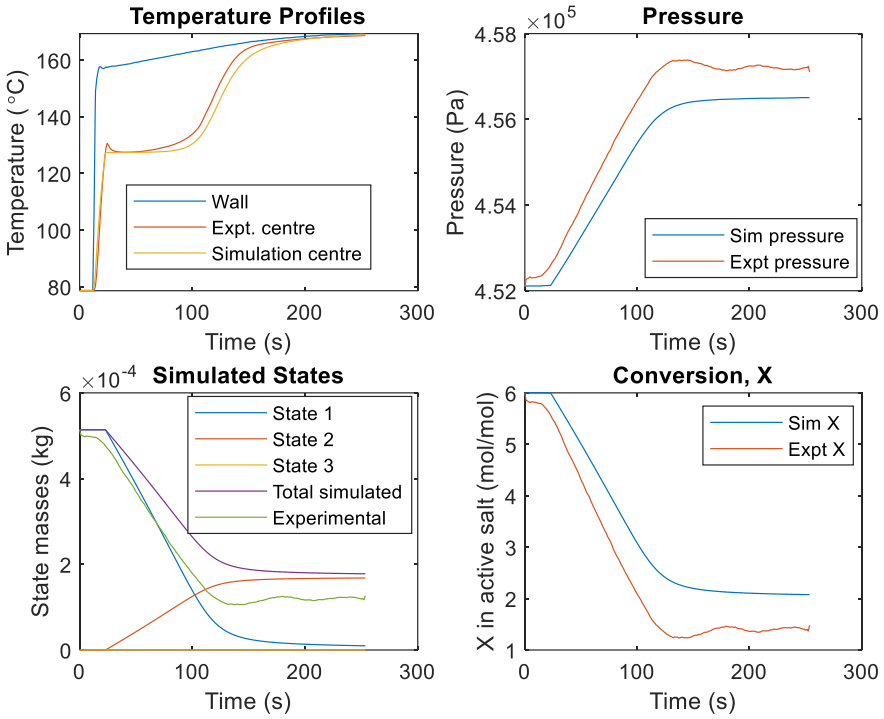

(a)

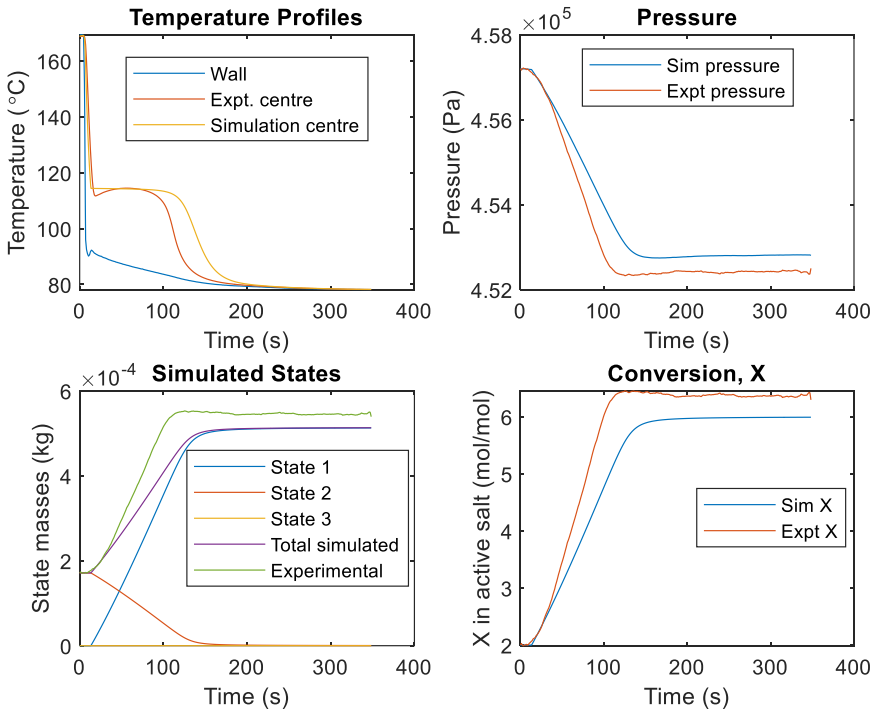

(b)

Figure 26 Simulation results for manganese chloride plotted against experimental results from the tube-side LTJ testing manganese chloride (test TA): (a) desorption at 4.5 bar; and (b) adsorption at 4.5 bar.

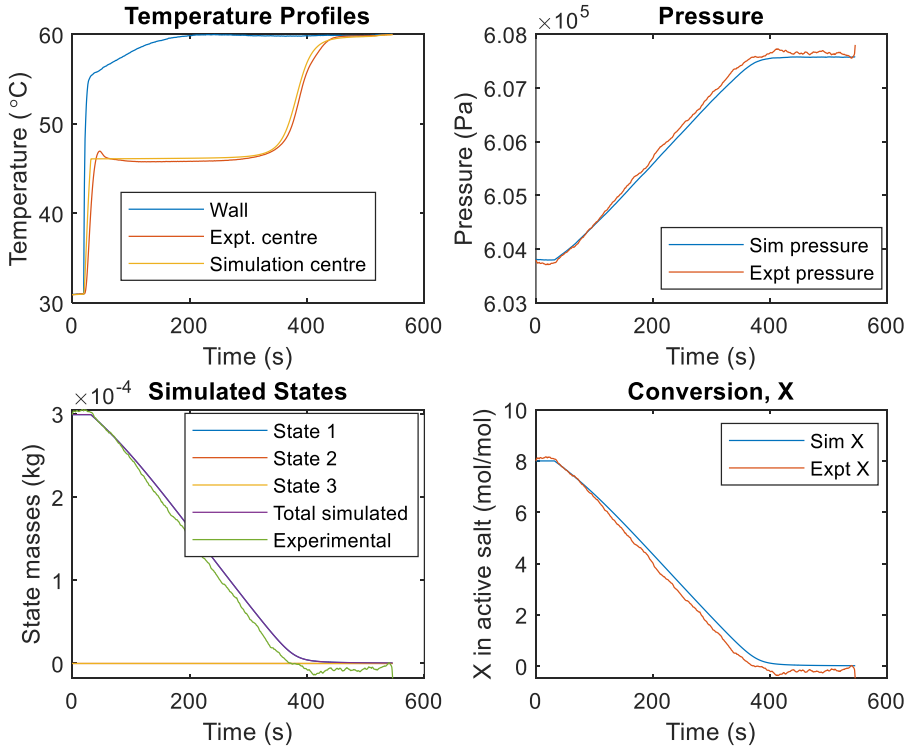

(a)

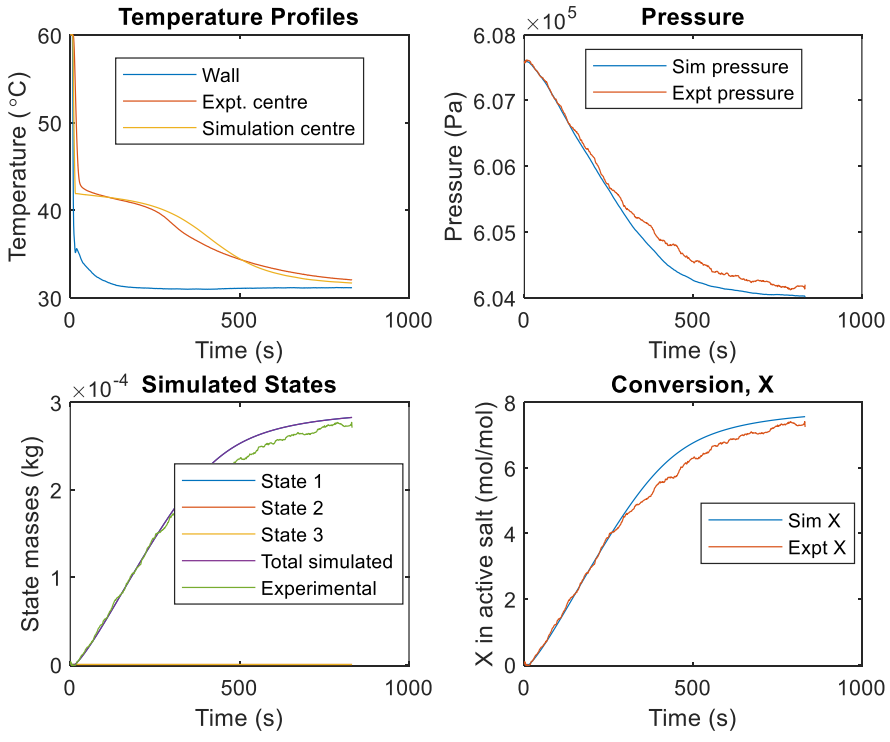

(b)

Figure 27 Simulation results for barium chloride plotted against experimental results from the tube-side LTJ testing barium chloride (test TB): (a) desorption at 6 bar; and (b) adsorption at 6 bar.

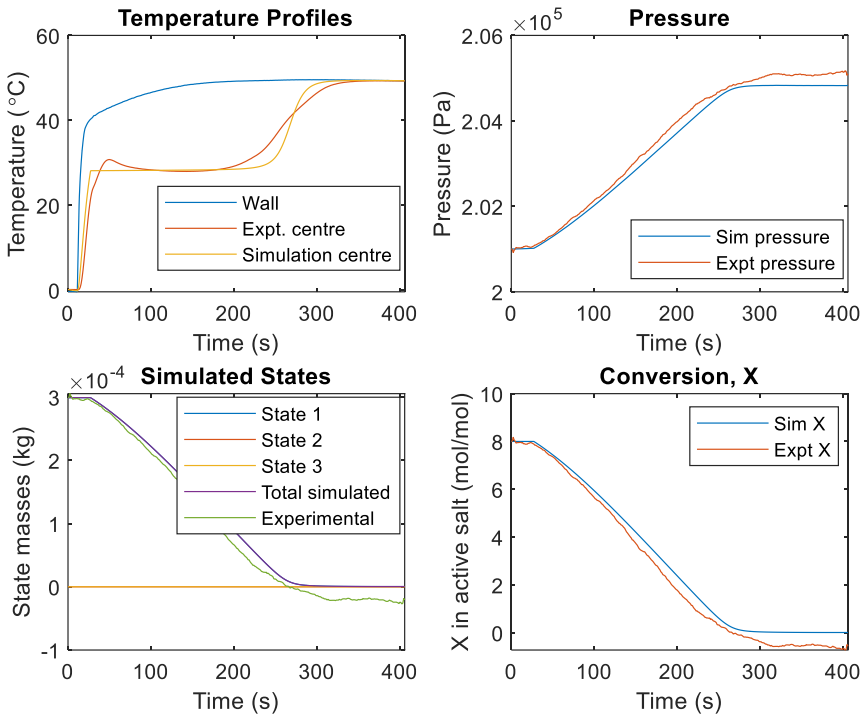

(a)

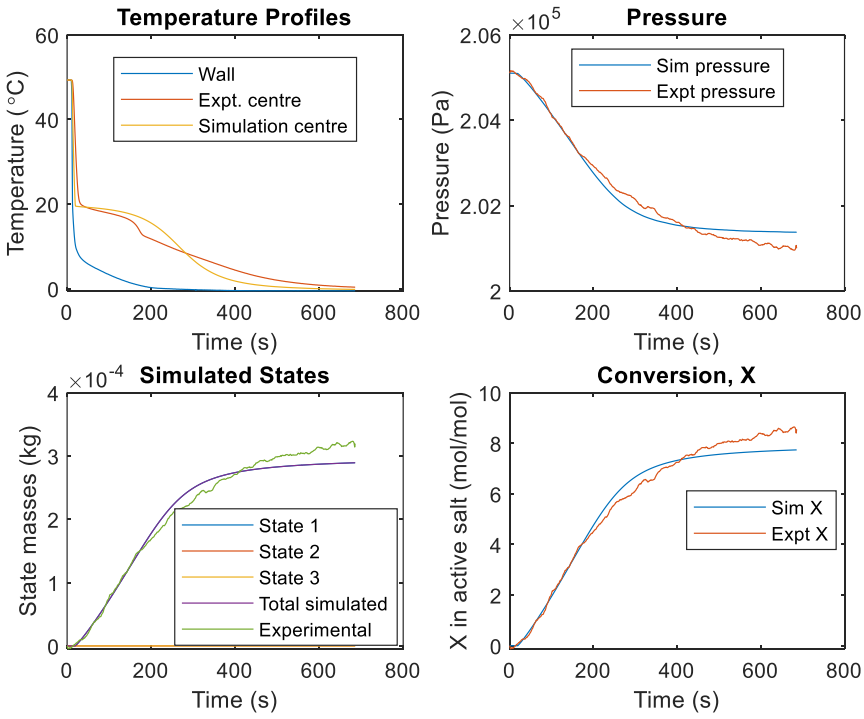

(b)

Figure 28 Simulation results for barium chloride plotted against experimental results from the tube-side LTJ testing barium chloride (test TB): (a) desorption at 2 bar; and (b) adsorption at 2 bar.

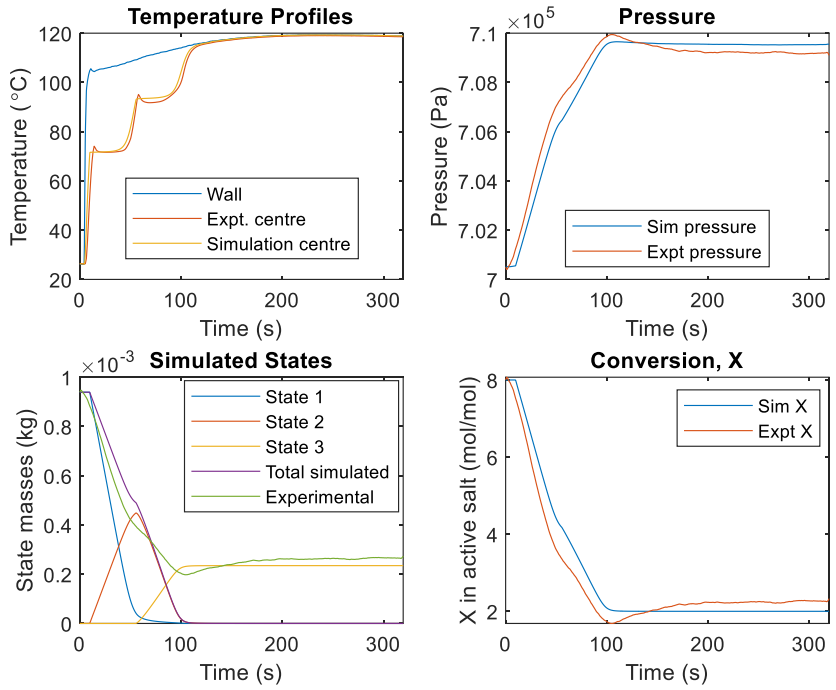

(a)

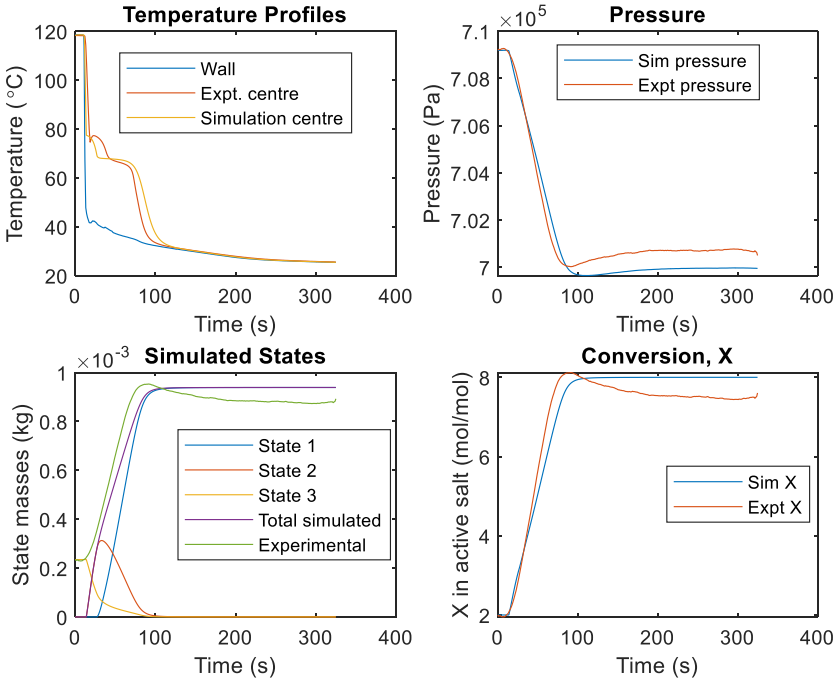

(b)

Figure 29 Simulation results for calcium chloride plotted against experimental results from the tube-side LTJ testing calcium chloride (test TD), across both state changes (8-4) and (4-2): (a) desorption at 7 bar; and (b) adsorption at 7 bar.

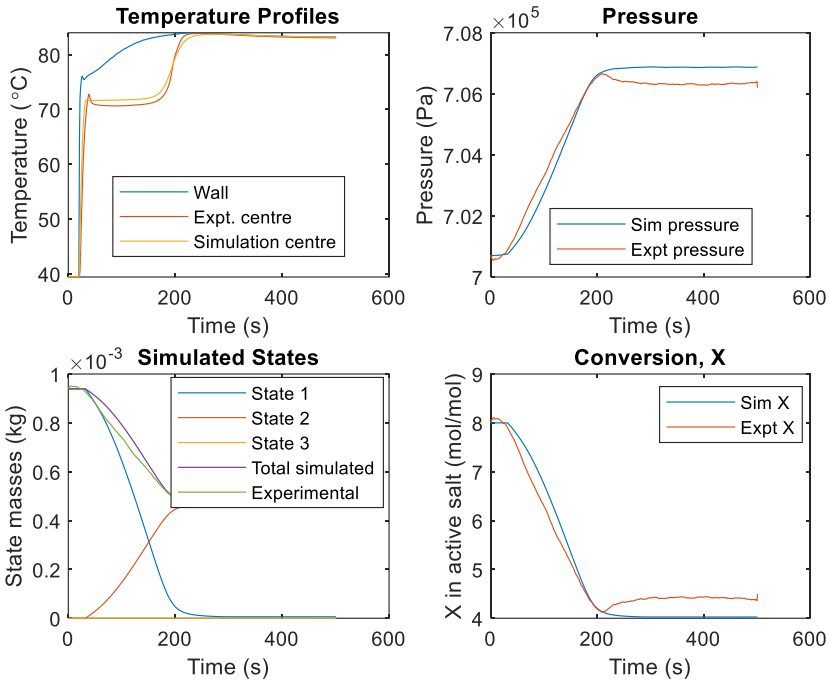

(a)

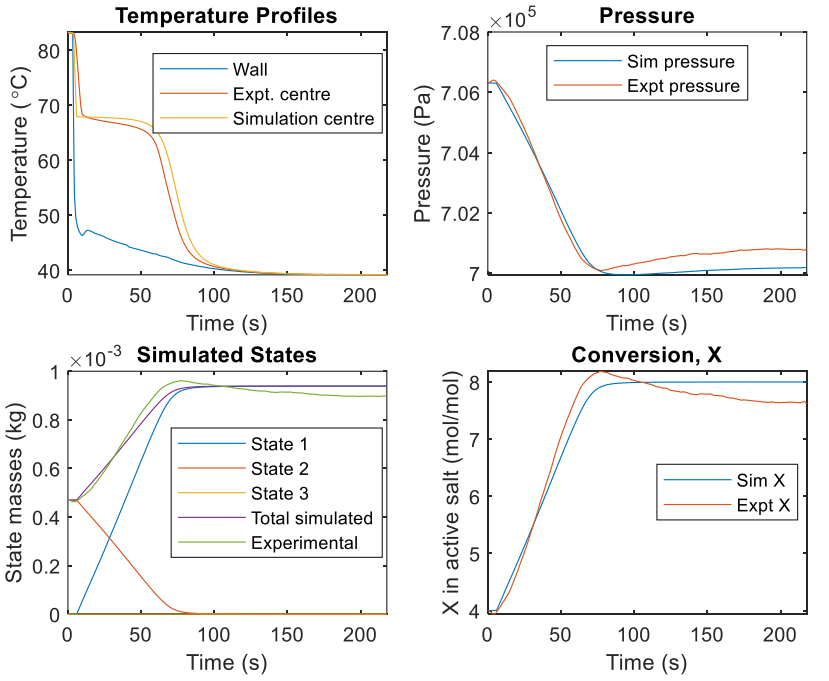

(b)

Figure 30 Simulation results for calcium chloride plotted against experimental results from the tube-side LTJ testing calcium chloride (test TD), across state change (8-4): (a) desorption at 7 bar; and (b) adsorption at 7 bar.

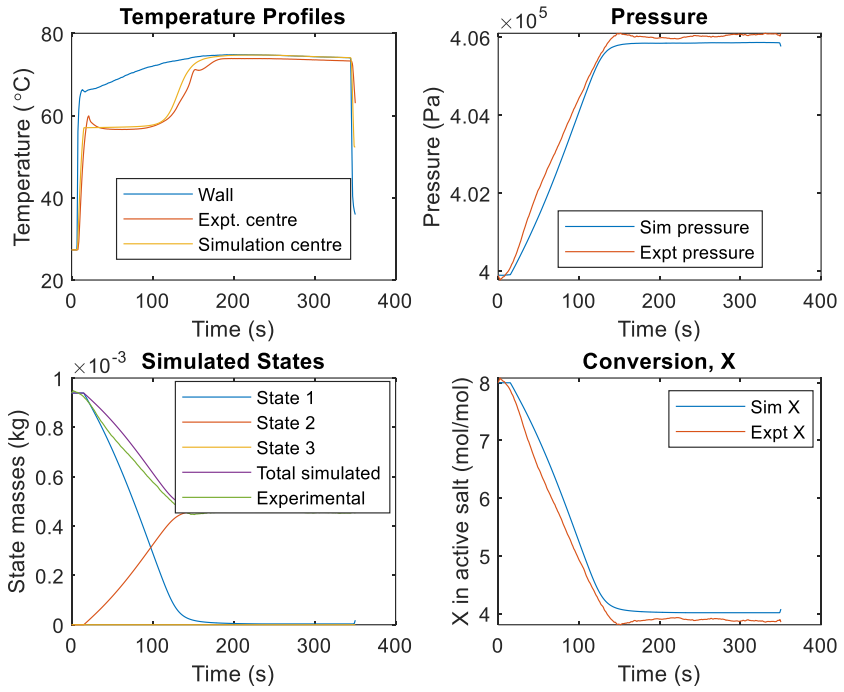

(a)

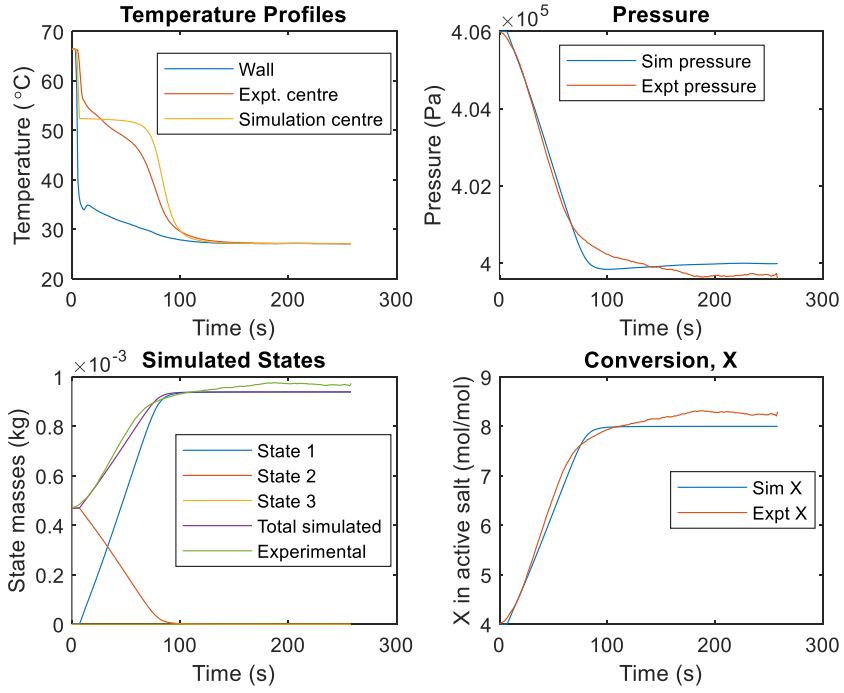

(b)

Figure 31 Simulation results for calcium chloride plotted against experimental results from the tube-side LTJ testing calcium chloride (test TD), across state change (8-4): (a) desorption at 4 bar; and (b) adsorption at 4 bar.

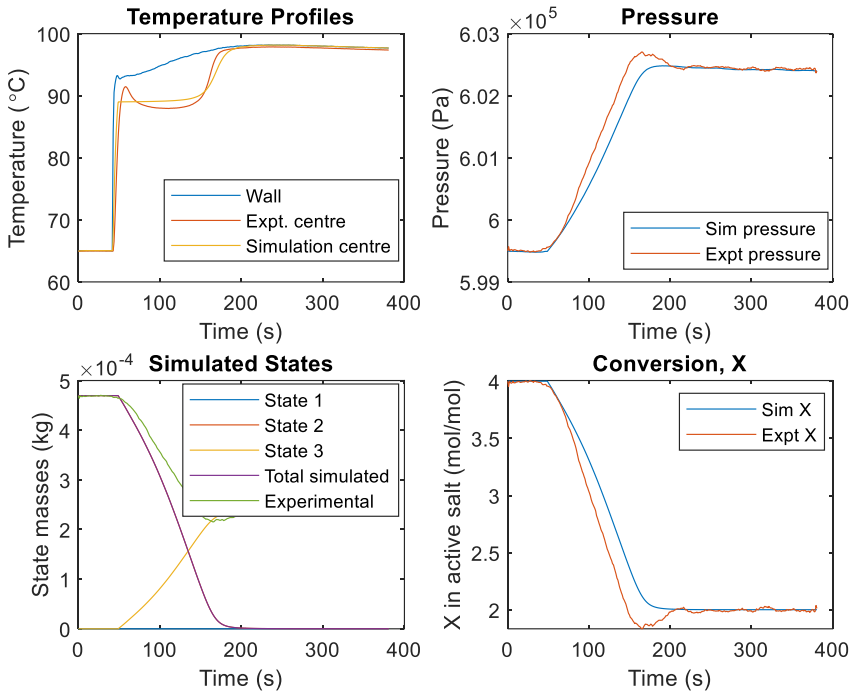

(a)

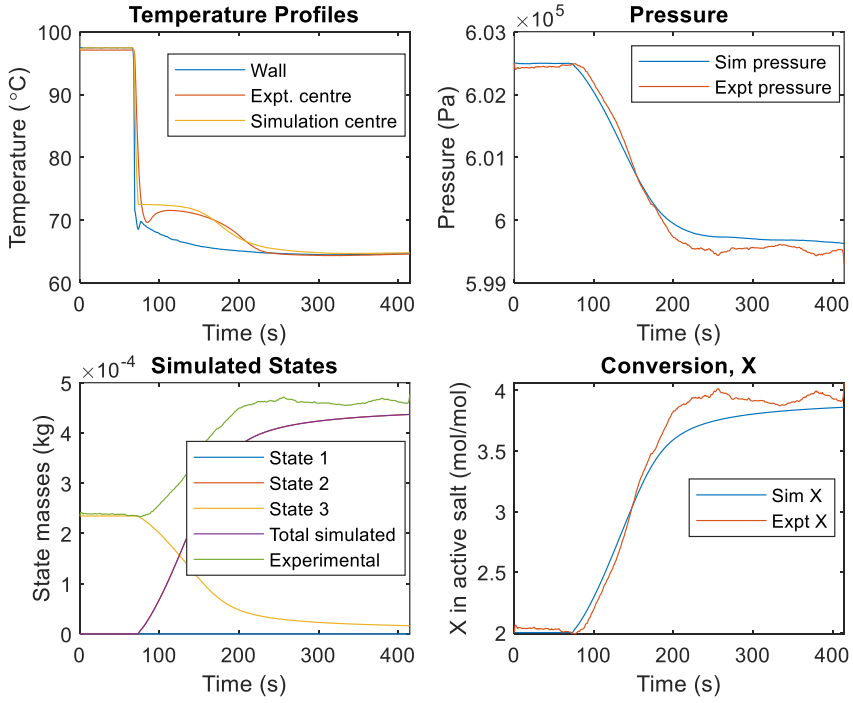

(b)

Figure 32 Simulation results for calcium chloride plotted against experimental results from the tube-side LTJ testing calcium chloride (test TD), across state change (4-2): (a) desorption at 6 bar; and (b) adsorption at 6 bar.

4.3.3 Shell-side with Best-fit Heat Transfer and Kinetic Constants LTJ Results

For further validation of the model, and to test sizes of samples similar to those being used in a full-size resorption machine, the shell-side rector was

designed (**section 3.3.3**). The process is the same but in this case the thermal fluid flows through the tube with the sorbent matrix in the shell.

Figure 33 and **Figure 38** show two different shell side tests. Some of the characteristics described within the tube side LTJ can still be seen such as the superheating effect, or subcooling effect. In **Figure 33** there is some pressure rise due to heating observed between 2000 and 3000 seconds. This is because the reaction has occurred over a much longer time period and the substantial thermal mass of the reactor became hot and heated gas in the system. This is avoided in the test shown in **Figure 38**, where heat transfer is improved and the heating time is less.

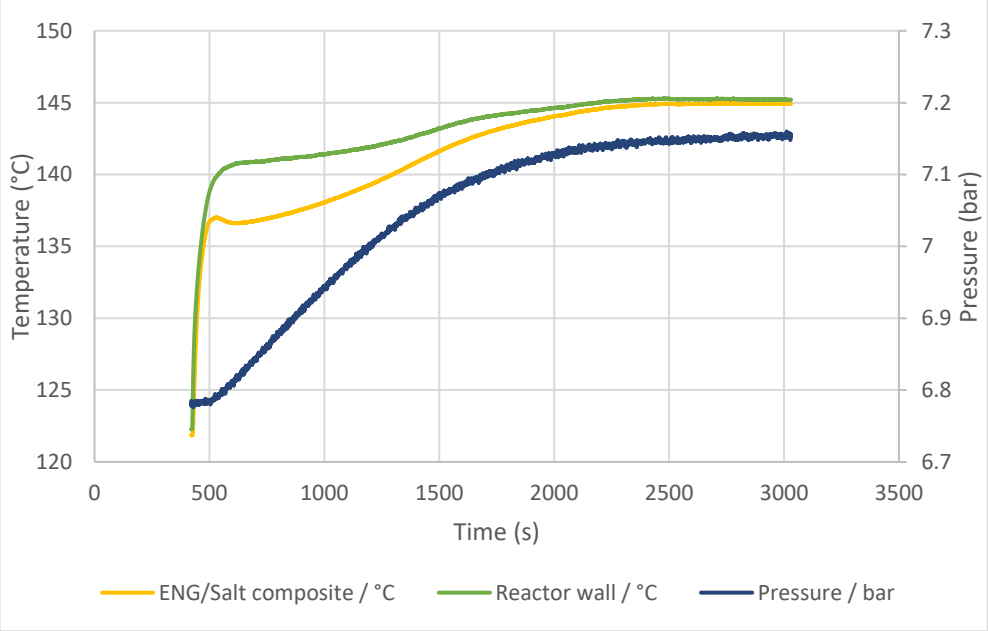

Figure 33 Shell-Side test for manganese chloride. Temperature of the ENG composite is an average of the two thermocouples TIT L1&L2 (test SA).

A further example is shown for calcium chloride in **Figure 34**. Both phase changes can be seen as well as the superheating and subcooling effects. Both the tests in **Figure 33 and Figure 34** used silicone oil as the heat transfer fluid, heated by Huber baths. When performing the tests, the temperature in the baths quickly recovers to the set point after the temperature jump. When we look at the temperature readings for the reactor wall temperatures in both these figures, we can see the wall temperature being held down by the composite. This is clearer in **Figure 34**, as the wall

temperature reading follows the same pattern as the salt temperature, being held down at two levels.

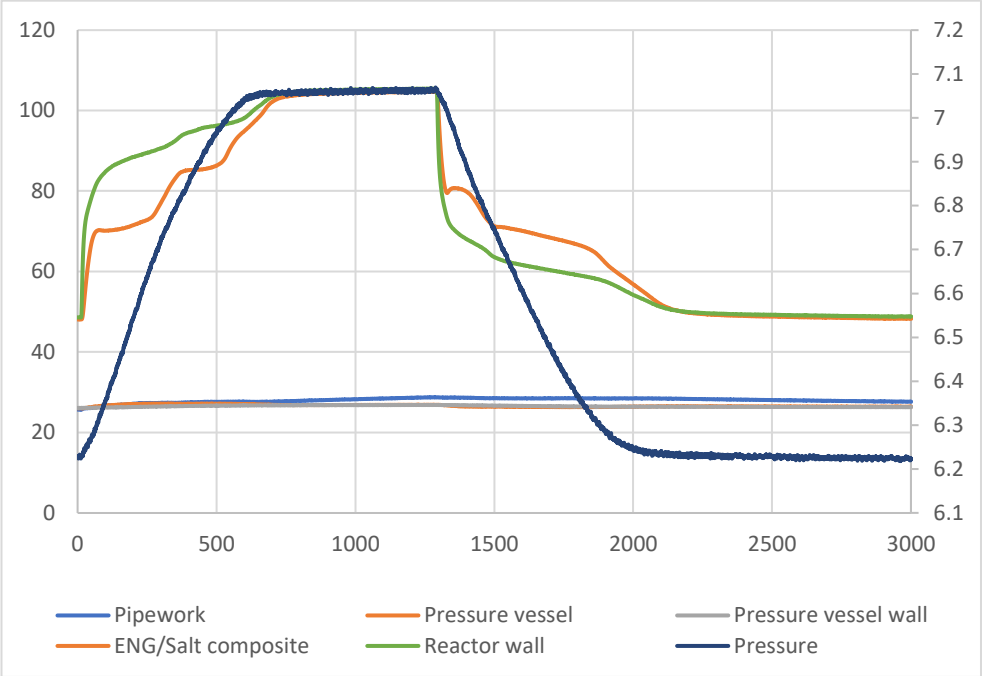

Figure 34 Shell-side test for calcium chloride. Temperature of the ENG composite is an average of the two thermocouples TIT L1&L2 (test SD).

The shell-side results have also been simulated using the model, this can be seen in **Figure 35.** This time in the model the first node is on the outer edge of the disc and the final node in contact with the wall which is a boundary condition of the model. The constants identified from the tube-side were applied to the shell-side but a new gap was identified. Contacting grounded thermocouples were again used and proved effective at delivering an accurate wall temperature of the tube, providing a basis for the boundary condition.

The simulations are effective at predicting the reaction kinetics. There is some minor divergence in the (external/sample) thermocouple reading from the simulated temperature of the first node, but this is likely due to the thermocouple being on the outside and in free space against the material as shown in **Figure 14**. Thermal resistance between the composite and the thermocouple will also take place. However, the simulation is effective at predicting the reaction rate, with comparable pressure curves and the reactions finishing at the same time, which provides confidence in the

results. Simulation results for some calcium chloride tests in the shell can also be seen in **Appendix 8.8.**

To check the validity of the model, a grid independence test for the number of nodes used in the finite difference model was conducted and can be seen in **Appendix 8.9**. The simulation results were tested over a range of nodes on both the tube side and larger shell side results. With 2 nodes, the simulation appeared to marginally differ (temperature and pressure profiles), but with more than 2 nodes the results were consistent. The number of nodes within the finite difference model was set to 5 (for tube and shell). This provided certainty in the accuracy and maintained computational efficiency when considering the time step. The time step needed to be small enough so that the model was stable and was typically between 0.01- 0.005 seconds.

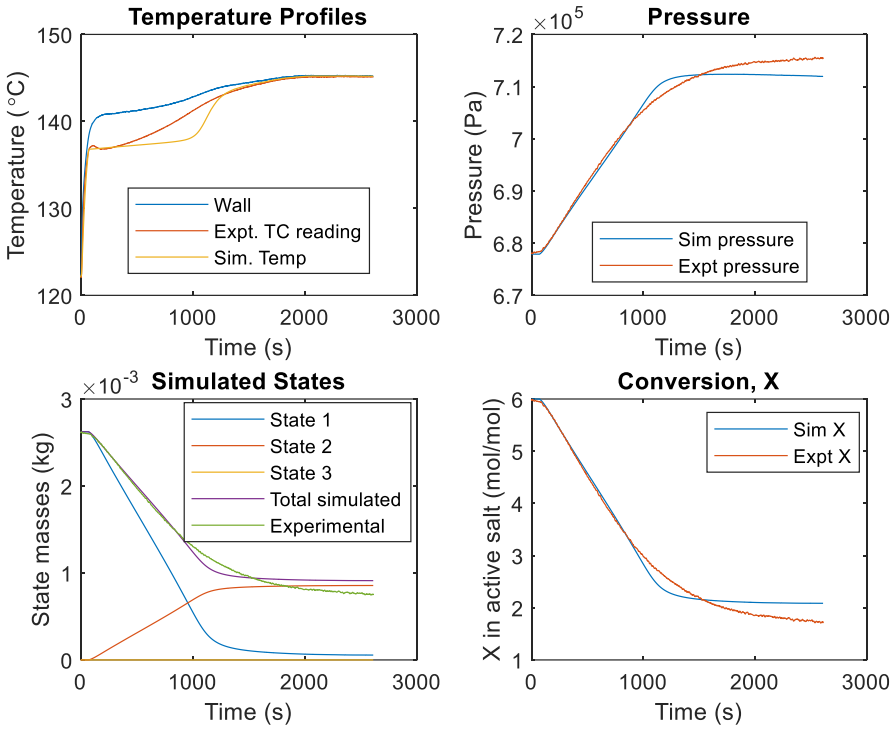

(a)

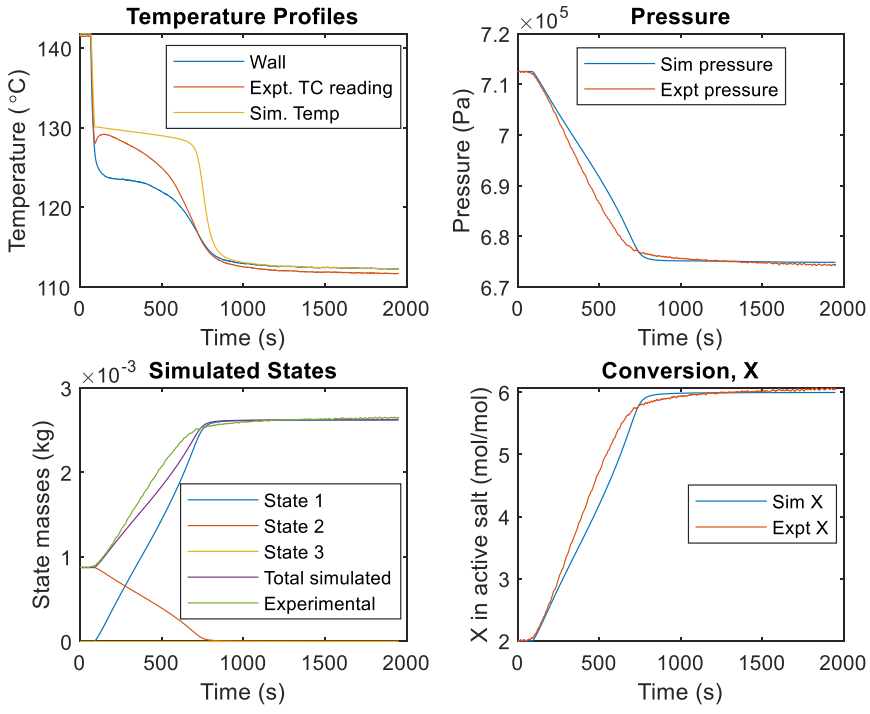

(b)

Figure 35 Simulations of the shell-side reactor plotted against the experimental results for manganese chloride (test SA): (a) desorption; (b) adsorption.

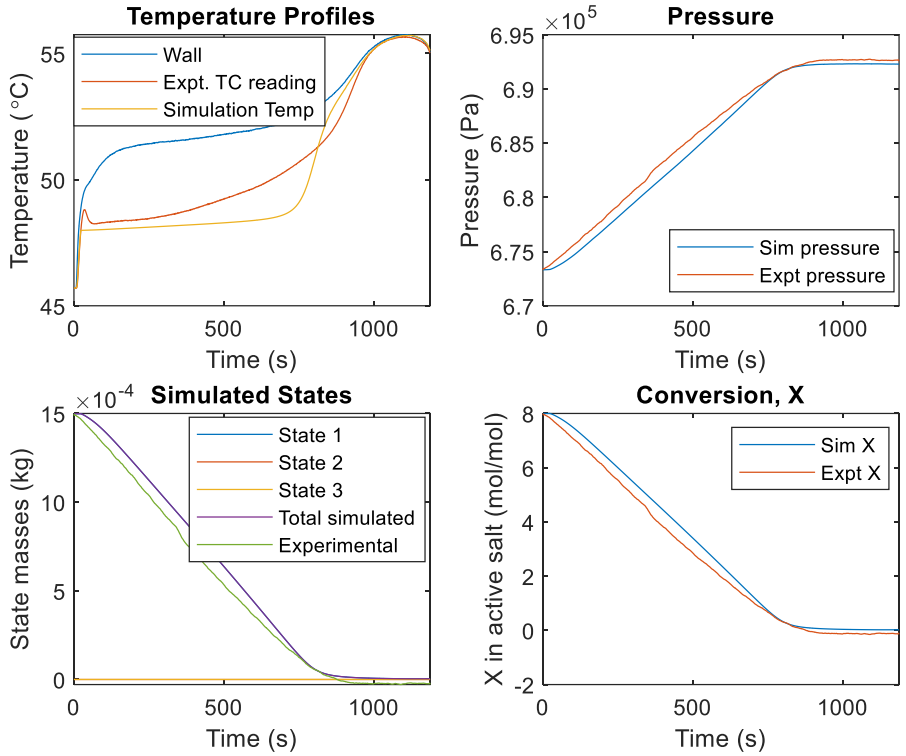

(a)

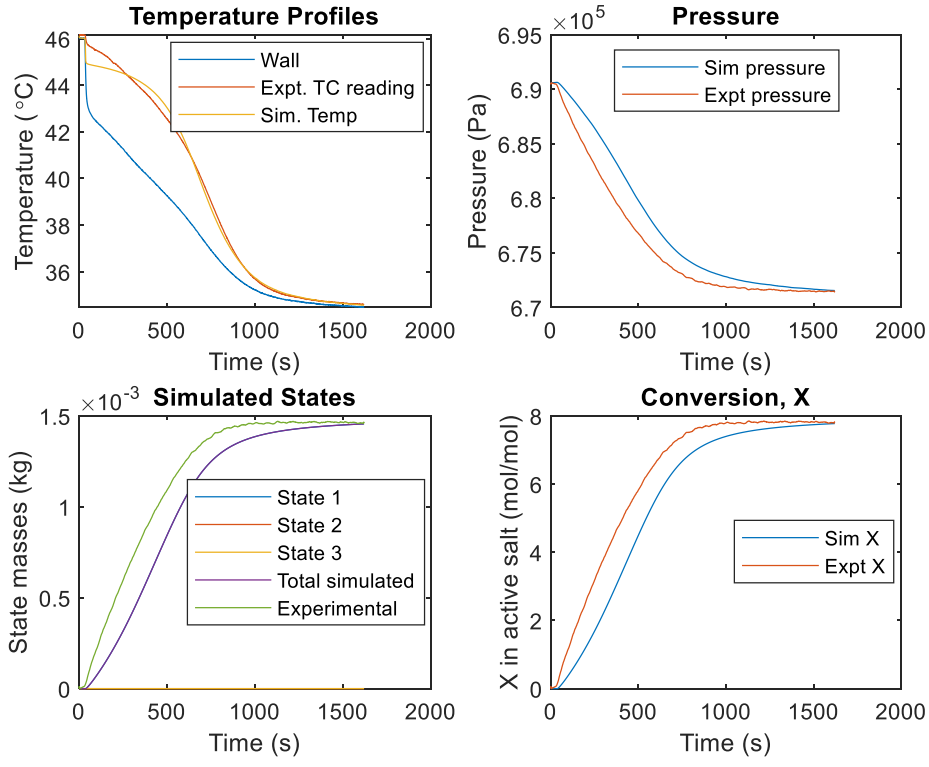

(b)

Figure 36 Simulation of shell side barium chloride results plotted against experimental results (test SB): (a) desorption; (b) adsorption

4.3.4 Heat Transfer Improvements

It has already been concluded that the process is heat transfer limited, this was observed as the 'gap' has the greatest effect on the rate of reaction; furthermore, adjusting the conductivity value for the composite had no observable effect (within reasonable bounds) on the rate of reaction. To improve the power density of potential systems, a higher rate of reaction is required. Therefore, heat transfer improvements are key to achieving a machine suitable for market. The tube side and initially the shell side LTJ experiment used silicone oil as the heat transfer fluid because of its wide operating range of temperatures. This was important for the testing of calcium chloride and manganese chloride which required testing at temperatures above 100 °C. When testing in the shell began, the wall temperature was observed to be notably different to the fluid temperature during the reaction. This was realised because after the temperature jump occurred, the Huber bath reservoir temperature would quickly recover to set point but the wall temperature stayed close to the reaction temperature; furthermore, when trying to produce a ΔT of 10 °C, the Huber bath set temperature had to be 20 °C above the reaction temperature (rather than 10 °C). The fluid temperature was not measured when silicone oil was used as it was impractical due to the oil exhibiting laminar flow, making obtaining an accurate fluid temperature challenging. Furthermore, the wall temperature was measured accurately and this was the boundary condition in the simulation. With the realisation that heat transfer was the most significant factor affecting the rate, it also became clear that heat transfer on the fluid side should be taken into consideration.

To improve the heat transfer to the sorbent/composite and to improve the reaction rate, it was necessary to improve contact with the tube. This was done by cutting discs with reducing central hole sizes, using custom-made hole saws. Testing was performed by cutting the smaller holes, then dosing the material with salt, and then pushing the progressively smaller discs over the tube (with manufactured tools) observing the integrity of the material

and testing until cracking. Pushing required 'pusher' tools to be manufactured to ensure the material did not fracture under an uneven distribution of force on the soft and slightly brittle material. These consisted of a conical receiver that slotted into the tube and a housing to push the samples on. The tools and hole saw as well as some discs and one that has fractured can be seen in **Figure 37**.

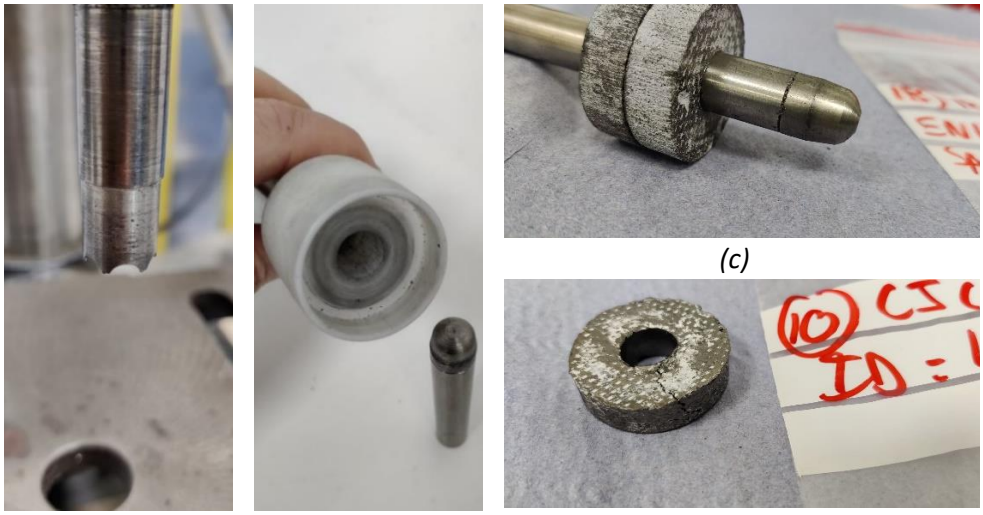

(a) *(b)* *(c)* *(d)*

Figure 37 Improving composite contact on the tube for shell-side samples: (a) Custom hole saw; (b) Pusher and conical receiver; (c) Samples on tube, again with conical receiver; (d) Cracked sample that yielded on testing.

The initial efforts at improving heat transfer were performed on the primary tube from the shell side reactor which was a ½" (12.7 mm OD) tube (with different flanges, the shell could have hosted a larger tube size). After testing the samples, the smallest size of hole saw OD was 11.9 mm, for which the sample did not fail, going down in increments of 0.1 mm. The samples actual ID might be greater due to a tolerance from the cut, but it is impossible to measure the sample ID accurately with callipers as the material is relatively soft.

To improve the heat transfer from the fluid side, the Huber baths were emptied, cleaned, and filled with water, resulting in an increased heat transfer coefficient compared to silicone oil. To further improve the heat transfer CALGAVIN hiTRAN® Thermal Systems tube inserts were used inside the tubes, these increased the turbulence of the fluid. The change to water

was considered realistic as a likely heat source for the transformer is steam condensate.

In **Figure 38** the results of improving the heat transfer can be seen; a much faster rate of reaction, a more constant temperature reading on the composite during the cycle and a very clear constant pressure rise. This further highlights the heat transfer limitation of the reaction rate. The cycle in **Figure 38** (*test SC)*, is a test for a hexagonal disc at the size chosen for samples (as described later), and this time water was used as the heat transfer fluid. As water was chosen, the fittings that fed the reactor were tapped to host Spectite TC fittings, and K type thermocouples were then used to measure the fluid temperature in and out of the reactor. The temperature difference between fluid and the central tube wall is similar to the difference between the wall and the outside radius of the ENG implying significant fluid-side heat transfer resistance. The heat transfer fluid was silicone oil in **Figure 34**, and water in **Figure 38**, the bath temperature (ΔT) was set much higher in **Figure 34**, but the latter reacts much quicker.

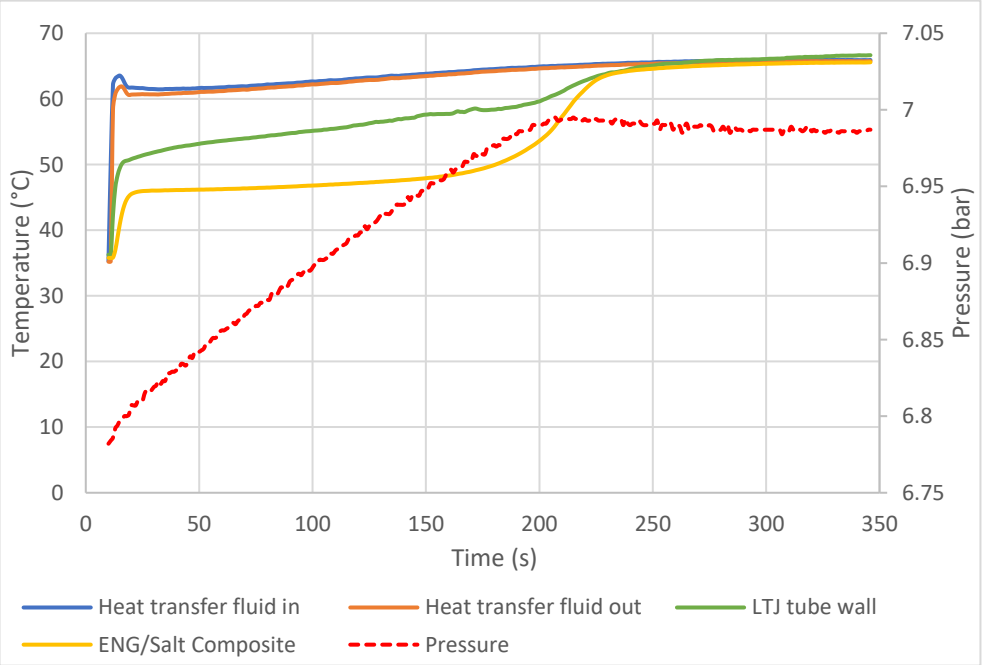

Figure 38 Shell side test for barium chloride (test SC). This time the LTJ was heated with water and had improved heat transfer, also the sample had a smaller central hole. This was a test with improved heat transfer, leading to a large reduction in heating time.

The result from **Figure 38**, was simulated using the model to assess the heat transfer, as shown in **Figure 29.**

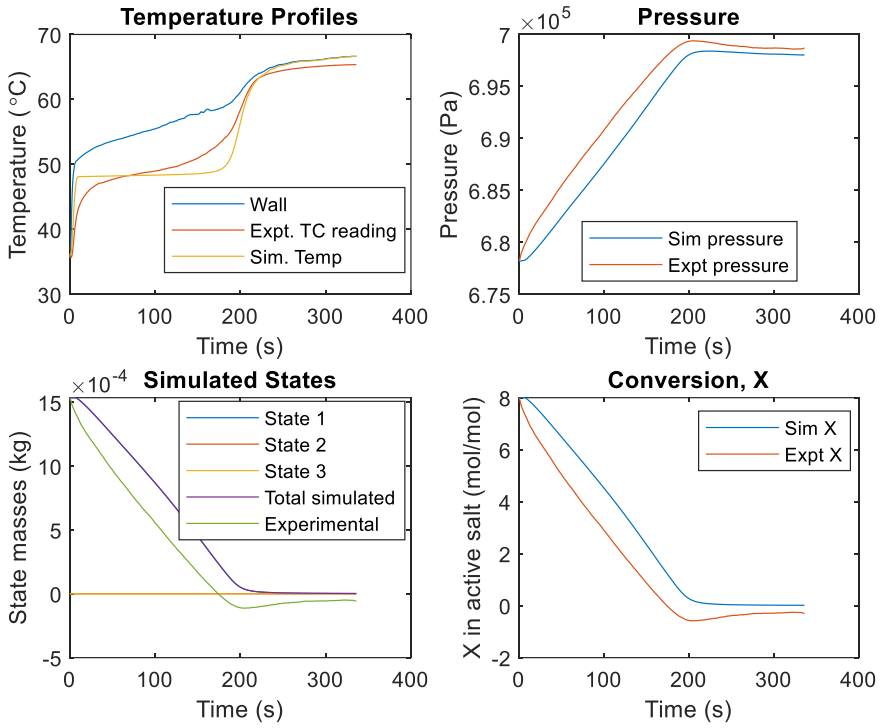

*Figure 39 simulation results of shell-side hexagon sample (test SC). The raw data can be seen in **Figure 38.***

The nominal gap sizes found for the barium tests were 0.15 mm and 0.043 mm for the samples in the tube and the shell respectively. After improving the heat transfer with the smaller ID disks, the nominal gap value was reduced to 0.0019 mm producing the result shown in **Figure 38** (test SC). This is a marked improvement, but the heat transfer resistance is still not negligible and could be improved further (in theory).

4.3.5 Simulation Error

Effort was taken to consider error by testing the instrumentation; the simulation results also presented a good prediction consistently of the real experimental results, particularly the predicted rate of reaction. Therefore, for the scale of machine presented in the next chapter (3 kW), error is not so much a concern. The challenge is that this technology could be designed at the megawatt scale, at which a 1% error could become noticeable. Therefore, a couple of calculations have been performed to evaluate the

simulation error. This has been done for the results shown in **Figure 35 (a)**, which shows a reasonable deviation in the temperature predictions. To consider the error, the first 2000 seconds of data were taken for the temperature plot and analysed to consider deviation. The last 1000 seconds were ignored as the results align. The temperature was taken as it is a key variable for the heat flux, and deviation observed overestimates the temperature difference and could overpredict the power. To consider the error over the dynamic operation the root-mean-square deviation was calculated, using the following equation:

$$RMSD = \sqrt{\frac{\sum(x - \hat{x})^2}{N}}$$

Where:

$RMSD$ = root-mean-square deviation

N = Number of data points

x = observed result

$\hat{x}$ = predicted result

The result is the square root of the average of the deviation from predicted results. The effect of the error from a data point is proportional to the size of the error and so a large deviation would have a disproportionately large effect. The final result was 0.941.

To evaluate further the mean absolute error was also calculated using the following equation:

$$MAE = \frac{\sum|x - \hat{x}|}{N}$$

The variables are the same (with an absolute value taken) and MAE is the mean absolute error. The result was 0.745. These values are very low, giving some confidence in the results. It is also likely some of the error may have come from the placement of the thermocouple which was in poor contact

with the material. However, it is worth noting that the deviation observed for a 10 °C temperature difference could become noticeable at scale. For this reason scaling up the design to megawatt scale should consider a factor for error. This could be as much as oversizing by 10%. When testing the 3 kW machine there should be some assessment into power and any underperformance

5 Geometry of Resorption Transformer

With an accurate model of the reaction kinetics, it is now possible to simulate a machine's performance and present an optimised design. The key factors to consider are the coefficient of performance (COP), and the peak specific mean power (SMP). There is a trade-off between the two. This is because optimal SMP can be seen when the material cycles quickly and rapidly delivers the reaction heat; this favours a thin layer of material against the steel, tending towards infinitely small layer (for the same nominal mass of material across an infinitely long tube). The COP has a limit equivalent to a ratio of active material to thermal mass of 1:0, which is a function of the specific heat capacity of the salt and the composite mass, and the reaction heat. The ideal COP is given by $\Delta H_{r,HTS}/(\Delta H_{r,LTS} + \Delta H_{r,HTS}) = 0.5$ (assuming parallel isosteres and therefore equivalent heats of reaction); the useful heat out, over the sum of the heats in (in an ideal system just the reaction heats are provided). The trade-off appears to be a high COP equals a low power density or vice versa. But this is not the entire story, as improving the heat transfer means a higher reaction rate; this means a larger mass of salt will produce a reasonable power density and also increase the COP.

As discussed in the **literature review 2.2**, for resorption to compete with existing absorption transformers, the systems need to have a relatively small footprint, and relatively fast cycle times [6]. This suggests that there should be more significance placed on the SMP than previously shown in the

literature, as high-power density would solve both these challenges. None the less, a minimum COP must also be achieved to ensure a heat efficiency within the system.

5.1 Specific Mean Power and Power Density

The reaction model observes a net flow of heat into or out of the boundary node, this induces the temperature rise (or fall) and thus the ΔT, that drives the reaction. Calculating heat flow or heat flux is therefore key to understanding performance in terms of power density. The total heat flow per volume of sample (and internal tube) divided by the time, produces a mean value for the specific mean power. Professor Critoph incorporated this into the MATLAB program and indexed the values in an array. The peak value of this (when the reaction is occurring) determines a measure of the power density. This is described as the peak specific mean power. An ideal control system would switch between adsorption and desorption when the peak is reached.

To further evaluate this, the model was developed to predict the performance of different samples subjected to a ramp in temperature (denoted by a step change in the wall temperature); simply done by creating the wall temperature array manually, rather than feeding in experimental results. This was purely a simulation without experimental data and neglected considerations into heat transfer to the wall; the wall temperature would change to a new value over a chosen time period, the initial temperature was set to the equilibrium line point, so the simulation would initiate the reaction instantaneously. The SMP (W/m^3) can be observed over the evolution of this simulated reaction and the peak value can be used to predict the power density of a machine. This can be used to understand performances of different sized samples on different tubes, before the sizes are tested in real conditions in the shell-side reactor. A reasonable value for the peak SMP would be 1 kW/litre. SMP is calculated from the sum of cumulative heat into (or from) the salt-ENG composite and the cumulative

heat to the steel and heat transfer fluid, divided by the time and the total volume of the cell. The peak is a local maximum observed during the reaction. The cell can be seen in **Figure 41**. The working machine is limited to a 10 °C driving temperature to reduce sensible heating impact on COP. Initially the program was set to ramp the wall temperature 10 °C and the SMP was observed over a range of standard tube sizes (½" ¾" 1" outer diameter tube) and a range of different sizes of samples (as shown in detail in **Appendix 8.12**). The next step was to test in the shell-side LTJ to assess real performance and to see if results were acceptable. There are a couple of factors to consider, as a larger tube with a thinner sample would have the most heat transfer and produce the highest SMP, (the corresponding COP needs to be considered,) but there is a practical limit to how thin the sample can be around the tube before it breaks. This approach was indicative of results before committing to testing or design. The approach was iterative, and modelling COP of sizes was done at the same time, using trial and error to assess what appeared to produce useful results. An example of an LTJ shell-side test result for barium chloride and the plot of SMP is shown in **Figure 40**.

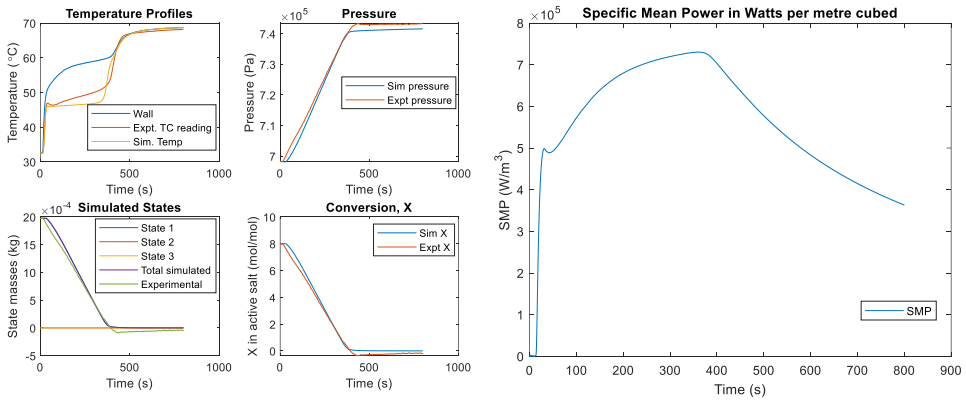

(a) *(b)*

Figure 40 Shell side LTJ test and SMP plotted versus time: (a) Simulation result; (b) Specific mean power plotted vs time. The peak value of SMP was 0.72434 kW/litre. The samples had a 35 mm outer diameter and fitted over a 12.7 mm tube.

The constraints when considering optimal sizing of a cell as in **Figure 41**, is that at lab scale the system would have to use standard tube sizes. This means that the internal diameter has to be either 12.7 mm (1/2" tube), 19.05 mm (3/4" tube) or 25.4 mm (1" tube). Tube-side geometry has been

disregarded as the COP performance would be unacceptable, due to the high ratio of thermal mass if used in a shell and tube bundle.

The results in **appendix 8.12** shows a correlation in the shell geometry between reducing the outer diameter (producing a thinner sample) presents a higher specific mean power, for the cell in **Figure 41**. When considering the larger size of tubes, the same conclusion can be made, but the SMP value derived from just the composite and not the steel or water (SMPW – ENG only), diverges more from the actual SMP as the thermal mass of the fluid and tube is larger. The larger tube size can appear to improve SMP due to the improved heat transfer, but as the tubes get bigger the ratio of the thermal mass of the fluid to the (relatively) thin composite causes the COP to be unacceptably low. The peak SMP and the COP are inversely proportional, assigning a size will be revisited in the **discussion section 6**.

5.2 COP Calculation

The COP can be calculated to assess the thermal efficiency of the system. This is an important assessment, to predict the effectiveness of recovering waste heat. Assessing the COP gives an understanding of the effect of the thermal masses involved and ensuring sensible heating losses are not too great, illustrating if a system is viable. As discussed in **section 2.5**, many papers have calculated the COP without using dynamic results (Lépinasse et al., 1994, Vasiliev et al., 2004, Li et al., 2010). The approach taken in this work is to calculate a COP to inform the design; any development and testing would then involve assessing the COP performance to understand why it may not have achieved desired results.

To assess the COP for potential sizing, a unit cell is defined to represent the reactor geometry. The assumption is that the reactor is comprised of uniform cells in a bundle arrangement with an equal ratio of materials per axial length throughout the bundle. A unit cell is defined in **Figure 41**. This comprises of salt-ENG composite, the stainless-steel tube and the heat transfer fluid per unit length. This mass ratio can be used to look at different

pairs when we factor in stoichiometric ratios and uptake of salt into the ENG. This can be used to assess both in tube and out of tube position of the composite, but external placement is most likely because inert thermal mass ratio would be lower. Further to this, van der Pal and Critoph's test used a tube bundle with fluid in the shell (in a shell and tube heat exchanger design), they suggest that if the reactor they tested was used in practice, a final COP of less than 0.1 would be achieved (van der Pal and Critoph, 2017). This design was not optimised, but if we consider that the shell would have to cycle with the temperature and the quantity of fluid in the shell it becomes clear the COP would be poor and the system would be massive.

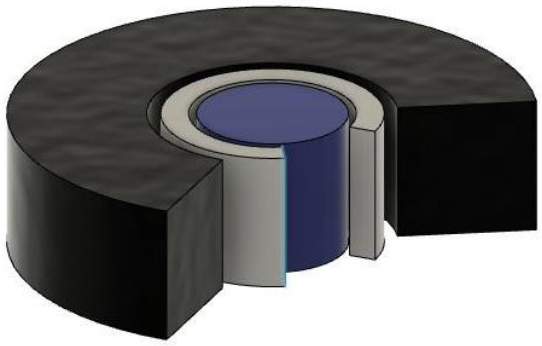

Figure 41 Cutaway, of a unit cell of a resorption generator, the central cylinder is water (the heat transfer fluid), the middle grey tube is stainless steel and the outer ring is ENG-salt composite. Key to assessing performance, is the ratio of component diameters.

The COP is calculated from the equation:

$$COP = \frac{Q_{HTS,ads.heat} - Q_{HTS,heating}}{Q_{LTS,heating} + Q_{gas,heating} + Q_{LTS,des.heat} + Q_{HTS,des.heat}} \quad (20)$$

This evaluates the heat in and useful heat out per mass of salt in the low temperature bed. The heat in, is assumed to be the sum of: the sensible heat to heat up the low temperature salt $Q_{LTS,heating}$; the sensible heat to heat the high temperature salt, $Q_{HTS,heating}$; the sensible heat to heat up the mass of ammonia gas desorbed during the high pressure phase, $Q_{gas,heating}$; the reaction heat of desorption in the low temperature bed during the high pressure phase, $Q_{LTS,des.heat}$; and the reaction heat of desorption in the high temperature bed during the low pressure phase,

$Q_{HTS,des.heat}$. The useful heat produced is the heat of adsorption recovered from the high temperature bed during the high-pressure phase of the process, $Q_{HTS,ads.heat}$; minus the sensible heat to heat the high temperature salt, $Q_{HTS,heating}$, this has to come from the adsorption heat due to the temperatures required. As mentioned, adsorption and desorption heats of reaction are the same, but these are separate to illustrate how the equation is defined. The $Q_{LTS,ads.heat}$ is not in the equation as this low temperature heat is lost (emitted to atmosphere). The calculation is conservative, and some of the sensible heat in both beds could be recovered by employing heat recovery—this will be discussed in the discussion section.

To initially review the COP, equation (20) is applied. To simplify the calculation, the assumptions are as follows:

- There is no reaction while the system transitions between the high pressure and low-pressure stages—therefore a constant maximum amount of adsorbed mass of ammoniate is heated, and in reverse the minimal amount of adsorbate is cooled.
- Initial calculations focus on geometry and sizing, therefore no thermal mass of ends and shell, are considered. This will be revisited, but for the case of optimising a design these values are nominally set and appear as not a variable; the key consideration is tube vs active materials. By incorporating a bundle form, some of the thermal mass will be reduced — then a larger rig for the same bundle size will have a better performance as the ratio of the ends to active material will be reduced. Furthermore, a full-size system will employ heat recovery between two pairs of beds reducing the thermal mass effects of the shell and ends.
- The adsorbate/ammoniate is considered as solid ammonia for its properties, as in the heat transfer model in **section 8.1**, where this is explained.
- The active fraction is applied, so that there is an inactive mass equal to the theoretical mass that is not cycled; i.e. an active fraction of 0.8

equates to a cycle between 10 and 90% adsorbed stoichiometric mass, the same assumption as made by Lépinasse et al. (Lépinasse et al., 1994).

- Sensible heat is not recoverable in this process in any way. In practice, a small amount of sensible heating in the high temperature bed will contribute to heat recovered.

Drawing the Clapeyron diagram for the salt pair helps to clarify how this is calculated. The sensible heating ($Q_{LTS,heating}$, $Q_{HTS,heating}$) occurs during the phases where the temperature is changing up and down the isosteres. The key temperature points are identified by the markers seen in **Figure 42.**

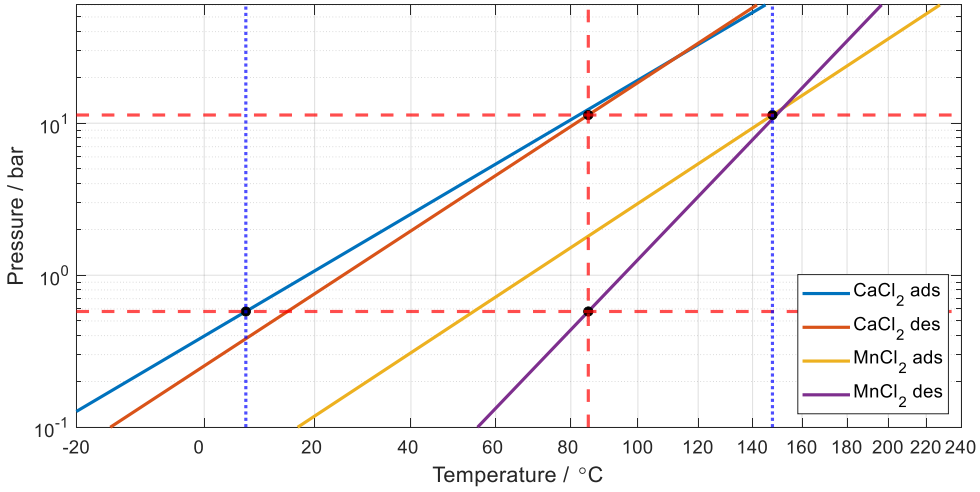

Figure 42 Clapeyron diagram for calcium chloride (8-4) and manganese chloride (6-2) pair, with a T_m of 85 °C

The calculations enable comparison of performance for different salt pairings. The operating temperatures and pressures for resorption are derived from the isosteres for the salt pairs observed in the LTJ tests. In practice, the isosteres would not cross at the high pressure and temperature conditions as this is impossible. The variables are the salt pairs, and the middle heat temperature. The middle temperature heat at T_m (which in this application is the waste heat, denoted by the vertical red dashed line), enables an upgraded heat temperature T_h (denoted by the right hand vertical blue dotted line) to be derived from the pressure at which the equilibrium changes for the Low Temperature Salt at T_m; and the heat sink

temperature T_l (denoted by the left hand vertical blue dotted line), is derived from the pressure that the equilibrium changes for the High Temperature Salt (HTS) at T_m. These form the high and low pressures respectively. This is represented in the cycle shown in **Figure 42**, where the horizontal lines are the pressures and the vertical lines are T_l, T_m, and T_h from left to right.

The calculation basis (mass) for calculating the COPs are tests SA, SB, and SD in

Table 2. The calculations were based on the low temperature salt (per mole of), to account for the different masses required for the paired salt (due to stoichiometry, and relative uptakes) a ratio can be determined to size the high temperature salt. This was done by calculating an equivalent length of samples required based on the same size of cell.

$$HTS_{length,factor} = \frac{(StoicheometricNH_{3,LTS} \times Mass_{LTS,sample}/RMM_{LTS})}{(StoicheometricNH_{3,HTS} \times Mass_{HTS,sample}/RMM_{HTS})}$$

$$Length_{HTS} = Length_{LTS} \times HTS_{length,factor}$$

The volume of salt is then calculated by the length times the sample CSA:

$$V_{LTS/HTS} = Length_{LTS/HTS} \times \left(\frac{(\pi \times 33.6 \times 10^{-3})^2}{4} - \frac{(\pi \times 12.7 \times 10^{-3})^2}{4}\right)$$

The lengths could be swapped for masses or number of samples (of unit length 9.5 mm). From this basis a mass of ENG and salt can be calculated for the high temperature bed as a function of the low temperature bed. The total volume is calculated from the mass fraction of salt per volume, denoted

as a density factor ρ'; rather than a real density, salt per volume of composite.

$$Mass_{HTS,salt}(LTS) = V_{HTS} \times \rho'_{HTS,sample}$$

N.B. these calculations were done based on two samples mass of the LTS, and an equivalent length of HTS required was scaled from this. This was done using empirical data for two samples that was obtained from shell side tests. Later work has calculated a COP based on expected lengths and total masses, some work was done evaluating a percentage of shell material heated (or shell heated a percentage of the ΔT); when the percentage was 0%, i.e., the same calculation as this but for a real length, the values returned the same COP results.

To then account for sensible heating, a mass ratio of stainless steel for the tubes can be calculated from the respective lengths as illustrated by the cell in Figure 41. This is presented for the basis of ½" tube, at 12.7 mm outer diameter. The calculation for the HTS reactor is shown:

$$Mass_{HTS,steel} = \left(\frac{(\pi \times 12.7 \times 10^{-3})^2}{4} - \frac{(\pi \times 10.88 \times 10^{-3})^2}{4}\right) \times Length_{HTS} \times \rho_{steel}$$

$$Mass_{HTS,water} = \frac{(\pi \times 12.7 \times 10^{-3})^2}{4} \times Length_{HTS} \times \rho_{water}$$

This presents a mass of a cell (calculated on a basis of LTS mass), the sensible heat and a reaction heat can now be calculated. The reaction heat is a function of all the masses and the specific heats of each component. The water mass is assumed a stagnant mass of water within the tube. The sensible heat is accounted for heating or cooling, when the process transitions between the high pressure and low pressure phase.

$$Q_{sensible\ heating,HTS} = \Delta T\big(Mass_{HTS,salt}C_{p,HTS} + mols_{\cdot NH_3,(ads)}C_{p,\cdot NH_3,(ads)} + Mass_{HTS,steel}C_{p,steel} + Mass_{HTS,water}C_{p,steel} + Mass_{ENG,HTS}C_{p,steel}\big)$$

$$Q_{Gas\ heating} = \Delta T(P_{eq}) \times (mols_{NH_3,(g)} \times RMM_{NH_3} \times C_{p,NH_3,(g)})$$

The sensible heating (or cooling of desorbed gas) can be calculated from the temperature difference between the reaction points at the high pressure or low-pressure phase. The reaction heat is calculated from the heat of reaction multiplied by the amount of material reacting, a molar basis was used.

$$Q_{Reaction\ heat,HTS} = \Delta H_{reaction,HTS} \times Mols_{NH_3,(g)}$$
$$Q_{Reaction\ heat,LTS} = \Delta H_{reaction,LTS} \times Mols_{NH_3,(g)}$$

The final COP can then be calculated from equation (20).

The most evident application for a transformer is the recovery of heat from steam condensate and transforming it to produce further steam. Absorption transformers typically raise heat from around 70 °C to 140 °C (Cudok et al., 2021), the aim is to have a lift in this range, similar to that proposed by Hitachi in **Figure 3**, recovering heat below 100 °C and raising it to a temperature to raise steam. To ensure heat transfer and a driving force for reactions, heat should be provided 10 °C hotter and emitted to 10 °C lower than the reaction temperatures. Therefore, as a rule of thumb T_m, the middle temperature which the waste heat is provided at is taken at ≤ 85 °C, and T_h must be high enough to raise steam. For a transformer to be applicable in the UK it needs to be able to expel heat at T_l to the UK climate. As a basis the hottest daily average temperature for the warmest month taken from Coventry UK is 21.6 °C (MetOffice), so for proof of concept approximately 30 °C is suitable; we will revisit the temperatures in the discussion section.

An evaluation of the sizes can be seen using manganese chloride and calcium chloride pair, considering different tube sizes in **Table 7**. In the case of index a) the actual composite would be 5.3 mm thick (the difference in radii rather than axial length of sample), which is too thin to push onto the tube with the same tightness and equivalent contact.

*Table 7 COP evaluations for different sizes, all cases are manganese chloride (6-2) and calcium chloride (8-4) pair at 85 °C T_m, with the equilibrium data from the LTJ. The conditions are the same as the last case (i) in **Table 8**. *Final selected sizing*

index	Tube OD (Cell ID mm)	Composite OD (mm)	COP	Volume of Cell (m^3)
a)	25.4 (1”)	36	0.197	0.00051
b)	25.4 (1”)	40	0.238	0.00075
c)	19.05 (3/4”)	36	0.293	0.00073
d)	19.05 (3/4”)	40	0.317	0.00097
e)	12.7 (1/2”)	33.6 *	0.356	0.00076

Table 7 results show that for the relative volume the ½” tube at 12.7 mm ID for the sample, has high relative COP. A larger volume of cell presented with index d) in a greater tube size has a lower COP, illustrating how although an increase in tube size may increase the SMP, even at the larger volume the COP is reduced by the greater thermal mass of water (SMP values can be seen in **appendix 8.12**). A ½” tube or 12.7 mm inner diameter sample presented the best option for COP; and after assessing the peak SMP the final size was produced, which proved reasonable when tested for peak SMP, and gives the value presented above in **Table 7** for COP.

5.2.1 Effect of Hysteresis on COP

The calculations for the COP used a basic MATLAB program to first derive the temperatures and then sum the heating effects and account for the thermal mass. The isosteres are plotted which show the temperatures and elucidate some of the challenges in **Appendix 8.10**. The resultant COPs and operation temperatures can be seen in **Table 8**. These values are calculated with the isosteres from the LTJ and the heat of reaction derived from the ITC.

Table 8 COP and temperature calculations for different pairs (with single reactions); equilibrium data from LTJ. calcium chloride as the LTS is (8-4) reaction and as HTS (4-2) reaction. (iv) is barium chloride calculation with single equilibrium line. The COPs are calculated for a 32 mm hexagonal sample, the final sizing.

	Pair (LTS + HTS)	T_m (°C)	T_h (°C)	T_c (°C)	COP
(i)	$CaCl_2$ + $MnCl_2$	70	127.5	-8.7	0.221
		80	141.1	2.0	0.209
		85	148.0	7.4	0.203
(ii)	$BaCl_2$ + $MnCl_2$	70	176.5	-15.7	0.192
		80	199.9	-6.9	0.159
		85	212.1	-2.5	0.141
(iii)	$BaCl_2$ + $CaCl_2$	70	118.5	26.1	0.372
		80	139.0	34.5	0.352
		85	149.6	38.7	0.342
(iv)		85	136.3	38.7	0.366

Looking at the initial results from **Table 8** and the plots in **Appendix 8.10** the resultant COPs and temperatures are lower than one would like, and generally the values for T_c are of some concern. The pair barium chloride (8-0) and calcium chloride (4-2) show the isosteres crossing in **Appendix 8.10** in **Figure 78**, which is impossible. If just the adsorption line is used for the calculation for a T_m of 85 °C it produces a higher COP, this is because the lift is slightly reduced and there is less heating of the gas between beds. This can be seen in a construction in **Figure 79** and is shown indexed in **Table 8** as *(iv);* the real result should be somewhere in the middle.

5.2.2 Reduced Hysteresis Effect on COP

It may be that the effects of hysteresis will be reduced in a full scale machine as suggested by van der Pal and Critoph who observed 'little to no' hysteresis in a full scale calcium chloride reactor (van der Pal and Critoph, 2017). To evaluate the hysteresis effect on the COP, and consider the enhancement of performance if it can be reduced, COP calculations have been performed using isosteres obtained from the ITC tests for the equilibrium lines (rather than from LTJ data). These calculations can be seen in **Table 9.**

Table 9 COP and temperature calculations for different pairs (with single reactions); equilibrium data from LTJ. Calcium chloride as the LTS is (8-4) reaction and as HTS (4-2) reaction. The COPs are calculated for a 32 mm hexagonal sample, the final sizing.

	Pair (LTS + HTS)	T_m (°C)	T_h (°C)	T_c (°C)	COP
(i)	$CaCl_2$ + $MnCl_2$	70	133.8	17.9	0.213
		80	148.2	25.6	0.196
		85	155.5	29.5	0.188
(ii)	$BaCl_2$ + $MnCl_2$	70	169.6	3.0	0.215
		80	185.4	9.9	0.200
		85	193.3	13.3	0.191
(iii)	$BaCl_2$ + $CaCl_2$	70	110.4	36.7	0.394
		80	122.4	44.5	0.389
		85	128.5	48.4	0.386

The equilibrium lines used to produce the results in **Table 9** can be seen in the constructions in **Appendix 8.11**. The equilibrium lines tend to cross, but this provides an estimate at the effect of reduced hysteresis with real data. Real results may not be this good, but this elucidates the effects of the hysteresis. The hysteresis does impact the COP results (lowering them); this is due to the increased *ΔTs* between points and therefore more sensible heating of gas and solids, as all calculations used the same heats of reaction. The main effect of hysteresis is to impact the operational envelope, making temperatures potentially impractical. More work may be required in reducing the effect of hysteresis.

5.2.3 Calcium Chloride, (8-4) and (4-2) Double Reaction

It may be possible that both phase changes can be used from calcium chloride. This is not something discussed by Goetz et al, when they discuss the concept and propose salt pairings (Goetz et al., 1993). The challenge to implementing two reactions is to understand and manage what occurs during the transition between the two reactions. The HTS will be adsorbing, so there could be a pressure drop which could affect performance, but the high *ΔT* should drive the LTS reaction onward. The question will be revisited in the **discussion section 6**. The value of utilising both reactions is that it will

raise the energy density in the LTS bed and reduce the thermal mass required to be sensibly heated, thus raising the COP. An example of what this may look like can be seen in **Figure 43**. The COP calculation results are presented in **Table 10.**

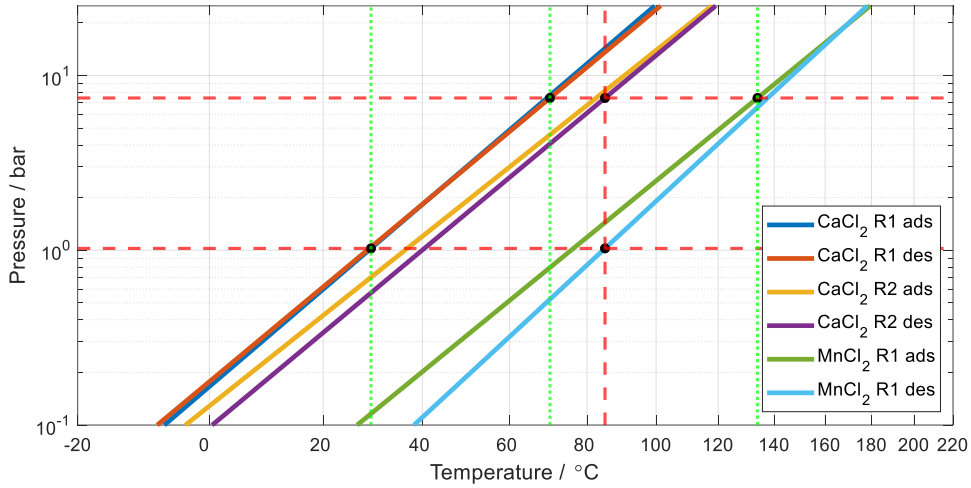

(a)

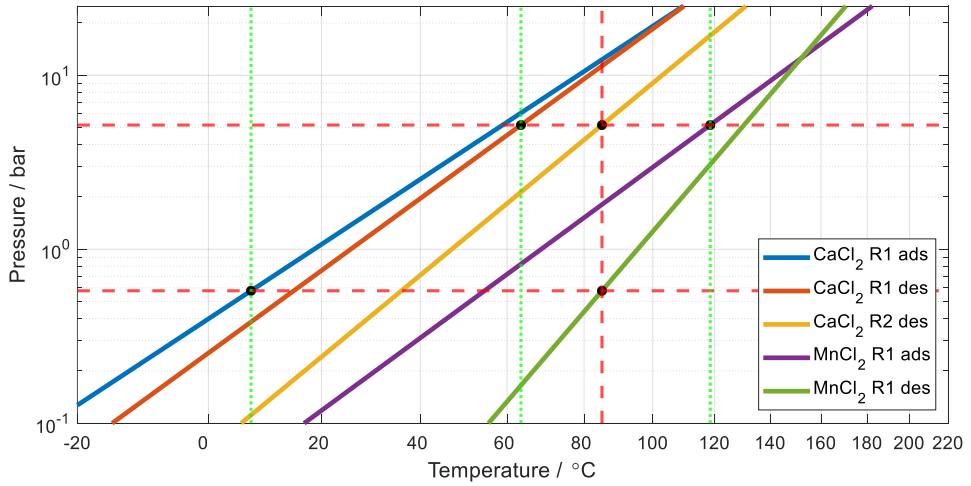

(b)

*Figure 43 Clapeyron relationship construction, for the pairing of calcium chloride and manganese chloride, utilising both calcium chloride reactions. T_m = 85 °C: (a) Plotted with equilibrium lines from the ITC; (b) plotted with the equilibrium lines with hysteresis from the LTJ. Plot (a) is plotted in **Appendix 8.10** with the adsorption line of reaction two, the hysteresis is so extensive it interferes with the visibility of this plot but this is of interest in its own right.*

The calculations use the higher values of T_m (85 °C), as this is the only case that presents a reasonable value for T_c. Because it uses the (8-4) reaction, and the way the temperatures are calculated, the other T_c values can be inferred from the results in **Table 8** for both calcium chloride reactions paired with manganese chloride. Using the LTJ equilibrium data: when T_m is at 85 °C, T_c is at 7.4 °C which is too low. But again, the reduced hysteresis

results present a case to be optimistic. An interesting observation is in the plot with both reactions showing hysteresis in **Appendix 8.10**, the adsorption line of the second reaction comes close to the adsorption line of the first reaction—this would not be an issue in practice, as both reactions occur and the driving temperature is 10 °C lower than the lower line—but the extent of the hysteresis in the (4-2) reaction is notable.

*Table 10 Double calcium chloride reaction COP calculation results using ITC obtained equilibrium lines. *Obtained with LTJ equilibrium lines which exhibit the hysteresis.*

Pair (LTS + HTS)	T_m (°C)	T_h (°C)	T_c (°C)	COP
$CaCl_2$ + $MnCl_2$	80	127.4	25.6	0.340
	85	134.0	29.5	0.335
*$CaCl_2$ + $MnCl_2$	80	112.0	2.0	0.361
	85	118.7	7.4	0.357

What can be seen in **Table 10**, is the calculations with reduced hysteresis have a lower value, this is due to the sensible heating term in the numerator in equation (20). The value of sensible heating appears reduced as the hysteresis reduces the delta T in the calculation.

Only the pair calcium chloride and manganese chloride are considered for the two-reaction option. Calcium chloride (with both reactions) cannot be used as a HTS as it would produce heat at two temperatures. The calcium chloride and manganese chloride pairing is of note because the resultant values of COP are well within the range of absorption transformers if they can be obtained.

6 Discussion and Design of a Resorption Thermal Transformer

The large temperature jump experiment has proven effective at observing the reactions between salt-ammonia, noting behaviours previously missed in gravimetric testing. Developments in the testing have also been important, with the ability to obtain an accurate heat of reaction (something

not previously achieved). Furthermore, the ability to measure the wall temperature accurately ensured that silicone oil could be used as the heat transfer fluid and enabled testing over a broad range of conditions. This was important in obtaining equilibrium data and an understanding of reaction behaviour at temperatures applicable to resorption transformers. The value in the presented LTJ design is its simplicity, which creates a basis for modelling and understanding the reaction kinetics. The system can now be used to rapidly test and evaluate different salts or salt mixtures, for future systems. The results obtained for barium chloride, calcium chloride, and manganese chloride are an important step towards the realisation of resorption systems.

The experimental results show the reaction rate (for this composite ENG sheet and halide salt) is limited by the rate of heat transfer. This limitation is characterised by a linear pressure change during the adsorption and desorption reactions. It was observed that adjusting the model terms n and A_r have limited effect on reaction rate but influence the shape of the plots, in particular the sigmoidal shape of the temperature curve. The wall heat transfer resistance—modelled by an ammonia gas-filled gap—was observed to have the greatest effect on reaction rate, illustrating how it is limited by rate of heat transfer. The findings and those to be discussed in this section, suggest that improving the heat transfer—primarily the contact resistance or gap, and the fluid to tube—will have the greatest prospect of further enhancing resorption system potential.

The model produced by Professor Critoph has proven effective at simulating the behaviour of the reactions, and the application of it in this work has identified reaction kinetic parameters enabling optimisation of composite dimensions for resorption systems. Mazet and Amouroux suggested the constants n and A_r in their model have no physical meaning and are pseudo in nature (Mazet et al., 1991). They present a range of values for the constants under different conditions, i.e., they are not truly constants. The work in this paper, as well as other work on improved composites such as by

An et al. (An et al., 2020a) illustrates more accuracy in the prediction of global rates of advancement by similar empirical kinetics functions, with unchanging constants. This is likely a product of better composite materials used, and better experimental instrumentation. The evidence makes further sense when the reaction behaviour is also considered. For example, the ENG matrix ensures a relatively even distribution of grains at a small and constant size while providing void pathway for the gases, and also being highly conductive with effective contact with the small grains of salt inside. When the model results are compared with the modelling by Lu, et al. which incorporates chemical kinetics, mass transfer into the grain, and heat and mass transfer within the grain; reaction times of hours are observed (Lu et al., 1996). The processes observed testing these salt composites in the tube-side LTJ, show short reaction times between 5 and 15 minutes with a linear reaction rate limited by the rate of heat transfer. This shows empirically that the reaction rate (within a somewhat homogenous conductive matrix) is dominated by the deviation from the equilibrium conditions, i.e., the temperature or pressure difference, and this is the dominant component of any kinetic function. This correlates with the limited effect of adjusting n and A_r, only affecting the curvature of temperature and pressure profiles into and out of the constant rate of change.

This makes further sense when the monovariant nature of the reaction is considered; once the equilibrium conditions are overcome, the reaction proceeds in one direction at a constant rate until completion as long as the driving force is maintained. Therefore, the simple advancement model (equations 33 & 34—**appendix 8.1.2**) will predict reaction kinetics for a resorption machine—as the rates of the processes will be driven by deviations from equilibrium conditions due to a change in system pressure, or imposed boundary temperature due to heat transfer. The composite material in these experiments performed well, reducing the rate limiting effects to the thermal resistance between the stainless-steel tube and the composite. The model would appear to predict the reactions for any driving

temperature as long as the initial superheating or subcooling effect is overcome so that the reactions initiate. These results suggest that the rate constants are truly constant for the application of salt when impregnated in ENG. This provides a good basis for designing a full-size generator since it is now possible to consistently predict the rate of reaction. The findings (about deviation from equilibrium conditions) further highlight the importance for future work to consider the heat transfer from fluid to the tube. Ensuring the heat transfer resistance between fluid and tube is reduced will be key to achieving a machine with good performance.

The observation of the metastate is important in understanding some of the hysteresis phenomena. When we consider equilibrium data published from gravimetric methods, these will show further hysteresis as the phase change will appear to occur at the peak (metastate) conditions and not the actual reaction temperature. Reduction or removal of the metastate could in part reduce the hysteresis. Observing accurate conditions for the reaction equilibrium (after the metastate) has been particularly important for simulating the reaction behaviour which has ensured ΔT values used are accurate.

When testing a resorption device, an important consideration is the level of hysteresis that is exhibited. If as some work suggests it will be reduced (van der Pal and Critoph, 2017), that will be important to ensure reasonable operating temperatures. Future work should consider how to reduce the hysteresis.

The active fraction found suggests that around 80% of the salt readily reacts to form an ammoniate during a cycle, for the three salts tested this appears a rough rule of thumb; this also aligns with the proposed conversions presented by Lépinasse et al. (Lépinasse et al., 1994). Identifying the oxide in manganese chloride—which isn't routinely discussed—was important for this work, the details can be found in **Appendix 8.2**. The observation was that incorrect preparation using anhydrous form of manganese chloride, leads to a brown oxide forming which affects active fraction. This was further

observed with samples left exposed to moisture from the air, with the effect of reducing the active fraction. This could also be observed in samples left in the oven for extended periods. This is important for preparation at scale as the number of samples required and the process of manufacture, could lead to lengthy exposure and oxide forming—reducing system performance. Further understanding the active fraction is important, and future work may find that different salts such as iodides have different values, or that the active fraction can be improved.

An important finding was a unified heat of reaction; previous work has not identified this. This could be the reason why work such as by An, et al observed up to ± 20% deviation in their simulation (An et al., 2020a). Having a unified heat of reaction means that COP can be estimated accurately for the first time. It is not clear how some of the COP calculations in the literature (discussed in **section 2.5**) were performed; the full-scale machines did not use dynamic data, so calculations lacked a measure of heat flow into or from the reactor, and the test cells in baths could not measure heat flow. Testing the design presented below can be used to evaluate a dynamic COP from measuring the heat in and out, and calculations can be done to understand if or why there is a drop in performance.

In the literature, two reactions in one salt (such as with calcium chloride 8-4 and 4-2) are discussed as occurring simultaneously. In some of the adsorption tests for calcium chloride, this effect can be noted. However, the model simulations predict one reaction then the other, which is perhaps expected with the homogenisation of the material that occurs within a finite difference model. It is hard to understand whether if the conditions are overcome for both reactions, if they actually occur simultaneously. In the ENG-salt composite, the conditions locally may overcome the requirements for the second reaction, this could mean a large salt grain is undertaking the first reaction, while a smaller grain could be undertaking the second reaction (after having finished the first). Presumably on a molecular level the first reaction is always a prerequisite for the second. This touches on chemistry

and crystallography and is perhaps a topic for chemists to consider in the future, but for the basis of applying the useful heating effects, the empirical modelling performed here works very well.

The approach to sizing presented what is effectively a trade-off between the COP and the peak SMP. Trial and error was applied to finding a sizing, by predicting the performance and evaluating the potential COP, before the resultant sizes were tested in the shell side LTJ to ensure results were effective. Improvements in the thermal contact between the sample and the tube and the heat transfer from the fluid to the tube, improved the peak SMP result observed in tests. Analysis of the values and discussion are presented in **section 6.1.**

6.1 Optimising Composite Dimensions

Shell-side tests have further validated the model, and the shell side LTJ is another key tool that can rapidly evaluate salt contenders for future systems. Using the heats of reactions identified with the ITC testing, and with the LTJ data, it is possible to estimate and consider optimal dimensioning. In the literature review, the resorption machines that have been tested are not published with their basis of design, they are usually built and then evaluated. Lepinassé was perhaps the most effective in system design and testing, with promising COP results (Lépinasse et al., 1994). But resorption as a concept has failed to advance since those tests in the ‘90s. The more contemporary work has focussed on more novel and complex systems, but has not addressed the challenges detailed and observed by Lepinassé. The concept of resorption is well proven and even further complex applications have proof of concept. Similarly different ammonia-salt systems have not advanced towards prototype systems. The reason significant advances have not occurred in the field of chemisorption is due to the lack of accurate modelling for optimising designs, and the omission of important data such as thermal masses of fluids. The absence of thermal mass reporting is well discussed by Gluesenkamp et al. (Gluesenkamp et al., 2020). Following from

Gluesenkamp et al. this work focuses on addressing some of these issues by discussing a system design and method in a transparent fashion.

As discussed in **section 5.1 and 5.2**, producing a final size of reactor was an iterative process and the intention was to present a size and geometry of composite adsorbent that met the objectives for COP and peak SMP. When considering different sizes, particularly bigger tubes, the samples had to be robust enough to not break, particularly when pushed onto the tube to ensure tightness as shown with testing in **section 4.3.4**, meaning there was a minimum thickness for a sample. When considering peak SMP, the initial result in **Figure 40** was not great enough and the driving temperature was greater than the specified 10 °C driving temperature, highlighting the need for considerations into heat transfer. The greatest peak SMP or power density comes from fastest reaction; as rapidly delivering the heat raises the power (and of course the peak). This is done by improving heat transfer as stated; this gives rise to the conclusion that a thinner layer of material provides a greater SMP. This is due to the relative heat transfer area increasing, thus improving rate of heat transfer. This can give rise to the assessment that increasing the tube size for the same volume of composite will bring optimal results as the relative heat transfer area is increased. On this basis when considering only the SMP, the optimal performance would come from an infinitely thin layer of composite. This is because it would react instantaneously and deliver its heat at the same rate. However, this assessment is to the detriment of the COP as such a system would have a COP of 0. The low COP would be due to the dominating effect of the thermal mass. For realistic tube sizes, the approach to increase relative tube size and heat transfer area decreases the COP to unsuitable levels as the results show in **Table 7**. One can see that at similar cell volumes the ½" tube produces a reasonable COP, at a reasonable volume of material. The challenge is to ensure that this is married with a SMP that is attractive.

To enhance the heat transfer the steps were taken as shown in **section 4.3.4**, to improve the composite-tube contact, and fluid turbulence in the tube

whilst measuring the fluid temperature. The silicone oil previously used as the heat transfer fluid, had a working range of -10 to 190 °C. But due to its viscous nature, its flow was laminar and therefore measuring the fluid temperature accurately in and out of the reactor would have been difficult. To measure the fluid temperature and to improve heat transfer, the heat transfer fluid was changed from oil to water. CALGAVIN hiTRAN® Thermal Systems tube inserts were also employed to increase turbulence, improving heat transfer and ensuring accurate temperature readings.

To evaluate the effects of the heat transfer improvements, samples were tested for their peak SMP during cycles, for sizes with COPs in an acceptable range. The final size settled upon was a 32 mm hexagon A/F (across flats) that was tested for its SMP to ensure the final chosen size was effective. This was tested in the shell-side LTJ with the resultant peak SMP (test SC

Table 2). The mass of salt was 3.095 g and the mass of ENG was 2.008 g in this sample. The sizing of the sample can be seen in **Figure 47**. The sample was again cut with the 11.9 mm hole saw.

When the 32 mm hexagon results were simulated, the peak SMP was about 1.4 kW/litre, which was a marked improvement in result and can be seen in **Figure 44** (The raw data is shown in **Figure 38**). The peak at 1.4 kW/litre can be seen at around 160 seconds, the initial spike in the plot is before the reaction begins. It is also of note that during the reaction the value for SMP is relatively constant, this suggests the heat was delivered during the cycle at a continuous rate, which is preferable for operation and an interesting observation.

The program (temperature change) simulation for the same sizing can be seen in **Appendix 8.12,** the same sample masses and size were evaluated against the 10 °C change over 40 seconds; this shows the overestimate of this calculation. This predicted an SMP of 1.92 kW/litre as shown in **Figure 45**. To test with no resistance, the gap was then reduced to zero; this presents an ideal performance, and produced a peak value at 2.2 kW/litre. If heat transfer on both the fluid and tube side could be improved, something nearer to 1.9 kW/litre would be the aim, ensuring a high-power density to maintain the appeal of the technology. Furthermore, the sizing of composite will need to increase to produce a more attractive COP.

It is not clear as to how either heat transfer resistances could be reduced further but marginal gains could be possible, and newer designs with enhanced heat recovery could present larger ratios of salt composite to thermal masses which will enhance resulting COPs.

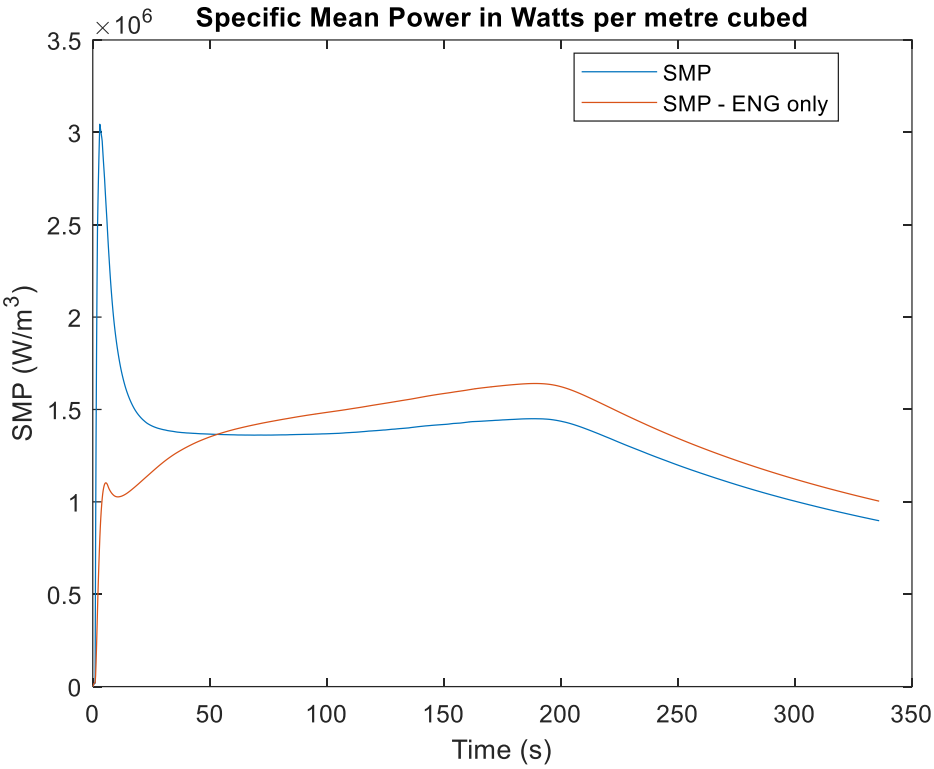

(a)

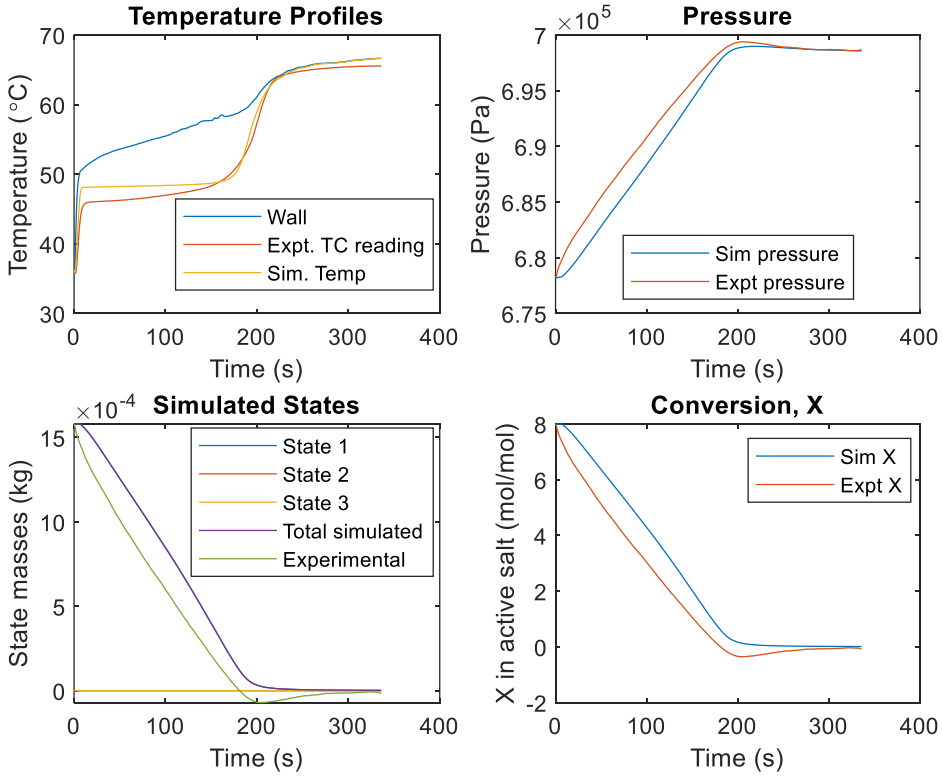

(b)

Figure 44 Results and simulation for 32 mm hexagon, the simulation uses the 33.6 mm circle as its basis and also how the SMP is calculated. The initial peak is not the reaction heat. The steady subsequent value greater than 1 kW/litre is from the reaction. The peak SMP is in excess of 1.4 kW/litre

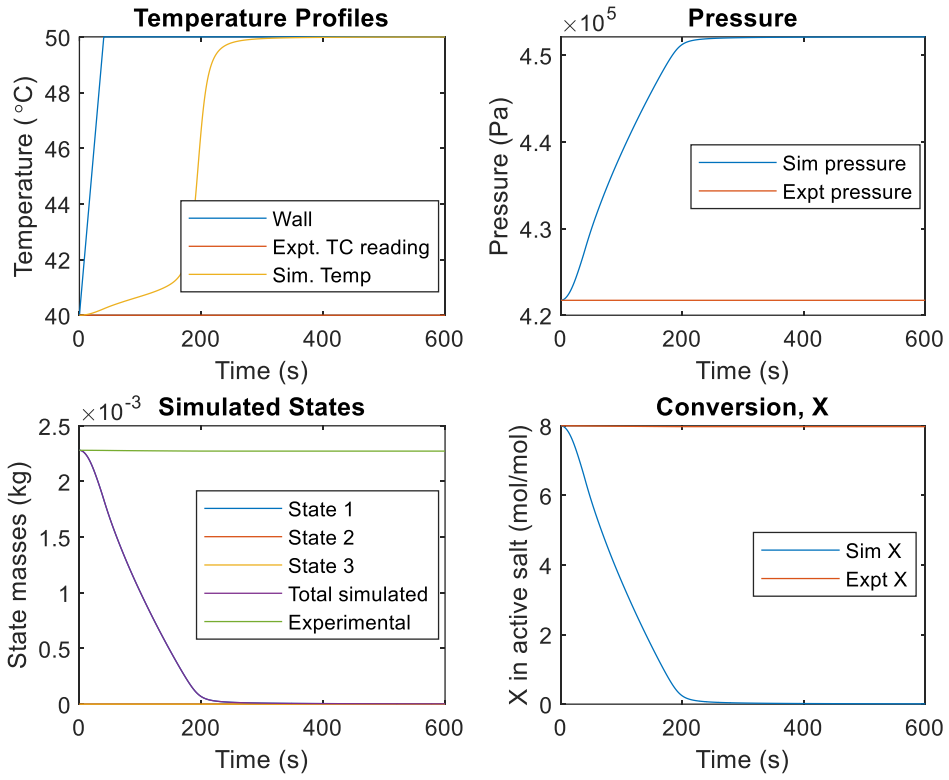

(a)

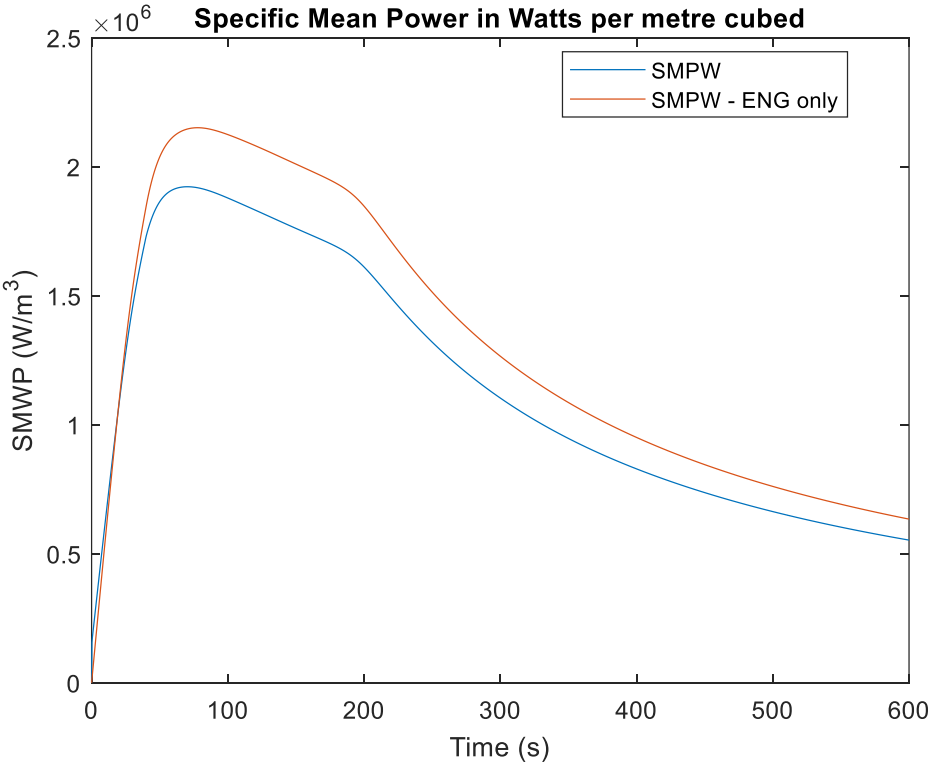

(b)

Figure 45 Program temperature change simulation for the 32 mm hexagon as illustrated in Figure 44. The simulation uses the 33.6 mm circle as its basis and also how the SMP is calculated. This provides a more optimistic performance value, as the 'wall' does not heat up as fast in practice. The peak SMP = 1.92 kW/litre

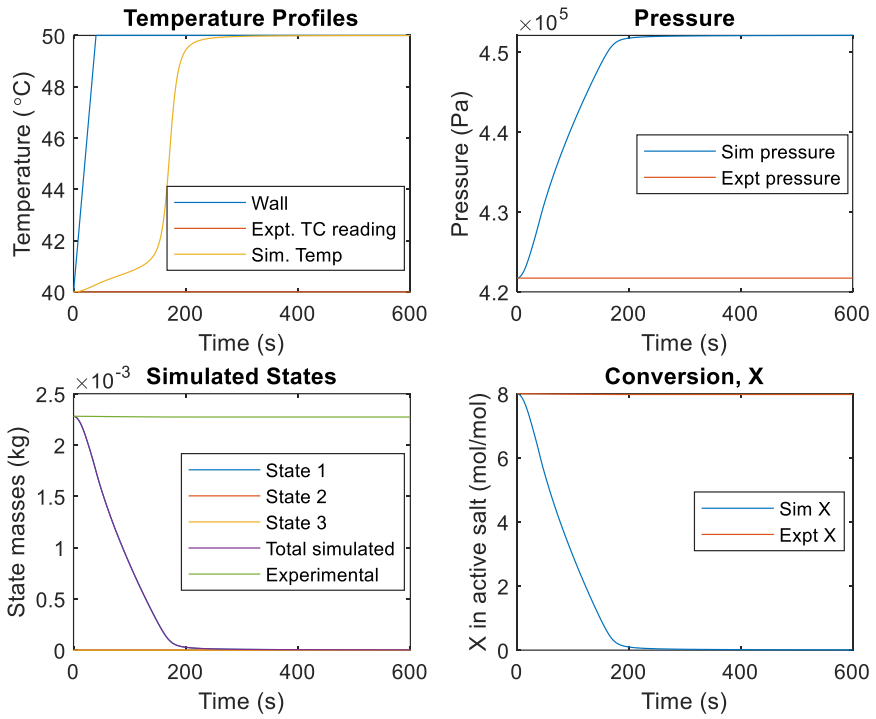

(a)

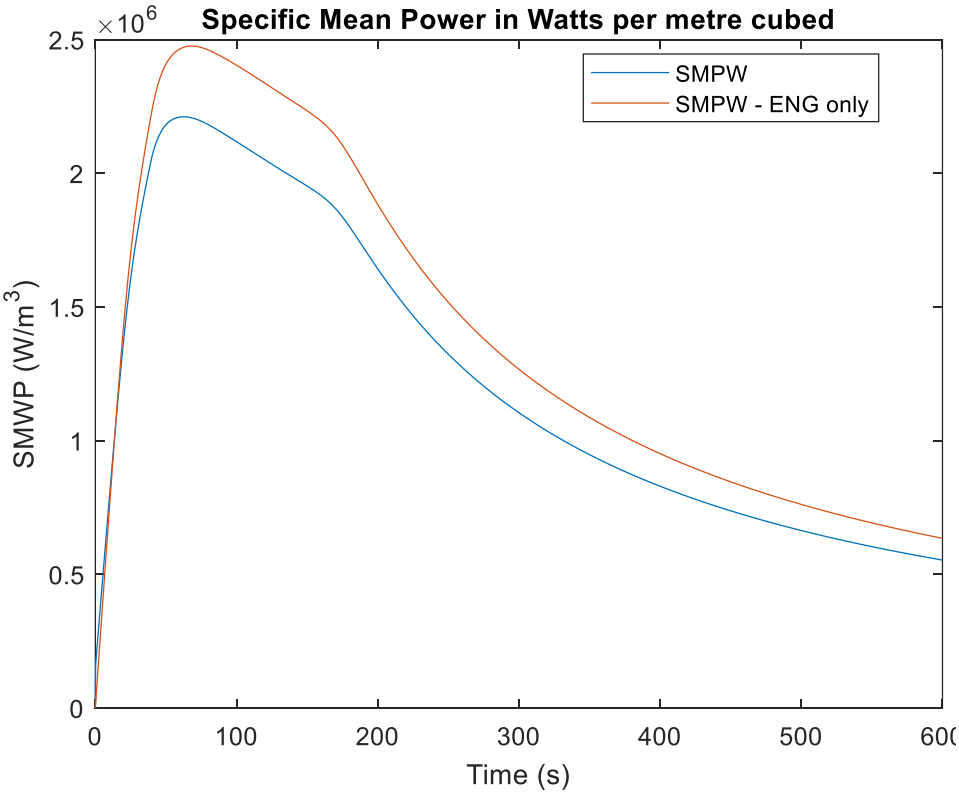

(b)

Figure 46 Program temperature change simulation for the 32 mm hexagon as illustrated in Figure 44. The simulation uses the 33.6 mm circle as its basis and also how the SMP is calculated. This time the gap is set to zero, this provides an ideal performance value. The peak SMP = 2.2 kW/litre

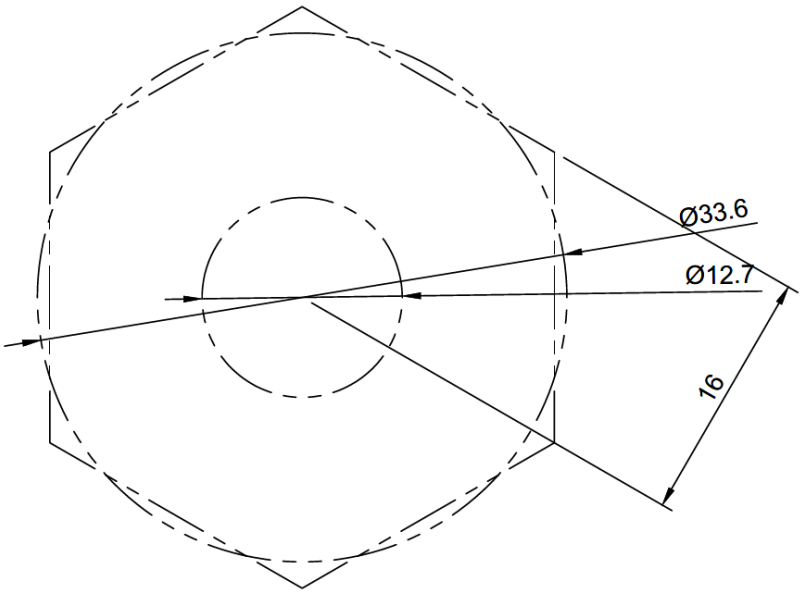

Figure 47 Diagram of 32 mm hexagon (16 mm apothem), taken as final sizing.

The result in **Figure 44** for the final sizing shows a driving temperature from the wall that is less than 10 °C. This is reasonable, but clearly the heat transfer from the fluid to the tube is an issue as the fluid ΔT is as much as 15-20 °C. The final sizing of a 32 mm hexagon (apothem 16 mm), provides a reasonable COP as shown in the calculations in **Table 7**. The size can be seen in **Figure 47**, as well as the circle with an equivalent area. A greater SMP could perhaps be obtained by improving the contact resistance with the material further. This could be done using graphite paint on the tube to reduce friction on the samples when inserted tightly on the tube, reducing the potential size of the ID hole further. It may be that with some empirical understanding of the gas channels and flow at low pressure, single plates which seven tubes fit into (rather than 7 discs) could be incorporated into the design, but the testing at this stage suggest pushing the material over a tube bundle may be impractical. It could also be that an improved tightness could be gained using samples that are not dosed, and then dosing the samples with salt on the tube, but care would have to be taken to assess performance as exposed surface area of disks may be key to salt uptake.

6.2 Sizing Reactors and Salt Pairings

6.2.1 Salt Pairing COP and Hysteresis

When considering the results from **section 5.2.** the pairs discussed here will require values for T_m to be 85 °C to provide temperature lifts to generate steam; these are in the range of the temperatures reported by Hitachi for their absorption systems on the market, discussed in the literature review (HITACHI, 2019). A heat source of 90-95 °C would be usable. The result in **Figure 44** does show promise but when considering the raw data (**Figure 38**) the fluid temperature was as much as 15 °C above the reaction temperature. This highlights the importance of considering the heat transfer in the future. As this section will discuss, the reduction of hysteresis may be key to ensuring T_m values are effective and could further improve performance. Also, as mentioned previously many times heat transfer improvements could reduce the driving temperature required ensuring these source temperatures work.

*Table 11 Pairings of salts from **section 5.2.** *Indicates calculations with hysteresis equilibrium data, other results use ITC data.*

Pair (LTS + HTS)	T_m (°C)	T_h (°C)	T_c (°C)	P_{high}(bar)	P_{low} (bar)	COP
*$CaCl_2$ + $MnCl_2$	85	148.0	7.4	10.1	0.6	0.356
$CaCl_2$ + $MnCl_2$	85	155.5	29.5	10.5	1	0.366
*$CaCl_2$ 8-4-2 + $MnCl_2$	85	118.7	7.4	5	0.67	0.411
$CaCl_2$ 8-4-2 + $MnCl_2$	85	134.0	29.5	7.5	1	0.417
*$BaCl_2$ + $CaCl_2$	85	136.3	38.7	12.3	5	0.416
$BaCl_2$ + $CaCl_2$	85	128.5	48.4	12.5	7.5	0.435
*$BaCl_2$ + $MnCl_2$	85	212.1	-2.5	45	0.58	0.364
$BaCl_2$ + $MnCl_2$	85	193.3	13.3	34	1	0.382

Table 11 shows all pairings which have been considered for a full-scale machine, with expected operating conditions and COP estimates based on the unit cell **Figure 41**. The results present the LTJ equilibrium data with hysteresis versus equilibrium lines from the ITC (with reduced hysteresis). Looking at the values in **Table 11**, one can see the effects of hysteresis in limiting whether systems can be realised. What can be observed is the hysteresis has a small effect on the COP values in the range of less than 5%, this is due to a change in sensible heating requirements (because of a change in the gradients of lines and therefore temperatures, and due to the form of the estimation). The main challenge of the hysteresis, is the changes in operation conditions at key points in the cycle. Specifically, the LTS desorption T_c and the HTS adsorption T_h. Because of the application as a transformer, the adsorption temperatures in the LTS and in the HTS are key to the performance of the system—this is where heat is emitted to rest the system or recovered after upgrading. The effect of the hysteresis is to cause

a large pseudo-equilibrium area, diverging where adsorption and desorption take place (the onset lines are moved apart with a greater difference in gradient. This leads temperatures T_c and T_h to the left of the Clapeyron diagram and at the same time T_m is effectively driven upwards/to the right, which is also a negative effect.

As stated, some of the hysteresis may be avoided (van der Pal and Critoph, 2017); this is a crucial factor to be monitored in any lab scale resorption machine when tested. In the large temperature jump, the rapid approach to the equilibrium may exacerbate the effects, particularly with the metastate that occurs. The conditions in the ITC are unlikely to be replicated in a full-size machine, but key to the ITC working was not completing the reactions. It would be interesting to consider whether a resorption machine could cycle within 95% of the active fraction, not completing either reaction, and what effect this has on the results. In a resorption machine, the majority of the time that the system is running is at the heat recovery high pressure point or the regeneration low pressure stage. In these conditions an equilibrium between both beds occurs where the mass adsorbed in the HTS is equivalent to the desorbed mass from the LTS. In essence this occurs under constant conditions, this could also reduce the hysteresis effects. Another prospect for the future, is that the addition of small amounts of another salt may reduce the hysteresis by weakening the crystal structure (akin to how impurities provide a point from which a lattice forms, or a weak point for it to break; pure water readily can be supercooled below 0 °C for example, impure freezes more readily). Manganese chloride exhibits extensive hysteresis and is a favourable HTS as these results show; therefore, reducing the hysteresis it exhibits would cause notable improvements. If it can be reduced, the pair calcium chloride and manganese chloride present the possibility of a system to compete with absorption transformers.

6.2.2 Length of Reactor

The 32 mm hexagon was observed as the optimal size at this scale based on SMP and COP considerations and was taken as a basis for design of the reactors for the resorption machine. The final value of SMP in kW/litre can be used to size a reactor. Using empirical data for salt uptake, and stoichiometric molar ratios for the reaction, it is possible to estimate the lengths of reactors required by other salts for the stoichiometric mass of ammonia desorbed—this provides a relative understanding of potential power densities (there is small difference in enthalpy values). The basis is the barium chloride samples (test SC), **Figure 47**. This produced a peak SMP of 0.7 kW/litre (this value comes from the 1.4 value observed, but halved as this drives the second bed and effectively halves the power density assuming equal bed size). The design is for a 3 kW resorption transformer therefore, 4.29 litres of barium chloride composite and tube is required. The calculations are as follows:

$$Power/SMP_{(peak)} = Volume_{reactor}$$

The SMP calculation included the tube and fluid volume, and is divided by the total cell volume to calculate the number of cells to derive a length (the cell illustrated in Figure 41).

$$\pi \frac{(33.6 \times 10^{-3})^2}{4} = Volume_{cell}$$

$$Volume_{reactor}/Volume_{cell} = Number\ of\ barium\ chloride\ samples$$

The number of barium chloride samples is the basis as the value of peak SMP was measured using barium chloride, but other salts volumes are calculated based on mass uptake and mass balance of ammonia adsorbed by them. As a rule of thumb, the salts' active fractions were 0.8 so the factor is equivalent across the calculations.

The calculation for the number of cells, presents a length of tube required. Initially this is a single tube length as shown in **Figure 48**.

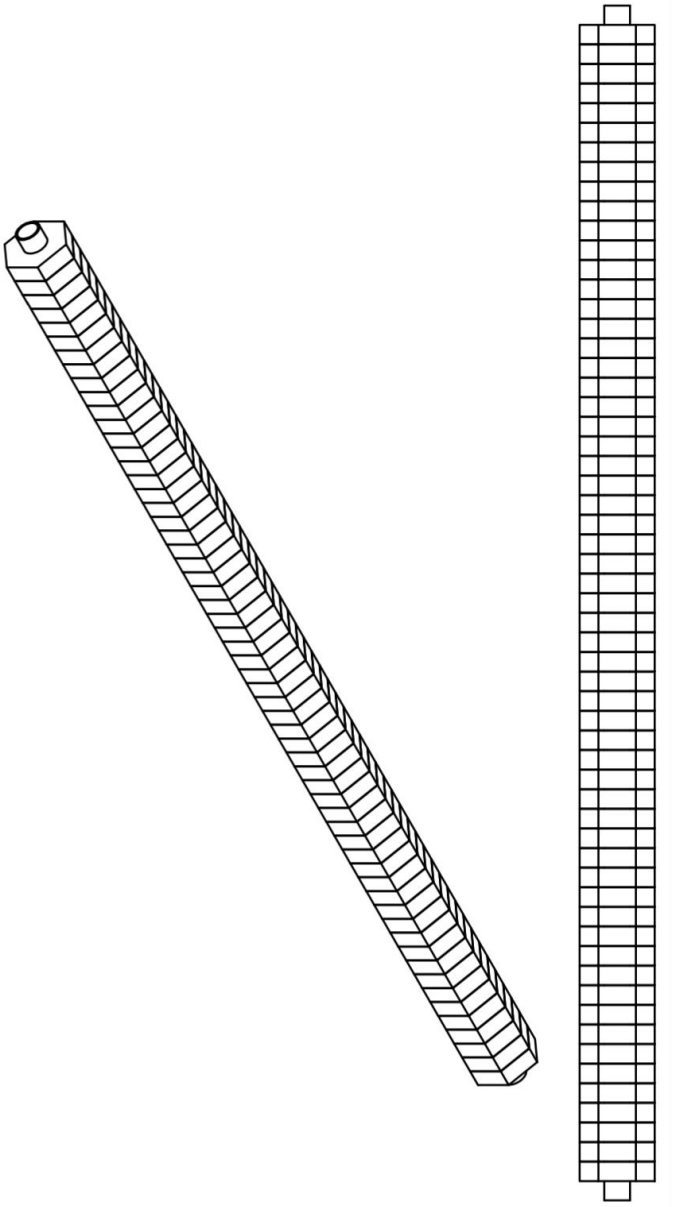

Figure 48 Initial calculation result is a number of cells, final value is just the length of cells and not the protruding tube, this sketch is taken from the drawing of the entire reactor but illustrates what is observed (not to scale, a 7^{th} of total required length seen here).

For practicality and to reduce some shell mass and void volume, the geometry will be a bundle of seven tubes rather than a single tube. Dividing the number of cells by seven and rounding provides a number (of composite samples) per length of tube in the bundle of seven, and an approximate initial length of reactor (before end of shell and flow distribution). This can be used to see how different salts have different power densities and the sizes required.

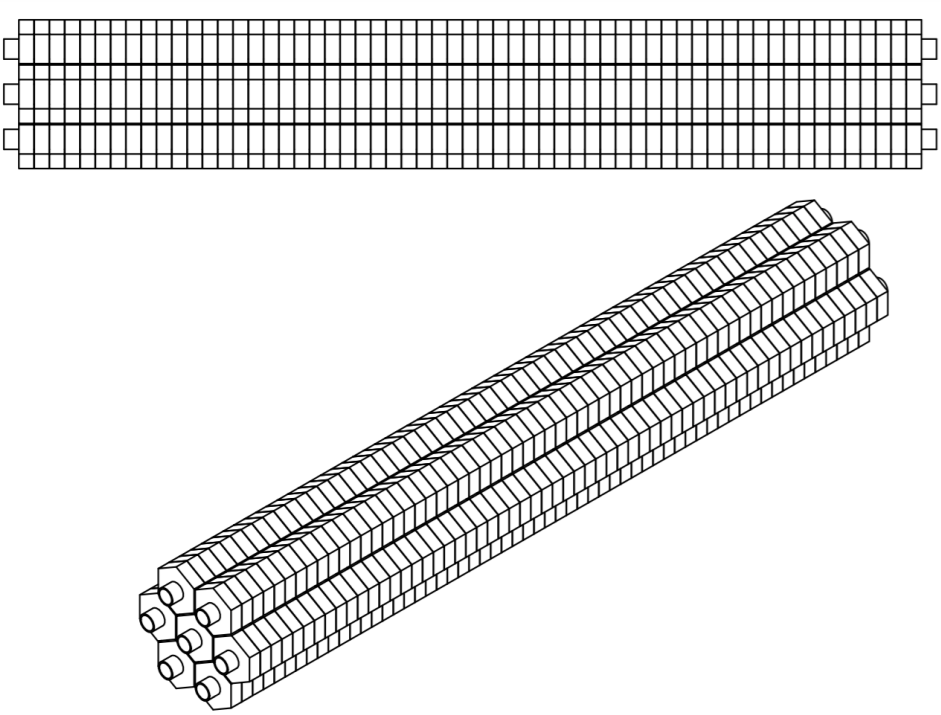

Figure 49 Bundle of tubes that forms reactor core. This drawing is to scale and is based on calcium chloride reactor that utilises both reactions.

The calculation basis is for barium, based on its measured SMP. Knowing the mass of salt expected per sample, a mass of required salt can be calculated, as well as a mass of ENG. Using measured data for the samples (mass of salt and ENG) is important because the true volume of material may be slightly different to the expected volume as the real hexagons may have some minor tapering due to the water jet cutting. The SMP is calculated from the expected volume, so no error for disc number can carry through the calculation and (in theory) sample preparation should produce on average the same expected mass uptake of ENG per volume. For this case, the calculation basis is the mass per disc ascertained by halving the value for (test SF) in

Table 2.

$$Mass_{BaCl_2} = Number\ of\ samples_{BaCl_2}/mass\ per\ disc_{BaCl_2}$$
$$mols_{BaCl_2} = Mass_{BaCl_2}/RMM_{BaCl_2}$$
$$mols_{NH_3} = mols_{BaCl_2} \times 8(stoichiometric\ ratio)$$

From the mass of barium chloride, a mass balance presents the mass of ammonia adsorbate. To ensure modularity of a test cell, this value should be equivalent for all beds henceforth and sized on this basis. Therefore, even if barium chloride is not a salt in use, two new salt reactors could be sized. A mass per disc is calculated for future salts based on dosing data obtained under usual conditions. For calcium chloride, this is as follows

$$mols_{CaCl_2} = mols_{NH_3}/stoichiometric\ ratio$$
$$Mass_{CaCl_2} = mols_{CaCl_2} \times RMM_{CaCl_2}$$
$$Number\ of\ samples_{CaCl_2} = Mass_{CaCl_2}/mass\ per\ disc_{CaCl_2}$$

This simply calculates the number of discs required to adsorb or desorb the same mass of adsorbate. This functionally defines lengths of reactors. The active fraction should be observed for future salts/salt mixtures in case this differs then the mass of adsorbate should account for this.

Dividing the number of samples by seven again, presents the number of samples required per tube. The ENG sheets appear to actually be 9.5 mm rather than 10 mm thick. Thus, multiplying the number of samples by this value presents the initial length based on active material.

The relative initial lengths of reactors have been calculated. This produces an idea of relative power densities of certain salts; more discs than barium chloride per tube, equates (relatively) to a lower power density.

Table 12 Number of discs calculated based on barium result for SMP

Salt	Number of Discs	Number of Discs per Tube	Mass of Salt (kg)	Moles of Salt (kmol)	Stoichiometric Reaction Ratio
*$BaCl_2$	509	73	0.787339	0.003781	8
$CaCl_2$ (4-2)	1266	181	1.678507	0.015124	2
$CaCl_2$ (8-4)	633	90	0.839254	0.007562	4

$CaCl_2$ (8-4-2)	422	60	0.559502	0.005041	6
$MnCl_2$	501	72	0.951628	0.007562	4

The relative lengths of tube required have been drawn up in CAD to illustrate the power density scale difference as shown in **Figure 50**. We can see that calcium chloride (4-2) reaction that could be used as a HTS would require a reactor length in excess of 1.7 metres, this is considerably larger than any other reactor, and can be assumed to have an exceptionally worse power density making it not suitable for practical use.

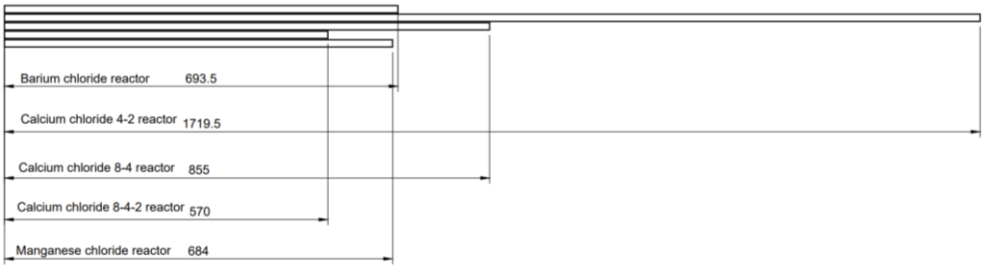

Figure 50 Relative reactor lengths calculated; the dimensions are millimetres.

The sizing of the reactor is not just based on the stoichiometric moles of ammonia the salt reacts with, but also the relative mass uptake of salt in the ENG, and furthermore the molecular mass. From the preparation method used this is intrinsically related to the solubility, and higher dosing could be produced perhaps if preparation occurs under conditions that raise the solubility. This could be from heating but saturation could lead to precipitation outside the ENG reducing uptake, if the solution cools while under vacuum.

The initial lengths presented here are just for active composite. Final reactor lengths will be longer to due ends to the shell and pipework. Fluid distribution and gas flow need to be considered and incorporated into the final lengths.

The low pressures that are noted in the calcium chloride and manganese chloride pair which can be seen in the Clapeyron diagram in **Figure 40** suggest that the ammonia mass velocity when the reactor bed begins desorbing could cause damage to the ENG matrix. To address this, a design

is proposed with gas channels to enable flow. The samples also swell on adsorption so this must be considered. Furthermore, the shell should be isolated from the hot gas that is being transferred during the reaction to reduce sensible heating. Insulation within the reactor is impractical and since much heat will be conducted from tubes and end plates to the shell, it may be ineffective and not reduce sensible heating to the shell. To overcome this a design is proposed as shown in **Figure 51**.

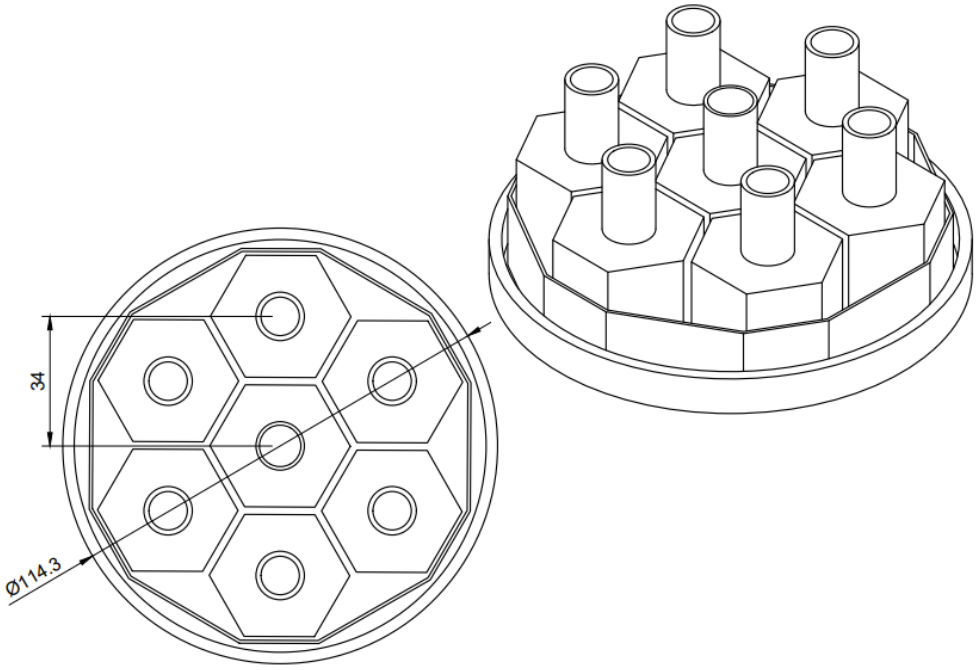

Figure 51 Engineering drawing of cross section of reactor, values in mm.

The design uses a folded aluminium sheet to isolate the gas channels which use the hexagon shape to create the triangular channels. At each end a narrow ring-plate—machined to form a tight fit—will hold the folded aluminium and ensure no gas flow or pathway external to the aluminium, keeping a stagnant gas volume to reduce heat loss. On the inside, the aluminium provides triangular gas channels. A pitch of 34 mm between tubes is proposed, this provides space for expansion of the 32 mm hexagons and some volume for gas flow so the central hexagon has access to the mass flow channels. The extra void volume of the gas channels and gas gap, is a relatively small increase as the ENG has a high void volume. The initial lengths defined in **Figure 50** are the lengths of active material. The final

length also includes: head space for gas, shell end plates, and a manifold that ensures equal flow distribution between the seven tubes. The manifolds are scaled based on a design calculated by George Atkinson, and are detailed later in this section. This additional end length can be considered as the same for each reactor regardless of active material length. Future work may optimise the dimensions of this further to reduce material, but extensive safety factors and ease of assembly are important at this stage.

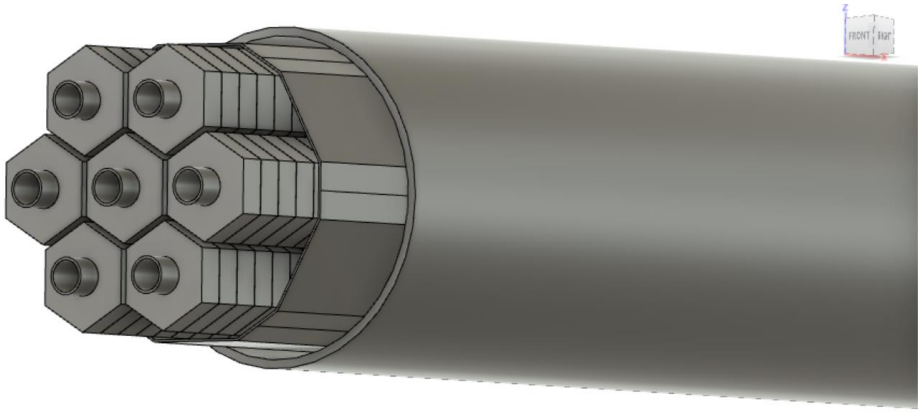

Figure 52 Diagram of internals of reactor, cut away. Isometric view shows the tubes, hexagonal disks around the tubes with spacing, aluminium folded plate, and shell.

Figure 53 Reactor end with ring plate sealing gas insulating gap. The aluminium plate is therefore hidden. Gas flow channels can still be seen.

The ends of the reactor appear as shown in **Figure 53**. To remove contact from the graphite there is one millimetre gap between the graphite and the ring, and an extra millimetre of folded aluminium plate on each end. An end void or head is maintained; with the length of plain tubes before the end plate, whose length is equal to the thickness of the shell. Structural stability comes from the welding of the end plate to the tubes.

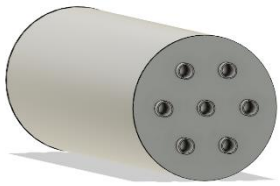

Figure 54 Reactor with end plate

To split the flow between the seven tubes a distribution manifold has been machined, this is based on a design produced and calculated by George Atkinson for a carbon ammonia reactor also using ½" tubing. The design constitutes two plates that clamp together with an orifice plate in the middle, the outer plates seal

with bolts and an O ring around the external perimeter and any nuts within to ensure no leakage. The orifice was defined to split the flow between 6 channels and the orifice, the cross-sectional area is equal across each but the radial dimensions are extended to fit this geometry. The result is an equal flow rate of pressurised water in all seven tubes, with a differing pressure between the outer tubes and inner tube. The manifold as acknowledged, was designed by Mr Atkinson and then replicated with scale adjustment for this design. It is included in the thesis due to its relevance for complete design and inclusion in thermal mass considerations.

The basic reactor is then formed of all these components. The final reactor will have a welded tube to the shell to connect to the other reactor, and inside the fluid tubes there will be CALGAVIN hiTRAN® Thermal Systems tube inserts, as described in the heat transfer improvements section.

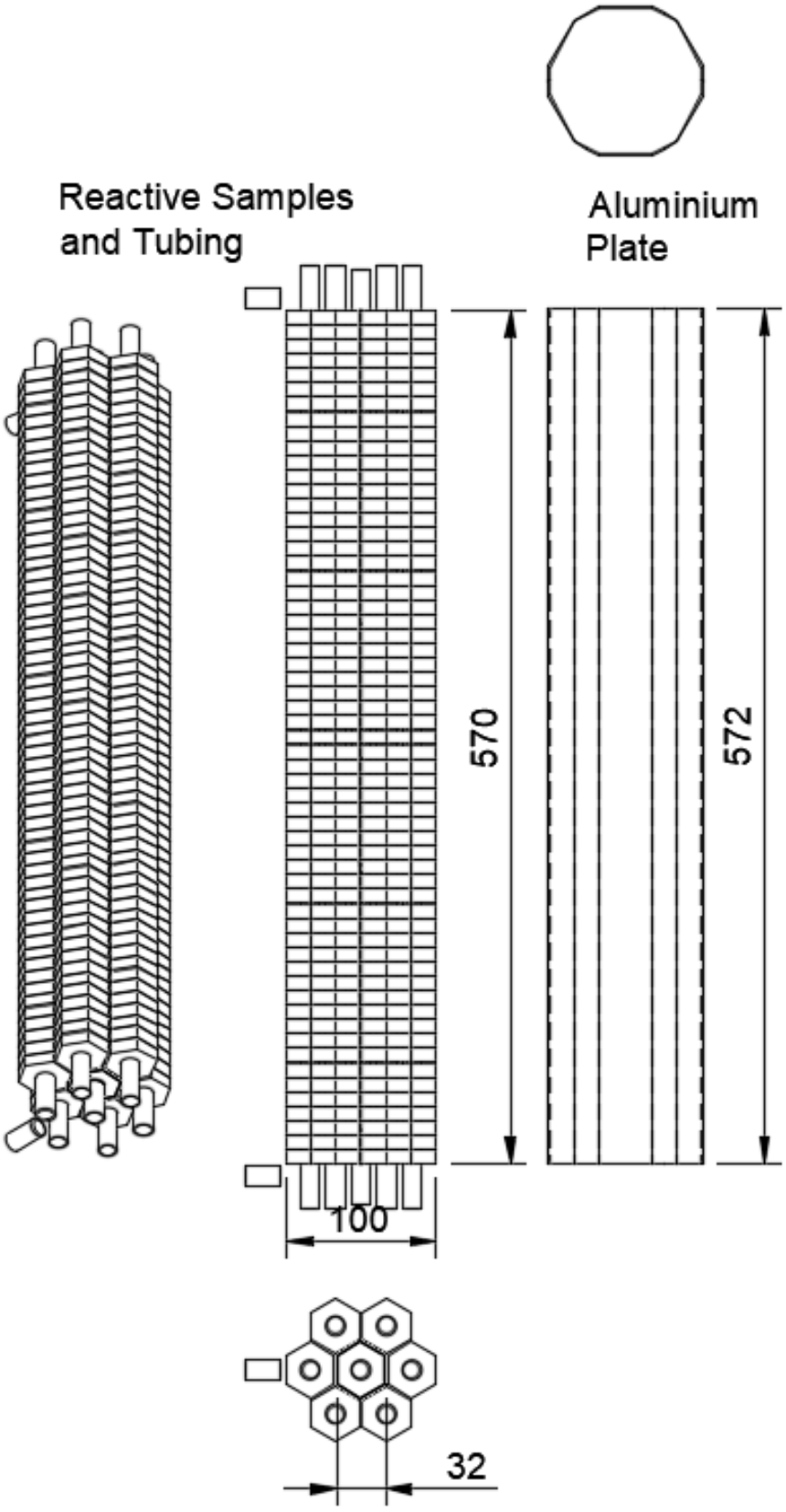

Figure 55 Reactor drawing and sizing for calcium chloride (8-4-2), dimensions in mm. The hexagons are 16 mm apothem and tubes are a 34 mm pitch. The aluminium plate folded to surround the samples is 1 mm longer at each end to maintain a gap.

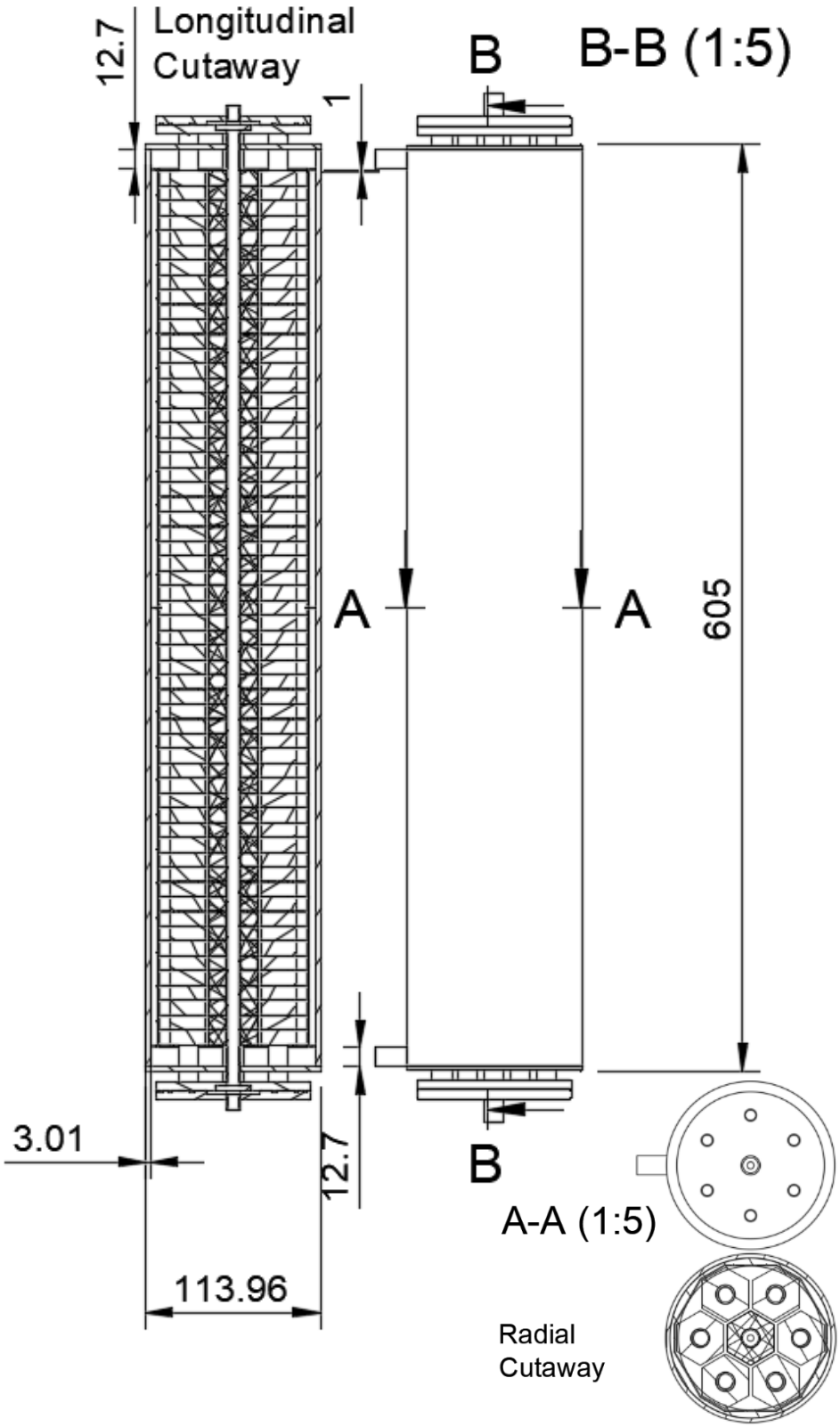

Figure 56 Reactor sizing and cutaway, distribution manifolds on the end. The longitudinal cutaway is shown from point B to B; it dissects the centre hexagonal sample. The radial cross section shows all the components. Cross section at the top is the view from the end including manifolds.

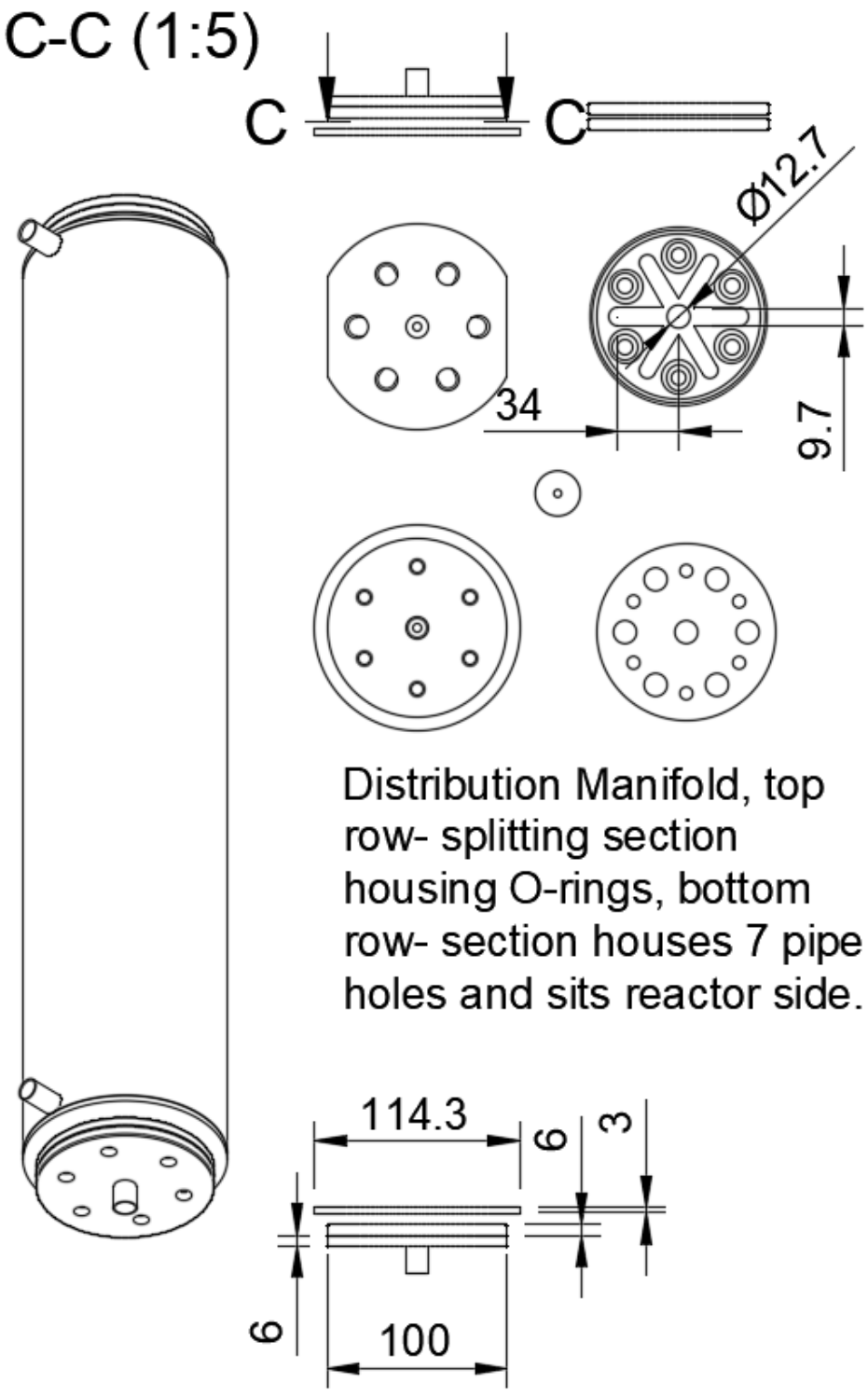

Figure 57 Isometric view of reactor with end plates and manifolds illustrated.

The dimensions and design of a 3 kW reactor for calcium chloride can be seen in **Figure 55, Figure 56, and Figure 57**. In **Figure 55** the aluminium folded sheet that is used to create a stagnant gas can be seen to be longer than the length of the composite (nominally this is 1 mm but for practical

purposes may need to be larger so that no contact can be assured when construction occurs). The aluminium is held in place by a ring of plate stainless steel, seen to be dimensioned at 1 mm. This could be held in position with some silver solder (in various positions around the radius) as it is not a structural component. In this design the tubes that will connect the reactors to the other reactors can be seen in **Figure 56**, this connects to headspace at the end of each reactor which is sized to 12.7 mm to house the connecting tube.

The connecting tube can be used to position the ring and other components in place and will be welded on the exterior of the shell, this will be connected with Swagelok to the other reactor via a flow meter. To hold things at the correct positions for welding a cylindrical insert at the size of the inner radius of the connecting tube can be inserted—the diameter of this will define the head space at each end of the shell, and will be removed after welding—the ring will fit against this at each end and hold the aluminium in place. As long as the composite is fitted at equal distance from each end of the tubes, an external spacer between the end of the shell and the manifolds will ensure equal distances and maintain the gaps internally. The spacers are only in place for the welding and will be removed, but will centre everything axially at the correct position down the length. Some consideration may want to be given to factor error in fitting the components together, but the method will ensure maintaining no contact between the active material and the shell components, ring and aluminium folded plate. Welding could begin on the shell with the external spacer in place and it could be removed once shell was welded up, to weld the tubes to the shell end plate before welding the manifold to the tubes.

Different salts' reactors are sized to have the same geometries, with the only difference being the lengths. From the design presented, it is therefore possible to assess the volume and mass of extra material in the design from initial investigations into COP. The thermal masses of the extra material can then be considered for their potential effect on the COP.

6.2.3 Thermal Mass and Material Considerations

The initial design steps have considered the composite and tubing which is fixed at this stage of system development. A full reactor design has been produced; incorporating an aluminium folded plate to potentially reduce sensible heating. It also includes a basic flow distribution device (manifold) to ensure equal mass flows of thermal fluid, and is completed with a shell that is produced from a standard pipe size. This is a reasonable best approximation at this stage of technology readiness.

As shown in the design produced in **Figure 55, Figure 56, and Figure 57**, the mass of extra material thermal masses can be calculated. This is presented based on standard sizing of tubes and materials, but it is a variable and could be optimised in further stages of development. The designs are such that each reactor has the equivalent masses on each end; of endplate and manifolds; and a mass of shell and aluminium plate derived from the length which is a ratio to the mass of tubes and material (as illustrated in **Figure 58**). Therefore, for each possible pairing in **Table 11**, for lengths derived in **Table 12**, the masses of the entire reactor can be calculated and thermal mass assessed and/or reported. To understand how the thermal mass could affect the COP, some basic *back of envelope* calculations can be done.

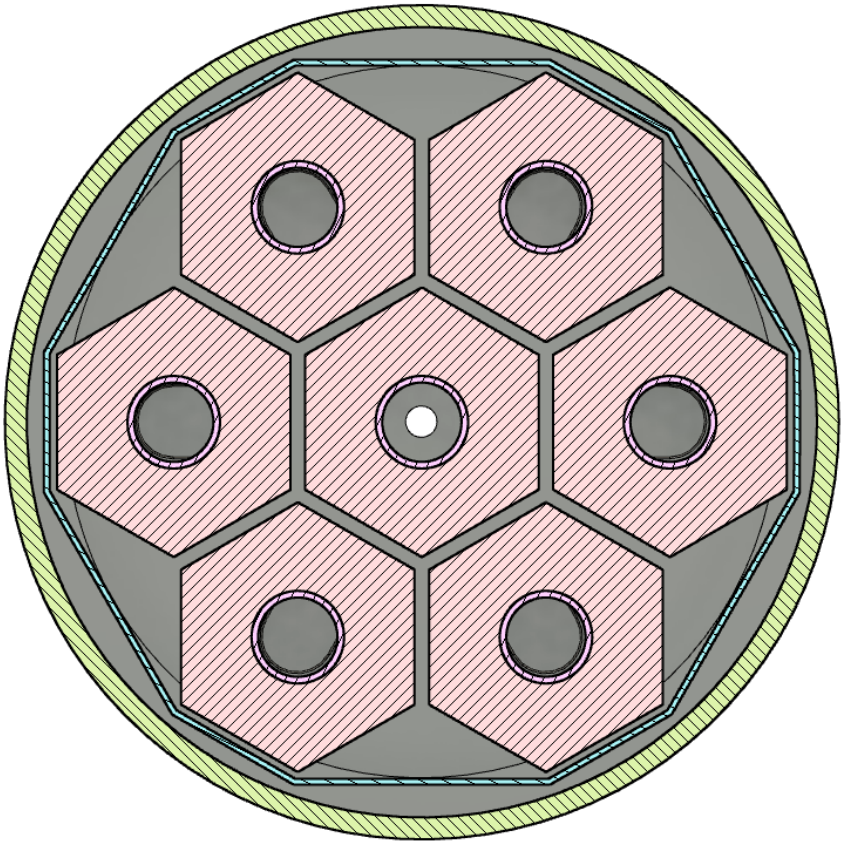

Figure 58 Cutaway of reactor, the ratio of shell and aluminium folded plate masses can be observed down the length of the samples; these are the cut sections displayed in colour and hatched.

When assessing the COP in **section 5.2** the sensible heating of the active material is calculated during a heating or cooling stage by the following equation:

$$Q_{sensible\ heating,HTS} = \Delta T\big(Mass_{HTS,salt}C_{p,HTS} + mols_{\cdot NH_3,(ads)}C_{n,\cdot NH_3,(ads)} + Mass_{HTS,steel}C_{p,steel} + Mass_{HTS,water}C_{p,steel} + Mass_{ENG,HTS}C_{p,steel}\big)$$

The thermal mass of the shell (and rest of reactor) is deduced from volume of material and described by the calculation:

$$Thermal\ Mass_{shell\ and\ ends} = CSA_{aluminium} \times \left(LTS_{Length} + 2 \times 10^{-3}\right) \times \rho_{Aluminium} \times C_{p,aluminium} + \left(\pi \times 57.15 \times 10^{-3^2} - \pi \times 54.15 \times 10^{-3^2}\right) \times LTS_{Length} \times \rho_{steel} \times C_{p,steel} + Volume_{ends} \times \rho_{steel} \times C_{p,steel}$$

The volume of the ends is composed of the ring that seals the insulating gas layer, some further shell, the plate at the end, extra lengths of tubing, the manifold volume (two plates and the orifice plate), and a section of connective tube from the manifold. This is calculated as followed, with the manifold volumes taken from the fusion 360 drawing (where **Figure 58** originates) in mm^3 and would of course be doubled:

$$End\ ring\ volume$$
$$= \left(\pi \times 54.15 \times 10^{-3^2} - \pi \times 48.8 \times 10^{-3^2}\right) \times 0.8 \times 10^{-3}$$
$$End\ shell\ volume$$
$$= \left(\pi \times 57.15 \times 10^{-3^2} - \pi \times 54.15 \times 10^{-3^2}\right) \times 4.2 \times 10^{-3}$$
$$End\ plate\ volume$$
$$= \left(\pi \times 57.15 \times 10^{-3^2} - 7 \times \pi \times 12.7 \times 10^{-3^2} \div 4\right) \times 3 \times 10^{-3}$$
$$Extra\ tube\ volume$$
$$= 6 \times \left(\frac{12.7 \times 10^{-3^2}}{4} - \frac{10.88 \times 10^{-3^2}}{4}\right) \times 21.5 \times 10^{-3} + \left(\frac{12.7 \times 10^{-3^2}}{4} - \frac{10.88 \times 10^{-3^2}}{4}\right) \times 18.5 \times 10^{-3}$$
$$Manifold\ volume = (74792.041 + 78681.748 + 2859.111) \times 10^{-9}$$
$$Manifold\ connection\ tube\ volume$$
$$= \left(\frac{12.7 \times 10^{-3^2}}{4} - \frac{10.88 \times 10^{-3^2}}{4}\right) \times 18 \times 10^{-3}$$

The total sum of these volumes presents the volume at one end of a reactor, these are the same for each reactor as they are identical.

When considering the thermal mass, at this stage it is not possible to predict the sensible heating that this thermal mass experiences without complex modelling. This is because the level of heating that the shell and these components experience is proportional to the reaction time; unlike the tube

and composite material, which will cycle the full temperature swing when reacting in the resorption machine. The shell will heat up based on conductance throughout the 3D geometry with primary conduction down the steel, and the extent of this depends on the reaction rate and is affected by the rate of the reaction in the other bed. The paired effect on the rate of reaction is not yet explored with this model or by the LTJ testing.

However, to consider the potential effect on the COP, this thermal mass has been added to the COP calculation and can be evaluated for each viable pairing, for a factor of heating which is a fraction of the ΔT between 1 and 0 SHF (sensible heat factor). This is a simple 'back of envelope' style calculation but enables different salts relative performance to be considered and also a very rough estimate as to how the final COP may be affected.

$$Q_{sensible\ heating,HTS} = \Delta T\big(Mass_{HTS,salt}C_{p,HTS} + mols_{\cdot NH_3,(ads)}C_{n,\cdot NH_3,(ads)} + Mass_{HTS,steel}C_{p,steel} + Mass_{HTS,water}C_{p,steel} + Mass_{ENG,HTS}C_{p,steel} + Thermal\ Mass_{shell\ and\ ends} \times SHF\big)$$

The effect on the COP of different values for the SHF can be seen for the pair manganese chloride-calcium chloride (both reactions 8-4-2), and manganese chloride-barium chloride in **Figure 59**. The exact values used to plot the graph can be seen in **Table 13**.

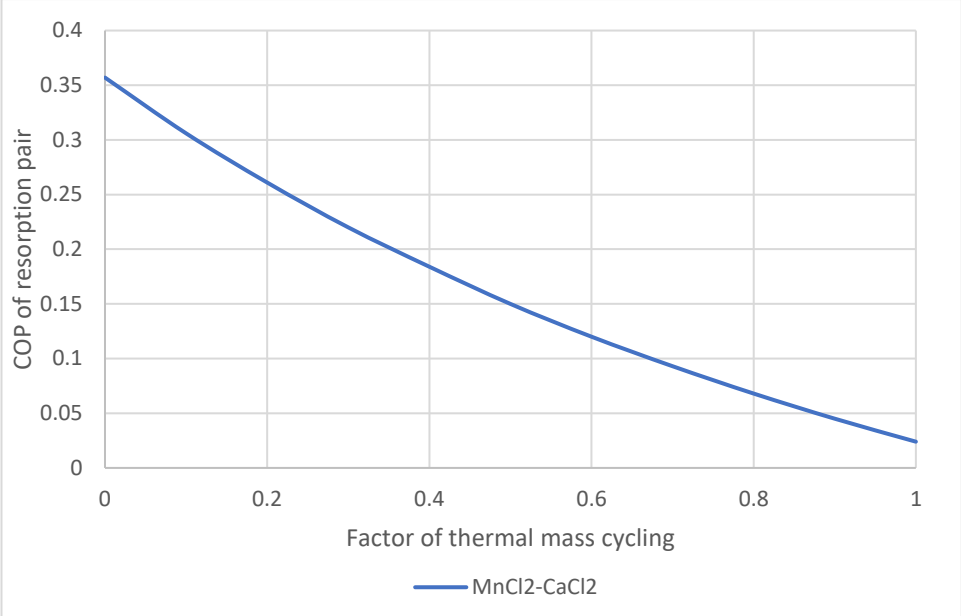

Figure 59 Thermal mass of shell evaluating potential effect on the COP

The results show that for the pair manganese chloride and calcium chloride, if the thermal mass of the shell and ends cycle for 50% of the temperature, (or 50% of the mass cycles the full temperature change through the whole cycle) the COP is 0.15. This highlights the necessity for employing heat recovery on a resorption system.

Table 13 COP based on thermal mass times a factor of the ΔT.

Factor *(SHF)*	$MnCl_2$-$CaCl_2$
1	0.024
0.9	0.045
0.8	0.068
0.7	0.093
0.6	0.120
0.5	0.150
0.4	0.184
0.3	0.220
0.2	0.261
0.1	0.306
0	0.357

By considering the 'fraction' of the shell material that cycles during the reaction, (or the mean fraction of temperature swing the shell undergoes,) it is possible to consider how improvements on COP may be facilitated. As one might expect, less sensible heating ensures better performance. There are two ways this can occur: faster reaction rate, or reduction of thermal

mass in the shell. Both of these are key things to consider in the next stages of development.

Heat recovery, using a second pair of reactors out of sync would present a pseudo-continuous process. Connecting the beds of the same salts during the transition change would reduce the sensible heating demand and improve the COP. To assess how this could improve the lab scale 3 kW test the effect can be estimated. This can be done conservatively by taking a SHF of 0.5 for the shell heating during a cycle presenting the COP at 0.15, the calculation can then consider recovering 70% of the sensible heat. This estimates the COP with heat recovery for manganese chloride and calcium chloride pair to be 0.40.

The reaction times in practice (in a working resorption machine) will dictate the amount of heat transfer to the shell; if performance is poor and reactions are slow then the COP will be lower, and vice versa. Accurate heat recovery effects could be modelled with dynamic results from a single pair of beds. There is reason to be optimistic that the 0.4 COP is achievable if heat recovery is employed. Furthermore, the results considering SHF illustrate that reducing heat transfer resistance and thus sensible heating will have a large impact improving performance.

6.3 Salt Pairings, Performance, and Considerations

The results from testing and analysis as well as initial design enable the primary contender of salt pairing to be determined. The primary choice is calcium chloride and manganese chloride, utilising both calcium chloride reactions. These results can be considered against the literature discussed in section **2.**, and the main points of consideration for testing and resorption system development.

Calcium chloride and manganese chloride

This pair is presented by Goetz et al. as a potential combination, utilising the single reaction of calcium chloride (8-4) (Goetz et al., 1993). They base this

from single equilibrium lines for each. When the equilibrium data from the LTJ (with hysteresis) are used to predict the performance, this can be seen in **Table 11**. The problem with this pair is that the value for T_c is too low when there is hysteresis, and even with reduced hysteresis it appears quite low. When both reactions of calcium chloride are considered (8-4-2), the results are more promising in **Table 11**. Again, the value for T_c is low which is of some concern. However, the improved COP is promising, and when the length of reactor is considered such as in **Figure 50**, calcium chloride with both reactions is the shortest and would have the highest SMP. It is odd that the work in the 90's such as by Goetz et al. did not consider the opportunity of both reactions (Goetz et al., 1993), as this would provide the highest power density. Van der Pal and Critoph test a calcium chloride reactor with the expectation of utilising both reactions for the purpose of a transformer, they also propose that in full scale reactors the conditions are apparent to reduce hysteresis effects (van der Pal and Critoph, 2017). This is promising particularly for resorption transformer application and shows this pair is the best contender from these results.

Barium chloride and calcium chloride

The resultant COPs when considering calcium chloride and barium chloride as a pairing with calcium chloride as the HTS are promising, with values in excess of 0.4 (based on initial internal reactor geometries). This pairing is suggested again by Goetz et al. (Goetz et al., 1993), where they propose that the temperature lift would be from T_m at 95 °C to T_h at 120 °C with T_c at 15 °C. It is not exactly clear where these values come from as in this work the lift appears better with a reasonable value for T_c as shown in **Table 11**. The problem with this pairing comes when we consider the required lengths of reactors as shown in **Table 12**, and in **Figure 50**. The reactor length for the calcium chloride reaction (4-2) as the HTS would be double the length of any other sized reactor for the same geometry. The power density and SMP for the calcium chloride (4-2) reactor must therefore be less than half that of the barium reactor, for which the value was measured. This would mean

reactors would be incredibly large and not feasible, and having a HTS reactor so much longer than the LTS would likely have further implication on the COP in dynamic behaviour due to the large sensible heating involved. For these reasons this pair is therefore unrealistic in practice.

Barium chloride and Manganese chloride

Barium chloride is presented in literature as a potential adsorption heat pump salt, particularly due to its large concentration change of the ammoniate during the cycle (Zhong et al., 2007). It is notable due to its low reaction temperatures (and pressures) and due to its simplicity to test and featuring in other pairs, it was also compared paired with manganese chloride. The simplicity is due to its single-phase change between 8 and 0 mols of ammoniate which presents a simple basis for starting out in developing an understanding of the sorption behaviour, and defining the model. As show in **Table 11**, the equilibrium lines for the pairing appear too far apart; so, whilst it presents a remarkable lift and a COP which is only marginally dampened by the large lift, the lower T_c temperatures are too low for reasonable application. This pairing does have a reasonable SMP and therefore reactor size/power density and so for other application such as chilling or heat pumping, it may be more effective.

Alternative pairs

Magnesium chloride is presented by Jegede as an option for the HTS in a resorption heat pump (Jegede, 2017). This salt was ruled out initially as when anhydrous manganese chloride is dissolved in water, it is extremely exothermic and the reaction causes the water to dissociate; the reaction heat causes hydrochloric acid to form, which jets off in a vapour, making it dangerous and impractical. The anhydrous form is produced from chemical synthesis rather than drying. The salt is soluble in ethanol, which is how Jegede uses it. But at room temperature the solubility is much lower than for other salts in water, and on reviewing the position of the line, it was not worth considering.

The results suggest that another salt with a Clapeyron line between calcium chloride and manganese chloride (to substitute one of that pair), may provide a better result with a higher T_c. Although due to the parallelogram geometry of the Clapeyron line relationship between the pairs—the system is quite sensitive to changes and the requirement is a higher T_c and T_h, but with a lower T_m, which may not be possible with parallel equilibrium lines. An alternative type of salt, like a bromide, or iodide, or even a sulphate may have a different gradient of Clapeyron line. The problem with this is that if we seek a new LTS paired with manganese chloride as the HTS, the LTS requires a steeper gradient, to raise T_c and drop the T_m values. The quasi-parallel nature of two chloride salts when paired are presented to have heats of reaction ΔH_r of the same order as proposed by the Clapeyron relationship. This means that the ideal COP is 0.5:

$$COP_{ideal} = \frac{\Delta H_{reaction,HTS}}{\Delta H_{reaction,HTS} + \Delta H_{reaction,LTS}} = \frac{1}{2}$$

If the ΔH_r for the LTS is greater than the value for the HTS, then the denominator of the ideal COP function will equal more than twice the numerator and thus the ideal COP would drop. There still could be opportunities with a different HTS and the numbers of salts to explore are innumerable. Future work could consider this and other salt pairs alternative to chlorides with the same anion.

What may be of interest and offer further enhancement is the effect of mixing salts. The potential for mixtures of salts in a single bed is discussed by Gordeeva et al., (Gordeeva et al., 2013). Gordeeva et al., show that an additive of one salt can shift “temperature necessary for regeneration of the sorbent by some 15 K”. Adjusting the temperatures as the they describe, applied to the results in **Table 11**, could prove beneficial. The addition of other salts may also reduce the hysteresis. The reduction of hysteresis is key to effective resorption systems, and the opportunity to alter the temperatures at which reactions occur is an important prospect for future applications and system development. The LTJ experimental rig and

methodology developed in this work, would enable rapid evaluation of modified salts, salt mixtures, or future pairs. Future work following the methodology and techniques used here could accurately derive equilibrium lines and heats of reaction, as well as test and model the reactions involved, this approach can lead to rapid development and ensure focus considers the challenges around heat transfer and hysteresis and ensure realisation of resorption systems.

7 Conclusions

The objective of this work was to design a resorption thermal transformer for the upgrading of waste heat. The approach to do so was evidenced and has presented a methodology for developing future resorption systems. If there had been more time and the practical work had not been interrupted by a pandemic, the system could have been built and initial tests undertaken.

The experimental work has proven insightful, the development of the LTJ test method presented in this work has recorded important new data and observed key characteristics not previously published. Significant findings:

1. The development and corroboration of a repeatable and successful methodology to test salts reacting with ammonia.
2. Identified the conditions at which the reactions occur and observed a metastate.
3. Reported a unified and accurate heat of reaction for the salts.
4. Identified an 'active fraction' of salt.
5. Successfully applied a model to identify empirical reaction kinetic constants and was able to simulate reaction data consistently — something not previously done.
6. Presented a test cell for testing full size composite for machines.
7. Proven the effectiveness of the ENG-salt composite and showed that it reduces the reaction limitation to only the rate of heat transfer.
8. Highlighted the importance in improving heat transfer for chemisorption systems and made initial steps to do so.
9. Identified a sizing of sample that offers a reasonable COP and high-power density.
10. Presented a reactor design and designing method for a resorption test scale reactor.

The methodology for analysing new salts for resorption systems—identified in this work—is as follows:

I. Determine potential salt/salt mixture
II. Produce samples for the tube-side LTJ and measure salt uptake
III. Test in the tube-side LTJ
    - Measure active fraction
    - Observe several tests over a range of conditions to determine equilibrium conditions for the onset of reaction
    - Record reaction data for analysis
IV. Test the salt in the ITC to estimate the heat of reaction
V. Model the salt behaviour using the reaction model and method
VI. Test a sample to the size specified in this paper in the shell-side LTJ, with a central hole cut to 11.9 mm with a hole saw
VII. Evaluate results, of the shell-side LTJ in the model considering SMP, potential COP
VIII. Resize and repeat testing in the shell-side, if necessary

The project has proven successful as significant advances have been made to understand the processes underlying ammonia-salt chemisorption. The literature review identified problems and challenges to the technology, and the method taking in this work has sought to address that with key considerations into heat transfer and identifying a reliable method to test the material. The results from the simulation are a major step, as now the reactions can be modelled reliably with repeatability which will be key for developing the technology to industrial scale.

The causes of the hysteresis have been discussed in the literature but are not fully understood, and different tests may show different extents of it. What is key is predicting the onset of reaction for the case being modelled, and having a correct heat of reaction to ensure the model is accurate (and also abides by the first law of thermodynamics). The test results and the application of the model by Critoph has proven effective in this work to simulate the reaction behaviour over a range of conditions and in different reactor geometries. The model has some limits but for the purpose of collecting data to design resorption systems, it has proven effective. This is

in part due to the improved composite which effectively reduces reaction rate limitations to just the rate of heat transfer.

The shell side test rig has also proven important, this was used for the ITC method but also provided empirical data for testing samples expected to be used in a full-scale design. A major finding from this work, scarcely discussed in contemporary chemisorption research, is the importance of heat transfer considerations. It is perhaps the most important element that should be considered in system development.

Future work should take the following steps to ensure the realisation of resorption systems to bring them to market:

The design presented in this thesis should form the basis of an experiment. The experiment should focus on dynamic data results, and evaluate actual COP. If a reasonable COP is observed, or an underperformance understood, this will signpost some of the future steps to be taken. There should also be some consideration into any error that could be important for scale-up to pilot or full scale that could come from a drop off in power.

Bench scale resorption testing should explore the hysteresis observed in practice. The hysteresis could make resorption systems impractical with its effects on the working temperatures. The extent of hysteresis that is observed will dictate the importance of improving the understanding of it, and exploring how to reduce it. Based on the literature, the best approach to date would be considering how mixtures or doping salts might either reduce hysteresis or change reaction temperatures. Exploring these factors will be key if hysteresis is an issue; or be valuable for future work, if operating temperatures can be fine-tuned.

As stated, the heat transfer is of vital importance. If the SMP is lower than expected due to slow reactions, improving this will be key. There should also be consideration in further increasing the power density of the process, and its COP. Future work may redesign the heat transfer equipment and choose something less conventional than a shell and tube type heat exchanger; or

consider a much greater scale of tube and sample, presenting an increased heat transfer area.

Ammonia-salt reactions for transformers are of great promise, if the hysteresis is reduced in practice as some work suggests, the systems could be scaled up quickly to compete with absorption transformer technology. The work here has given an insight into the salt behaviour and laid the groundwork for major developments in resorption technology.

8 Appendices

8.1 Modelling the Ammonia-Salt Reaction

The thermodynamic reaction model and finite difference heat transfer model were derived by Professor Critoph, who then computed them into a MATLAB model. The model was able to replicate the LTJ data and simulate results by devising a step change in temperature, it could also measure the heat flow in and out of the salt based on the energy balance and therefore produce a value for the specific mean power. Mr G. Atkinson and I checked the model derivation. I altered the MATLAB program to accept the data files with results from the LTJ, and then used it to identify: the heat transfer coefficient ('gap'); the active fraction of salt; the constants within the chemical kinetic equation; and the specific mean power of later results. The derivation and explanation of the model is within this thesis due to its importance in evaluating and understanding the experimental results, how they are processed, and identifying the kinetic parameters as well as later calculations for resorption system design. The work in this section was published in the international journal of refrigeration and edited by myself (Hinmers et al., 2022).

8.1.1 Energy Balance of a Unit Cell

Figure 60 shows a discretised unit cell of ENG impregnated with salt and possibly also containing solid adsorbate. The diagram illustrates how the

model conceptualises the changes during sorption in a lumped parameter model, illustrating the change in a single unit cell or element. Between times *t* and *t+dt*, a mass of adsorbate $dm_{REACT_{AB}}$ in the form of A (indicated by the left-hand dotted line in a) has reacted to form adsorbate in the form B. Simultaneously, a mass of adsorbate $dm_{REACT_{BC}}$ in the form of B (indicated by the right-hand dotted line in a) has reacted to form adsorbate in the form C. These might be, for example, $CaCl_2 \bullet 8NH_3$, $CaCl_2 \bullet 4NH_3$ and $CaCl_2 \bullet 2NH_3$. The model accounts for gas flow to or from the control volume and the resultant change in pressure. The model copes with either all the adsorbate reacting from form A to B, before then reacting B to C or the situation when both transitions occur simultaneously, as seen in salts like $CaCl_2$, as observed by van der Pal (van der Pal and Critoph, 2017). The approach here applies the same reaction equation for both phase changes and therefore differs to the work by Mazet, et al. (Mazet et al., 1991).

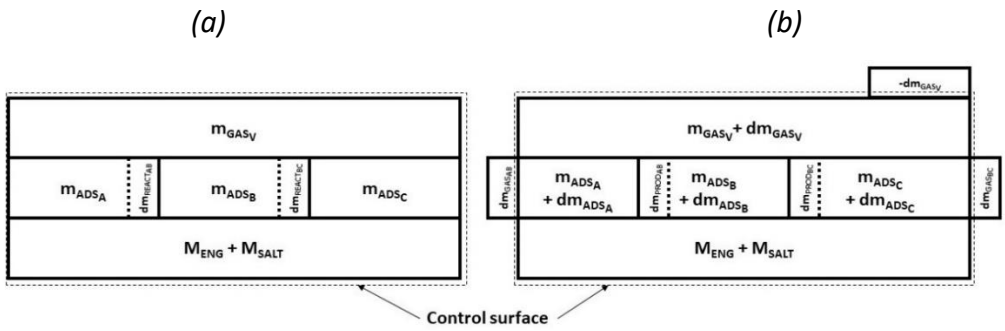

Figure 60 Unit cell masses at time t (a) and time t + dt (b).

The unit cell is small enough to be used in a finite difference program that assumes it is all at the same temperature and pressure. The unit cell volume is fixed but can be any geometry: cylindrical, rectangular, etc. The ENG and the un-ammoniated salt are characterised by their mass, density and specific heat and the whole volume has a fixed conductivity, nominally that of the ENG matrix. There are also masses of adsorbate types A, B, C (e.g. $\cdot 8NH_3$, $\cdot 4NH_3$ and $\cdot 2NH_3$) which have their own densities and specific heats, assumed to be those of solid ammonia as observed by Fujioka et al., and Hirata and Fujioka (Hirata and Fujioka, 2003, Fujioka et al., 1996). Considering desorption between time *t* and *t* + *dt*, a small mass of type A,

$m_{REACT_{AB}}$ reacts, some being converted to $m_{PROD_{AB}}$ and the remainder becoming gas $dm_{GAS_{AB}}$, which leaves the control volume. Some of type B reacts to form type C plus some expelled gas in similar fashion. There is also a gas void volume within the control volume, being the ENG pore volume not occupied by salt (fixed), or adsorbate (variable). Changes in pressure and temperature will affect m_{GAS_V}, the mass of gas in the void volume, as well as any portion of it leaving the volume, $-dm_{GAS_V}$.

The first law for the unsteady control volume in desorption is given by equation (21)

$$\begin{aligned} \Delta Q &= \Delta U_{ENG} + \Delta U_{SALT} + \Delta U_{ADS} + \Delta U_{GAS_V} + dm_{GAS_{AB}} h_{out} \\ &\quad + dm_{GAS_{BC}} h_{out} - dm_{GAS_V} h_{out} \\ &= MC_p dT + \Delta U_{ADS_A} + \Delta U_{ADS_B} + \Delta U_{ADS_C} + \Delta U_{GAS_V} \\ &\quad + dm_{GAS_{AB}} h_{out} + dm_{GAS_{BC}} h_{out} - dm_{GAS_V} h_{out} \end{aligned} \tag{21}$$

where ΔQ is the total heat entering the control volume in time *dt*.

The terms are either changes in internal energy U of the different masses of ENG, salt, adsorbate and gas within the control volume, or the enthalpy of the masses of gas entering or leaving the control volume. The MC_p term is the thermal mass (J/K) of the ENG plus the salt, whether accessible to the reaction or not. In desorption, ΔQ is positive and the enthalpy of the outlet streams h_{out} is that for the control volume temperature. In adsorption, ΔQ is negative and h_{out} is for the temperature of the incoming gas, which in an LTJ experiment is the expansion vessel temperature T_E.

The terms can be considered separately: that associated with type A and conversion to/from B and the gas entering or leaving, that associated with type B and conversion to/from C and the gas entering or leaving, the sensible heating of C, and the sensible heating of the salt and ENG.

First considering type A:

$$\begin{aligned}&\left(\Delta U_{ADS_A} + dm_{GAS_{AB}} h_{out}\right)\\ &\qquad = \Delta U_{NR-ADS_A} + \Delta U_{R-ADS_A} + dm_{GAS_{AB}} h_{out}\\ &= \Delta(mu)_{NR-ADS_A} + \Delta(mu)_{R-ADS_A} + dm_{GAS_{AB}} h_{out}\\ &= m_{NR-ADS_A} du_{NR-ADS_A} + dm_{PROD_{AB}} u_B - dm_{REACT_{AB}} u_A\\ &\qquad + dm_{GAS_{AB}} h_{out}\\ &= (m_{ADS_A} - dm_{REACT_{AB}}) c_{V_{ADS}} dT + dm_{PROD_{AB}}\left(h_B - pv_{ADS_B}\right)\\ &\qquad - dm_{REACT_{AB}}\left(h_A - pv_{ADS_A}\right) + dm_{GAS_{AB}} h_{out}\\ &= m_{ADS_A} c_{V_{ADS}} dT + dm_{GAS_{AB}} \Delta h_{AB} - dm_{PROD_{AB}} pv_{ADS_B}\\ &\qquad + dm_{REACT_{AB}} pv_{ADS_A}\end{aligned} \tag{22}$$

where NR and R indicates non-reacting and reacting, and PROD and REACT indicate product (time *t*) and reactant (time *t*+*dt*). Δh_{AB} is the enthalpy of reaction per unit mass.

Given that:

$dm_{REACT_{AB}} = dm_{ADS_A}$ The only change in dm_{ADS_A} is due to the AB reaction.

$dm_{PROD_{AB}} = dm_{ADS_A} \times \frac{B}{A}$ Change from .A mols to .B mols

$pv_{ADS_A} = pv_{ADS_B} = pv_{ADS}$ Specific volume of all ammoniate assumed equal to that of solid NH_3.

Then:

$$\begin{aligned}\Delta U_{ADS_A} + dm_{GAS_{AB}} h_{out}&\\ &= m_{ADS_A} c_{V_{ADS}} dT + dm_{GAS_{AB}} \Delta h_{AB}\\ &\quad + dm_{ADS_{AB}} pv_{ADS}\left(1 - \frac{B}{A}\right)\end{aligned} \tag{23}$$

The first term on the right-hand side of the equation is sensible heating of adsorbate A, the second is the reaction enthalpy term. The third term is the work associated with shrinkage or expansion; the term is quite small although the expansion of adsorbate can be considerable. Keeping account of the changing volume of solid within the control volume is important since expansion of the solid reduces the gas space available and expels gas from the control volume. The flow work done by gas expelled from the control

volume is accounted for by h_{out}. It is preferred to keep small terms for completeness since they do not slow the numerical solution significantly.

A similar argument applies to the terms in Equation (21) relating to conversion between forms B and C:

$$\begin{aligned} \Delta U_{ADS_B} + dm_{GAS_{BC}} h_{out} \\ = m_{ADS_B} c_{V_{ADS}} dT + dm_{GAS_{BC}} \Delta h_{BC} \\ + dm_{ADS_{BC}} pv_{ADS} \left(1 - \frac{C}{B}\right) \end{aligned} \tag{24}$$

The remaining terms in equation (21) are:

$$\Delta U_{ADS_C} = m_{ADS_C} c_{V_{ADS}} dT \tag{25}$$

Sensible heat only; there is no C to D reaction considered.

And for the gas void volume:

$$\begin{aligned} \Delta U_{GAS_V} - dm_{GAS_V} h_{out} = \Delta(mu)_{GAS_V} - dm_{GAS_V} h_{out} \\ = m_{GAS_V} du_{GAS_V} + u_{GAS_V} dm_{GAS_V} - dm_{GAS_V} h_{out} \\ = m_{GAS_V} c_{V_{GAS}} dT + dm_{GAS_V} \left(u_{GAS_V} - h_{out}\right) \\ = m_{GAS_V} c_{V_{GAS}} dT - pv_{GAS_V} dm_{GAS_V} \end{aligned} \tag{26}$$

The first term is the change in internal energy and the second is the positive work done in expansion.

Now if all the separate terms are substituted into equation (21) we obtain:

$$\begin{aligned} dQ = MC_p dT + \left(m_{ADS_A} + m_{ADS_B} + m_{ADS_C}\right) c_{V_{ADS}} dT \\ + dm_{GAS_{AB}} \Delta h_{AB} + dm_{ADS_{AB}} pv_{ADS} \left(1 - \frac{B}{A}\right) \\ + dm_{GAS_{BC}} \Delta h_{BC} + dm_{ADS_{BC}} pv_{ADS} \left(1 - \frac{C}{B}\right) \\ + m_{GAS_V} c_{V_{GAS}} dT - dm_{GAS_V} pv_{GAS_V} \end{aligned} \tag{27}$$

The first line is sensible heating/cooling of ENG, salt and adsorbate, the second is reaction and expansion work in AB, the third is reaction and expansion work in BC, and the fourth is sensible heating and expansion of the gas.

dm_{GAS_V} may be calculated from perfect gas law assumptions and the pressure and temperature changes. If the expelled volume due to gas void temperature change dT and pressure change dp is dV:

$$dV_{GAS\,V} = V_{GAS\,V}\left(\frac{\frac{dT}{T} - \frac{dp}{p}}{1 + \frac{dp}{p}}\right) = dm_{GAS_V} p v_{GAS_V} \tag{28}$$

which is substituted into eq. (26) to give:

$$\begin{aligned} dQ = dT\Bigg(& MC_p + \sum_A^C m_{ADS}\, c_{V_{ADS}} + m_{GAS_V} c_{V_{GAS}} - \frac{\frac{pV_{GAS_V}}{T}}{1 + \frac{dp}{p}} \Bigg) \\ & + dm_{GAS_{AB}} \Delta h_{AB} + dm_{ADS_{AB}} p v_{ADS}\left(1 - \frac{B}{A}\right) \\ & + dm_{GAS_{BC}} \Delta h_{BC} + dm_{ADS_{BC}} p v_{ADS}\left(1 - \frac{C}{B}\right) \\ & + \frac{dpV_{GAS_V}}{1 + \frac{dp}{p}} \end{aligned} \tag{29}$$

For the purposes of simulating the process in a program, this is rearranged to solve for dT:

$$dT_{des} = \frac{\begin{pmatrix} dQ - dm_{GAS_{AB}} \Delta h_{AB} - dm_{ADS_{AB}} p v_{ADS}\left(1 - \frac{B}{A}\right) - dm_{GAS_{BC}} \Delta h_{BC} \\ -dm_{ADS_{BC}} p v_{ADS}\left(1 - \frac{C}{B}\right) - \frac{dpV_{GAS_V}}{1 + dp/p} \end{pmatrix}}{\left(MC_p + \sum_A^C m_{ADS}\, c_{V_{ADS}} + m_{GAS_V} c_{V_{GAS}} - \frac{\frac{pV_{GAS_V}}{T}}{1 + dp/p}\right)} \tag{30}$$

The analysis is slightly different in adsorption when gas entering the control volume can (generally in an LTJ test) cool it.

The equation for dT becomes:

$$dT_{ads} = \frac{\begin{pmatrix} dQ - dm_{GAS_{AB}}\Delta h_{AB} - dm_{ADS_{AB}} pv_{ADS}\left(1 - \frac{B}{A}\right) - dm_{GAS_{BC}}\Delta h_{BC} \\ -dm_{ADS_{BC}} pv_{ADS}\left(1 - \frac{C}{B}\right) - \frac{dpV_{GAS_V}}{1 + \frac{dp}{p}} + \\ m_{GAS_V} \frac{\frac{dp}{p}}{1 + \frac{dp}{p}} c_p (T - T_E) \end{pmatrix}}{\begin{pmatrix} MC_p + \sum_A^C m_{ADS}\, c_{V_{ADS}} + m_{GAS_V} c_{V_{GAS}} \\ -\frac{\frac{pV_{GAS_V}}{T}}{1 + \frac{dp}{p}} + m_{GAS_V} \frac{\frac{1}{T}}{1 + \frac{dp}{p}} c_p (T - T_E) \end{pmatrix}} \quad (31)$$

The final terms in both numerator and denominator account for the sensible heating or cooling of gas entering the control volume at temperature T_E.

Whilst complicated, given an assumed pressure rise the change in temperature and then the mass of ammonia in gaseous or adsorbed states A, B, and C can be calculated.

8.1.2 Reaction Rate Equations

m_{ADS_A}	m_{ADS_B}	m_{ADS_C}
m_{SALT_A}	m_{SALT_B}	m_{SALT_C}

$m_{ADS_A} + dm_{ADS_A}$	$m_{ADS_B} + dm_{ADS_B}$	$m_{ADS_C} + dm_{ADS_C}$
$m_{SALT_A} + dm_{SALT_A}$	$m_{SALT_B} + dm_{SALT_B}$	$m_{SALT_C} + dm_{SALT_C}$

Figure 61 Unit cell salt and adsorbate masses at time t (a) and time t + dt (b)

In **Figure 61** the m_{ADS} terms are the masses of adsorbate of types .A mols, .B mols and .C mols of adsorbed ammonia and the m_{salt} terms are the masses of salt associated with the A B and C forms.

The reaction rate equations used are based on those of Mazet (Mazet et al., 1991, Mazet and Amouroux, 1991):

$$\frac{dX}{dt} = (1 - X)^n A_r \frac{p_{eq} - p}{p} \quad (32)$$

where:

X is the advancement of the reaction (from zero to unity)

p is the pressure

p_{eq} is the equilibrium pressure

A_r and n are constants. $A_r$is an Arrhenius term that is actually a function of temperature but can be successfully assumed constant over the ranges used in this work.

Whilst generally used in molar form the same numerical values of A_r and n apply when using mass formulation. Thus, when expressing reaction AB in differential form:

From A to B (desorbing)

$$\frac{dm_{SALT\ A\ to\ B}}{dt} = (m_{SALT\ A} + m_{SALT\ B}) \left(\frac{m_{SALT\ A}}{m_{SALT\ A} + m_{SALT\ B}}\right)^{n_{AB}} A_{r_{AB}} \frac{p_{eq\ AB} - p}{p} \quad (33)$$

From .B to .A (adsorbing)

$$\frac{dm_{SALT\ B\ to\ A}}{dt} = (m_{SALT\ A} + m_{SALT\ B}) \left(\frac{m_{SALT\ B}}{m_{SALT\ A} + m_{SALT\ B}}\right)^{n_{BA}} A_{r_{BA}} \frac{p_{eq\ BA} - p}{p} \quad (34)$$

Similarly, for the BC reaction:

From B to C (desorbing)

$$\frac{dm_{SALT\ B\ to\ C}}{dt} = (m_{SALT\ B} + m_{SALT\ C}) \left(\frac{m_{SALT\ B}}{m_{SALT\ B} + m_{SALT\ C}}\right)^{n_{BC}} A_{r_{BC}} \frac{p_{eq\ BC} - p}{p} \quad (35)$$

From C to B (adsorbing)

$$\frac{dm_{SALT\ C\ to\ B}}{dt} = (m_{SALT\ B} + m_{SALT\ C}) \left(\frac{m_{SALT\ C}}{m_{SALT\ B} + m_{SALT\ C}}\right)^{n_{CB}} A_{r_{CB}} \frac{p_{eq\ CB} - p}{p} \quad (36)$$

The change in the adsorbate mass is readily used to calculate the new values of all the masses of salt and adsorbate plus the masses of gas adsorbed or

desorbed at the next time step, taking account of conditions under which the masses of .B may be the result of simultaneous A to B and B to C reactions.

The derivation of this model goes back to fundamentals when looking at simultaneous reactions, and enables the model to replicate reaction behaviour over a number of conditions accounting for different phase changes. Mazet et al. presented equation (37) and for subsequent reactions presented this kinetic equation with Y describing the extent of the second reaction:

$$\frac{dY}{dt} = ([1 - Y]X)^n \cdot A_r \cdot \frac{p - p_{eq}}{p} \tag{37}$$

The results presented by Mazet et al. suggest that the constants (A_r and n) vary depending on conditions (Mazet et al., 1991). They quote: 'These remarks do not therefore allow us to obtain coefficients which are valid over the whole range of experimental constraint temperatures at a given pressure P. It would therefore seem that a phenomenon influencing the rate of reaction has not been taken into account in the model.' In this study, the composite material and the detailed approach in modelling with attention to the heat transfer shows that the rate of heat transfer is the limiting factor and single values of A_r and n are identified. This contradicts the work by Mazet et al., and by identifying single parameters differs from other literature (Wu et al., 2019, Jegede, 2017, Yuan et al., 2019). This approach has also been tested in adsorption, and a similar single value for each constant has been identified but this differs between adsorption and desorption.

8.2 Manganese Oxide Formation

Initial samples of manganese chloride were prepared with flaked anhydrous manganese chloride. The analysis showed that the active fraction was 0.7; lower than barium chloride and calcium chloride which were 0.8. Granular pellets of manganese chloride were used to prepare a solution which turned

opaque and translucent, and gave off considerable heat in the process. This was attempted again with distilled water with granular salt but there was still a clear precipitate. This has been assumed to be manganese oxide (as taken from not very reputable online forums). It was found that using tetrahydrate flake and tap water or distilled water was capable of producing manganese chloride solution that was pink and translucent, and samples with an active fraction in excess of 0.8.

(a) *(b)* *(c)*

Figure 62 Manganese chloride solutions showing a precipitate that lowered the active fraction of samples: (a) granular pellets of manganese chloride; (b) opaque solution that occurred rapidly when using samples; (c) samples floating in solution that has precipitate in, it should appear pinker and the more translucent and sediment can be seen at the bottom of the beaker.

8.3 First Iteration of Shell Reactor Design

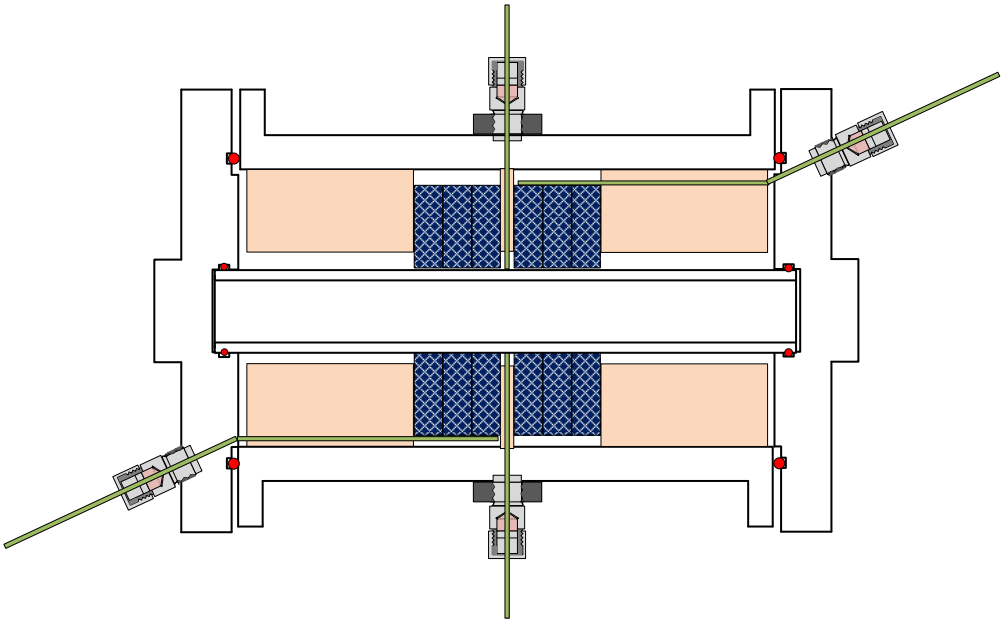

Figure 63 First shell-side reactor design. It was also longer than the final design which made it harder to install and align the thermocouples. The PEEK plastic was used in an attempt to mimic the tube-side design with its PTFE. But in the end it performed better just with blank ENG samples due to less thermal mass.

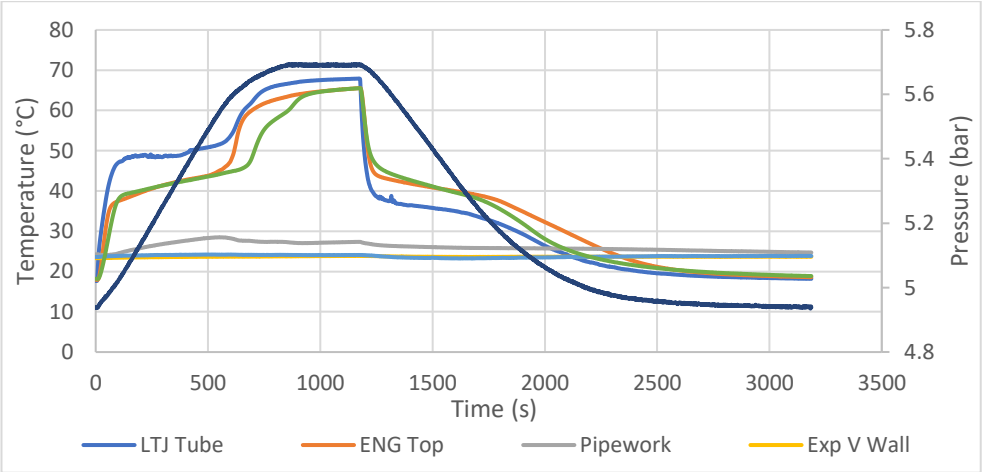

Figure 64 Shell side tests with thermoplastic PEEK filling the void volume, Initial shell results with PEEK show major lagging in the thermocouple readings and an inability to record the oil temperature at the end of the reaction.

8.4 Thermocouple Error Test

Thermocouples were placed inside an insulated vessel (not mixed) with hot water and then left to cool while the temperature readings were monitored. The standard deviation was plotted and used to show error bounds from the mean average temperature reading. This was performed as the most likely error will come from the data acquisition device itself. The DAQ device was

an NI 9214 TC module plugged into a cDAQ-9178 chassis. The largest error is likely to come from the cold junction; however, the module used has an isothermal terminal block to reduce this. The quoted typical value of error (not the maximum value), at high resolution sampling at 100 °C and 0 °C is ±0.37 °C and ±0.36 °C respectively. The standard deviation plot is well within this value. Because the values presented in this thesis are largely using dynamic data this was deemed as an acceptable validation. The equilibrium results for onset of reaction was the 'least dynamic' (for lack of a better phrase) as this used the average reading of 5 samples, but is a best fit plot over many tests over different and the same conditions. The irreproducibility of the reported results will come from the salt itself as many factors could affect the onset of reaction—such as the purity of the water used to prepare the samples, or whether the salt has been left overnight before the test runs. None the less the constants derived in the model—which aren't derived from temperature readings—still approximate the reaction rate well giving confidence in all results. Furthermore, published results for the data can regularly come from gravimetric testing methods, the findings in this thesis dispute their accuracy entirely; these isosteres for the basis of producing a model are accurate enough and a better estimate than those published previously. The values from the test can be seen in **Figure 65**, they are indeterminable but this illustrates the form of the test. These values are published as supporting data for a paper seen following this link: http://wrap.warwick.ac.uk/152152/

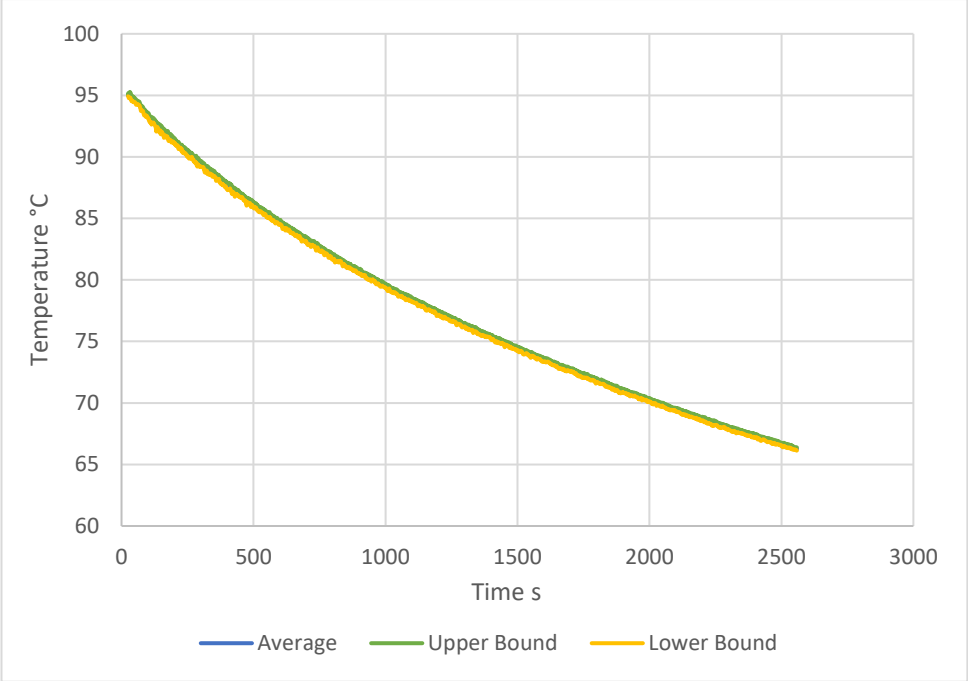

Figure 65 Thermocouple average readings over the length of the test and upper and lower bounds.

A clearer plot with error boundary from the standard deviation is shown in **Figure 66**. These tests were using all thermocouples used in the either LTJ set up.

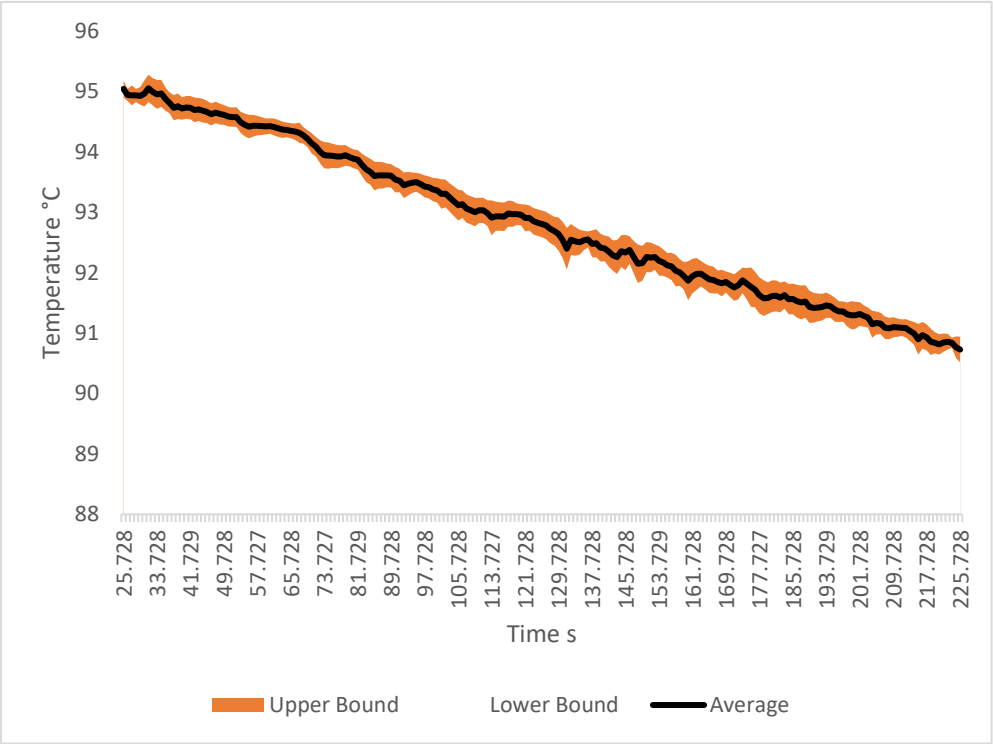

(a)

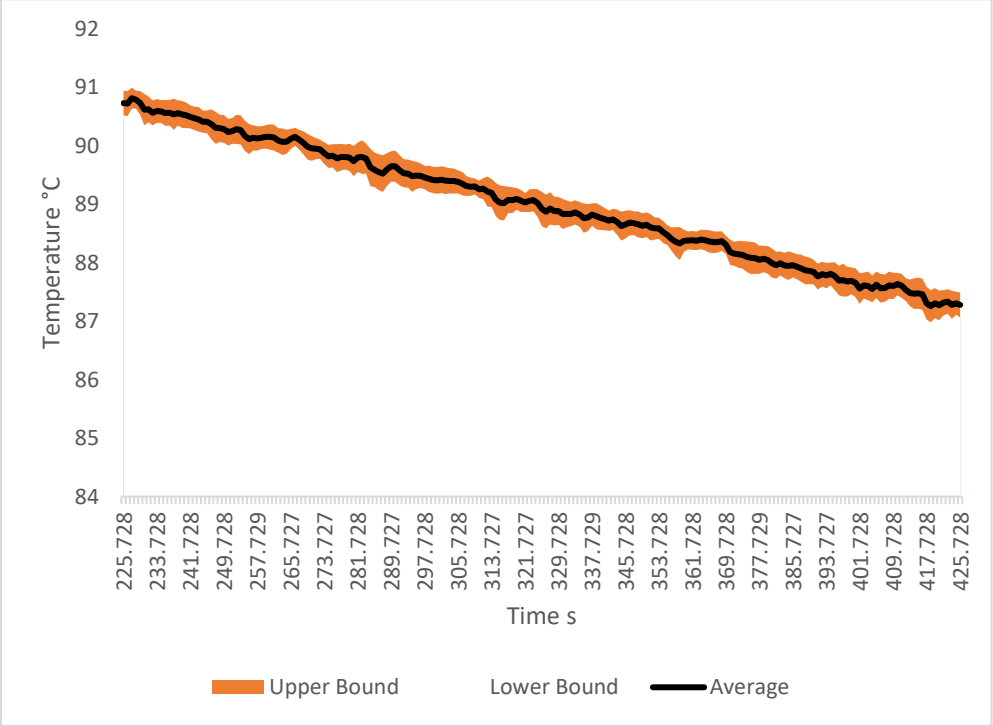

(b)

Figure 66 Standard deviation plots with error boundary of confidence. (a) and (b) are plotted against their time step, (b) follows (a).

8.5 Deadweight Pressure Test Calibration

A deadweight pressure test was performed using a deadweight pressure gauge. The reading of ambient pressure was taken using a mercury barometer and then accounted for in the calculation. A larger error was noted at the beginning. An average was taken of the error values and was 0.17%, removing the first data point and the error was 0.13%. This is well within quoted error values of 0.8%. Dynamic data was not presented typically as stated in **appendix 8.4**, and this value was taken as acceptable for the same reasons. This data is also available at: http://wrap.warwick.ac.uk/152152/

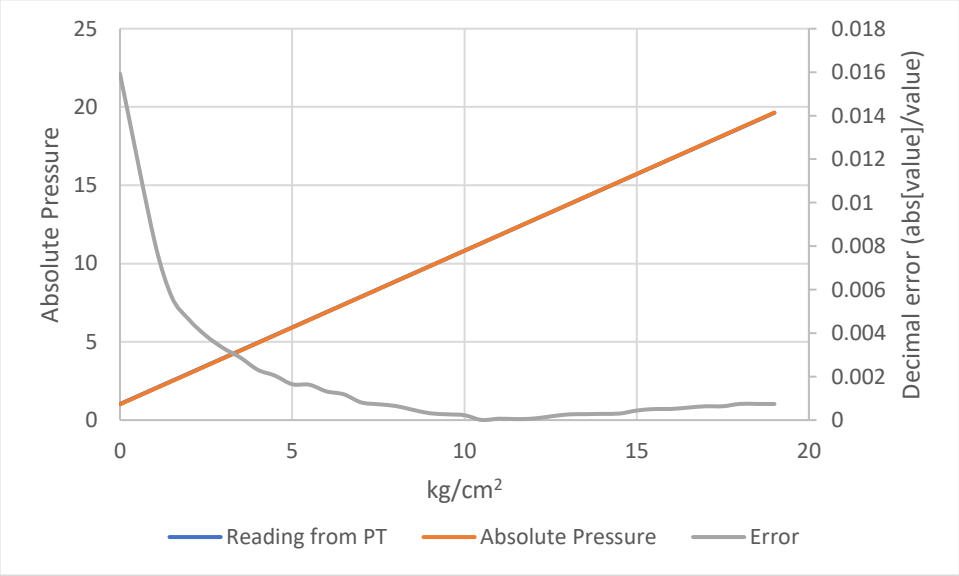

Figure 67 Absolute pressure and pressure transducer reading, plotted with error for each data point. Error plotted on right hand scale.

8.6 ITC Results Plots

The results for barium chloride and calcium chloride were obtained as described in **section 4.1.3**. In some cases, obtaining the results required yet slower ITC tests, in the case of the calcium chloride (2-4) reaction cycles were running for 10 or 12 hours. It was tricky obtaining a clear straight line in the calcium chloride (2-4) cycles, so linear sections from 3 different tests (3 adsorption and 3 desorption) were taken and an average gradient was approximated from those. To illustrate this, an average line is calculated and plotted in **Figure 72**. What provides some confidence in the value is the

similarity in gradient to the line presented by Neveu and Castaing (Neveu and Castaing, 1993). When we look at all the ITC plots and compare them to the lines presented by Neveu and Castaing, although in a different position, they are all approximately equal in gradient to the ITC results.

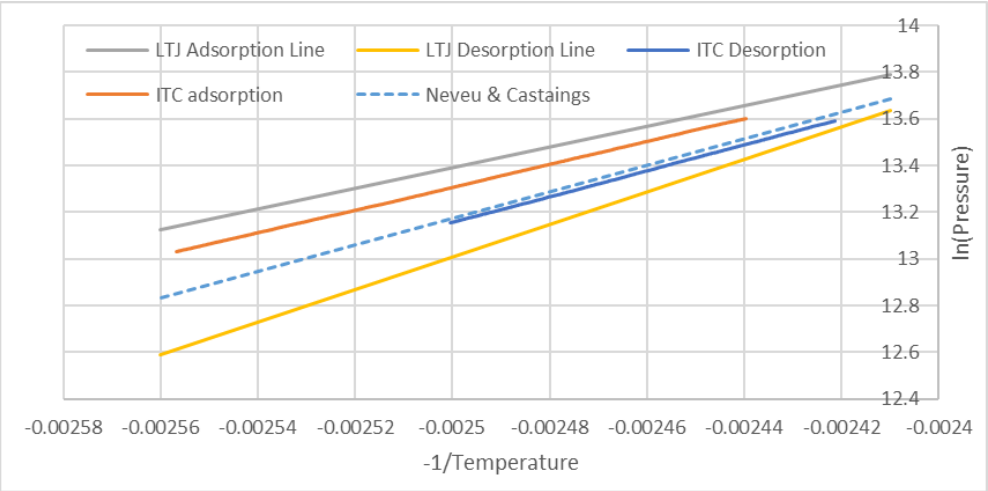

Figure 68 ITC construction lines for manganese chloride plotted with the line from literature (Neveu and Castaings (Neveu and Castaing, 1993)).

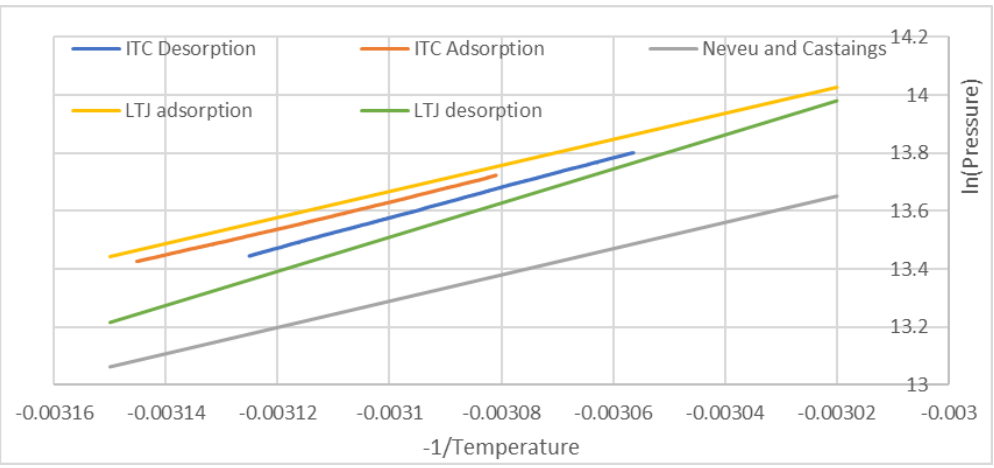

Figure 69 ITC construction lines for barium chloride heat of reaction, also plotted is the line from literature (Neveu and Castaings (Neveu and Castaing, 1993)).

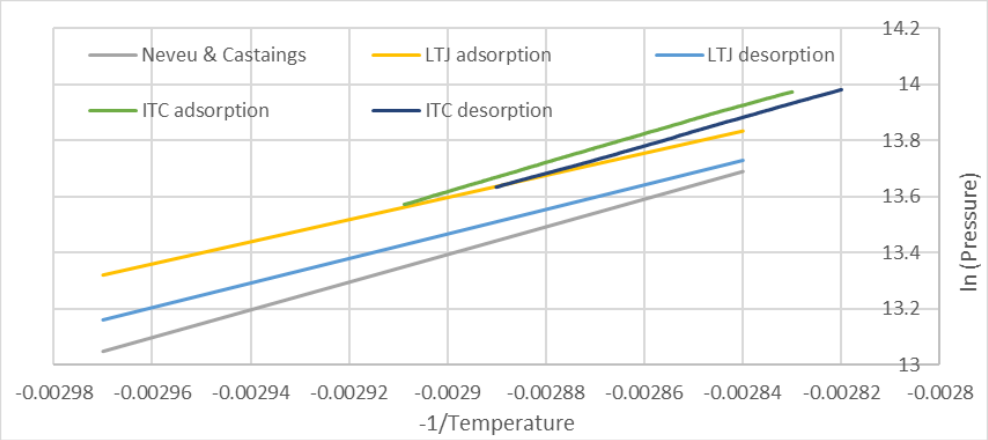

Figure 70 ITC construction lines for calcium chloride (8-4) reaction, also plotted is the line from literature (Neveu and Castaings (Neveu and Castaing, 1993)).

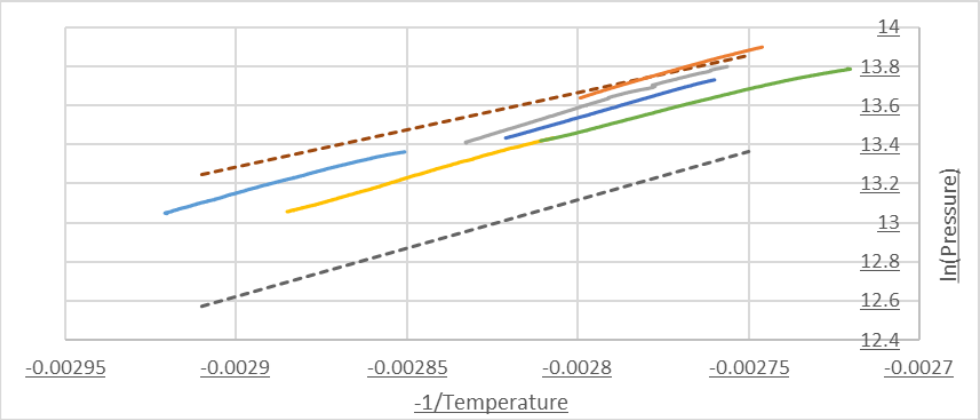

Figure 71 ITC construction lines for calcium chloride (4-2) reaction, the dashed lines indicate the lines obtained from the LTJ, the solid lines are from the ITC, the top 3 lines are from 3 different adsorption and the bottom 3 lines are from desorption.

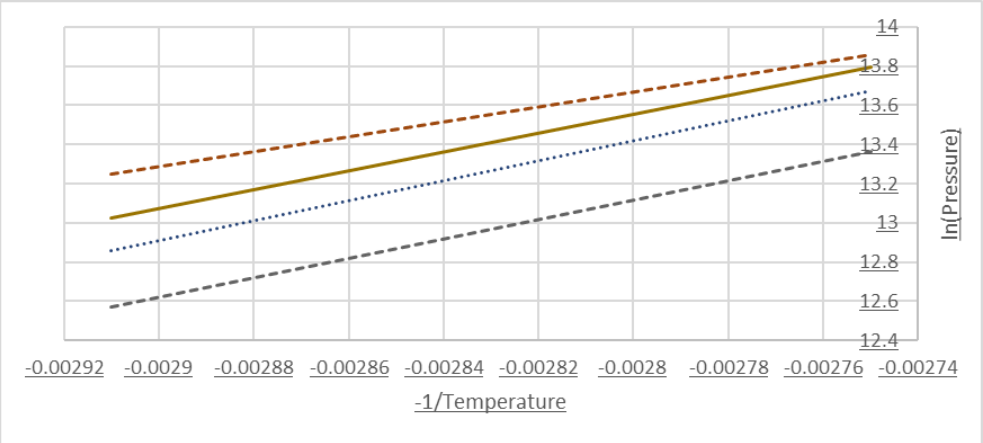

Figure 72 ITC construction line for calcium chloride (4-2) reaction, this time the solid line is the average lines of those in Figure 71; the dashed lines are the LTJ onset of reaction isosteres; and the dotted line is from Neveu and Castaings (Neveu and Castaing, 1993).

8.7 Simulation of ‘single’ Adsorption Reaction Across two Phase Changes

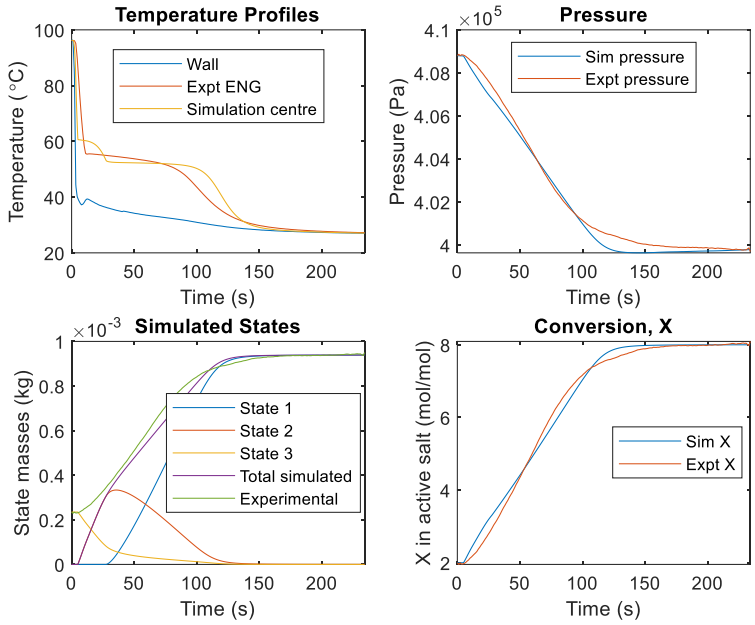

(a)

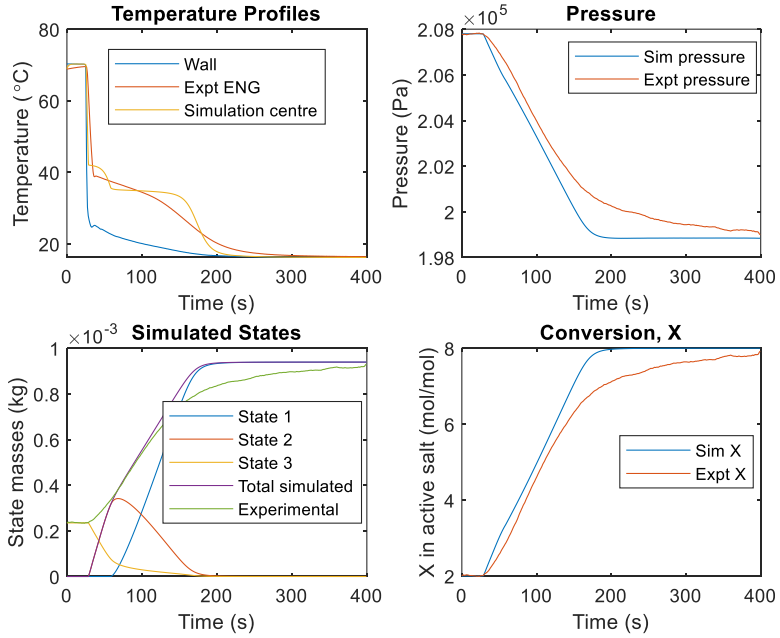

(b)

Figure 73 Calcium chloride adsorption simulation where one reaction appears to occur, across two changes in ammoniated state.

Data points collected for calcium chloride adsorption at the conditions for the onset of reaction (after any superheating/subcooling effect). The plot titles based on the change in the number of adsorbed moles. In the case

when during adsorption, seemingly a single-phase change occurred these were plotted and the trend line can be seen in the middle of the two reactions.

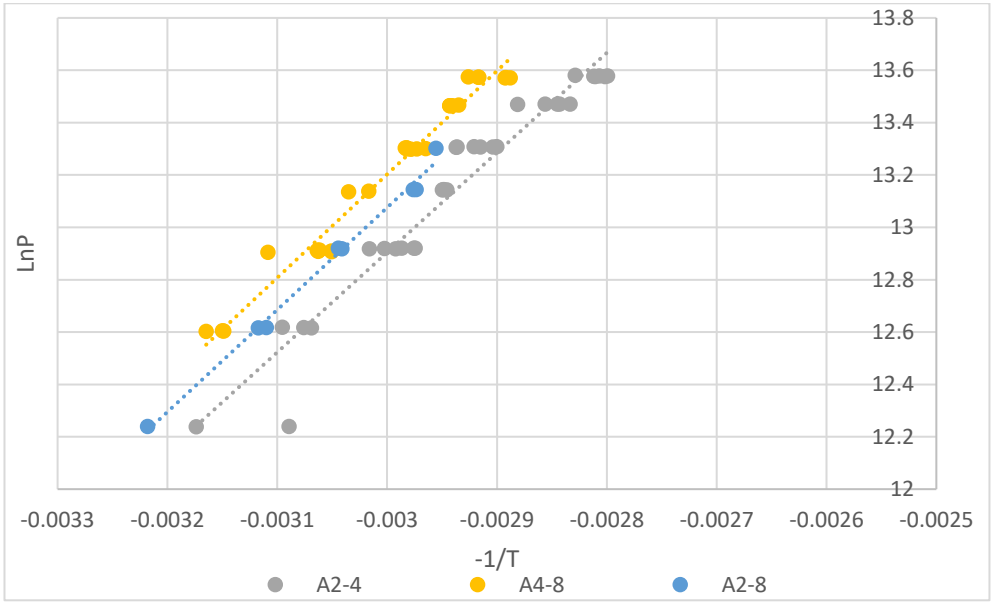

Figure 74 Data points for the onset of reactions for adsorption in calcium chloride, A2-4 is adsorption between 2 and 4 moles of ammoniate. The trend line plotted for the points where seemingly one reaction occurs (as opposed to two), is notably in the middle of the two other lines.

8.8 Shell-side Calcium Chloride Simulations

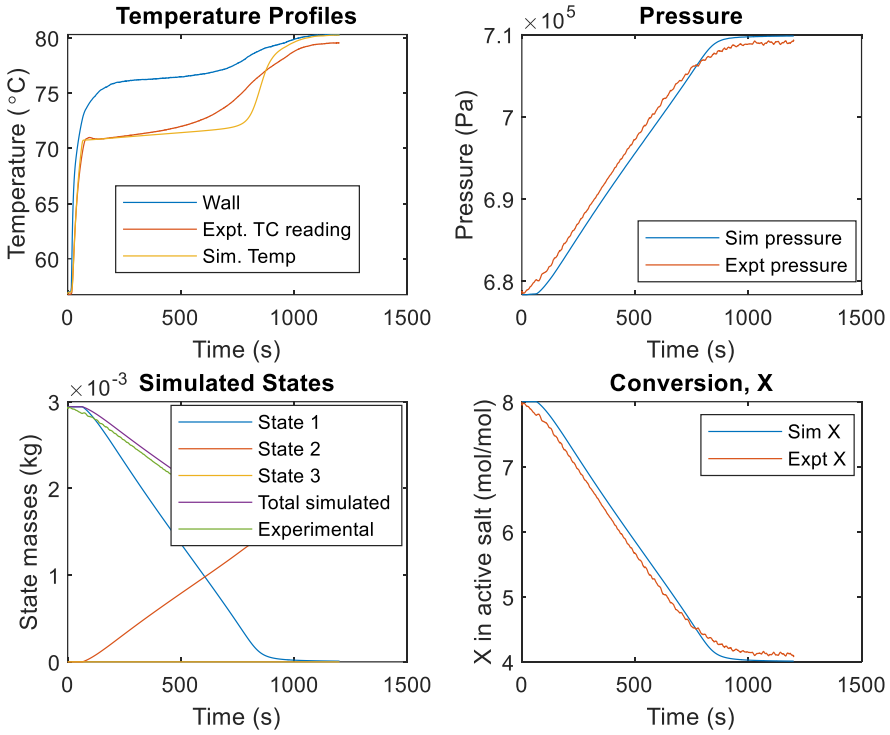

(a)

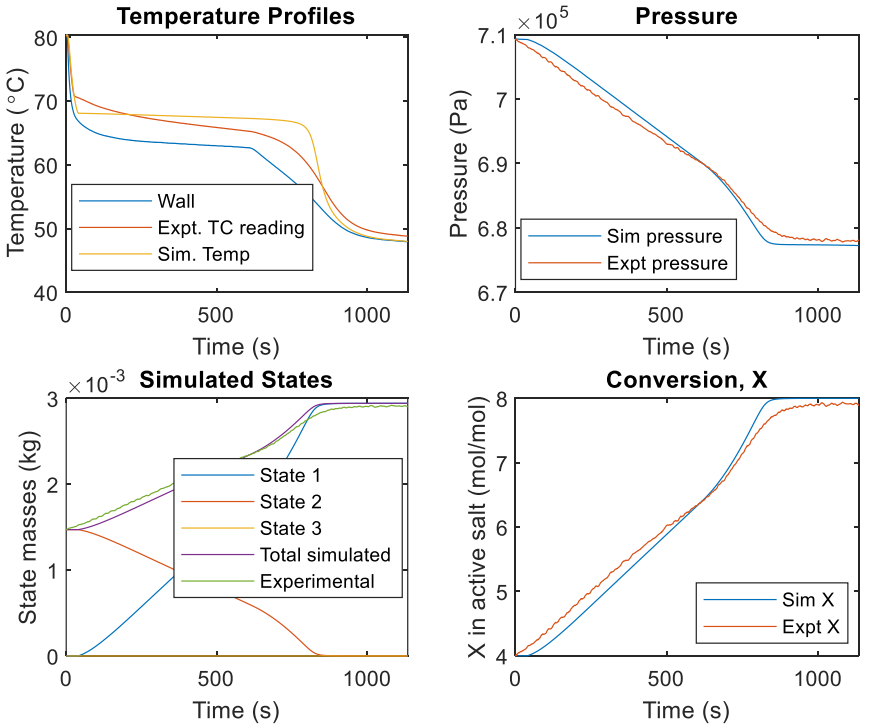

(b)

Figure 75 Calcium chloride shell-side tests simulation results, (test SD) the nominal gap in this case was 0.015 mm.

8.9 Grid Independence Test for Number of Nodes

Results from varying the number of nodes, done using the shell manganese chloride test to confirm the number of nodes within the finite difference model.

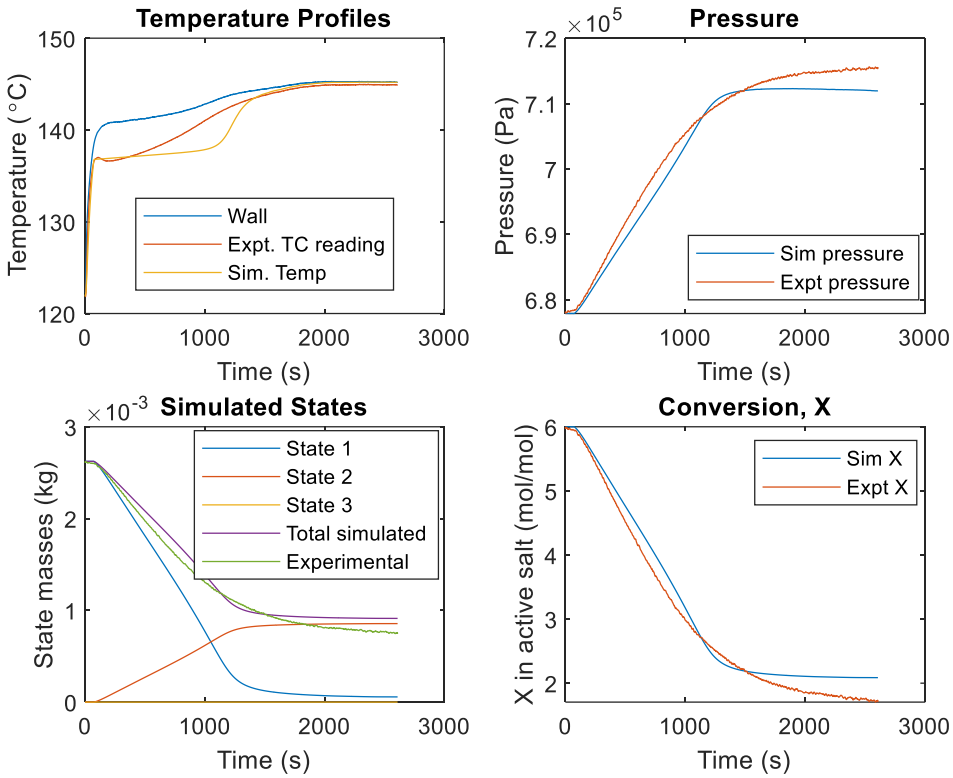

Shell side result with a 2-node simulation.

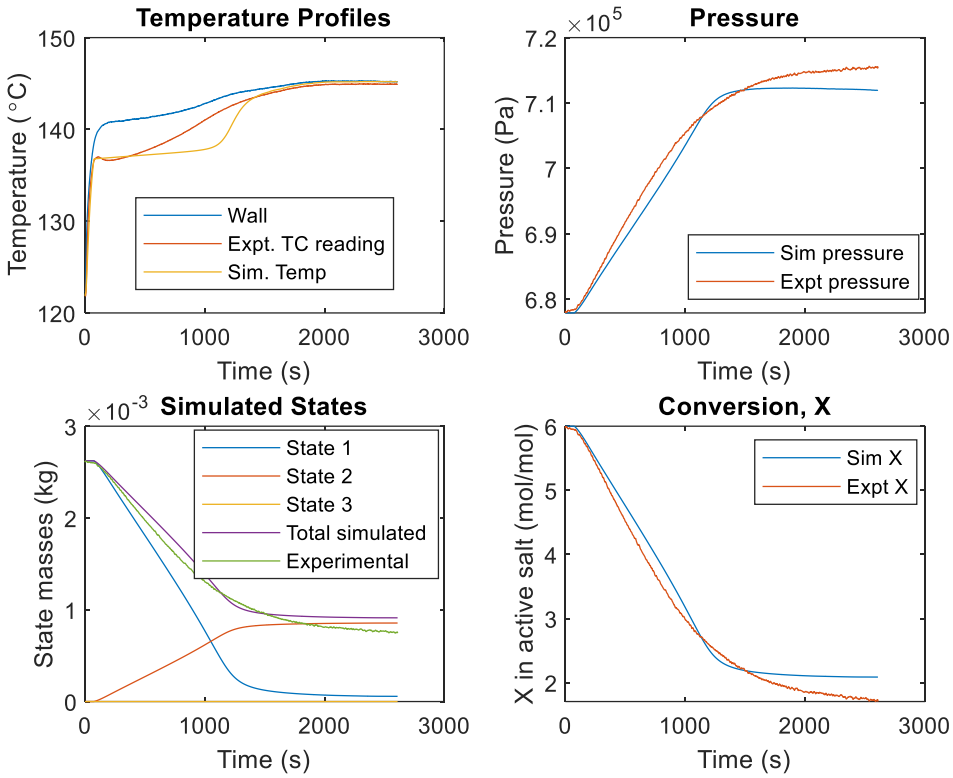

Shell side with 3 nodes simulation.

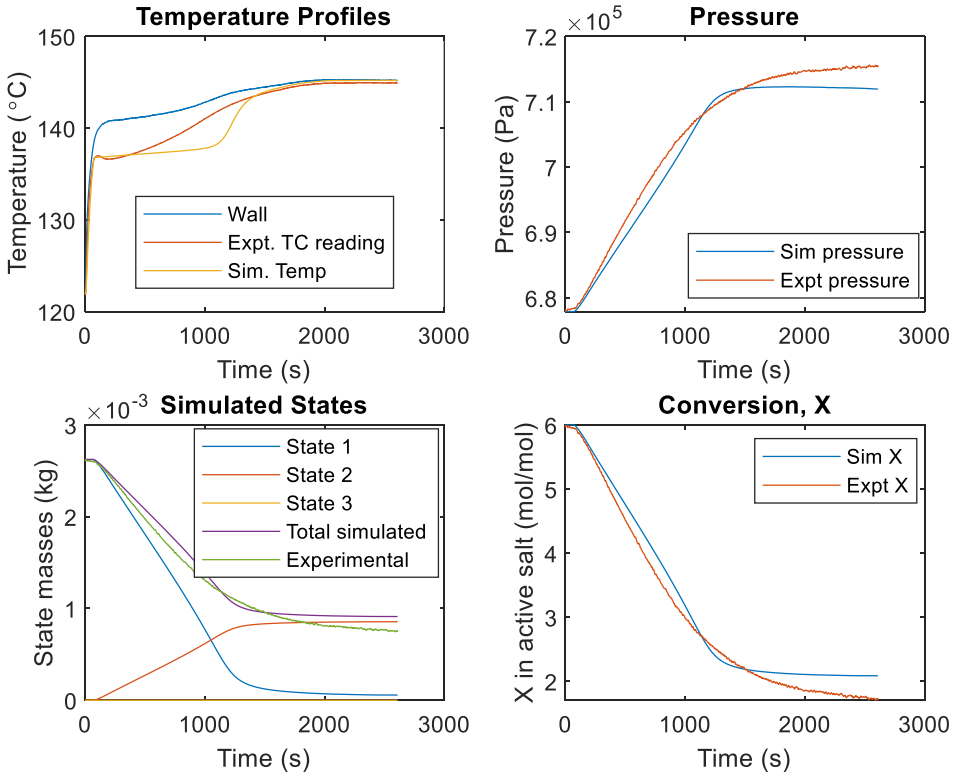

Shell side result with 4 nodes simulation.

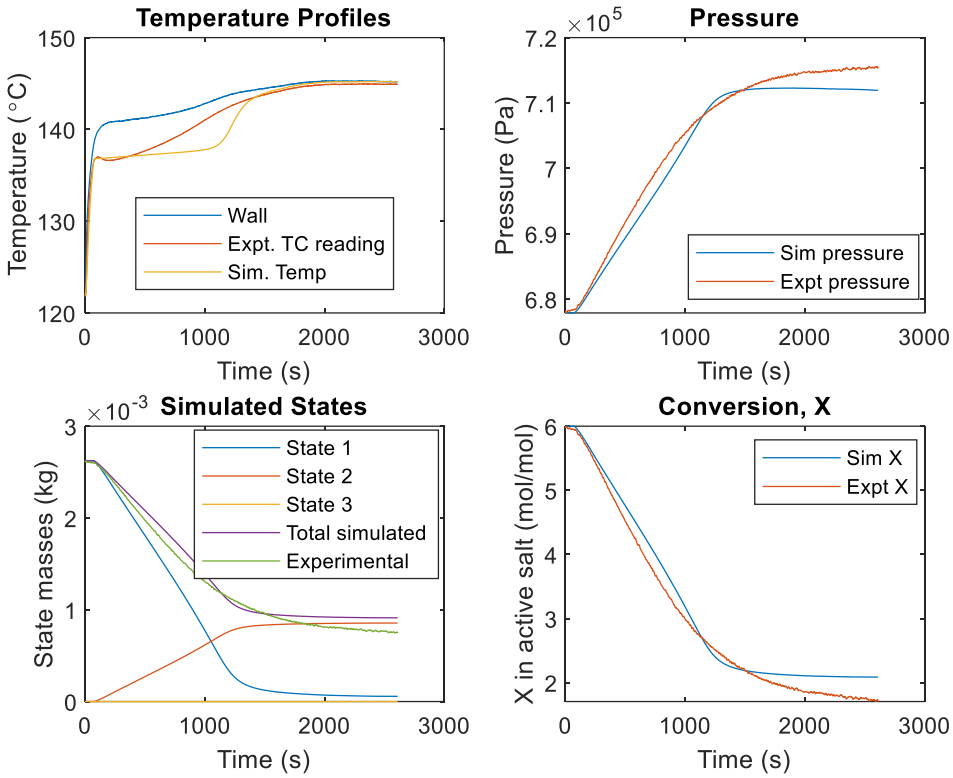

Shell side result with 5 nodes simulation.

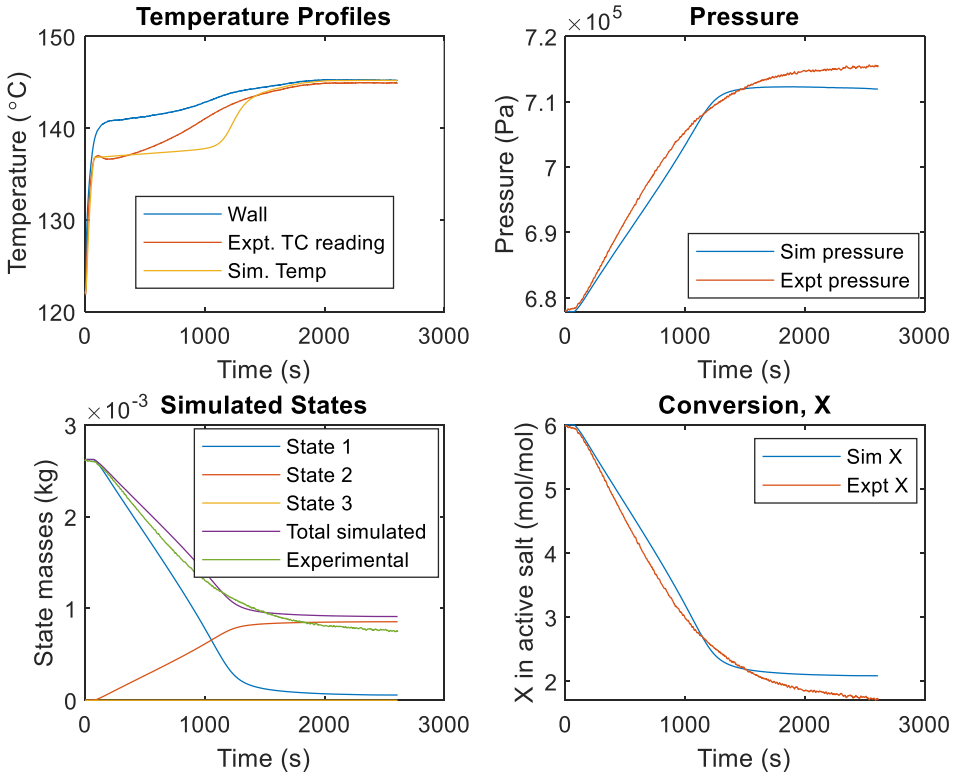

Shell side result with 10 nodes simulation.

8.10 Clapeyron Relationships Constructions to Assess the COP

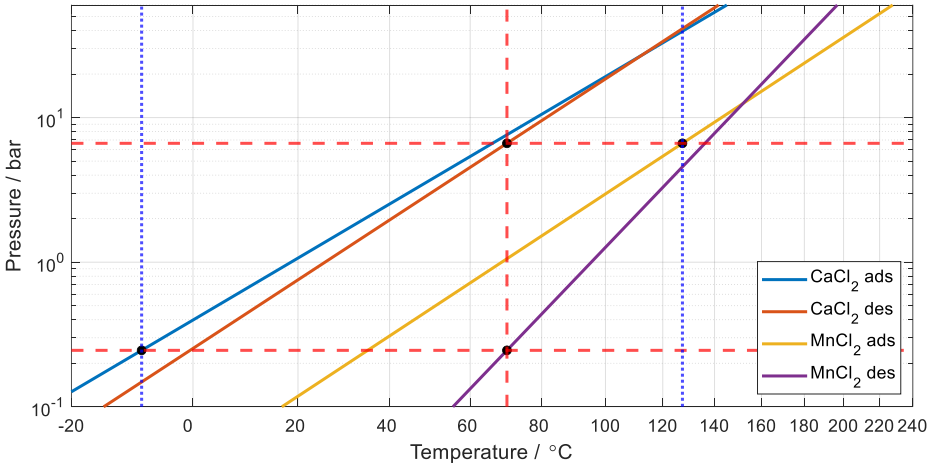

(a)

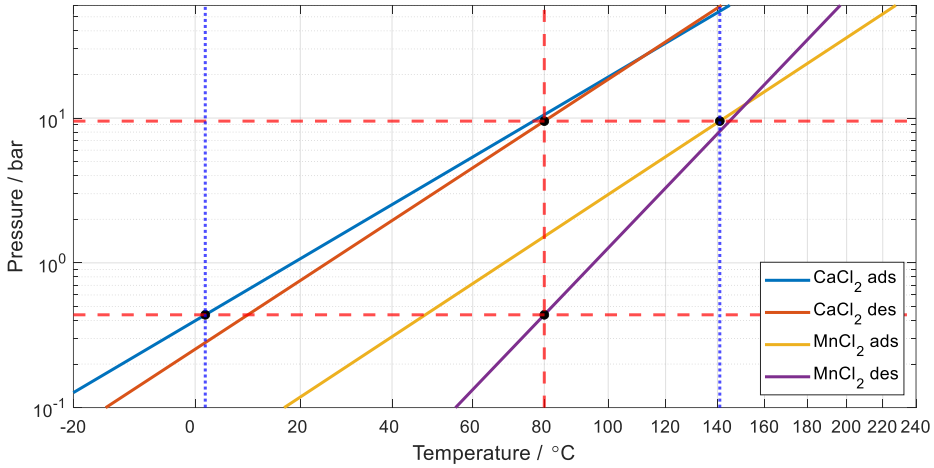

(b)

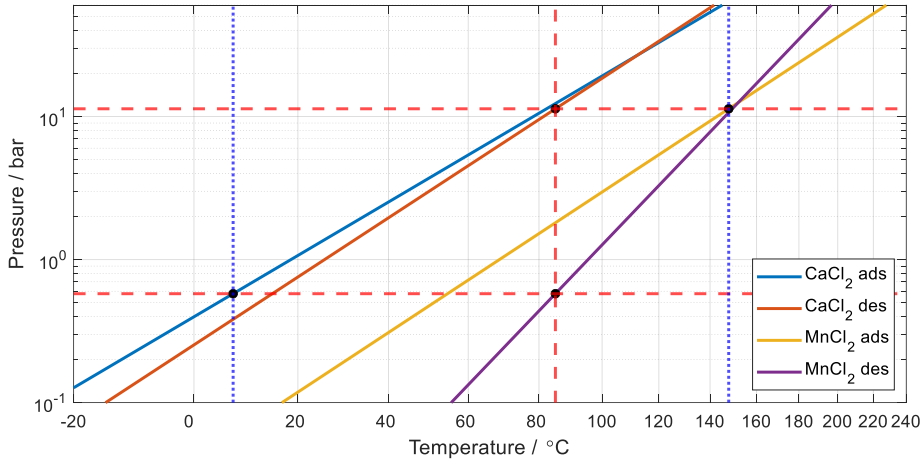

(c)

Figure 76 Clapeyron relationships for the pair calcium chloride (8-4), manganese chloride (6-2). This is indexed as (i) in ***Table 8****: (a) 70 °C T_m; and (b) 80 °C T_m; (c) 85 °C T_m*

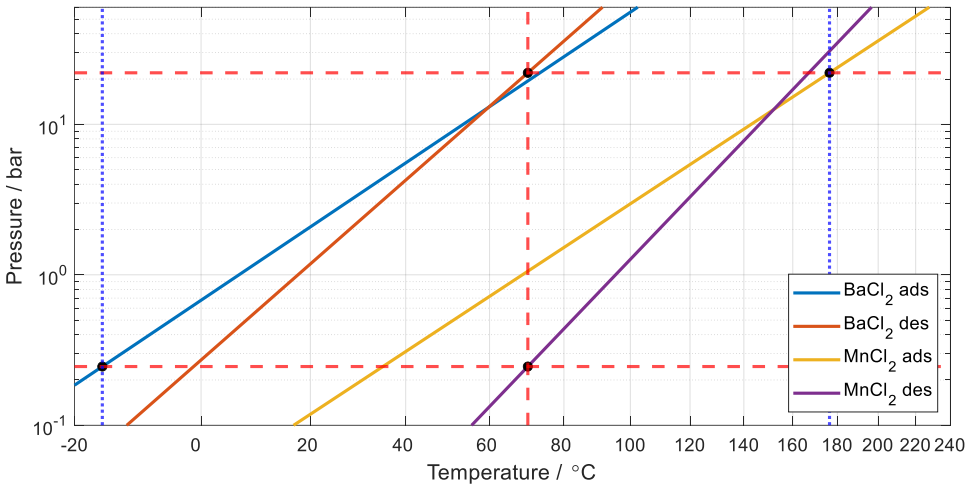

(a)

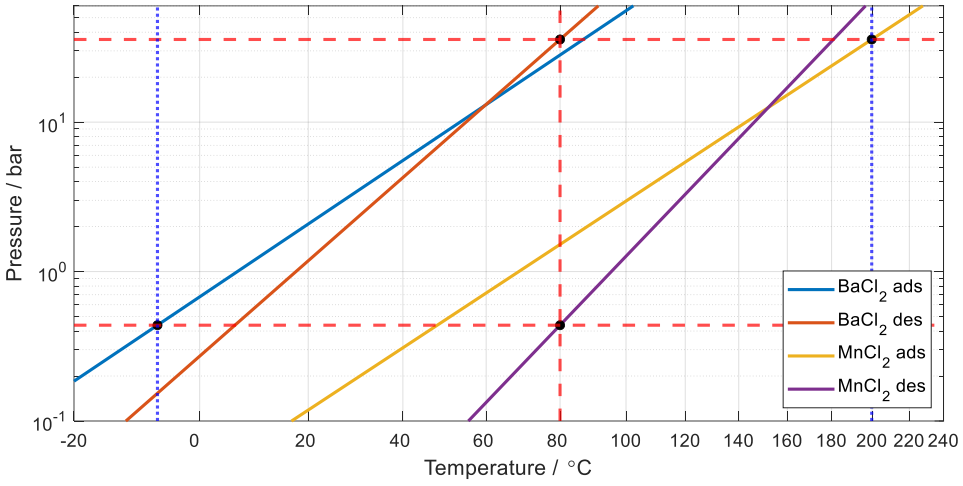

(b)

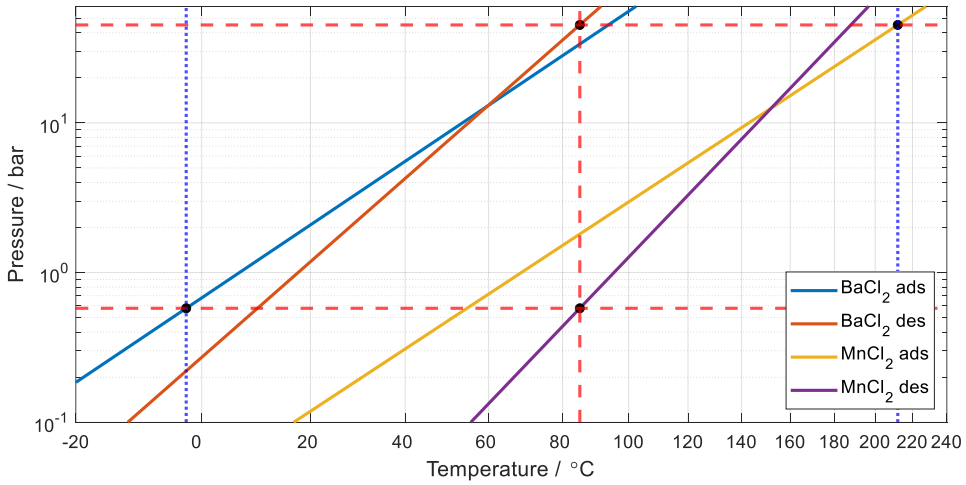

(c)

*Figure 77 Clapeyron relationships for the pair barium chloride (8-0), manganese chloride (6-2). This is indexed as (ii) in **Table 8**: (a) 70 °C T_m; (b) 80 °C T_m; and (c) 85 °C T_m.*

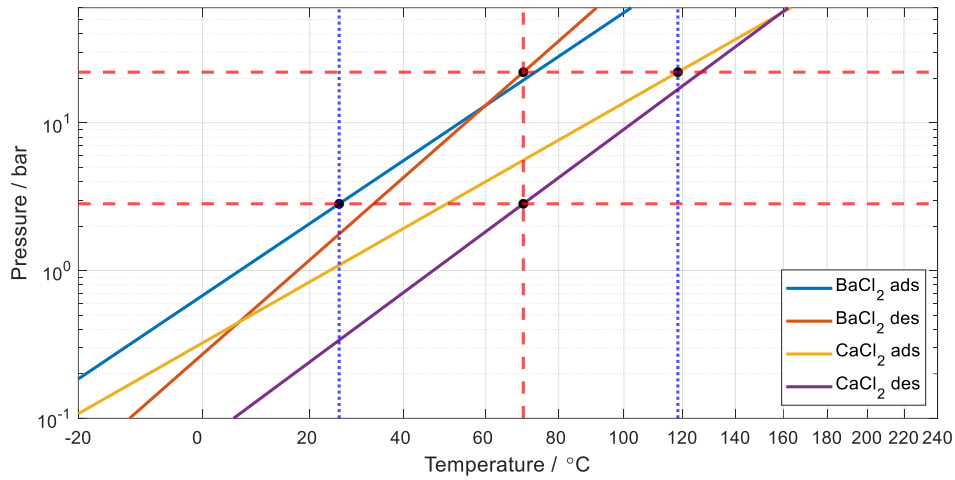

(a)

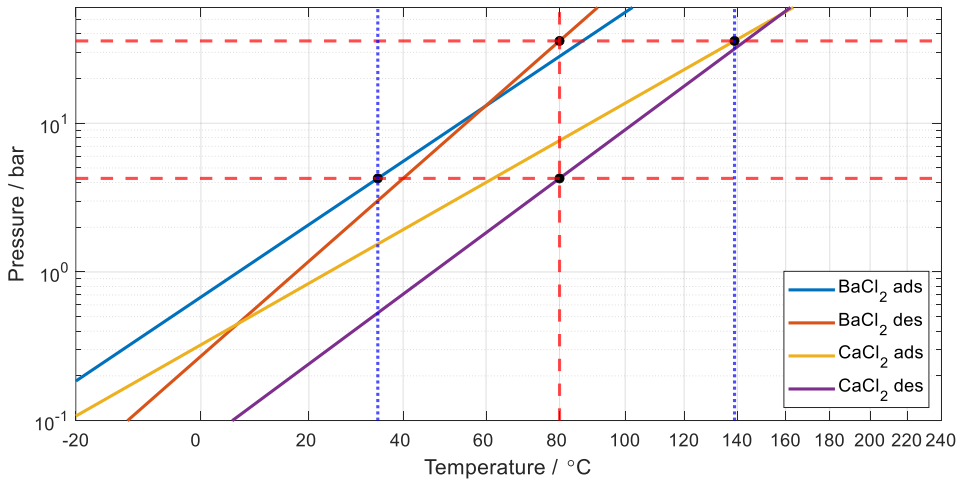

(b)

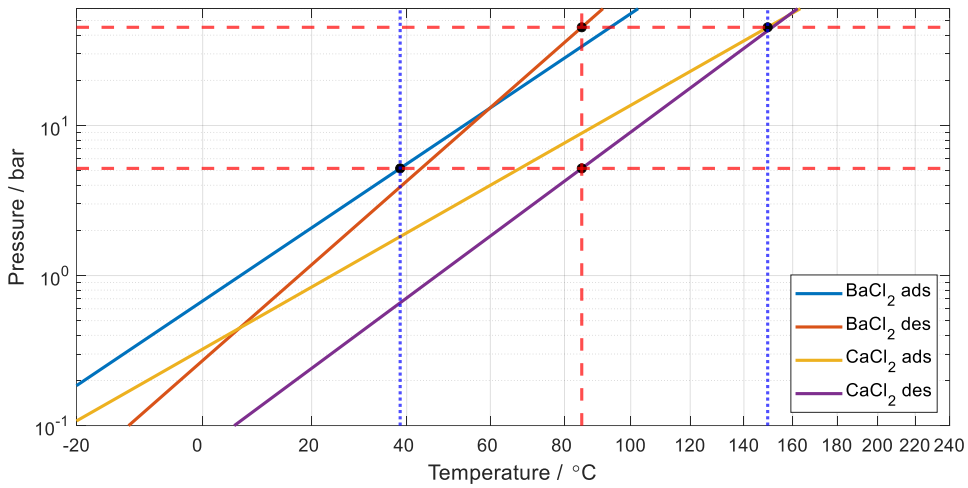

(c)

Figure 78 Clapeyron relationships for the pair barium chloride (8-0), calcium chloride (8-4). This is indexed as (iii) in ***Table 8****: (a) 70 °C T_m; (b) 80 °C T_m; and (c) 85 °C T_m.*

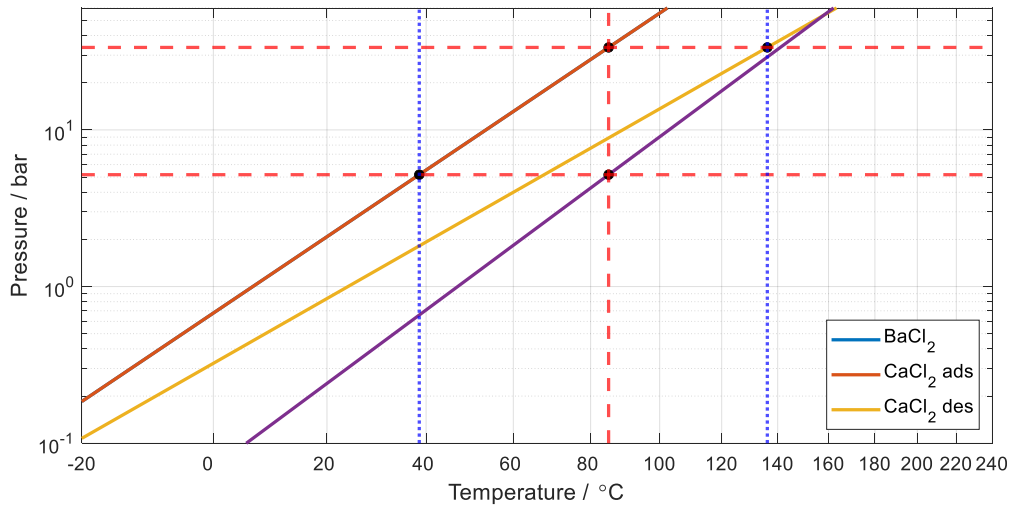

Figure 79 Clapeyron relationships for the pair barium chloride (8-0), calcium chloride (4-2). This is indexed a (iv) in ***Table 8****, illustrative example with only the adsorption line: T_m= 85 °C; T_h= 136.3 °C; and T_l= 38.9 °C. The COP = 0.316*

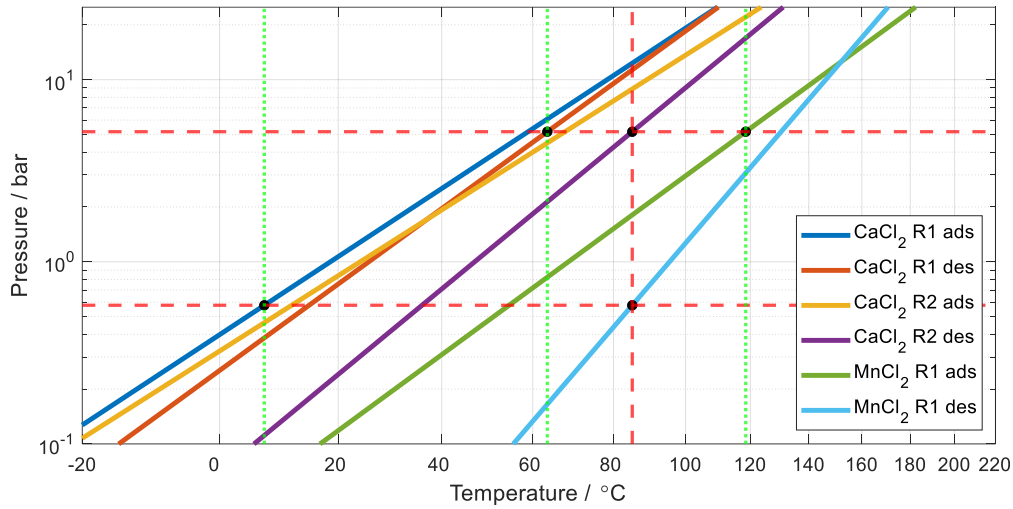

Figure 80 Clapeyron relationships for calcium chloride (8-4-2), both reactions with hysteresis. The adsorption line of calcium chloride visually interferes with the LTS plots. The same as shown in plot ***Figure 43****.*

8.11 Clapeyron Relationships Construction to Assess COP with Reduced Hysteresis

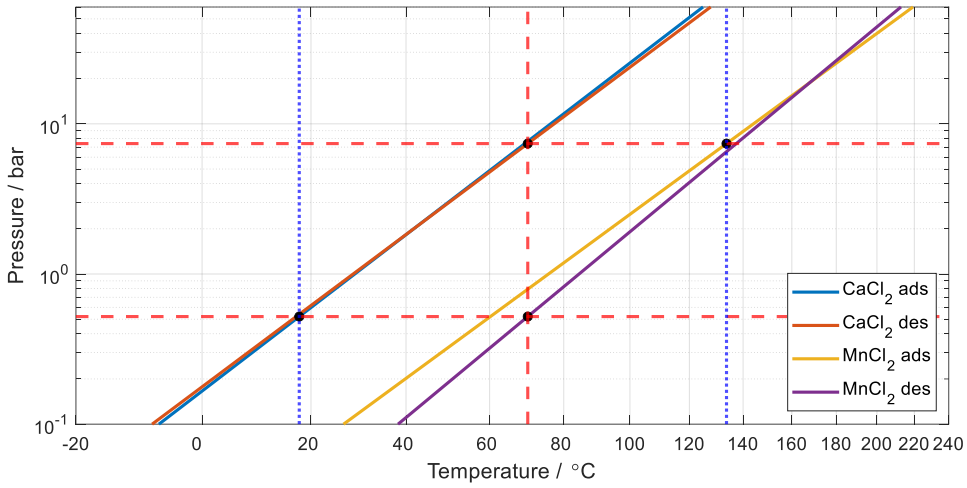

(a)

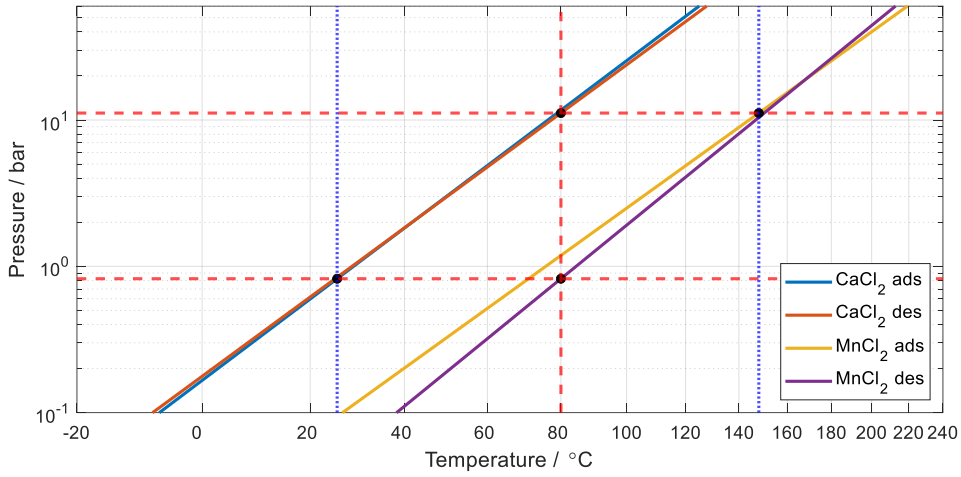

(b)

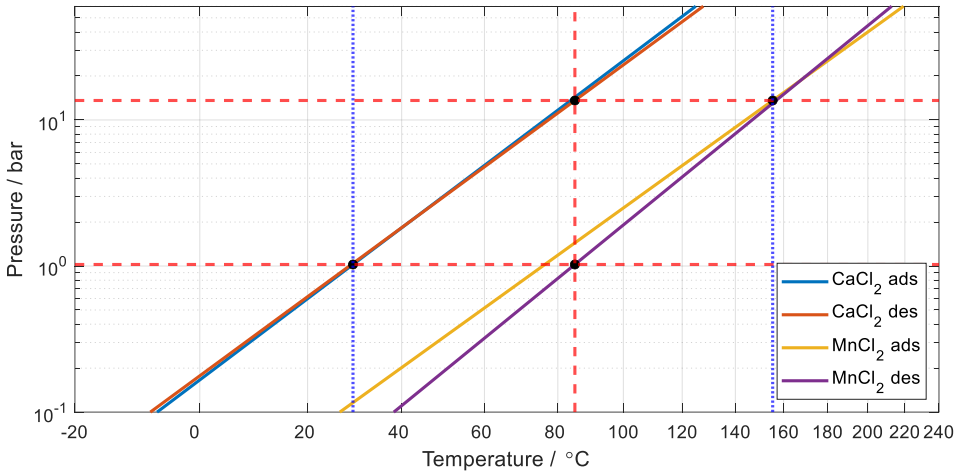

(c)

Figure 81 Clapeyron relationships for the pair calcium chloride (8-4), manganese chloride (6-2) with reduced hysteresis. This is indexed as (i) in ***Table 9****: (a) 70 °C T_m; (b) 80 °C T_m; and (c) 85 °C T_m.*

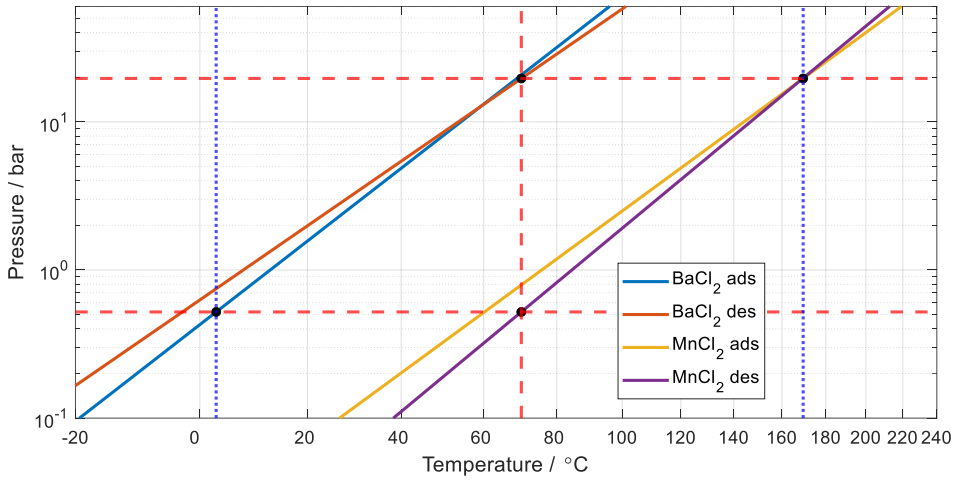

(a)

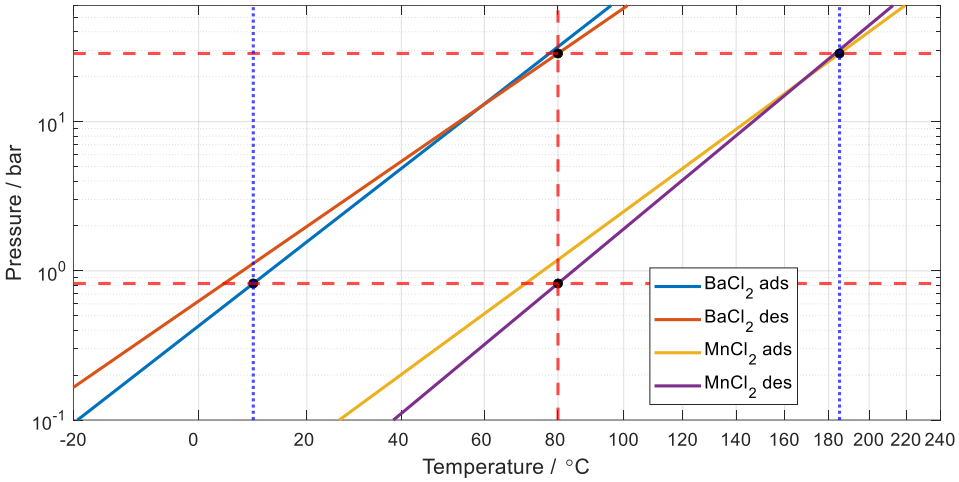

(b)

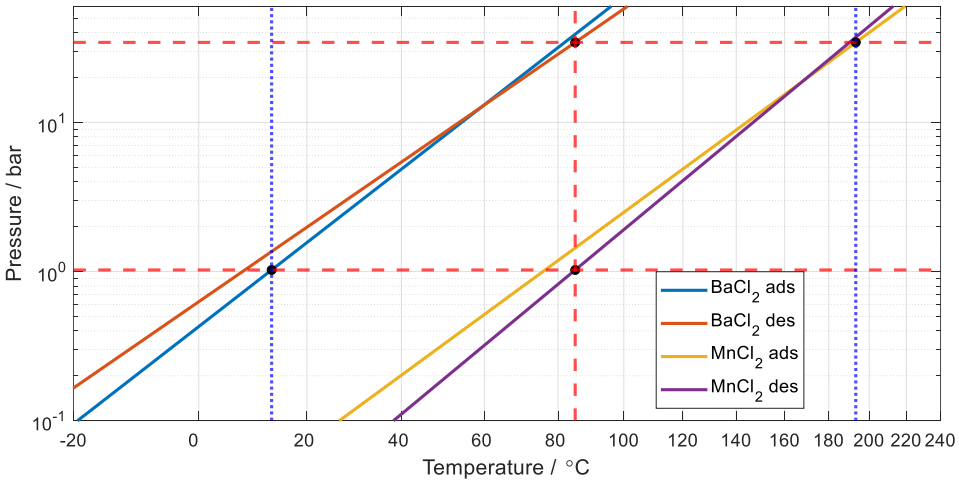

(c)

Figure 82 Clapeyron relationships for the pair barium chloride (8-0), manganese chloride (6-2) with reduced hysteresis. This is indexed as (ii) in ***Table 9****: (a) 70 °C T_m; (b) 80 °C T_m; and (c) 85 °C T_m.*

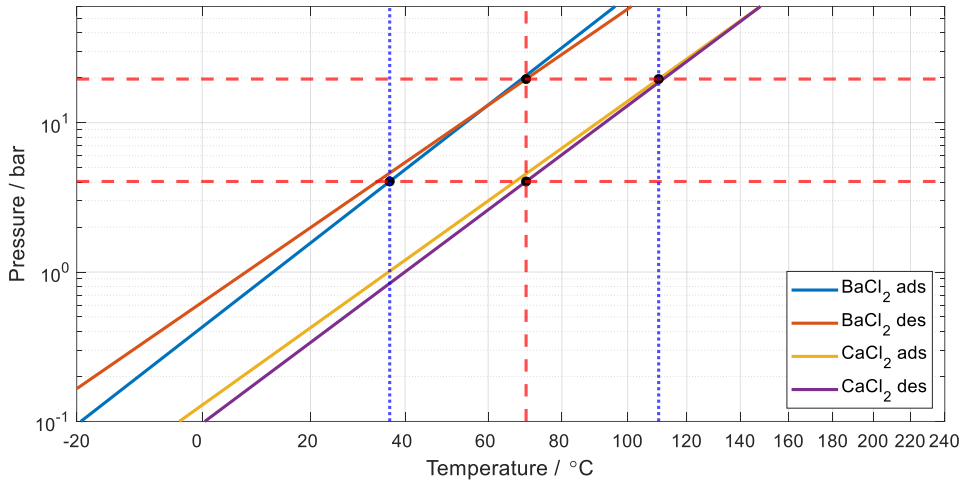

(a)

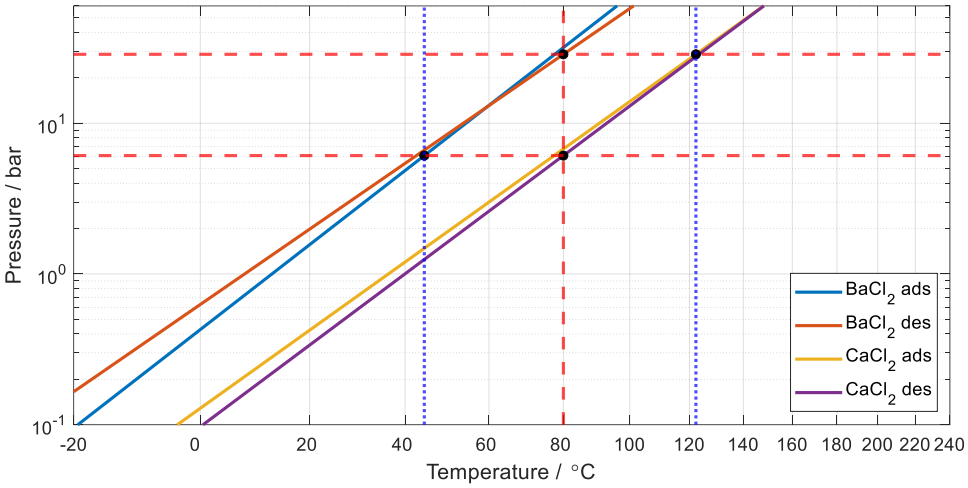

(b)

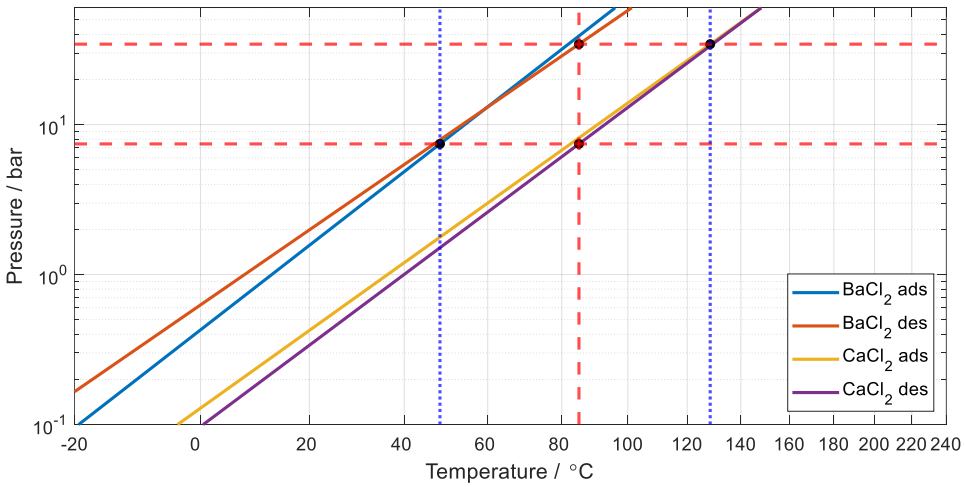

(c)

Figure 83 Clapeyron relationships for the pair barium chloride (8-0), calcium chloride (4-2) with reduced hysteresis. This is indexed as (iii) in ***Table 9****: (a) 70 °C T_m; (b) 80 °C T_m; and (c) 85 °C T_m*

8.12 Temperature Ramping SMP Tests

The program was set to simply ramp the temperature to a new value, the starting temperature was at the equilibrium conditions and the ramp time was set to 40 seconds. The driving temperature was set at 10 °C. It was soon realised the heating time was optimistic but the basis of the size effects were presented and could be weighed against the COP results for the same size. The approach was iterative as conclusions could be validated by testing in the shell side LTJ. The SMP value for ENG was the value only for the composite, it is therefore unimportant, but during the initial testing, one could observe the effect of the thermal mass of fluid and steel.

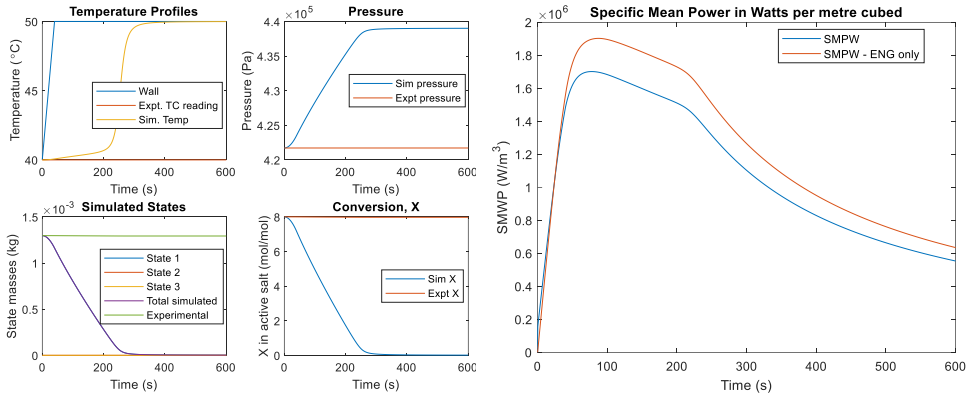

(a) *(b)*

Figure 84 Ramping simulation for barium chloride, sample sized for ½" tube (12.7 mm ID) with 30 mm outer diameter: (a) simulation results; (b) recorded SMP

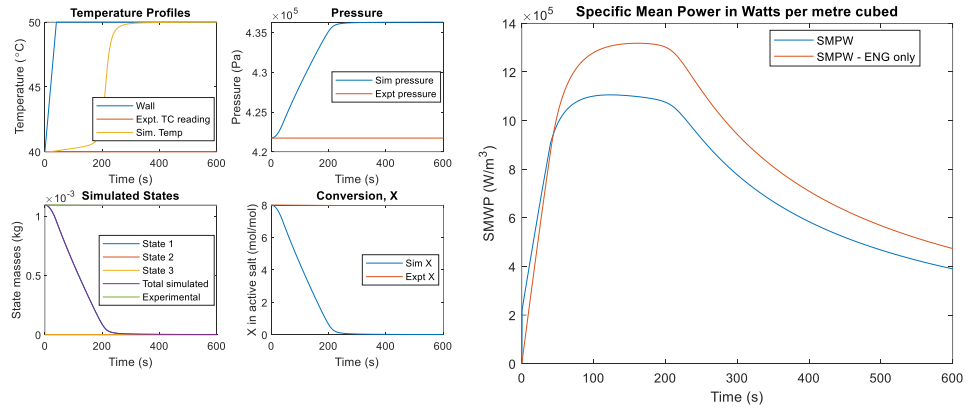

(a) *(b)*

Figure 85 Ramping simulation for barium chloride, sample sized for ½" tube (12.7 mm ID) with 28 mm outer diameter: (a) simulation results; (b) recorded SMP

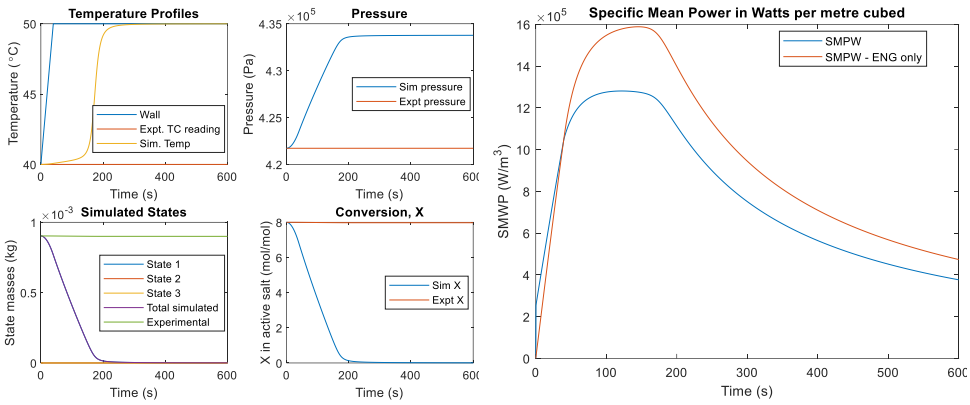

(a) *(b)*

Figure 86 Ramping simulation for barium chloride, sample sized for ½" tube (12.7 mm ID) with 26 mm outer diameter: (a) simulation results; (b) recorded SMP

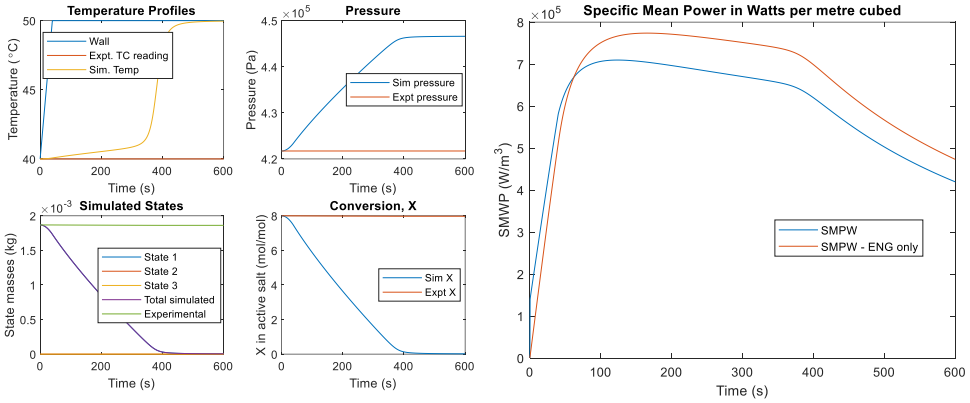

(a) *(b)*

Figure 87 Ramping simulation for barium chloride, sample sized for ½" tube (12.7 mm ID) with 35 mm outer diameter: (a) simulation results; (b) recorded SMP

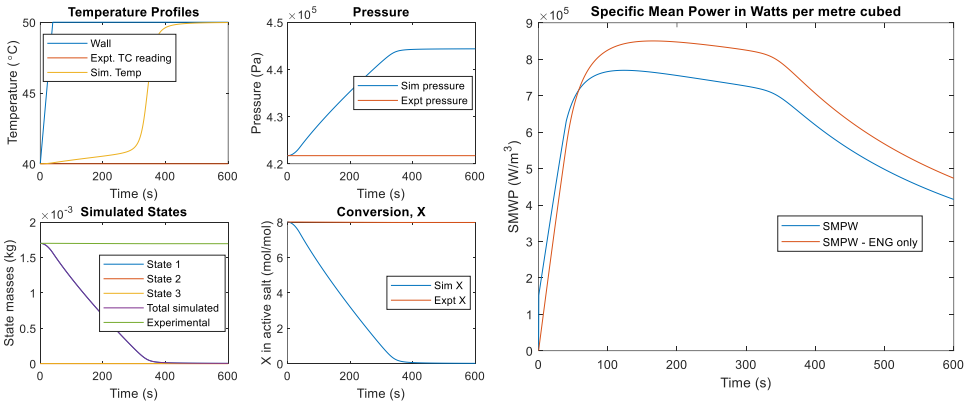

(a) *(b)*

Figure 88 Ramping simulation for barium chloride, sample sized for ½" tube (12.7 mm ID) with 33.6 mm outer diameter: (a) simulation results; (b) recorded SMP. Size basis of hexagonal final sample.

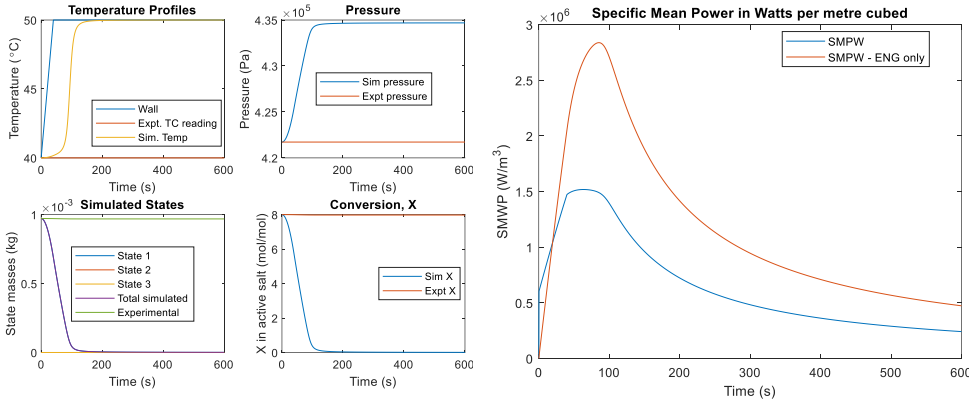

(a) *(b)*

Figure 89 Ramping simulation for barium chloride, sample sized for 1" tube (25.2 mm ID) with 36 mm outer diameter: (a) simulation results; (b) recorded SMP.

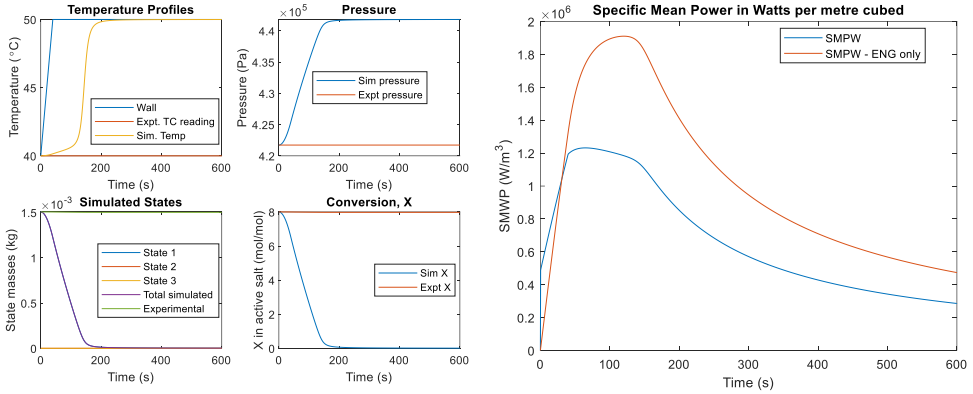

(a) *(b)*

Figure 90 Ramping simulation for barium chloride, sample sized for 1" tube (25.2 mm ID) with 40 mm outer diameter: (a) simulation results; (b) recorded SMP.

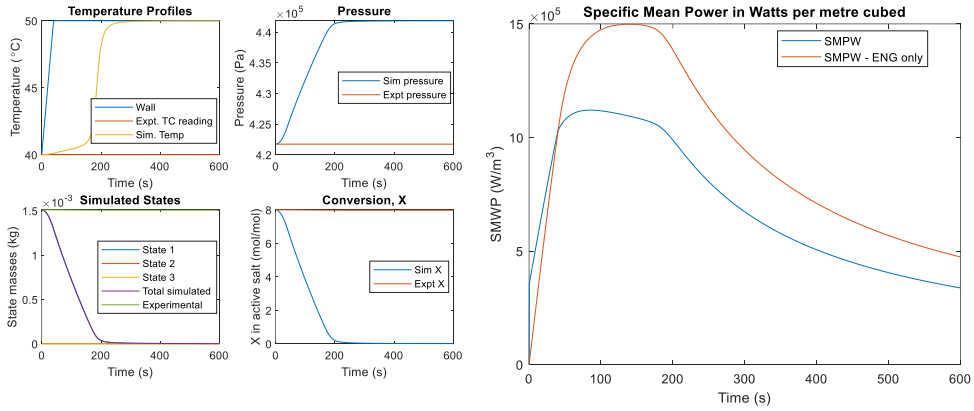

(a) *(b)*

Figure 91 Ramping simulation for barium chloride, sample sized for 3/4" tube (19.05 mm ID) with 36 mm outer diameter: (a) simulation results; (b) recorded SMP.

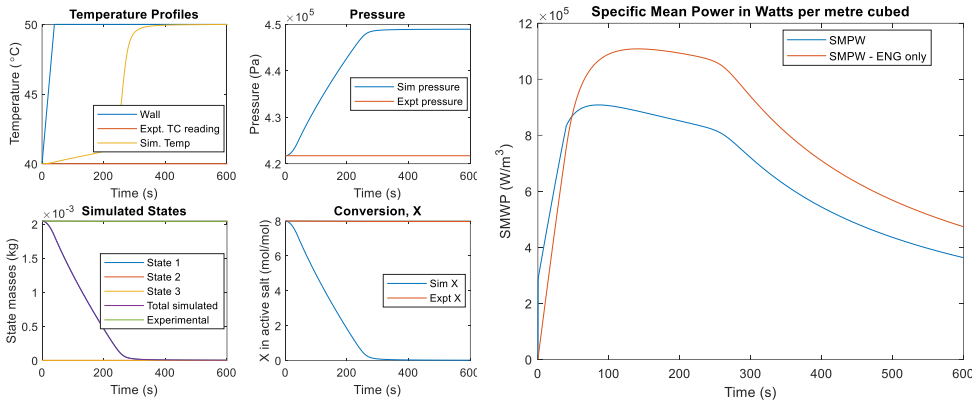

(a) *(b)*

Figure 92 Ramping simulation for barium chloride, sample sized for 3/4" tube (19.05 mm ID) with 40 mm outer diameter: (a) simulation results; (b) recorded SMP.

9 Bibliography

AITTOMÄKI, A. & HÄRKÖNEN, M. 1988. Modelling of zeolite/methanol adsorption heat pump process. *Heat Recovery Systems and CHP,* 8**,** 475-482.

AN, G., LI, Y., WANG, L. & GAO, J. 2020a. Wide applicability of analogical models coupled with hysteresis effect for halide/ammonia working pairs. *Chemical Engineering Journal,* 394**,** 125020.

AN, G. L., WANG, L. W., GAO, J. & WANG, R. Z. 2018. A review on the solid sorption mechanism and kinetic models of metal halide-ammonia working pairs. *Renewable and Sustainable Energy Reviews,* 91**,** 783-792.

AN, G. L., WANG, L. W. & ZHANG, Y. H. 2020b. Overall evaluation of single- and multi-halide composites for multi-mode thermal-energy storage. *Energy,* 212**,** 118756.

ARISTOV, Y. I. 2013. Experimental and numerical study of adsorptive chiller dynamics: Loose grains configuration. *Applied Thermal Engineering,* 61**,** 841-847.

ARISTOV, Y. I. 2017. "Heat from Cold" – A new cycle for upgrading the ambient heat: Adsorbent optimal from the dynamic point of view. *Applied Thermal Engineering,* 124**,** 1189-1193.

ARISTOV, Y. I., DAWOUD, B., GLAZNEV, I. S. & ELYAS, A. 2008. A new methodology of studying the dynamics of water sorption/desorption under real operating conditions of adsorption heat pumps: Experiment. *International Journal of Heat and Mass Transfer,* 51**,** 4966-4972.

ARMAREGO, W. L. F. & CHAI, C. L. L. 2009. Chapter 5 - Purification of Inorganic and Metal-Organic Chemicals: (Including Organic compounds of B, Bi, P, Se, Si, and ammonium and metal salts of organic acids). *In:* ARMAREGO, W. L. F. & CHAI, C. L. L. (eds.) *Purification of Laboratory Chemicals (Sixth Edition).* Oxford: Butterworth-Heinemann.

ATKINSON, G. H., HINMERS, S., CRITOPH, R. E. & VAN DER PAL, M. 2021. Ammonium Chloride (NH4Cl)—Ammonia (NH3): Sorption Characteristics for Heat Pump Applications. *Energies,* 14.

BAO, H. S., OLIVEIRA, R. G., WANG, R. Z., WANG, L. W. & MA, Z. W. 2011. Working pairs for resorption refrigerator. *Applied Thermal Engineering,* 31**,** 3015-3021.

BAO, H. S., WANG, R. Z., OLIVEIRA, R. G. & LI, T. X. 2012. Resorption system for cold storage and long-distance refrigeration. *Applied Energy,* 93**,** 479-487.

BEIS 2021. Quarterly Energy Prices: December 2021. *Energy and climage change: evidence and analysis.* London: Department for Business Energy and Industrial Strategy,.

CHEKIROU, W., BOUKHEIT, N. & KARAALI, A. 2016. Heat recovery process in an adsorption refrigeration machine. *International Journal of Hydrogen Energy,* 41**,** 7146-7157.

CRITOPH, R. E. 1989. Activated carbon adsorption cycles for refrigeration and heat pumping. *Carbon,* 27**,** 63-70.

CUDOK, F., GIANNETTI, N., CIGANDA, J. L. C., AOYAMA, J., BABU, P., CORONAS, A., FUJII, T., INOUE, N., SAITO, K., YAMAGUCHI, S. & ZIEGLER, F. 2021. Absorption heat transformer - state-of-the-art of industrial applications. *Renewable and Sustainable Energy Reviews,* 141**,** 110757.

DAINTITH, J. 2008. *A Dictionary of Chemistry*, Oxford University Press.

DAWOUD, B. & ARISTOV, Y. 2003. Experimental study on the kinetics of water vapor sorption on selective water sorbents, silica gel and alumina under typical operating conditions of sorption heat pumps. *International Journal of Heat and Mass Transfer,* 46**,** 273-281.

DONKERS, P., PEL, L., STEIGER, M. & ADAN, O. 2016. Deammoniation and ammoniation processes with ammonia complexes. *Energy,* 4.

ELEMENTENERGY 2014. The potential for recovering and using surplus heat from industry. London.

FARADAY, M. 1823. On the Condensation of Several Gases into Liquids. *Philosophical Transactions of the Royal Society of London,* 113**,** 189-198.

FUJIOKA, K., KATO, S.-I., FUJIKI, S. & HIRATA, Y. 1996. Variations of Molar Volume and Heat Capacity of Reactive Solids of CaCl2 Used for Chemical Heat Pumps. *JOURNAL OF CHEMICAL ENGINEERING OF JAPAN,* 29**,** 858-864.

GLUESENKAMP, K. R., FRAZZICA, A., VELTE, A., METCALF, S., YANG, Z., ROUHANI, M., BLACKMAN, C., QU, M., LAURENZ, E., RIVERO-PACHO, A., HINMERS, S., CRITOPH, R., BAHRAMI, M., FÜLDNER, G. & HALLIN, I. 2020. Experimentally Measured Thermal Masses of Adsorption Heat Exchangers. *Energies,* 13**,** 1150.

GOETZ, V., ELIE, F. & SPINNER, B. 1993. The structure and performance of single effect solid-gas chemical heat pumps. *Heat Recovery Systems and CHP,* 13**,** 79-96.

GOETZ, V. & MARTY, A. 1992. A model for reversible solid-gas reactions submitted to temperature and pressure constraints: simulation of the rate of reaction in solid-gas reactor used as chemical heat pump. *Chemical Engineering Science,* 47**,** 4445-4454.

GOETZ, V., SPINNER, B. & LÉPINASSE, E. 1997. A solid-gas thermochemical cooling system using BaCl2 and NiCl2. *Energy,* 22**,** 49-58.

GORDEEVA, L., GREKOVA, A., KRIEGER, T. & ARISTOV, Y. 2013. Composites "binary salts in porous matrix" for adsorption heat transformation. *Applied Thermal Engineering,* 50**,** 1633-1638.

GORDEEVA, L. G. & ARISTOV, Y. I. 2011. Composite sorbent of methanol "LiCl in mesoporous silica gel" for adsorption cooling: Dynamic optimization. *Energy,* 36**,** 1273-1279.

GORDEEVA, L. G. & ARISTOV, Y. I. 2012. Composites 'salt inside porous matrix' for adsorption heat transformation: a current state-of-the-art and new trends. *International Journal of Low-Carbon Technologies,* 7**,** 288-302.

HAMMOND, G. P. & NORMAN, J. B. 2014. Heat recovery opportunities in UK industry. *Applied Energy,* 116**,** 387-397.

HERNÁNDEZ-MAGALLANES, J. A., RIVERA, W. & CORONAS, A. 2017. Comparison of single and double stage absorption and resorption heat transformers operating with the ammonia-lithium nitrate mixture. *Applied Thermal Engineering,* 125**,** 53-68.

HINMERS, S., ATKINSON, G. H., CRITOPH, R. E. & VAN DER PAL, M. 2022. Modelling and Analysis of Ammonia Sorption Reactions in Halide Salts. *International Journal of Refrigeration*.

HIRATA, Y. & FUJIOKA, K. Thermophysical properties and heat transfer characteristics of CaCl2 heat pump reactor associated with structural change of reactive salts. V Minsk international seminar ''Heat pipes, heat pumps, refrigerators., 2003.

HITACHI. 2019. *Absorption heat pump Type2 - Hitachi* [Online]. Available: https://industrial.hitachiaircon.com/en/chiller/waste-heat/heat-pump-2 [Accessed 17th January 2022].

IEDEMA, P. D. 1984. *The Absorption Heat Pump.* Delft University of Technology.

JEGEDE, O. O. 2017. *Concept Design of a ThermoChemical Heat Pump Using Calcium Chloride-NH_3 and Magnesium Chloride-NH_3 Working Pairs.* PhD, University of Warwick.

JEGEDE, O. O. & CRITOPH, R. E. 2016. Extraction of heat transfer parameters in active carbon–ammonia large temperature jump experiments. *Applied Thermal Engineering,* 95**,** 499-505.

JIANG, L., WANG, L. W., ZHOU, Z. S., ZHU, F. Q. & WANG, R. Z. 2016. Investigation on non-equilibrium performance of composite adsorbent for resorption refrigeration. *Energy Conversion and Management,* 119**,** 67-74.

KIPLAGAT, J. K., WANG, R. Z., OLIVEIRA, R. G., LI, T. X. & LIANG, M. 2013. Experimental study on the effects of the operation conditions on the performance of a chemisorption air conditioner powered by low grade heat. *Applied Energy,* 103**,** 571-580.

LEBRUN, M. 1990. Simulation for the development of solid—gas chemical heat pump pilot plants Part II. simulation and optimization of Discontinuous and pseudo-continuous operating cycles. *Chemical Engineering and Processing: Process Intensification,* 28**,** 67-77.

LEBRUN, M. & SPINNER, B. 1990a. Models of heat and mass transfers in solid—gas reactors used as chemical heat pumps. *Chemical Engineering Science,* 45**,** 1743-1753.

LEBRUN, M. & SPINNER, B. 1990b. Simulation for the development of solid—gas chemical heat pump pilot plants Part I. simulation and dimensioning. *Chemical Engineering and Processing: Process Intensification,* 28**,** 55-66.

LÉPINASSE, E., GOETZ, V. & CROSAT, G. 1994. Modelling and experimental investigation of a new type of thermochemical transformer based on the coupling of two solid-gas reactions. *Chemical Engineering and Processing: Process Intensification,* 33**,** 125-134.

LÉPINASSE, E., MARION, M. & GOETZ, V. 2001. Cooling storage with a resorption process. Application to a box temperature control. *Applied Thermal Engineering,* 21**,** 1251-1263.

LEVENSPIEL, O. 1999. *Chemical Reaction Engineering,* New York, John Wiley & Sons.

LI, T. X., WANG, R. Z., KIPLAGAT, J. K. & CHEN, H. 2010. Experimental study and comparison of thermochemical resorption refrigeration cycle and adsorption refrigeration cycle. *Chemical Engineering Science,* 65**,** 4222-4230.

LING-CHIN, J., BAO, H., MA, Z., TAYLOR, W. & ROSKILLY, T. 2019. State-of-the-Art Technologies on Low-Grade Heat Recovery and Utilization in Industry.

LU, H.-B., MAZET, N., COUDEVYLLE, O. & MAURAN, S. 1997. Comparison of a general model with a simplified approach for the transformation of solid-gas media used in chemical heat transformers. *Chemical Engineering Science,* 52**,** 311-327.

LU, H.-B., MAZET, N. & SPINNER, B. 1996. Modelling of gas-solid reaction—Coupling of heat and mass transfer with chemical reaction. *Chemical Engineering Science,* 51**,** 3829-3845.

MA, L., RUI, Z., WU, Q., YANG, H., YIN, Y., LIU, Z., CUI, Q. & WANG, H. 2016. Performance evaluation of shaped MIL-101–ethanol working pair for adsorption refrigeration. *Applied Thermal Engineering,* 95**,** 223-228.

MAZET, N. & AMOUROUX, M. 1991. Analysis of Heat Transfer in a Non-isothermal Solid-Gas Reacting Medium. *Chemical Engineering Communications,* 99**,** 175-200.

MAZET, N., AMOUROUX, M. & SPINNER, B. 1991. Analysis and Experimental Study of the Transformation of Non-isothermal Solid-Gas Reacting Medium. *Chemical Engineering Communications,* 99**,** 155-174.

METCALF, S., RIVERO-PACHO, Á. & CRITOPH, R. 2021. Design and Large Temperature Jump Testing of a Modular Finned-Tube Carbon–Ammonia Adsorption Generator for Gas-Fired Heat Pumps. *Energies,* 14**,** 3332.

METOFFICE. *UK Climate Averages, Coventry* [Online]. Available: https://www.metoffice.gov.uk/research/climate/maps-and-data/uk-climate-averages/gcqfjn5xn [Accessed].

MOUNDANGA-INIAMY, M. & TOUZAIN, P. 1992. The Reaction between Ammonia and Magnesium Chloride Graphite Intercalation Compounds. *MSF Materials Science Forum,* 91-93**,** 823-828.

NEVEU, P. & CASTAING, J. 1993. Solid-gas chemical heat pumps: Field of application and performance of the internal heat of reaction recovery process. *Heat Recovery Systems and CHP,* 13**,** 233-251.

OFFENHARTZ, P. O. D., BROWN, F. C., MAR, R. W. & CARLING, R. W. 1980. A Heat Pump and Thermal Storage System for Solar Heating and Cooling Based on the Reaction of Calcium Chloride and Methanol Vapor. *Journal of Solar Energy Engineering,* 102**,** 59-65.

OFFENHARTZ, P. O. D., MALSBERGER, R. E., RYE, T. V. & SCHWARTZ, D. 1981. METHANOL-BASED HEAT PUMP FOR SOLAR HEATING. COOLING AND STORAGE. PHASE III. Springfield, VA: MATERIALS CHEMISTRY AND ENERGY CONVERSION DIVISION DERARTMENT OF ENERGY AND ENVIRONMENT BROOKHAVEN NATIONAL LABORATORY ASSOCIATED UNIVERSITIES. INC.

PAN, Z. H. & ZHAO, C. Y. 2017. Gas–solid thermochemical heat storage reactors for high-temperature applications. *Energy,* 130**,** 155-173.

RIVERO-PACHO, A. M., CRITOPH, R. E. & METCALF, S. J. 2017. Modelling and development of a generator for a domestic gas-fired carbon-ammonia adsorption heat pump. *Renewable Energy,* 110**,** 180-185.

SGL CARBON 2020. Sigratherm L and LN - Lightweight graphite board for thermal management. *In:* SGL CARBON GMBH (ed.) *Graphite Materials and Systems.* Germany: SGL Carbon SE.

SHARMA, R., ANIL KUMAR, E., DUTTA, P., SRINIVASA MURTHY, S., ARISTOV, Y. I., TOKREV, M. M., LI, T. X. & WANG, R. Z. 2021. Ammoniated salt based solid sorption thermal batteries: A comparative study. *Applied Thermal Engineering,* 191**,** 116875.

SUPEKAR, S. D. & SKERLOS, S. J. 2015. Reassessing the Efficiency Penalty from Carbon Capture in Coal-Fired Power Plants. *Environmental Science & Technology,* 49**,** 12576-12584.

TOUZAIN, P. Thermodynamic values of ammonia-salts reactions for chemical sorption heat pumps. *In:* C, S., ed. PROCEEDINGS OF THE INTERNATIONAL SORPTION HEAT PUMP CONFERENCE, 1999 Munich, Germany. ZAE Bayern, 225-238.

TOUZAIN, P., ATIFI, A. E. & MOUNDANGA-INIAMY, M. 1994. Reaction of Metal Chloride Graphite Intercalation Compounds with Ammonia. *Molecular Crystals and Liquid Crystals Science and Technology. Section A. Molecular Crystals and Liquid Crystals,* 245**,** 231-236.

TOUZAIN, P. & MOUNDANGA-INIAMY, M. 1994. Thermochemical Heat Transformation: Study of The Ammonia/Magnesium Chloride-Gic Pair in A Laboratory Pilot. *Molecular Crystals and Liquid Crystals Science and Technology. Section A. Molecular Crystals and Liquid Crystals,* 245**,** 243-248.

TRUDEL, J., HOSATTE, S. & TERNAN, M. 1999. Solid–gas equilibrium in chemical heat pumps: the NH3–CoCl2 system. *Applied Thermal Engineering,* 19**,** 495-511.

TYAGI, K. P. 1987. Aqua-ammonia heat transformers. *Heat Recovery Systems and CHP,* 7**,** 423-433.

VAN DER PAL, M. & CRITOPH, R. E. 2017. Performance of CaCl 2 -reactor for application in ammonia-salt based thermal transformers. *Applied Thermal Engineering,* 126.

VAN DER PAL, M., DE BOER, R., SMEDING, S. & VELDHUIS, J. B. J. 2009. Thermally driven ammonia-salt type II heat pump: Development and testing of a prototype. *Heat Powered Cycles Conference.* Berlin.

VASILIEV, L. L., MISHKINIS, D. A., ANTUKH, A. A., KULAKOV, A. G. & VASILIEV, L. L. 2004. Resorption heat pump. *Applied Thermal Engineering,* 24**,** 1893-1903.

VESELOVSKAYA, J. V., CRITOPH, R. E., THORPE, R. N., METCALF, S., TOKAREV, M. M. & ARISTOV, Y. I. 2010. Novel ammonia sorbents “porous matrix modified by active salt” for adsorptive heat transformation: 3. Testing of “BaCl2/vermiculite” composite in a lab-scale adsorption chiller. *Applied Thermal Engineering,* 30**,** 1188-1192.

VESELOVSKAYA, J. V. & TOKAREV, M. M. 2011. Novel ammonia sorbents “porous matrix modified by active salt” for adsorptive heat transformation: 4. Dynamics of quasi-isobaric ammonia sorption and desorption on BaCl2/vermiculite. *Applied Thermal Engineering,* 31**,** 566-572.

VESELOVSKAYA, J. V., TOKAREV, M. M., GREKOVA, A. D. & GORDEEVA, L. G. 2012. Novel ammonia sorbents ‘‘porous matrix modified by active salt” for adsorptive heat transformation: 6. The ways of adsorption dynamics enhancement. *Applied Thermal Engineering,* 37**,** 87-94.

WANG, C., ZHANG, P. & WANG, R. Z. 2010. Performance of solid–gas reaction heat transformer system with gas valve control. *Chemical Engineering Science,* 65**,** 2910-2920.

WARUDKAR, S. S., COX, K. R., WONG, M. S. & HIRASAKI, G. J. 2013. Influence of stripper operating parameters on the performance of amine absorption systems for post-combustion carbon capture: Part I. High pressure strippers. *International Journal of Greenhouse Gas Control,* 16**,** 342-350.

WU, S., LI, T. X., YAN, T. & WANG, R. Z. 2019. Advanced thermochemical resorption heat transformer for high-efficiency energy storage and heat transformation. *Energy,* 175**,** 1222-1233.

XU, J., OLIVEIRA, R. G. & WANG, R. Z. 2011. Resorption system with simultaneous heat and cold production. *International Journal of Refrigeration,* 34**,** 1262-1267.

YUAN, Y., BAO, H., MA, Z., LU, Y. & ROSKILLY, A. P. 2019. Investigation of equilibrium and dynamic performance of SrCl2-expanded graphite composite in chemisorption refrigeration system. *Applied Thermal Engineering,* 147**,** 52-60.

ZHONG, Y., CRITOPH, R. E., THORPE, R. N. & TAMAINOT-TELTO, Z. 2009. Dynamics of BaCl2–NH3 adsorption pair. *Applied Thermal Engineering,* 29**,** 1180-1186.

ZHONG, Y., CRITOPH, R. E., THORPE, R. N., TAMAINOT-TELTO, Z. & ARISTOV, Y. I. 2007. Isothermal sorption characteristics of the BaCl2–NH3 pair in a vermiculite host matrix. *Applied Thermal Engineering,* 27**,** 2455-2462.